IN MEMORY OF MY PARENTS

GAMMA-RAY STUDIES OF SOME LIGHT NUCLEI

by

Frederick Chao-Pang Huang

A Thesis submitted to
the Australian National University
for the Degree of Doctor of Philosophy

Canberra
March, 1968

PREFACE

This thesis describes a series of experiments which were carried out in the Department of Nuclear Physics, the Australian National University.

The study of the $^{13}C(p,\gamma)$ reaction (Chapter 3) was carried out under the supervision of Dr. D.F. Hebbard. Approximately 50% of the supervised effort was my own.

The study of the $^{14}N(p,\gamma)$ reaction (Chapter 4) was carried out in collaboration with Mr. C.H. Osman under the supervision of Dr. D.F. Hebbard. In the later stage of the experiment, Dr. T.R. Ophel suggested coincidence measurements and actively engaged in the analysis of data while Dr. Hebbard was on leave. Again 50% of the effort was my own.

The study of the $^{26}Mg(p,\gamma)$ reaction with a Ge(Li) detector described in Chapter 5 and 6 was carried out under the supervision of Dr. T.R. Ophel. Both the experimental work and analysis were divided evenly between us.

It is a pleasure to thank the many people who have helped in the work described in this thesis. I wish to acknowledge my debt to Dr. D.F. Hebbard for his help and guidance in the early stage of my study and to Dr. T.R.

Ophel for his excellent supervision and helpful comments in all aspects of this thesis.

I would like to express my gratitude to Professor E.W. Titterton for his encouragement and support of the projects and to the Australian National University for the award of a scholarship.

Thanks are also to Mr C.H. Osman for his hospitality shown to me during my stay in Australia and to members of the technical staff for their assistance in operation of accelerators.

No part of this thesis has been submitted for a degree at any other university.

F C P Huang

TABLE OF CONTENTS

		page
CHAPTER I	GENERAL INTRODUCTION	1
CHAPTER II	ANALYSIS OF GAMMA-RAY SCINTILLATION SPECTRA	5
	1. Introduction	5
	2. Interaction of Gamma-Rays with Matter	6
	3. Response of NaI(Tl) Crystal to Gamma-Rays	8
	4. Measurement of Standard Gamma-Ray Line Shapes	12
	5. Generation of Line Shapes of Energies Other Than Those Measured	15
	5.1 Function Fits	15
	5.2 Methods of Interpolation	19
	6. Coincidence Sum Spectrum	21
	7. Method of Least Squares Analysis	23
CHAPTER III	THE 8.49 MeV STATE OF ^{14}N	28
	1. Introduction	28
	2. Experimental Procedure	35
	3. Results	38
	4. Discussion	44
	5. Summary	51
CHAPTER IV	THE INVESTIGATION OF THE $^{14}N(p,\gamma)^{15}O$ REACTION IN THE PROTON ENERGY RANGE 1.7 TO 3.0 MeV	55
	1. Introduction	55
	2. Specific Problems	57
	3. Experimental Details	59
	4. Measurement of Target Composition	61
	5. Analysis of Data	64
	6. Results	68
	7. Discussion	74

		Page
CHAPTER V	THE 20 c.c. Ge(Li) DETECTOR	80
	1. Introduction	80
	2. Performance of the Spectrometer	82
	2.1 Resolution	83
	2.2 Energy Linearity and Calibration	86
	2.3 Calculation of Detector Efficiencies and Angular Correlation Attenuation Factors	94
	2.4 Photopeak Efficiency	99
	2.5 Double Escape Peak Efficiency	103
	3. Line Shape Analysis	105
	4. Application	108
CHAPTER VI	THE $^{26}Mg(p,\gamma)^{27}Al$ REACTION	113
	1. Introduction	113
	2. Specific Problems Concerning Levels of ^{27}Al	117
	2.1 The Spin of the 3.00 MeV Level	117
	2.2 The 3.68 MeV Level	118
	2.3 The 3.96 MeV Level	121
	2.4 The 4.41 MeV Level	122
	3. Experimental Methods	123
	4. The 662 keV Resonance	128
	5. The 719 keV Resonance	130
	5.1 Decay Scheme of the 719 keV Resonance	130
	5.2 Angular Correlation Measurements at the 719 keV Resonance	134
	6. The 809 keV Resonance	137
	6.1 Decay Scheme of the 809 keV Resonance	137
	6.2 Decay Scheme of the 4.41 MeV Level	138
	6.3 Angular Correlation Measurements at the 809 keV Resonance	139
	7. The 839 keV Resonance	143
	8. The 954 keV Resonance	145
	8.1 Decay Scheme of the 954 keV Resonance	145

Page

8.2 Angular Correlation Measurements at the 954 keV Resonance 151
9. The 982 keV Resonance 154
10. Branching Ratios of Bound States 157
11. Spins 162
12 Discussion 163

REFERENCES 167

APPENDIX COMPUTER PROGRAMS 173

CHAPTER I

GENERAL INTRODUCTION

A major portion of research in nuclear physics is directed toward systematic identification of the position and properties of energy levels in various light nuclei.

With the existence of a level established, the parameters appropriate to an energy level which can be obtained experimentally are the excitation energy of the level, the transition probability or lifetime, the partial lifetimes or widths for decay via the various energetically possible channels, the total angular momentum or spin, the parity and whenever applicable, the isobaric spin quantum number. Two other ground state level parameters may sometimes be obtained for excited states. These are the magnetic dipole moment and the electric quadrupole moment.

Gamma-ray spectra constitute an essential part of the data required for the derivation of nuclear level schemes. The information obtainable from observations of γ-ray transitions can be classified into three categories:

1. The transition energies of γ-rays determine the energy differences between levels.

2. The geometrical properties of a γ-ray, i.e., the angular distribution of its intensity and polarization determine the multipole character of the radiation and the spin and parity of the levels involved.

3. Gamma-ray branching ratios of bound states and the multipole admixtures of the cascade members provide sensitive tests of predictions based on various nuclear models.

Gamma-ray spectroscopy lacked the precision possible with various methods of particle spectroscopy for many years and was handicapped by the fact that the energy response of detectors is much more complicated than those of charged particle detectors. Furthermore, particle capture reactions, which are potentially the most valuable means of exploiting gamma-ray spectrocopy, are weaker by several orders of magnitude than reactions which proceed by way of particle emission.

Scintillation methods of γ-ray detection with NaI(Tl) crystals, which provided high counting efficiency and moderate resolution to resolve γ-ray energies, greatly extended experimental possibilities especially with regard to γ-γ coincidence measurements. The recent advent of

Ge(Li) detectors has been a major advance in γ-ray spectroscopy; the high resolution and moderate counting efficiency of the detector enabling γ-ray spectroscopy to be more accurate in many respects than magnetic particle analysis. The high resolution and the corresponding accuracy with which gamma-ray energies may be determined has allowed identification of γ-rays in complex singles spectra with more confidence. Thus pre-measurements of γ-ray spectra with a Ge(Li) detector have become an essential prerequisite to guide in the selection of cascade gamma-rays for γ-γ coincidence correlation measurements with NaI(Tl) detectors.

It is the purpose of this thesis to study the de-excitation process of several capture reactions with NaI(Tl) and Ge(Li) detectors. Studies of $^{13}C(p,\gamma)^{14}N$ and $^{14}N(p,\gamma)^{15}O$ reactions were made using 5" x 4" NaI(Tl) detectors. Accordingly, the analysis of γ-ray scintillation spectra using the method of least squares line shape fitting is described in Chapter II.

Chapter III describes angular distribution measurements of γ-rays de-exciting from a weakly excited state in ^{14}N. The spin and parity of the level were uniquely determined.

Chapter IV describes the measurements of excitation functions of γ-rays from the reaction $^{14}N(p,\gamma)^{15}O$ in the

proton energy range of 1.7 to 3.0 MeV. This reaction is of particular astrophysical importance because its reaction rate at stellar proton energies determines the abundance of ^{14}N in equilibrium in burning stars. The possible effect of resonances at higher proton energies on the cross section at stellar energies is examined.

Chapter V describes the properties of a large volume Ge(Li) detector available in this department and the analysis of γ-ray complex spectra obtained with the detector. Though the method of line shape analysis is similar to that used in the analysis of scintillation detector spectra, it was considered desirable to separate the discussion from Chapter II since many of the techniques appropriate to its use and analysis of data from the detector had to be developed.

In Chapter VI the application of the Ge(Li) detector to the study of $^{26}Mg(p,\gamma)^{27}Al$ resonances, in which the decay schemes of resonance levels at 662, 719, 809, 839, 954 and 982 keV were deduced, is described. Angular distribution measurements at 719, 809 and 954 keV resonances have established the spins of a number of excited states.

CHAPTER II

ANALYSIS OF GAMMA-RAY SCINTILLATION SPECTRA

1. Introduction

The analysis of complex γ-ray spectra is complicated by the interaction of γ-rays with the detecting crystal through three different processes, namely, the photoelectric effect, the Compton effect and pair production, which are energy dependent and by the pulse distributions due to these processes which further depend on the crystal dimensions, detector geometry and the angular distribution of the γ-rays. The response function, which is defined as the set of pulse height distributions due to different processes as a function of γ-ray energy, must be known for all γ-rays which exist in the complex spectra before any analysis can be made. Since it is impractical and almost impossible to provide all response functions which have the energies required in the spectra to be analyzed, they were obtained by interpolation procedures.

In the analysis of a complex γ-ray spectrum, the method was the following:

(1) establish the gain (energy/channel) and zero intercept of the spectrum to be analyzed

(2) subtract the room background

(3) identify the energies of all γ-ray components in the spectrum

(4) for each γ-ray component, generate the line shape by interpolation

(5) determine the intensity of each γ-ray component by the method of least squares

(6) correct each intensity by the detector efficiency appropriate to the γ-ray energy.

The method described above was used in the analysis of γ-ray spectra obtained from the reactions $^{13}C(p,\gamma)^{14}N$ and $^{14}N(p,\gamma)^{15}O$. Since 5" x 4" NaI(Tl) crystals were used for measurements of both reactions to detect γ-rays emitted as the result of proton bombardment, the spectrometer assemblies were similar and the techniques involved in the analysis of data were not very different, they are summarized in one chapter.

2. Interaction of gamma-rays with matter

The mechanisms of γ-ray interaction with matter are briefly discussed here, since an understanding of them is important for γ-ray spectroscopy.

Gamma-rays interact with matter by one of the three processes: the photoelectric effect, the Compton effect and pair production.

In the photoelectric process, the γ-ray is absorbed by a bound electron in atom with the result that the electron is ejected from the atom with an energy equal to the incident γ-ray energy less the binding energy of the electron to the atom. The photoelectric absorption cross section in the K-shell is expressed by Heitler (HE 54) as

$$\sigma_{photo} \propto Z^5 E_\gamma^{-3.5} \quad \ldots\ldots (2.1)$$

where Z = atomic number,

E_γ = γ-ray energy.

Thus the photoelectric absorption increases very rapidly with atomic number and decreases very rapidly with γ-ray energy.

In the Compton effect, the γ-ray is inelastically scattered by a virtually free electron; the cross section is given by Klein and Nishima as

$$\sigma_{Compton} \propto Z E_\gamma^{-1} [\log(2E_\gamma/mC^2) + 1/2]^{-1} \quad \ldots\ldots (2.2)$$

where m = electron mass,

C = light velocity.

Thus the Compton cross section increases linearly with Z and decreases approximately linearly with γ-ray energy. The energy of the scattered electron ranges from zero to a

maximum value Ec corresponding to γ-rays being scattered through 180^{o}. Ec is calculated from equation (2.3).

$$Ec = E_{\gamma}/(1 + mC^2/2E_{\gamma}) \quad \ldots\ldots (2.3)$$

The scattered photon may escape from the absorbing material or may be further absorbed.

In pair production, a γ-ray with energy greater than 1.022 MeV ($2mC^2$), the threshold energy for this process, can lose its energy by creating an electron-positron pair in the field of a nucleus. Any γ-ray energy in excess of 1.022 MeV appears as kinetic energy of the outgoing pair. The pair production cross section is expressed by Heitler (He 54) as

$$\sigma_{pair} \propto Z^2[\log(2E_{\gamma}/mC^2) - 218/27] \quad \ldots\ldots (2.4)$$

Thus the pair production cross-section increases rather rapidly with atomic number and γ-ray energy. Associated with pair production is the subsequent creation of two 511 keV photons from the annihilation of positrons when they come to rest in matter.

3. Response of NaI(Tl) crystal to gamma-rays

When γ-rays interact with a NaI(Tl) crystal, the photon energy is absorbed in the crystal through the three principal processes described previously. The result of the interaction is the transfer of photon energy partially or completely to electrons or electrons and positrons

depending on the absorption processes which occur. The electrons or positrons in turn produce scintillations in passing through the phosphor; the total light output is proportional to the electron energy and is independent of the processes by which the γ-ray energy is absorbed. The electron energy is in fact transferred back to photons of an energy detectable by a photomultiplier coupled to the phosphor. To conclude, one photon of energy E_γ is transformed into a light pulse of approximately constant wave length but with an intensity directly proportional to the energy deposited in the crystal.

From this complex process, the resultant pulse distribution (or γ-ray line shape) is not only a function of photon energy and crystal dimensions, but also depends on the impinging direction of the γ-ray and the position at which it interacts with the crystal. Thus detector geometry and the γ-ray angular distribution affect the γ-ray line shape.

When a γ-ray impinges on the center of a crystal, the probability of all of the photon energy being absorbed in the crystal is much higher than when it impinges on the edge of the crystal. This is because in the former case, the likelihood of the scattered γ-rays and annihilation γ-rays escaping from the crystal is reduced. The same

result is obtained if a large crystal is used. Edge effects become important when the γ-ray distribution is very anisotropic or when a small detector is used.

For a given experimental arrangement, the γ-ray line shape is mainly determined by photon energy. The γ-ray line shape of NaI(Tl) crystals is discussed below according to the photon energy is greater or smaller than the pair production threshold energy.

When the γ-ray energy is below 1.022 MeV, only the photoelectric and Compton scattering processes can take place. Absorption by the photoelectric process produces a well defined peak of approximately Gaussian distribution corresponding to the incident γ-ray energy due to the absorption of the photoelectron and the iodine K X-ray. Though the X-ray of energy 28 keV may escape from the crystal, the effect is negligible when γ-ray energy is above 250 keV, since the γ-ray penetrates more deeply before most of its energy is absorbed. The Compton scattering shares the incident γ-ray energy between an electron and a scattered photon which may escape from the crystal or may further interact to deposit some or all of its energy in the detector. The pulse distribution which results is a continuum extending from just below the photopeak to zero energy. The Compton edge appears at energy Ec of equation (2.3).

Not all Compton interactions contribute to the Compton distribution, a complete secondary absorption of scattered quanta will lead to light yields equal to that from the direct photoelectric effect. This is true for all cases, namely, if a γ-ray is completely absorbed by any combination of the three processes the resultant pulse will appear in the photopeak, for this reason the photopeak is often referred to as the full energy peak.

For γ-ray energies above 1.022 MeV, production of a positron and electron pair is possible, though in NaI(Tl) crystal this process does not become significant until the photon energy is above about 2.5 MeV. The γ-ray energy in excess of 1.022 MeV appears as kinetic energy shared between electron and positron. The higher energies of the electrons and positrons make the bremsstrahlung losses more significant than in the other two processes which dominate at low photon energies; however, the kinetic energy of the electron-positron pair can be nearly completely absorbed in the crystal, though there is a chance for the bremsstrahlung to escape from the crystal and to contribute a 'tail' in the spectrum.

When the positron comes to rest in the crystal, annihilation with a nearby electron produces two photons of 511 keV γ-ray which may escape from the crystal.

Assuming total absorption of electron and positron energy, peaks appear in the pulse distribution depending on whether both photons are detected in the crystal (full energy), only one is detected (single escape) or both escape from the crystal (double escape).

From the foregoing discussion it follows that the response of NaI(Tl) crystal to a monochromatic γ-ray is to produce a complicated pulse height distribution which is mainly determined by the incident γ-ray energy and the experimental arrangement. To analyze a complex spectrum obtained from the simultaneous detection of several monochromatic γ-rays, the individual γ-ray line shapes or the response function must be known.

4. Measurement of standard gamma-ray line shapes

In principle, the response function of a NaI(Tl) crystal to γ-rays can be calculated by Monte Carlo methods though the procedure is tedious and time consuming. The advantage of experimentally measuring the standard γ-ray line shapes is that the standards can be measured under the conditions which are identical to those under which the collection of the γ-ray spectra are performed.

In choosing sets of standard γ-ray line shapes, the energy range of the γ-rays was chosen according to the γ-ray components in the spectra to be analyzed which

during the present work extended over the energy range of 2.5 to 10.0 MeV. To span this range, five line shapes corresponding to γ-ray energies of 2.367, 4.433, 6.129, 8.060 and 10.540 MeV were measured. Table 2.1 summarizes the reactions and bombarding energies used to obtain the γ-rays. The reactions were chosen on the basis that they provided reasonable γ-ray yields of relatively monochromatic γ-rays with energies dividing the energy range of interest into roughly equal intervals and that the targets were simple and available.

Table 2.1

Reactions used in the measurement of standard γ-ray line shape

E (Mev)	Reaction	Ep (keV)
2.367	$^{12}C(p,\gamma)^{13}N$	459
4.433	$^{15}N(p,\alpha\gamma)^{12}C$	429
6.129	$^{19}F(p,\alpha\gamma)^{16}O$	597
8.060	$^{13}C(p,\gamma)^{14}N$	554
10.540	$^{27}Al(p,\gamma)^{28}Si$	759 (BA 61)

To generate a standard γ-ray line shape from the γ-ray spectrum collected from a nuclear reaction, the room background was subtracted and an estimate of the

continuum made for the low energy portion of the spectrum. The 'tail' was assumed to be flat to the zero channel. This approximation was necessary because of low energy γ-rays existing in the spectra. Figure 2.1 shows the 8.060 MeV γ-ray line shape as measured from the reaction $^{13}C(p,\gamma)^{14}N$ at the Ep = 554 keV resonance. The solid line shows the tail. This raw line shape was then divided into a number of intervals and a function fit was used to fit the line shape of each interval. The original line shape was then re-generated from the function, thereby eliminating any statistical fluctuations in the line shape. Due to the initial estimate of the continuum the five line shapes so obtained were not exact. In order to refine the result, least squares fitting to the measured spectra was used to estimate the intensities of low energy γ-rays superposed on the continuum. The low energy γ-ray line shapes were obtained by interpolation between the raw line shapes. The low energy γ-rays were subtracted from the measured spectra to obtain a flat region representing the true continuum. Figure 2.2 shows the flat region as obtained from the method of least squares fit. It can be seen that the first approximation of the continuum was too high.

Figure 2.1

The 8.06 MeV γ-ray line shape as measured from the reaction $^{13}C(p,\gamma)^{14}N$ at Ep = 554 keV resonance. The solid line shows the first approximation to the tail.

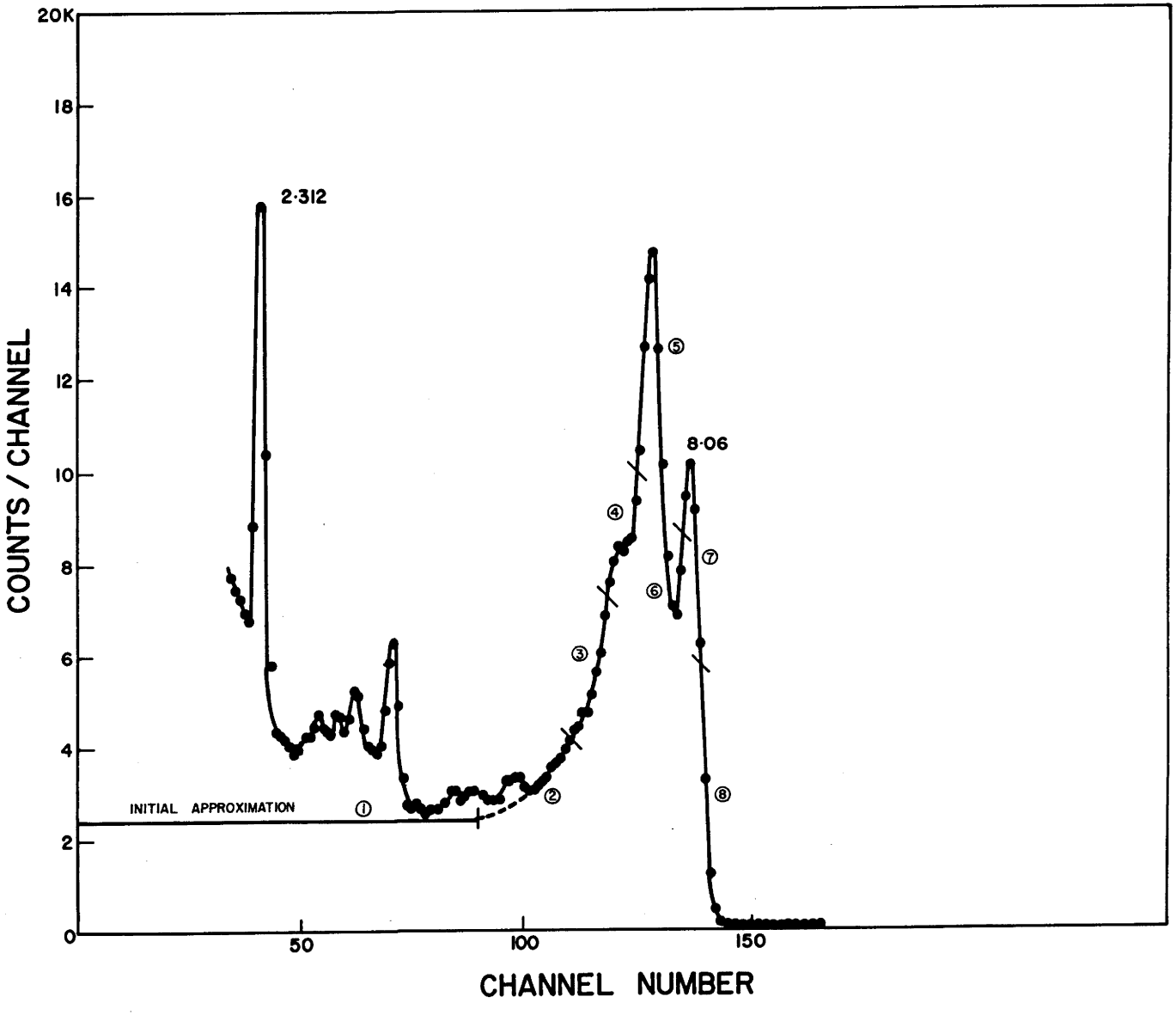
20K
18
16
14
12
10
8
6
4
2
0
COUNTS / CHANNEL
2·312
8·06
INITIAL APPROXIMATION
①
②
③
④
⑤
⑥
⑦
⑧
50
100
150
CHANNEL NUMBER

Figure 2.2

The 8.06 MeV γ-ray line shape with the tail estimated from the subtraction of low energy γ-rays, the intensities of which were obtained from least squares analysis. The solid line shows the first approximation to the tail.

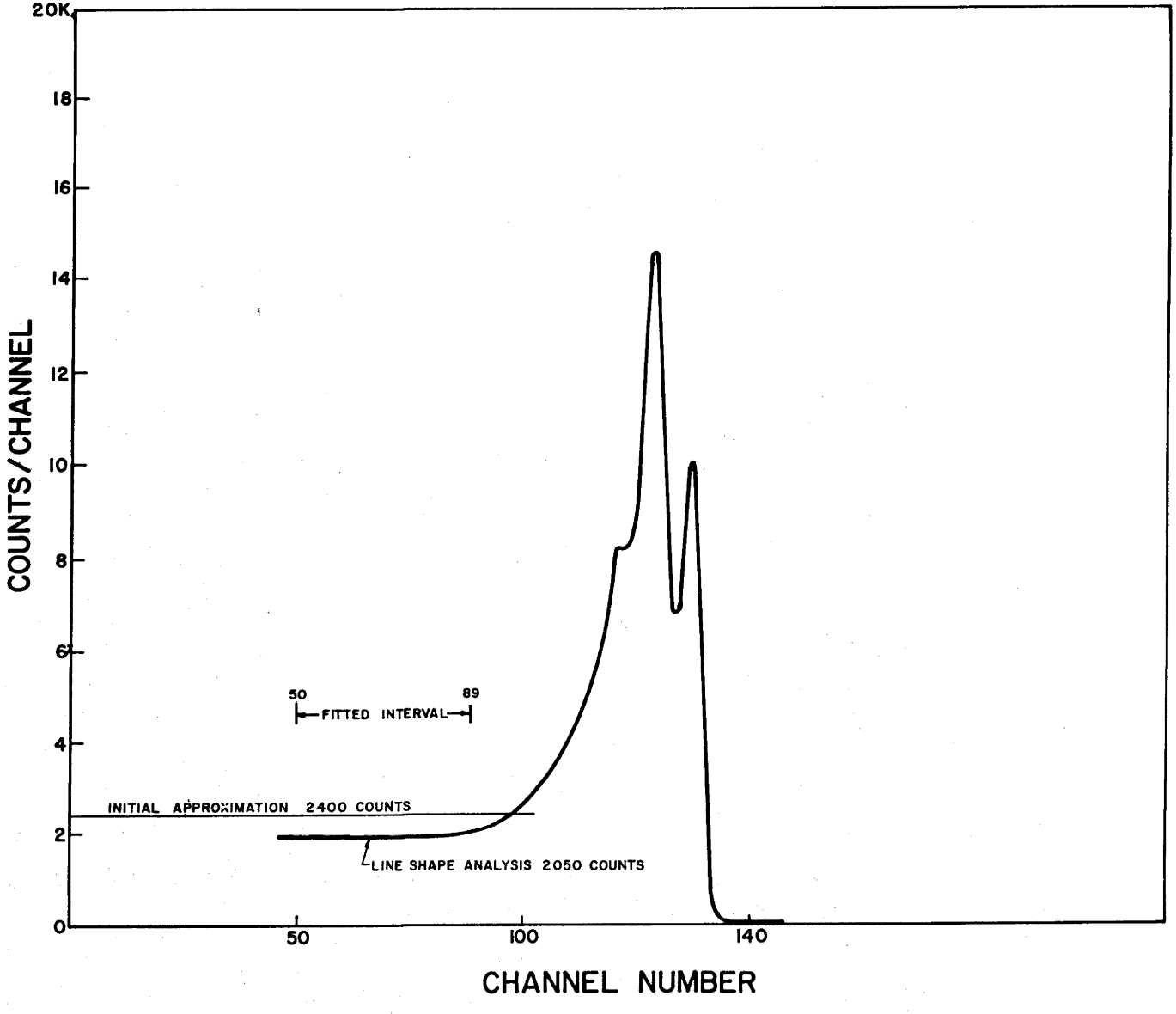
20K
18
16
14
12
10
8
6
4
2
0
COUNTS/CHANNEL
50
89
FITTED INTERVAL
INITIAL APPROXIMATION 2400 COUNTS
LINE SHAPE ANALYSIS 2050 COUNTS
50
100
140
CHANNEL NUMBER

Figure 2.3

The standard γ-ray line shapes of energy 2.367, 4.433, 6.129, 8.060 and 10.540 MeV with each line shape normalized to have an integrated intensity of 500,000 counts.

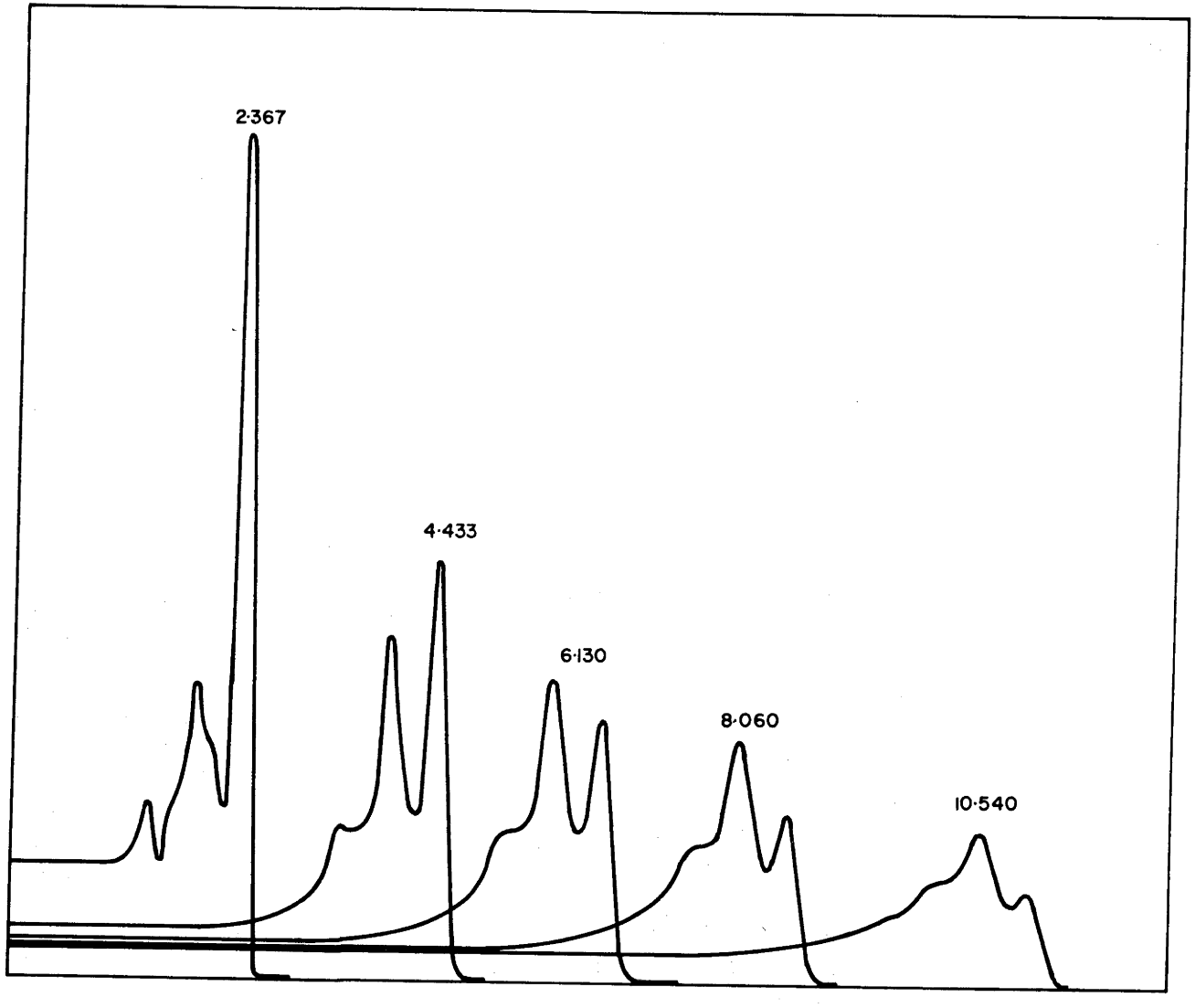
2·367
4·433
6·130
8·060
10·540

Similar procedures were used to generate the other standard γ-ray line shapes. Figure 2.3 shows the standard γ-ray line shapes with each line shape normalized to an integrated intensity of 500,000 counts. The variations of relative height of the full energy peak, single escape peak, double escape peak and Compton continuum according to γ-ray energy are evident.

5. Generation of line shapes of energies other than those measured

5.1 Function fits

Statistical scatter within the line shapes can be smoothed out by fitting an anlytic function to the γ-ray line shapes. A computer program called FUNFIT (see Appendix) was developed to generate a set of coefficients

$$A,\ B,\ B_1,\ B_2,\ \ldots\ldots,\ B_{15}$$

such that the analytic function

$$A + B(X - X_0) + \sum_{k=1}^{15} B_k \sin\left(\frac{k\pi}{X_1 - X_0}(X - X_0)\right)$$

is a fit to the spectrum in the range of channels X_0 to X_1 (interval of fit). The total spectrum was divided into a number of intervals and fitted interval by interval. In applying the function fit to a particular interval, the number of coefficients and the magnitude of the sum of the squares of residuals are specified. After

a set of coefficients has been generated, the program regenerates the original spectrum with original gain, zero and intensity from the analytic function. The fits to original data points were examined carefully and the number of coefficients for each interval readjusted until the original line shape was reproduced faithfully from the function. To obtain a smoothing effect, the number of coefficients should be less than the number of data points in that interval. The residuals (FIT - DATA) for each point were calculated in the program and the sum of the squares of residuals (σ_s^2) for each interval was calculated. This value was compared to the value which was specified before the fitting. An exact reproduction of original line shape ($\sigma_s^2 = 0$) will not attain the purpose of smoothing. The statistical nature of the data suggests the best value of σ_s^2 to be specified is of the order of the total counts of spectrum fitted in that interval. The program automatically increases the number of coefficients by one if the value of σ_s^2 is greater than the value specified and re-calculates a set of coefficients.

To obtain a smooth transition between neighbouring intervals, an interval of use is used to define a common boundary. The interval of use nests in the interval of

fit. The coefficients of the standard line shapes were all normalized in the program to have specific values for gain (50 keV/channel), zero (0 channel) and intensity (one). This has the advantage that each γ-ray line shape can be measured with different gains and zeros which could result from gain shifts in the system.

Ferguson (FE 62) used polynomials to fit γ-ray line shapes instead of the Fourier series as described above. Each spectrum was divided into four regions according to (a) full energy peak, (b) single escape peak, (c) double escape peak and (d) Compton distributions. This is different from the method described here where as many intervals as are required can be used allowing the function to converge to the original shape much faster within a small interval with only a few coefficients. A large interval needs more coefficients to represent the line shape, a ninth degree polynomial was used by Ferguson to represent each of the four regions defined above. Since each polynomial has ten coefficients, a total of 40 coefficients represents the entire spectrum. Because of the high degree of polynomial used, the polynomial approximations generally rapidly diverge to $\pm \infty$ beyond the range of approximation. To eliminate this rapid fluctuation a variable ξ, given by

$$\xi = 1 - \frac{2}{\frac{E_\gamma}{E_0} + 1}$$

was introduced to represent each of the 40 coefficients. E_γ is the γ-ray energy of the line shape and E_0 is an arbitrary energy chosen near the middle of the range of energies to be represented. The 40 coefficients are now represented by polynomials in ξ. The degree of the polynomial to represent the ξ variation is determined by the number of standard line shapes used, for five sets of standard line shapes the degree is four, i.e., five constants. So for five sets of standard line shapes, a total of 200 coefficients are required by Ferguson.

Fourier series use sine functions to represent γ-ray line shapes so that there is no exponentiation of high power which could introduce truncation errors in computer calculations due to the large numbers encountered. The function generated in this way can be used successfully for interpolation as well as for extrapolation.

Another method of line shape fitting has been described by Heath et al. (HE 67), in which a 'modified Gaussian' function of the form

$$y(x)=y_0\left[1+\alpha_1(x-x_0)^4+\alpha_2(x-x_0)^{12}\right] \exp\left\{-(x-x_0)^2/b_0\right\} \quad .. \quad (2.5)$$

was used to fit the photopeak shapes, while the low energy part of line shape was fitted with a Fourier series similar to the method used in this experiment. For each photopeak, five parameters i.e., x_0, y_0, b_0, α_1 and α_2 are required to determine the peak shape. In equation (2.5), y is the calculated count at channel x, x_0 and y_0 is the channel number and counts at the center of the peak, b_0 is related to the full width at half maximum of the peak, α_1 and α_2 are represented by polynomials of the form

$$\log \alpha = a_0+a_1(\log x_0)+a_2(\log x_0)^2+a_3(\log x_0)^3 \quad \ldots \quad (2.6)$$

The complications introduced by equations (2.5) and (2.6) have not much physical meaning in themselves, the method used in this experiment seems to include the advantages of Ferguson and Heath and retain its simplicity.

5.2 Methods of Interpolation

After five standard line shapes were obtained to comprise the response function, the line shape appropriate to a γ-ray of intermediate energy can be generated by interpolation. The coefficients of each γ-ray line shape was first normalized to the gain and zero of the experimental spectrum to be analyzed and the actual γ-ray line shapes of each standard were reproduced from the function.

To obtain a point in the interpolated spectrum there is a maximum of five points to be used in interpolation. The polynomial interpolation described by Ferguson would use all five points to determine the value of ξ, so for every interpolated γ-ray line shape, 5 x 40 polynomial constants were calculated. The line shape of required energy was then reproduced from these coefficients. Heath (HE 66) varied the number of points used in the interpolation so as to obtain best fit to the data points. Since the shapes of the various prominent features such as photopeak, Compton shoulder and pair peaks vary very rapidly with energy, only γ-ray line shapes of nearest energy should be used for interpolation. Two points and three points have been used to analyze the present data.

The actual interpolation was carried out channel by channel using Lagrange's interpolation formula (WH 44). If y is the number of counts of a point in the interpolated spectrum of energy E_γ, and three points y_1, y_2 and y_3 corresponding to the counts of three standard γ-rays of energies $E_{\gamma 1}$, $E_{\gamma 2}$ and $E_{\gamma 3}$, then y is expressed as

$$y=\frac{(E_\gamma-E_{\gamma 2})(E_\gamma-E_{\gamma 3})y_1}{(E_{\gamma 1}-E_{\gamma 2})(E_{\gamma 1}-E_{\gamma 3})}+\frac{(E_\gamma-E_{\gamma 1})(E_\gamma-E_{\gamma 3})y_2}{(E_{\gamma 2}-E_{\gamma 1})(E_{\gamma 2}-E_{\gamma 3})}+\frac{(E_\gamma-E_{\gamma 1})(E_\gamma-E_{\gamma 2})y_3}{(E_{\gamma 3}-E_{\gamma 1})(E_{\gamma 3}-E_{\gamma 2})}$$

The interpolation of γ-ray line shapes from an analytic function has the advantage that the gain and zero

Figure 2.4

The standard γ-ray line shapes of energy 2.367, 4.433, 6.129, 8.060 and 10.540 MeV with the full energy peaks of each γ-ray line shape aligned and normalized to the same height.

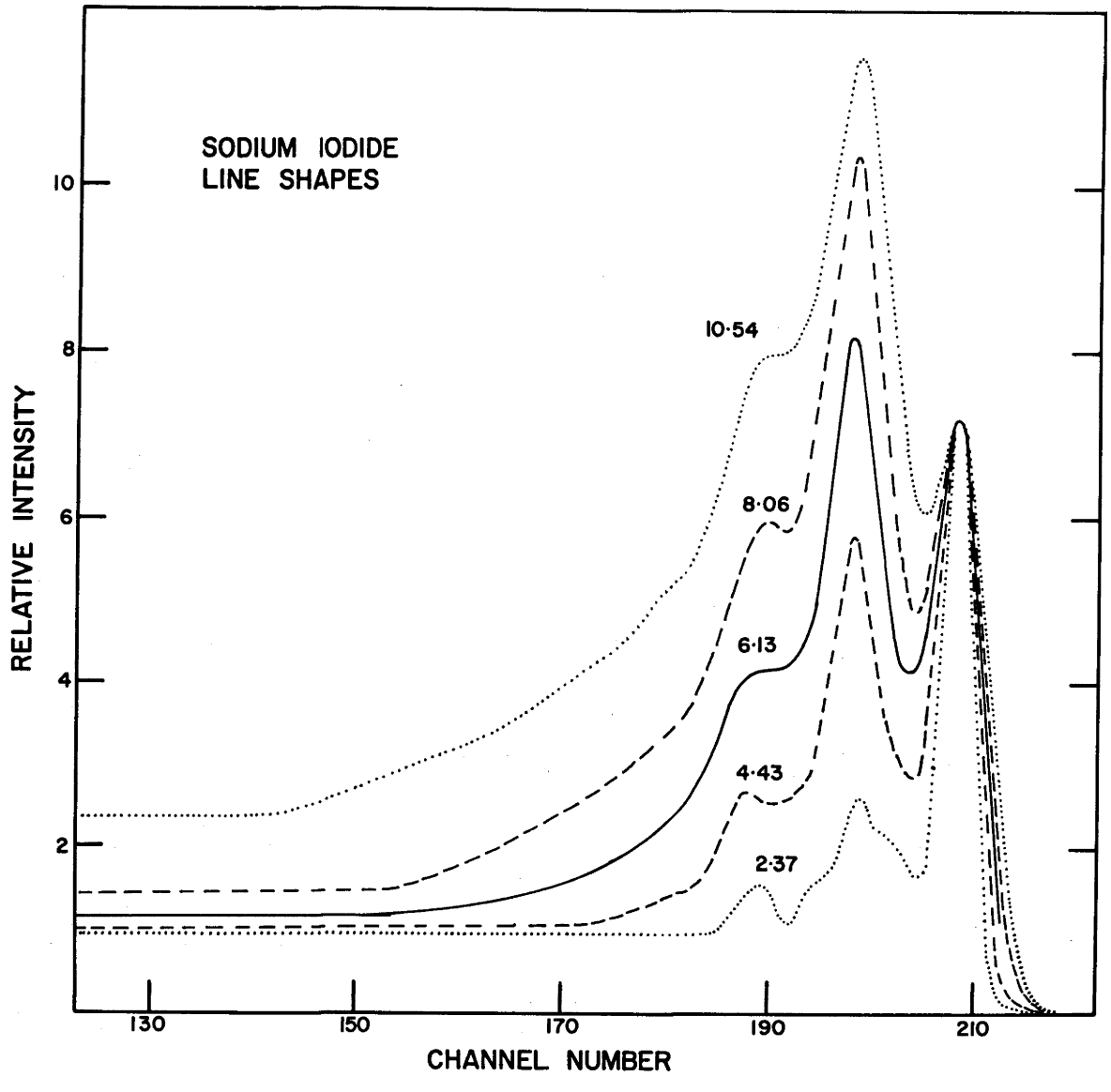
SODIUM IODIDE
LINE SHAPES
10·54
8·06
6·13
4·43
2·37
RELATIVE INTENSITY
10
8
6
4
2
130
150
170
190
210
CHANNEL NUMBER

of interpolated spectrum can be easily adjusted to the experimental spectrum by re-calculating the coefficients. However, this method is subject to hidden errors due to insufficient representation of line shape by analytic functions. To avoid this, interpolation of γ-ray line shape of intermediate energy can be carried out from the smoothed standard line shapes. To achieve this, the full energy peaks of each γ-ray line shape were aligned and normalized to the same height as shown in Figure 2.4. The interpolated spectrum was then re-adjusted to the required gain and zero of the experimental spectrum. Two subroutines called PUSH and PULL were developed to compress or expand the interpolated spectrum if the gain of the experimental spectrum was greater or smaller than the gain of the standard line shapes.

6. Coincidence sum spectrum

The coincidence sum spectrum discussed here is different from random coincidences due to uncorrelated radiations which are detected within the resolving time of detection system. Due to the low yields of γ-rays emitted from the reactions studied random summing was small and not considered in the analysis.

The summing effect, due to true coincidences between two cascading radiations, results in a pulse distribution

from the minimum detectable height to the sum of the maximum pulse height obtainable from the individual γ-rays. The most prominent feature of the spectrum is that it contains sum peaks which result from coincident detection of pulses from full energy peaks and pair peaks of the two coincident γ-rays. The sum spectrum was calculated in the subroutine called SUMSPE. The pulse height spectra for the two coincident γ-rays $G_1(x)$ and $G_2(x)$ were first generated from the interpolation between the standard γ-ray line shapes. Let the probability of simultaneously detecting gamma 1 in channel x_1 and gamma 2 in channel x_2 be the product $G_1(x_1)G_2(x_2)$ which is the probability of producing a pulse in the sum spectrum in channel (x_1+x_2). The total contribution to any channel x of the sum spectrum is equal to the sum of contributions from all pairs of channels for which $x_1+x_2=x$. This is expressed as

$$S(x) = \sum_{n=1}^{x} G_1(x_1)G_2(x - x_1)$$

In principle the summation due to three or four γ-rays in cascade could be calculated. These were actually not considered in the analysis due to low detection efficiencies of the experimental set up. The effect of γ-ray angular distribution was not taken into account in generating the coincidence sum spectrum in the present work.

7. Method of least squares analysis

If the number of γ-ray components present in the spectrum to be analyzed and their energies are known, the least squares method of analysis can be programmed for computer analysis to obtain their intensities. These requirements are not as restrictive as it might seem to be since the result of first estimates may be observed and the second estimates with corrections in these specifications were made until a good fit to the data is obtained. This method was used by Ferguson (FE 62) and Helmer et al. (HE 67a) and proved to be more satisfactory than graphical techniques.

If a_{ij} is the counts in channel i of the j th component which has an intensity of X_j and if there are m components contributing to channel i to make a total counts of b_i in the experimental spectrum, then

$$b_i = \sum_{j=1}^{m} a_{ij} X_j + z_i \qquad \ldots\ldots (2.7)$$

where z_i is the random error.

If there are n data points ($n \geq m$), the best value of X_j are obtained by minimizing R, the sum of the squares of z_i.

$$R = \sum_{i=1}^{n} w_i z_i^2 = \sum_{i=1}^{n} w_i \left[b_i - \sum_{j=1}^{m} a_{ij} X_j \right]^2 \qquad \ldots\ldots (2.8)$$

where w_i is the weighting factor.

R is minimized by differentiating equation (2.8) partially with respect to X_j and equating to zero. A set of m linear simultaneous equations are obtained and may be solved to obtain values for X_j's.

$$\sum_{j=1}^{m} x_j \sum_{i=1}^{n} w_i a_{ik} a_{ij} = \sum_{i=1}^{n} w_i a_{ik} b_i \quad (k=1,2,3,\ldots,m) \quad .. \quad (2.9)$$

The solution of the normal equations is most conveniently done by matrix techniques, which have the advantage that the mean square deviation of each X_j is equal to the jj th diagonal element of the inverse matrix. If equations (2.9) are written in matrix form

$$CX = Y$$

then the solution is $X = C^{-1}Y$.

The inverse matrix C^{-1} is calculated in a subroutine called MATINV.

Since each data point has statistical distribution, each value of X_j calculated is also accompanied by statistical variation, the mean square deviation for j th component is expressed by Rose (RO 53) as (assuming $w_i = \frac{1}{\sigma_i^2}$)

$$\sigma^2(X_j) = C_{jj}^{-1} \qquad \ldots\ldots \quad (2.10)$$

where C_{jj}^{-1} is the jj th diagonal matrix element of the inverse matrix C^{-1}. This is a measure of the deviation of X_j to be expected on purely statistical bases. Other

sources of error due to experiment and line shapes may actually occur. The test of the fit is expressed as chi-square, and is defined as

$$\chi^2 = \sum_{i=1}^{n} w_i (FIT_i - b_i)^2 \qquad \ldots\ldots (2.11)$$

where $FIT_i = \sum_{j=1}^{m} a_{ij} X_j$

The value of χ^2 should be of the order of n - m, number of degrees of freedom, for an ideal fit. A value of $\chi^2/(n - m)$ appreciably greater than unity implies that errors other than those due to statistics have been introduced into the system. Wrong energy assignments and an insufficient number of components used in the fit will also increase the value of χ^2. The mean error in X_j has been given by Rose as

$$(X_j) = \sqrt{\frac{\chi^2}{(n - m)} C_{jj}^{-1}} \qquad \ldots\ldots (2.12)$$

The mean error includes all sources of error and not just the statistical errors.

The weight w_i for each data point is governed by the equation (2.11) which shows weight is inversely proportional to σ^2. If the normalization constant is ignored, w_i is expressed as

$$w_i = \frac{1}{\sigma_i^2(b_i)}$$

Since the values of $\sigma_i^2(b_i)$ for each data point will not be known until an actual least squares fit is performed and the residuals calculated for every point; as a first approximation unit weight to every data point could be used and iterative procedures used to correct weights by the value obtained from previous fit until a required precision has been obtained. This elaborate procedure of analysis, however, was not attempted in this work. The reason is that the value of χ^2 which is based on equation (2.11) does not necessarily mean a good fit when it is minimized by iterative procedures; on the other hand a plot of data and fit after first approximation shows the direction to improve the fit. The Poisson distributions of data points which are true for nuclear disintegration events suggest for the weight the inverse of data as the first approximation, since the standard deviation is equal to the square root of the total counts accumulated in that channel. Ferguson used an inverse of fit as weight, since fit is not available before least squares analysis is performed an iterative program was used for the analysis. In the present work, weight equal to unity and inverse of data for each data point were both used in the analysis.

Figure Captions

Figure 2.1 The 8.06 MeV γ-ray line shape as measured from the reaction $^{13}C(p,\tilde{\gamma})^{14}N$ at Ep = 554 keV resonance. The solid line shows the first approximation to the tail.

Figure 2.2 The 8.06 MeV γ-ray line shape with the tail estimated from the subtraction of low energy γ-rays, the intensities of which were obtained from least squares analysis. The solid line shows the first approximation to the tail.

Figure 2.3 The standard γ-ray line shapes of energy 2.367, 4.433, 6.129, 8.060 and 10.540 MeV with each line shape normalized to have an integrated intensity of 500,000 counts.

Figure 2.4 The standard γ-ray line shapes of energy 2.367, 4.433, 6.129, 8.060 and 10.540 MeV with the full energy peaks of each γ-ray line shape aligned and normalized to the same height.

CHAPTER III

THE 8.49 MeV STATE OF ^{14}N

1. Introduction

In a recent report (EA 64) on the $^{14}N(p,p')$ reaction, a low energy particle group was observed but its properties were not well determined. If the group was assumed to be inelastic protons from ^{14}N, then an excitation energy in ^{14}N of 8.57 $\pm$ 0.05 MeV, intermediate between a known level (AJ 59) at 8.63 MeV and the state reported by Miller et al. (MI 56) at 8.45 $\pm$ 0.07 MeV, was indicated. No check on the type of particle or on the mass of residual nucleus was made since the particle group was only observed at low energies and a forward angle.

Later measurements at higher incident proton energies have shown that the observed particle group was actually two overlapping groups of comparable intensity. One of these was from the $^{14}N(p,d)$ reaction to the ^{13}N ground state while the other was from the $^{14}N(p,p')$ reaction to a ^{14}N state estimated to be at 8.52 $\pm$ 0.05 MeV. The identification was made by varying the gas pressure, by interposition of foils and by kinematic checks for the mass of the target nucleus (HE 64).

The state in ^{14}N at 8.52 $\pm$ 0.05 MeV is certainly the same state as the one seen at 8.45 $\pm$ 0.07 MeV by Miller et al. (MI 56). Comparisons with the more precise determination of 8.49 MeV by Armstrong et al. (AR 61, DE 65), using the $^{13}C(p,\gamma)^{14}N$ reaction, show good agreement for both the $^{14}N(p,p')$ and the $^{14}N(\alpha,\alpha')$ reactions (EA 64, MI 56). For the remainder of this chapter, the state will be referred to as the 8.49 MeV state. Observation of inelastic α-particle scattering to the 8.49 MeV state establishes its T = 0 character.

Following the arousal of interest in 8.49 MeV state, an attempt was made to determine the spin and parity of the state by angular distribution and yield measurements of the $^{13}C(p,\gamma)$ reaction in the vicinity of 1012 keV resonance. Meanwhile, Detenbeck et al. (DE 65) measured and published yields and angular distributions of gamma-rays from several small resonances in the $^{13}C(p,\gamma)$ reaction. However, recent correspondence (DE 67) has disclosed an unsatisfactory feature of the angular distribution measurements of these workers.

Because of problems with target uniformity and stability, Detenbeck et al. used a multiple detector array with several runs at interlaced angles. The extracted γ-ray intensities were used as input data for an analysis of the angular distribution curve, with the

Legendre polynomial coefficients and the relative normalizations for the individual runs being adjusted to achieve a least squares fit. In the extraction of the γ-ray intensities, large corrections were needed (DE 67) for γ-ray attenuation in the target and the target chamber. These corrections were uncertain (DE 67) because the attenuator angular structure was smaller than the detector aperture and because the corrections were based on the attenuation of an isotropic distribution in a situation of good geometry.

The corrections, if large, cannot be evaluated satisfactorily unless the angular distribution is known or assumed beforehand. In addition, the different detectors in the multi-detector array were not all at the same distance (DE 67) from the target making it difficult to apply accurately the correction to the angular distribution coefficients needed to allow for the finite size of the detectors. Detenbeck et al. chose not to apply this finite size correction but claim (DE 67) to absorb the uncertainty in the errors attached to the angular distribution coefficients.

This claim is unfounded, as can be demonstrated by an application of the correction appropriate to the approximate detector geometry described (DE 65). The corrections so obtained are increases of 8%, 27% and 70%

respectively for the P_2, P_4 and P_6 coefficients. If one allows for a $\pm$ 25% uncertainty in estimating the magnitude of these increases, then the corrected experimental angular distribution of Table 2, ref. (DE 65) would become

$W(\theta)=1+(0.59\pm0.06)P_2(\cos\theta)-(0.61\pm0.08)P_4(\cos\theta)+(0.12\pm0.12)P_6(\cos\theta)$.

This is to be compared with the published uncorrected distribution.

$W(\theta)=1+(0.55\pm0.05)P_2(\cos\theta)-(0.48\pm0.06)P_4(\cos\theta)+(0.07\pm0.07)P_6(\cos\theta)$.

It will be noted that the change in the magnitude of the $P_4(\cos\theta)$ coefficient is large compared with the assigned error and that the magnitude of the $P_2(\cos\theta)$ coefficient is also changed significantly.

The extra smearing caused by the γ-ray attenuation is to be combined with the effect already calculated. As a result of the correction not made, the comparisons of the theoretical and smeared experimental angular distributions in Table 2, ref. (DE 65) are meaningless. Table 2 was calculated for those J^{π} assignments considered possible on the basis of intensity and branching ratio measurements of the three J^{π} assignments in this Table, the 3^+ assignment is the only one still able to match the revised experimental angular

distribution coefficients. This assignment is discarded because it would require approximately equal E3 and E1 intensities and therefore a very large E3 enhancement ($\approx 10^5$), as already discussed (DE 65). The best fit for a 4^- assignment is still the distribution for pure channel spin 0 given by Detenbeck et al.

$$W(\theta) = 1 + 0.51P_2(\cos\theta) - 0.37\ P_4(\cos\theta)$$

The assignment of the quoted theoretical distribution in Table 2, ref. (DE 65), for pure channel spin 1 formation of a 4^- state is in error. It is actually the distribution for pure channel spin 0.

The differences of the theoretical $P_2(\cos\theta)$ and $P_4(\cos\theta)$ coefficients from the revised experimental values are now 2 and 3 times the quoted errors respectively. The disagreement of the revised experimental coefficients with the best fit for a 2^- assignment is similar.

Detenbeck et al. originally rejected a 2^- assignment for the 8.49 MeV state on the basis of the required inhibitions for several E1 and M1 transitions to lower lying levels. The transitions involved are between T = 0 levels in a self-conjugate nucleus and hence are expected (WI 60) to be inhibited. The assumed M1 radiations would have strengths of the order of 10^{-3}. Weisskopf units, which are typical values (WI 60) for inhibited M1

transitions. When the strengths of the assumed E1 transitions are compared with the histogram (WI 60) for inhibited E1 transitions, it is seen that two of the strengths can fall in the known range while two can fall just outside the known range of strengths. The latter strengths ($<10^{-5}$ Weisskopf units to the 3.95 MeV state and $<2 \times 10^{-6}$ Weisskopf units to the ground state) are out of the known range by factors of approximately 2 and 10 respectively. However, the known range of strengths has a wide distribution, covering 3 orders of magnitude. Furthermore, these two strengths are of a magnitude comparable with the strength (NE 65) of the known inhibited E1 transition between the 5.10 MeV state and ground state. Again, the two strengths in question are both larger than a known uninhibited E1 transition in a neighbouring nucleus (from the $\frac{1}{2}^+$ state at 7.55 MeV in ^{15}O to the $\frac{1}{2}^-$ ground state, having a strength of approximately 10^{-6} Weisskopf units). Therefore, contrary to the previous assertion (DE 65), a 2^- assignment cannot be ruled out on the basis of intensity measurements alone.

Recently, Gallmann et al. (GA 68) have populated the 8.49 MeV state of ^{14}N by means of the reaction $^{12}C(^3He,p)^{14}N$. The proton group to the 8.49 MeV state was detected near 180^o and the angular correlations of γ-rays in time coincidence were studied. Certain

numerical relationships must hold between the angular distribution coefficients measured in the $^{13}C(p,\gamma)$ reaction at 8.49 MeV state and the coefficients measured for the same transition when the populating reaction is $^{12}C(^{3}He,p)$ with the protons detected close to 180^{o}.

Defining the ratio:

R_2 = (coefficient of P_2 in $^{13}C(p,\gamma)$)/(coefficient of P_2 in $^{12}C(^{3}He,p\gamma)$)

and a similar ratio R_4; it follows that for a J^{π} assignment to the 8.49 MeV state:

$0.50 \leq R_2 \leq 1.00$ for $J^{\pi} = 2^{\pm}, 3^{\pm}, 4^{\pm}$

$0.50 \leq R_4 \leq 1.00$ for $J^{\pi} = 4^{\pm}$

$0.17 \leq R_4 \leq 3.00$ for $J^{\pi} = 3^{\pm}$

$-\infty \leq R_4 \leq \infty$ for $J^{\pi} = 2^{\pm}$

Gallmann et al., after a small correction for the finite size of their detector, find, for the 8.49 MeV to 5.10 MeV transition:

$W(\theta) = 1+(0.40\pm0.13)P_2(\cos\theta)-(0.17\pm0.17)P_4(\cos\theta)$

If this is compared with the revised coefficients of Detenbeck et al. (with zero $P_6(\cos\theta)$ coefficient), there is only 5% probability that the ratio R_2 is in the valid range and only a 2% probability that the R_4 ratio is in the valid range for a 4^- assignment. These probabilities reinforce one another, but to an uncertain extent because the correlations between the errors in the P_2 and P_4

coefficients for these experiments are not known. However, it is clear that either the 4^- assignment (DE 65) to the 8.49 MeV state is incorrect or else that at least one of the angular distributions that have just been compared is incorrect.

In conclusion, no satisfactory spin and parity assignment has yet been made for the 8.49 MeV state of ^{14}N.

2. Experimental procedure

The 1.2 MV Cockcroft-Walton accelerator at the Australian National University was used to accelerate protons for the study of the 1012 keV resonance in $^{13}C(p,\gamma)$. After passing through a 90^o magnetic analyzer, the beam incident on the target had approximately a 2 keV energy spread caused by the voltage ripple on the accelerator. The beam current was integrated in order to normalize the spectra taken at the different angles.

The target, approximately 6 keV thick for protons at the resonance energy, was one that had already been used extensively in low energy measurements (HE 60) of the $^{13}C(p,\gamma)$ cross section. It was made by cracking methyl iodide, enriched to 61% ^{13}C, onto a clean 0.5 m.m. thick tantalum disc, so that the carbon layer thickness was approximately 20 $\mu gm\ cm^{-2}$. The target was operated at

red heat (> 10 watts dissipation) which prevented the build-up of a residue from vapours in the vacuum system. No deterioration of this target has been observed after approximately 1 coulomb of bombardment.

The target chamber preserved cylindrical symmetry, apart from the target and the beam inlet pipe. The range of detector angles was chosen so that the beam inlet did not produce any appreciable effect on the angular distribution. The maximum angle between the detector axis and the target normal was 45^{o}, so that angles for which the target would have been viewed edge-on were avoided. Absorption effects for the 3.4 MeV γ-rays emerging from the target chamber were 2% in the target chamber walls and a further 3.5% to 5% for those γ-rays which passed through the target backing. The detector, which could be rotated in a horizontal plane around the vertical axis of the target chamber, was an unshielded 12.7 cm diameter x 10.2 cm thick NaI(Tl)crystal located with its front face 15.6 cm from the target. Standard electronics was used to accumulate 200 channel spectra in a pulse height analyzer.

The spectra were analyzed by using the methods described in the previous chapter. The summing effect due to the simultaneous detection of both members of a cascade was not included in the analysis. Though such

double detections may cause the spectrum to be analyzed to contain contributions to the full energy peak from more than one cascade this was neglected because the amount is only approximately 1% at resonance and less off resonance. However, an additional component, being the response of the detector and its surroundings to the neutron flux from a nearby tandem accelerator being operated independently was found to be needed in the analysis. Figures 3.1 and 3.2 show the range and quality of the fits achieved.

In this way, sets of angular distribution measurements for the different gamma rays in the $^{13}C(p,\gamma)$ reaction were extracted from the complex spectra accumulated just below, on and just above the 1012 keV resonance. In addition, excitation functions for the $^{13}C(p,\gamma)$ radiations were extracted from data taken over the proton energy range from 785 keV to 1158 keV in order to define more accurately the non-resonant yield underlying the data taken at the 1012 keV resonance. These sets of data affirm the stability of the target and the adequacy of the normalization by beam current integration. The excitation functions showed a smooth dependence with satisfactory repeatability. The angular distribution of the ground state gamma ray was also smooth and repeatable above, on and below the resonance.

Figure 3.1

A gamma-ray spectrum from the $^{13}C(p,\gamma)$ reaction, obtained at a proton energy just below the 1012 keV resonance, at an angle of 90^{o} to the beam. The solid line shows the extent and quality of the fit achieved as discussed in the text.

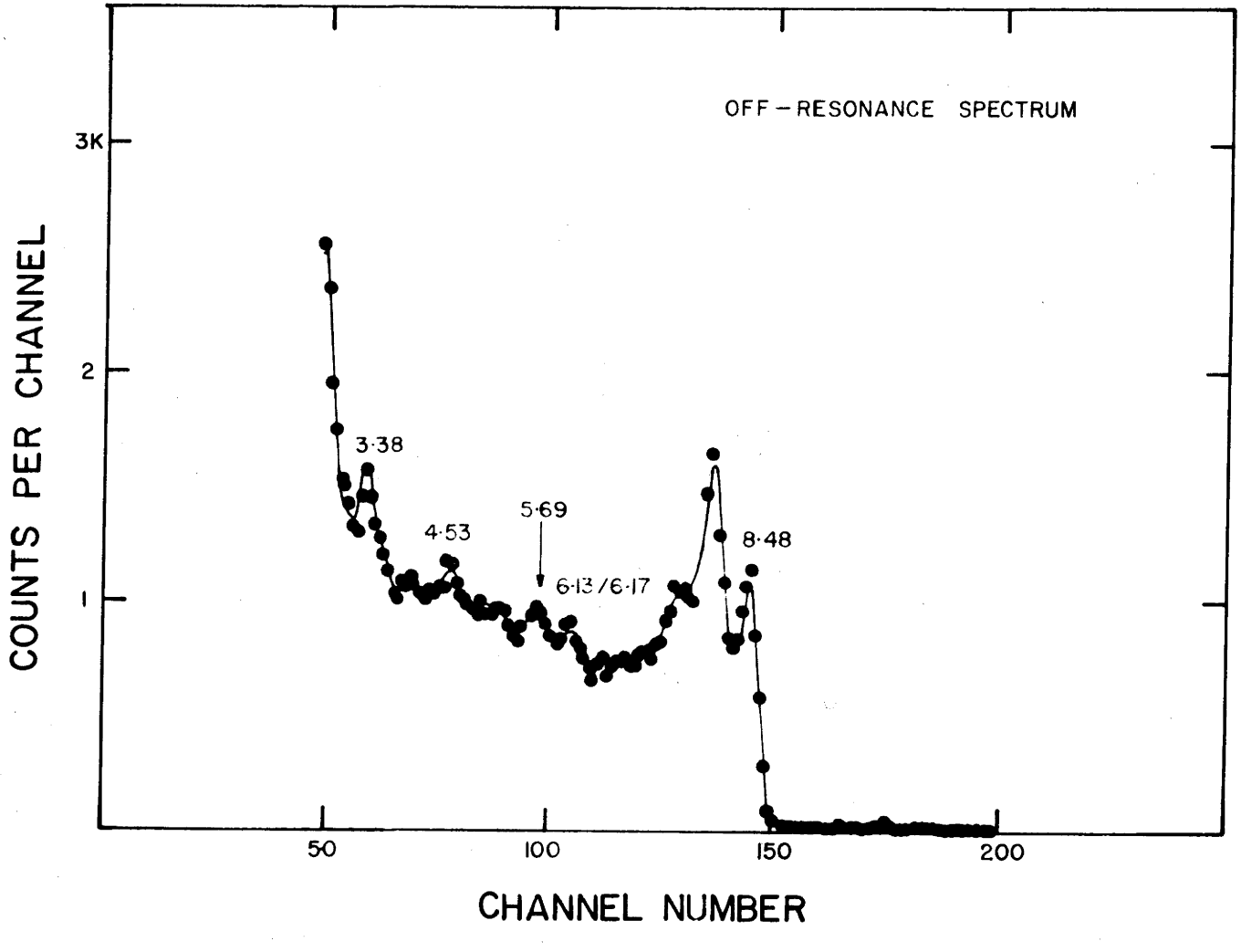
OFF – RESONANCE SPECTRUM
COUNTS PER CHANNEL
3K
2
1
3·38
4·53
5·69
6·13/6·17
8·48
50
100
150
200
CHANNEL NUMBER

Figure 3.2

A gamma-ray spectrum from the $^{13}C(p,\gamma)$ reaction, obtained at the 1012 keV resonance, at an angle of 90^{o} to the beam. The solid line shows the extent and quality of the fit achieved as discussed in the text.

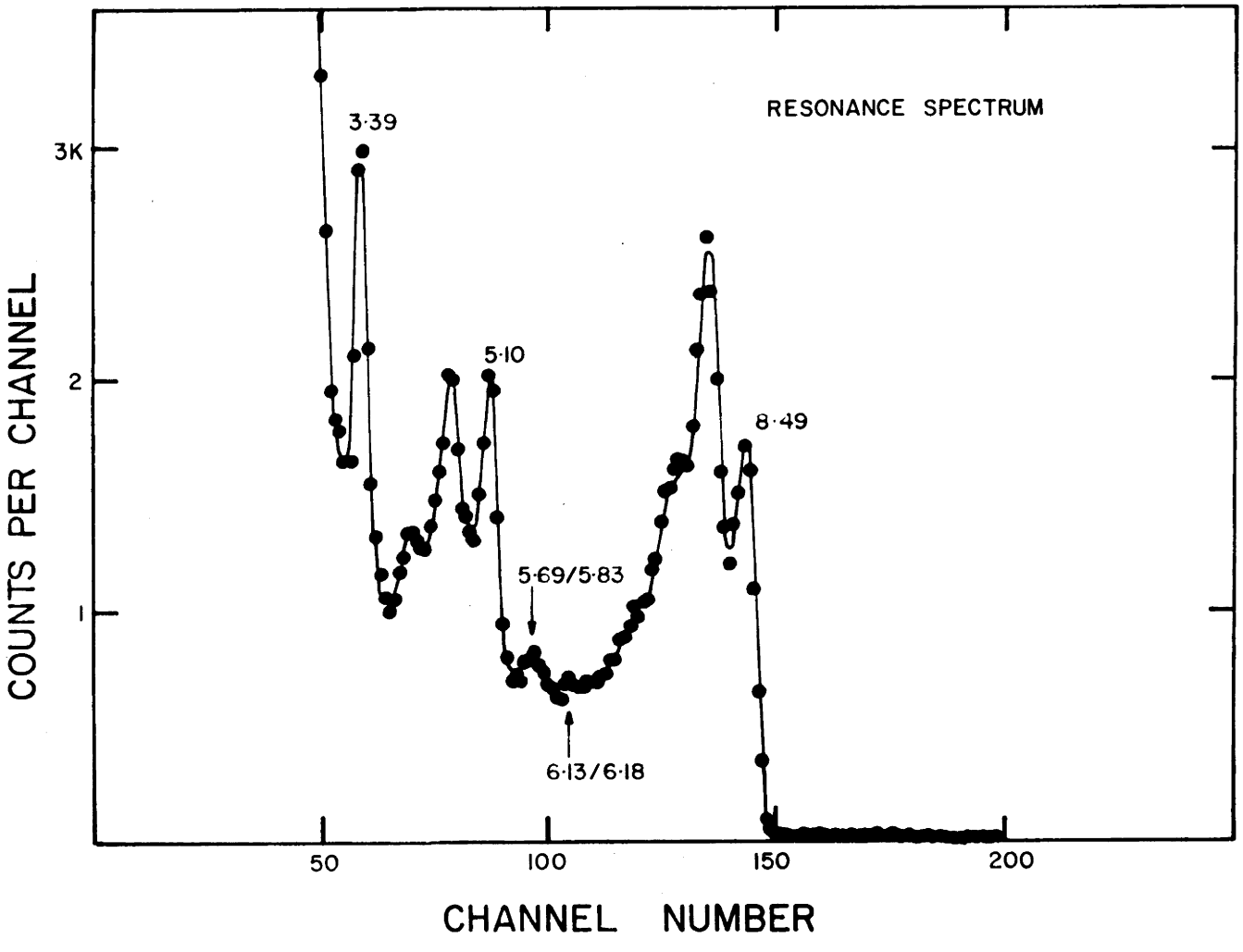
RESONANCE SPECTRUM
3·39
5·10
8·49
5·69/5·83
6·13/6·18
3K
2
1
COUNTS PER CHANNEL
50
100
150
200
CHANNEL NUMBER

However, some difficulty was experienced in keeping the proton beam at the resonance energy, within the limits imposed by the target thickness and the beam energy spread. This was checked by a determination of the intensity of the radiation from the 5.10 MeV state to the ground state. This radiation is negligible off resonance. Because of the uncontrolled radiation from the neutron flux already mentioned, it was not satisfactory to use a single channel analyzer window set to count the 5.10 MeV radiation in a monitor crystal. Instead, after computer analysis, those spectra that showed a reduced intensity of 5.10 MeV radiation were rejected. Those spectra rejected also showed, in approximately the same ratio, a reduction in the intensity of the other resonant gamma rays observed. The spectra remaining were used as the basis for the results given in the next section.

3. Results

The principal means of de-excitation of the 8.49 MeV state is by a cascade through the 5.10 MeV state. Figures 3.3 and 3.4 show the extracted intensities of the transitions from the 8.49 MeV state to the 5.10 MeV state and from the 5.10 MeV state to the ground state respectively at proton energies below, at and above

Figure 3.3

The angular distribution of 3.38 MeV gamma-rays observed above, on and below the 1012 keV resonance in $^{13}C(p,\gamma)$ is shown. The curves are the least-squares fits to the data.

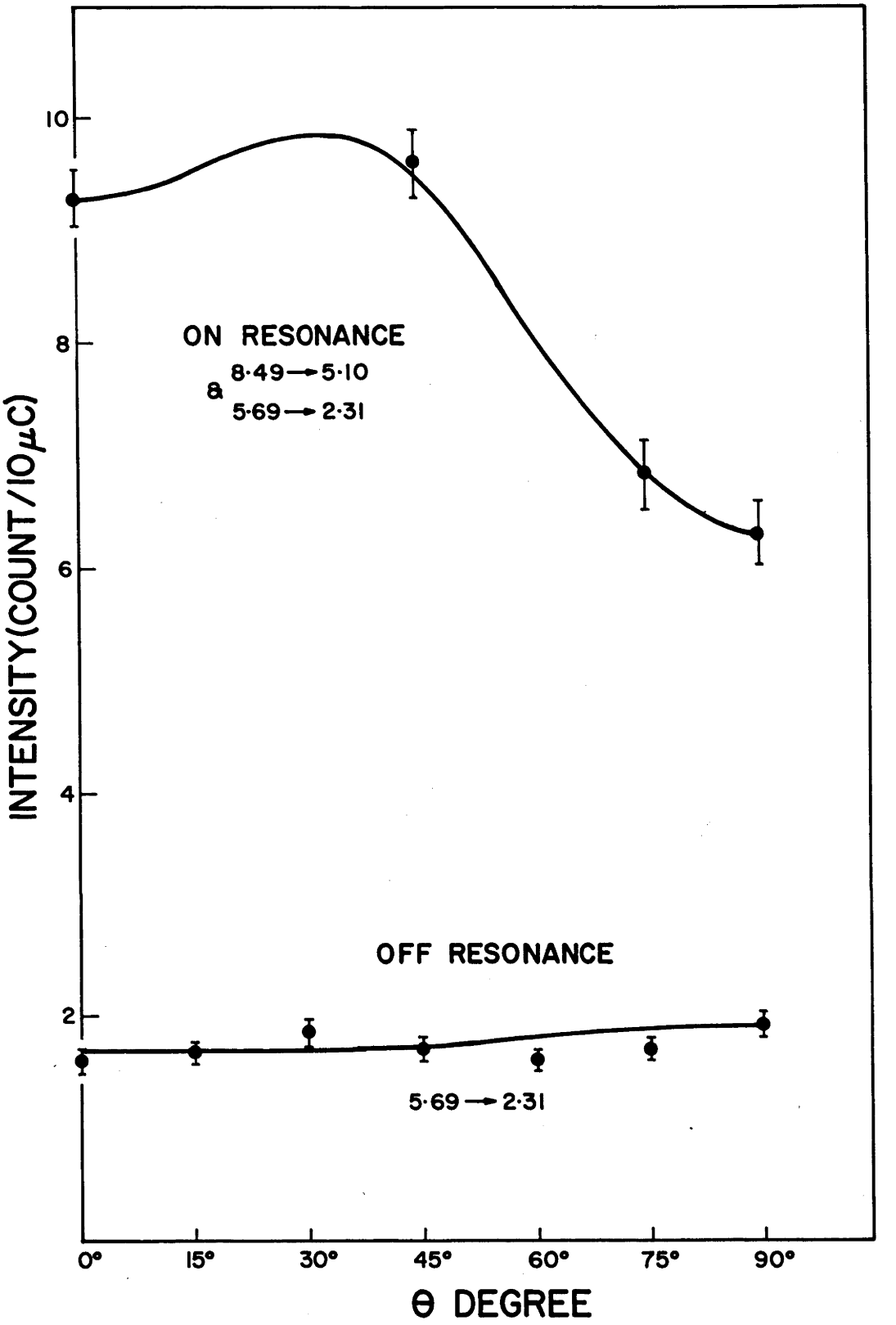
10
8
6
4
2
INTENSITY(COUNT/10μC)
ON RESONANCE
8·49→5·10
&
5·69→2·31
OFF RESONANCE
5·69→2·31
0°
15°
30°
45°
60°
75°
90°
θ DEGREE

Figure 3.4

The angular distribution of 5.10 MeV gamma-rays observed above, on and below the 1012 keV resonance in $^{13}C(p,\gamma)$ is shown. The curves are the least squares fits to the data.

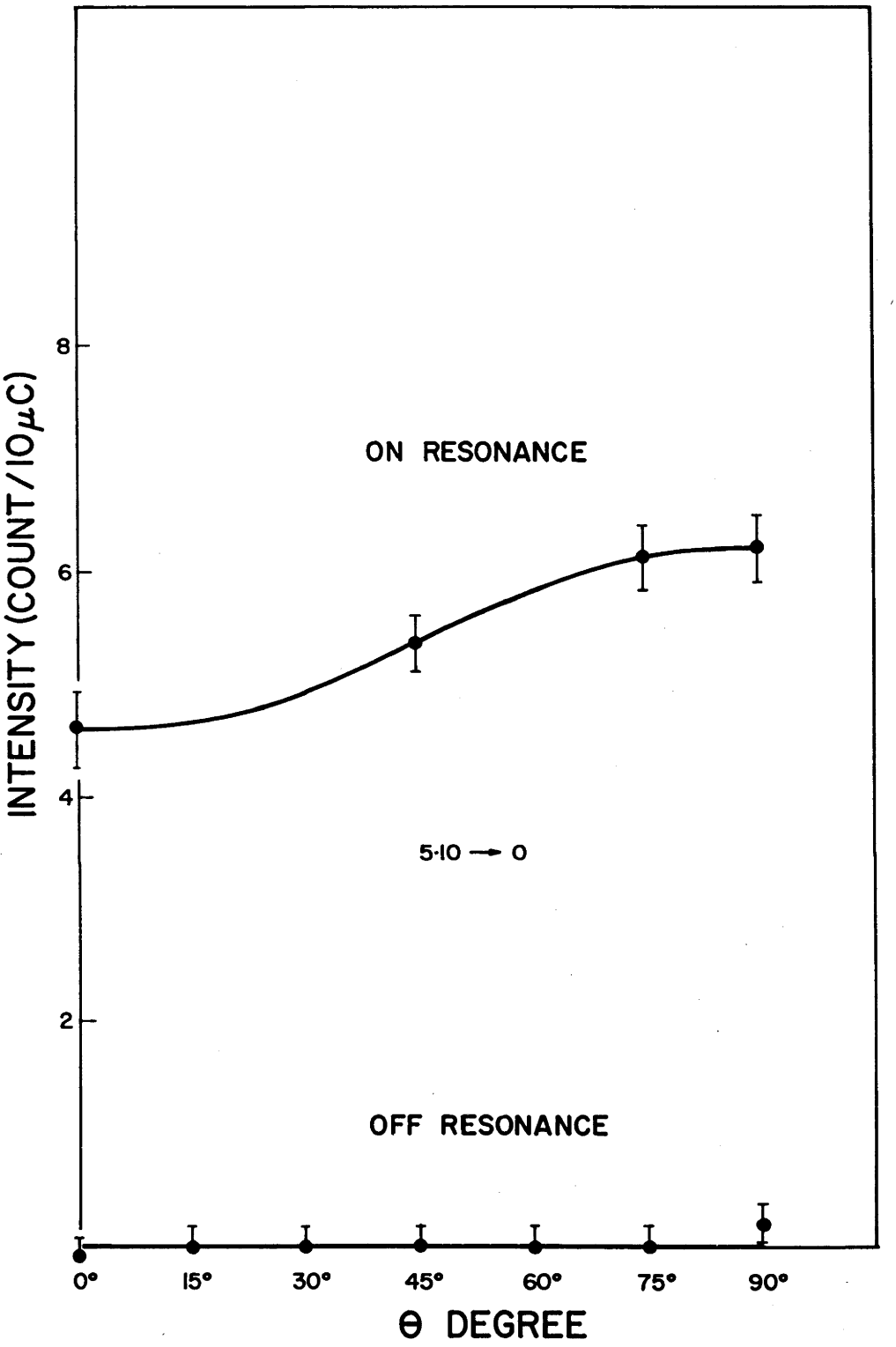
INTENSITY (COUNT / 10μC)
8
6
4
2
ON RESONANCE
5·10 → 0
OFF RESONANCE
0°
15°
30°
45°
60°
75°
90°
θ DEGREE

Figure 3.5

The angular distribution of 5.69 MeV gamma rays observed above, on and below the 1012 keV resonance in $^{13}C(p,\gamma)$ is shown.

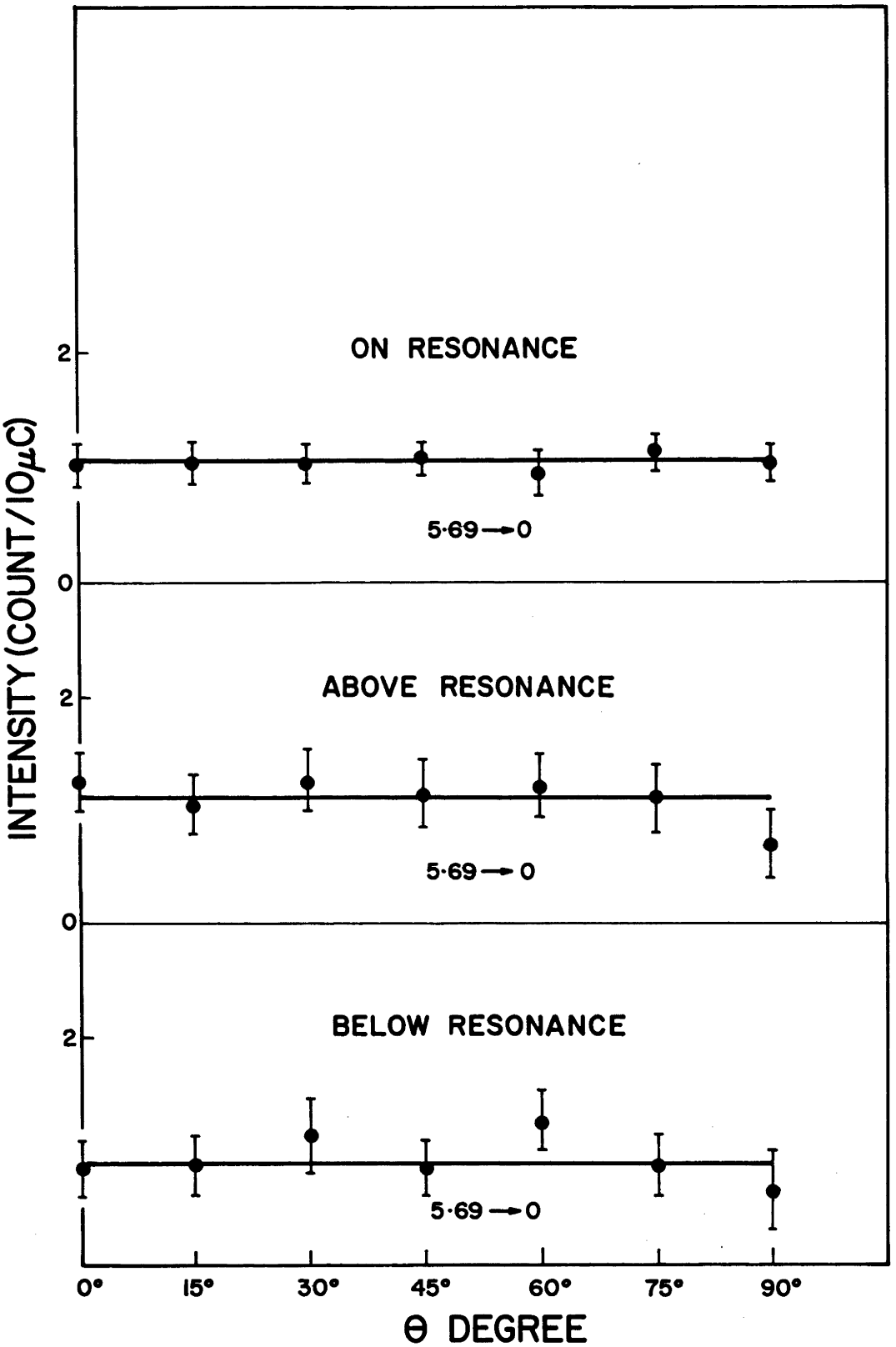
ON RESONANCE
5·69 → 0
ABOVE RESONANCE
5·69 → 0
BELOW RESONANCE
5·69 → 0
2
0
2
0
2
INTENSITY (COUNT/10μC)
0°
15°
30°
45°
60°
75°
90°
Θ DEGREE

resonance. The intensity of 5.10 MeV radiation is negligible off resonance implying that the observed off resonance yield of 3.38 MeV γ-rays (Figure 3.3) is not from a transition populating the 5.10 MeV state. The transition between the 5.69 and 2.31 MeV states has the same energy. Non-resonant transition from the 5.69 MeV state to the ground state was observed (Figure 3.5) with an intensity consistent with the known cascade branching ratio (WA 64) assuming that the observed 3.38 MeV γ-rays are, off resonance, entirely due to the transition from the 5.69 to the 2.31 MeV state. Therefore, Figure 3.3, on resonance, is interpreted as the sum of the resonant transition from the 8.49 to 5.10 MeV state and the non-resonant transition from the 5.69 to the 2.31 MeV state.

In the vicinity of the resonance, a 2.80 MeV γ-ray was observed and its intensity was extracted. This exhibited resonant behavior with an appreciable anisotropic non-resonant component. The resonant part has been interpreted as the transition between the 5.10 and the 2.31 MeV states. The observed intensity is consistent with the known branching ratio (WA 64) of the 5.10 MeV state and the observed intensity of the transition between the 5.10 MeV state and the ground state. The non-resonant part of the observed 2.80 MeV γ-ray intensity is the sum of the transitions from the

continuum to the 5.69 MeV state and from the $^{12}C(p,\gamma)^{13}N$ reaction. Radiation from the latter is expected to come from the target with a yield of the same order of magnitude as the other 2.8 MeV γ-rays. It may also originate on nearby collimators which are cooler than the target and thus more likely to build up contamination. This may be the cause of some of the anisotropy of this composite radiation. The uncertainties in composition mean that little information has been extracted from the 2.80 MeV γ-ray intensity.

Detenbeck et al. (DE 65) have found that the 5.83 MeV state is populated in approximately 20% of the decays of the 8.49 MeV state. The decay of the 5.83 MeV state is predominantly (AJ 59) by a transition to the 5.10 MeV state with a small branch to the ground state. No attempt was made to extract intensities for the transitions from the 8.49 MeV state to the 5.83 MeV state or from the 5.83 MeV state to the 5.10 MeV state, but a search for 5.83 MeV radiation showed that no significant amount was present. On the basis of the measurements of Detenbeck et al. and the known branching ratio of the 5.83 MeV state, the intensity expected was comparable with the estimated errors in the extraction. However, there is an excess of γ-rays de-exciting the 5.10 MeV state compared with those populating it directly.

This excess is in good agreement with the measurements of Detenbeck et al. on the strength of the cascade through the 5.83 MeV state. Thus Figure 3.4, on resonance, is interpreted as the sum of two angular distributions in which the 5.10 MeV state is populated by two different transitions. The direct transition should account for approximately 85% of the decays of the 5.10 MeV state.

Small amounts of radiation populating and de-exciting the 4.91 MeV state were found to be needed. These radiations were non-resonant, as was the radiation populating the 3.95 MeV state. The decay of the 3.95 MeV state is known (AJ 59) to proceed predominantly via the 2.31 MeV state. As a simple check on the extracted intensities, the strength of a 3.95 MeV component was estimated and was found to be negligible at all energies and angles. Negligible intensities were also found for assumed transitions from the 6.21, 6.44 and 7.03 MeV states to the ground state ($< 1\%$ of the non-resonant transitions and $< 3\%$ of the decays of 8.49 MeV state).

Radiation from the continuum to the 2.31 MeV state would have an energy, at the resonance, of 6.18 MeV. This was used as a component in the spectrum fits. However, close inspection of Figure 3.1 shows that a slightly lower component (6.13 MeV) would have provided a better fit. In addition, the yield was lower in the

sequence of runs taken at the resonance than in the sequences taken immediately ($\pm$ 10 keV) above and below resonance as can be seen immediately in Figures 3.1 and 3.2. This anomalous behaviour has been attributed to ^{19}F contamination, either on the target or on nearby collimators. The nearest $^{19}F(p,\alpha\gamma)^{16}O$ resonance is at a proton energy of 935 keV (Γ = 8.6 keV) and is predominantly (AJ 59) a transition through the 6.13 MeV state of ^{16}O. The level of contamination, if assumed to be on the surface of the target, would be approximately 5×10^{-9} gm cm^{-2}. Such a level of contamination has been found often in low-intensity γ-ray experiments and is likely to vary substantially between sequences of runs. Because of the masking effect of the contamination, only an upper limit of 8% to the strength of resonant transitions to the 2.31 MeV state can be given.

The remaining transition is from the continuum to the ground state. It is the most intense in the spectrum and is well resolved. The intensities measured above and below are consistent with the excitation function measured over a wider range of energies and allow interpolation to find the non-resonant yield at the resonance energy. When this is done, an excess count rate at the resonance of 0.18 $\pm$ 0.38 count/10 μC is found. This excess count includes the double detection effect in

the resonant 2-step cascade. On the assumption of no angular correlation in the cascade, the estimated effect is 0.15 count/10 μC. If a subtraction of 0.15 ± 0.15 count/10 μC is made to allow for this effect, the resonant ground state transition intensity is 0.0 ± 0.4 count/10 μC corresponding to an upper limit for the resonant ground state transition of 4% of the decay of the 8.49 MeV state. The present estimate is approximately 40% of the upper limit set by Detenbeck et al. (DE 65).

The data of Figure 3.3 have been analyzed separately, on and off resonance, into sums of Legendre polynomials which were subtracted to give the angular distribution of the resonant γ-ray. After correction for the finite size of the detector, the angular distribution for the transition from the 8.49 MeV state to 2^- state at 5.10 MeV is

$$W(\theta) = 1 + (0.47 \pm 0.06)P_2(\cos\theta) - (0.34 \pm 0.08)P_4(\cos\theta)$$

The angular distribution of the radiation from the 5.10 MeV state to the ground state, from Figure 3.4 after correction for the finite size of the detector, is found to be

$$W(\theta) = 1 - (0.21 \pm 0.05)P_2(\cos\theta) + (0.02 \pm 0.08)P_4(\cos\theta)$$

When the analyses included a coefficient for $P_6(\cos\theta)$, this was found to be consistent with zero and the lower order coefficients were unchanged.

4. Discussion

The comparison of the above angular distributions with the theoretical predictions can be limited to those assignments to the 8.49 MeV state with $J \leq 4$. Likewise, only dipole and quadrupole radiation from the 8.49 MeV state to the 5.10 MeV state need be considered. The measured strength of the transition from the 8.49 to the 5.10 MeV state is $w\Gamma_\gamma\Gamma_p/\Gamma = 0.008$ eV, in agreement with the measurement of Detenbeck et al. (DE 65). Any octupole radiation of sufficient strength to affect the angular distribution coefficients would require an unreasonable large enhancement ($\rangle 10^3$) over the Weisskopf single particle estimate (WI 60).

Of the spin assignments to the 8.49 MeV state with $J \leq 4$, $J = 0^{\pm}$ and $J = 1^{\pm}$ can be rejected immediately because of the observed complexity of the distribution of Figure 3.3. The assignment $J = 3^-$ may be rejected because it predicts only a positive P_4 coefficient in Figure 3.3 for any mixture of d and g wave protons and any mixture of M1 and E2 radiation in the first transition.

The assignment $J = 3^+$ is rejected on two grounds. Firstly, to fit the angular distribution for the transition from the 8.49 MeV state to the 5.10 MeV state, the parameters are such that an E3 enhancement of approximately 3×10^4 is required. Secondly, the parameters required to fit the first transition are not consistent with the second transition (5.10 MeV state to the ground state) using the known E3/M2/E1 mixing (NE 65, GO 66, WA 65) of the second transition.

As mentioned in the introduction, a 2^- assignment cannot be rejected on the basis of intensity measurements. A 2^+ assignment can be shown, from intensity measurements, to be unlikely. The f:p wave penetrability ratio is $\approx$ 1:400 while the required f:p wave intensity ratio, for a fit to the angular distribution, is $\approx$ 1:4. Also the enhancement of the M2 radiation strength required for a fit to the angular distribution data is approximately 30 times the Weisskopf single particle estimate. Both these intensities are improbable. However, using the known parameters (NE 65, GO 66, WA 65) of the transition from the 5.10 MeV state to the ground state, both the 2^- and the 2^+ assignments may be rejected. They both lead to a $P_2(\cos\theta)$ coefficient for the second transition that is close to zero and is significantly different from the experimental value of -0.21 ± 0.05.

An assignment of 4^+ to the 8.49 MeV state allows a fit to the angular distribution for the first transition with pure f-wave formation and pure M2 decay. The same parameters fit the angular distribution of the second transition, using known parameters (NE 65, GO 66, WA 65). However, the M2 enhancement in the first transition is required to be 40 times the Weisskopf estimate. Since this M2 transition would be expected to be inhibited (WA 58) rather than enhanced, it is concluded that the 4^+ assignment can be rejected on the basis of these intensity measurements.

The assignment of 4^- to the 8.49 MeV state allows a fit to the angular distribution for the first transition. The theoretical distribution for formation by pure channel spin 0 is

$$W(\theta) = 1 + 0.51\ P_2(\cos\theta) - 0.37P_4(\cos\theta)$$

and by pure channel spin 1 is

$$W(\theta) = 1 + 0.43P_2(\cos\theta) - 0.18P_4(\cos\theta)$$

while the experimental distribution is

$$W(\theta) = 1+(0.47\pm0.06)P_2(\cos\theta)-(0.34\pm0.08)P_4(\cos\theta)$$

Agreement with the distribution for pure channel spin 0 is good, but we cannot rule out a considerable contribution from channel spin 1.

The 4^- assignment would require an enhancement of a factor of 5 for E2 radiation to the 5.10 MeV state. It

Figure 3.6

The relationship between the mixing ratios M2/E1 and E3/E1 is shown for the transition from the 5.10 MeV state of ^{14}N to the ground state. The limits of the diagram are based approximately on limits given by Warburton *et al.* (WA 65). The solid curves are based on the angular distribution results, $W(\theta) = 1 + A_2P_2(\cos\theta) + A_4P_4(\cos\theta)$, of the present experiment. The hatched area (one of four, the others being excluded (WA 65) by Warburton *et al.*) defines the region of mixing ratios acceptable ($\pm$ standard deviation) to the present experiment. Also shown on the diagram are the regions acceptable to other experiments (NE 65, WA 64, GQ 66, WA 65, BI 64, WA 59).

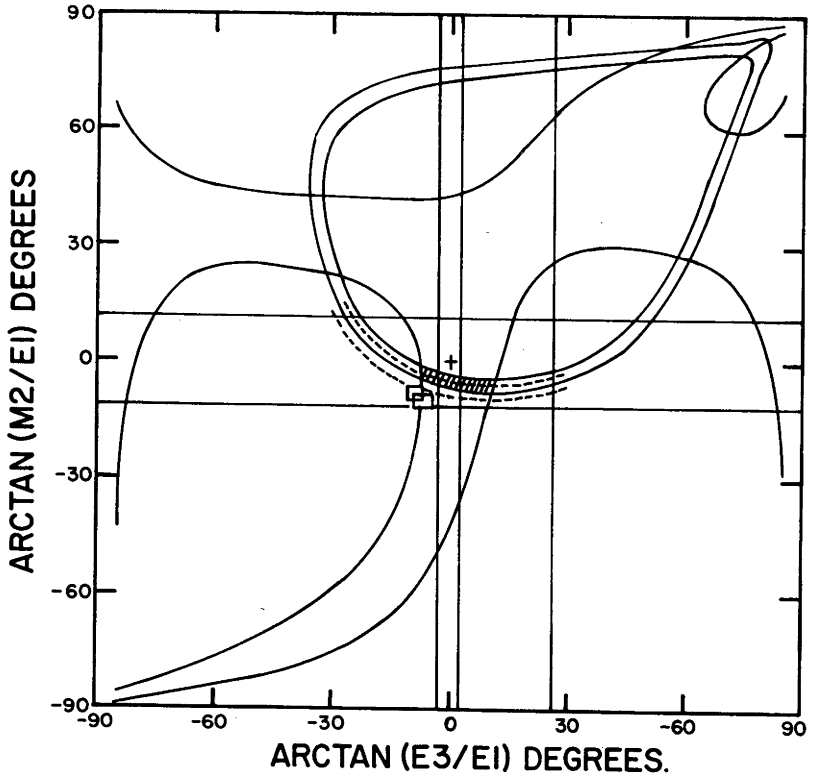

a.) OVERALL VIEW

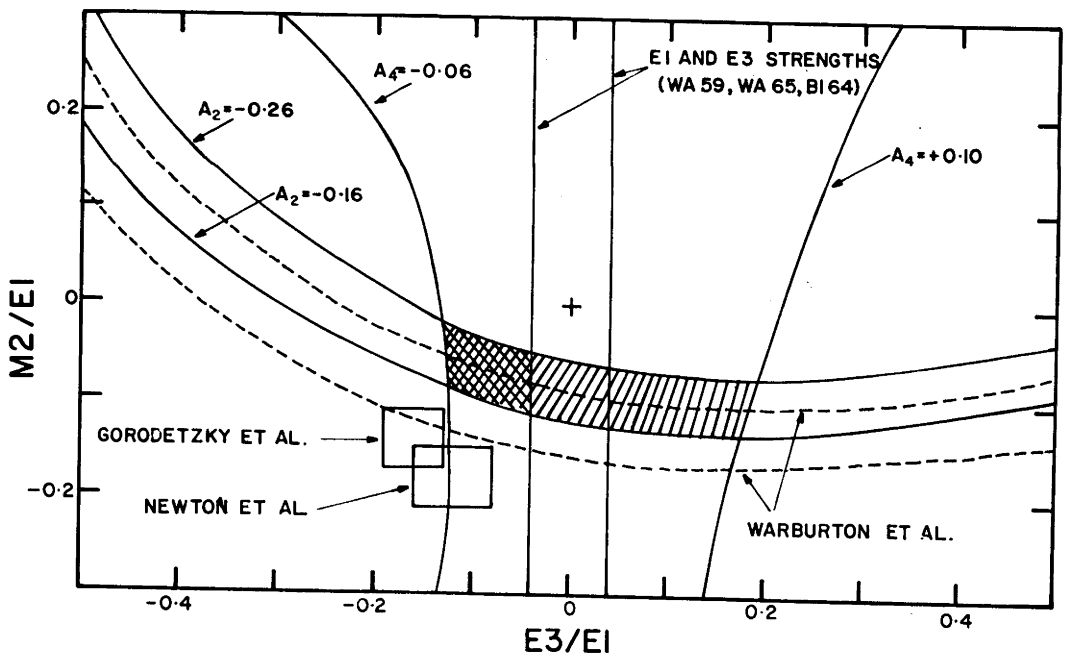

b.) EXPANDED VIEW

also requires an inhibition by a factor of 5×10^{-4} for M1 radiation to the 5.83 MeV state and by a factor of at least 10^{-4} for E1 radiation to the 6.44 MeV state. Both enhancements are reasonable (WI 60, WA 60) and the inhibitions required for the dipole radiations are also consistent with experience (WI 60).

For the second transition (from the 5.10 MeV state to the ground state) the coefficients of the angular distribution are insensitive to the channel spin mixture required for formation of a 4^- state at 8.49 MeV. They are also not significantly affected by the population ($\approx 15\%$) of the 5.10 MeV state through a cascade involving the 5.83 MeV state.

The angular distribution coefficients for the second transition may therefore be used to derive values of the E1/M2/E3 mixing ratios for the second transition. The results are shown in Figure 3.6 where a comparison is made with other experiments. It is seen that the early result of Warburton et al. (WA 64, WA 65) defines a region of the diagram which is consistent with all other measurements (NE 65, GO 66, BI 64, WA 59) including the present ones.

A further test may be applied to the present results, viz., a comparison with the $^{12}C(^3He,p\gamma)$ experiment of Gallmann et al. (GA 68). The ratios R_2 and R_4 already

defined are used. As remarked earlier, the limits to these ratios apply to comparisons of the $^{12}C(^{3}He,p\gamma)$ and $^{13}C(p,\gamma)$ angular distribution coefficients for the same transition, regardless of the complexity of the path by which that transition is reached. The only restriction is the limitation of the $^{12}C(^{3}He,p\gamma)$ reaction to the population of M = 0 and $\pm$ 1 substates in the initial state of ^{14}N(with $2 \leq J \leq 4$).

Gallmann et al. quote an angular correlation for the first transition of

$$W(\theta) = 1+(0.40\pm0.13)P_2(\cos\theta)-(0.17\pm0.17)P_4(\cos\theta)$$

and for the second transition

$$W(\theta) = 1+(0.13\pm0.10)P_2(\cos\theta)-(0.08\pm0.12)P_4(\cos\theta)$$

The first transition gives a satisfactory comparison with ratios R_2 and R_4 of approximately unity indicated, consistent with the hypothesis of a spin and parity assignment of 4^- to the 8.49 MeV state. For the second transition, the ratio R_4 is not well defined and so does not give a useful comparison. The ratio R_2 has a very small probability of being in the valid range and close to unity as suggested by the first transition. This suggests that either one or both of the experimental distributions is in error or that unrealistic estimates of the standard deviations may have been made. It should also be noted that the $P_2(\cos\theta)$ coefficient quoted by

Gallmann et al. is not in good agreement with a 4^- assignment to the 8.49 MeV state. Depending upon the source of information about the mixing ratios in the second transition (NE 65, GO 66, WA 65) the probability lies between 3.5% and 0.5% that the discrepancy observed (between the $P_2(\cos\theta)$ coefficient of Gallman et al. and the coefficient predicted by assuming a 4^- state at 8.49 MeV) is due to chance.

Because of the trouble experienced, during the present experiment, in keeping to the optimum beam energy, the possibility must be considered that the data retained may have been distorted by a drift from the resonance. It is possible that the selection of data has introduced a slight bias in the results by rejecting results which had suffered a statistical fluctuation downward in intensity. There were, however, few ambiguous results. Such a bias could change the angular distribution coefficients slightly and thus affect, to a small degree, the mixing ratios derived from the present experiment. It could not alter the spin and parity assignment itself.

It is believed that a major normalization of the present data may be rejected on two grounds. Firstly, the χ^2 test shows a good fit to the data for both transitions, so that a $P_6(\cos\theta)$ coefficient is not needed. With significantly distorted data, there is a

very high degree of probability that a $P_6(\cos\theta)$ coefficient would be needed to fit four data points. Secondly, no major renormalization exists that will simultaneously make probable the validity of the ratio R_2 for both the first and the second transition in the comparison of the work of Gallmann et al. with the present work. The valid range of R_2 is independent of the possible spin and parity assignments of the 8.49 MeV state.

For instance, a renormalization of the data on the second transition to an extent that makes it just probable to have a valid ratio R_2 for the second transition has already increased the ratio R_2 for the first transition enough to make its validity improbable.

A renormalization of the data for the first transition to match the revised coefficients of Detenbeck et al. (DE 65) would involve the rejection of the 4^- assignment, leaving only 2^- as a possible assignment that gives a fit to the first transition and that is not rejected by intensity arguments. With this renormalization, a large $P_4(\cos\theta)$ coefficient would be generated in the second transition distribution, sufficient to reject the 2^- assignment, leaving no satisfactory assignment. In addition, with this renormalization, there is a difficulty with the validity

of R_2 in the comparison of the $^{12}C(^3He,p\gamma)$ and the $^{13}C(p,\gamma)$ data for the first transition.

5. Summary

It has been shown that the revised data of Detenbeck et al. (DE 65) are inconsistent with the assignment 4^- to the 8.49 MeV state of ^{14}N. In addition, these revised data are inconsistent with the results of Gallmann et al. (GA 68) on the transition from the 8.49 to the 5.10 MeV state. A revision of the data (DE 65) because of the omission of the correction for the finite size of the γ-ray detectors results in systematic changes in the angular distribution coefficients which are inconsistent with the results of Gallmann et al. and with the present results. Accordingly, the $^{13}C(p,\gamma)$ measurements of Detenbeck et al. are rejected.

The present experiment, measuring both the transition from the 8.49 MeV state to the 5.10 MeV state and from the 5.10 MeV state to the ground state, is consistent with a 4^- assignment and with the mixing parameters already known for the second transition. There is agreement between the results of the present experiment and the results of Gallmann et al. for the first transition. For the second transition, there is disagreement with the results of Gallmann et al., which

are also in marginal disagreement with the assignment 4^-. The disagreement is in the magnitude of the coefficient of $P_2(\cos\theta)$. However, the value of this coefficient predicted by the 4^- assignment lies between the experimental values in disagreement. It is possible to reconcile the experimental values with the predicted value by increasing slightly the estimate of the standard deviation of the experimental results or by relaxing slightly the standards required for agreement. As they stand at present, a numerical value may be chosen for the $P_2(\cos\theta)$ coefficient which is just on 2 standard deviations from both the experimental values and which is consistent with other knowledge of the second transition.

It would be preferable that both experiments should be repeated in order to resolve the disagreement. However, these relaxations in the standard required for agreement are not such as to allow the assignment 2^- to become a possibility. It is therefore believed that the present measurements establish uniquely the assignment 4^- to the 8.49 MeV state of ^{14}N.

FIGURE CAPTIONS

Figure 3.1 A gamma-ray spectrum from the $^{13}C(p,\gamma)$ reaction, obtained at a proton energy just below the 1012 keV resonance, at an angle of 90^{o} to the beam. The solid line shows the extent and quality of the fit achieved as discussed in the text.

Figure 3.2 A gamma-ray spectrum from the $^{13}C(p,\gamma)$ reaction, obtained at the 1012 keV resonance, at an angle of 90^{o} to the beam. The solid line shows the extent and quality of the fit achieved as discussed in the text.

Figure 3.3 The angular distribution of 3.38 MeV gamma-rays observed above, on and below the 1012 keV resonance in $^{13}C(p,\gamma)$ is shown. The curves are the least-squares fits to the data.

Figure 3.4 The angular distribution of 5.10 MeV gamma-rays observed above, on and below the 1012 keV resonance in $^{13}C(p,\gamma)$ is shown. The curves are the least-squares fits to the data.

Figure 3.5 The angular distribution of 5.69 MeV gamma rays observed above, on and below the 1012 keV resonance in $^{13}C(p,\gamma)$ is shown.

Figure 3.6 The relationship between the mixing ratios M2/E1 and E3/E1 is shown for the transition from the 5.10 MeV state of ^{14}N to the ground state. The limits of the diagram are based approximately on limits given by Warburton et al. (WA 65). The solid curves are based on the angular distribution results, $W(\theta) = 1 + A_2P_2(\cos\theta) + A_4P_4(\cos\theta)$, of the present experiment. The hatched area (one of four, the others being excluded (WA 65) by Warburton et al.) defines the region of mixing ratios acceptable ($\pm$ standard deviation) to the present experiment. Also shown on the diagram are the regions acceptable to other experiments (NE 65, WA 64, GO 66, WA 65, BI 64, WA 59).

CHAPTER IV

THE INVESTIGATION OF THE $^{14}N(p,\gamma)^{15}O$ REACTION IN THE PROTON ENERGY RANGE 1.7 TO 3.0 MeV

1. Introduction

The rate of the $^{14}N(p,\gamma)^{15}O$ reaction is of interest in the C-N-O cycle of stellar nuclear reactions since the abundance of ^{14}N in equilibrium is determined by this reaction rate at stellar proton energies. The non-resonant radiation from the $^{14}N(p,\gamma)$ reaction has been studied by Hebbard et al. (HE 63) in the proton energy range from 210 to 1070 keV. In order to calculate the cross sections at stellar energies for each of the transitions through bound states in ^{15}O and the ground state, the experimentally obtained intensities were fitted with theoretical resonant and non resonant curves as a means of extrapolating the calculated cross section factors to the stellar proton energies. Calculations were made using the work of Christy and Duck (CH 61) for the direct capture amplitude and a constant amplitude was included to account for any distant broad s-wave resonances. The two resonances explicitly introduced were the 278 keV($\frac{1}{2}^+$) resonance and the 1060 keV ($\frac{3}{2}^+$) resonance. Because of the unknown characteristics of any

distant levels, different extrapolations could be produced by using different components in the fit.

The present work aimed to extend the measurements from 1.7 to 3.0 MeV to obtain information concerning the higher energy resonances in order that the low energy analysis could be performed with more certainty. Furthermore, there is current interest in the mirror nuclei ^{15}O and ^{15}N (WA 65a, EV 66). Comparison of experimental data on level positions provides tests of the assumptions of shell model theory and charge independence of nuclear forces.

The decays of the resonance levels in the incident proton energy range 1.82 to 3.0 MeV have not been well studied. Duncan and Perry (DU 51) measured the yield of positrons from the decay of ground state of ^{15}O for bombarding proton energies between 0.25 and 2.5 MeV. Absolute cross sections were obtained and all of the presently known levels in the region of excitation energy 7.5 to 9.6 MeV were observed. The reaction $^{14}N(p,\gamma)$ in the energy range studied has been suggested previously (FE 59, BA 63, EV 66, EV 67) as the combination of non-resonant direct capture and resonant compound nucleus processes. The resonant portion was attributed to a broad level, the width of which is about 300 keV (EV 67, LA 67), centered at 2.40 MeV and two narrow resonances at

Figure 4.1

Energy levels and decay scheme of ^{15}O.

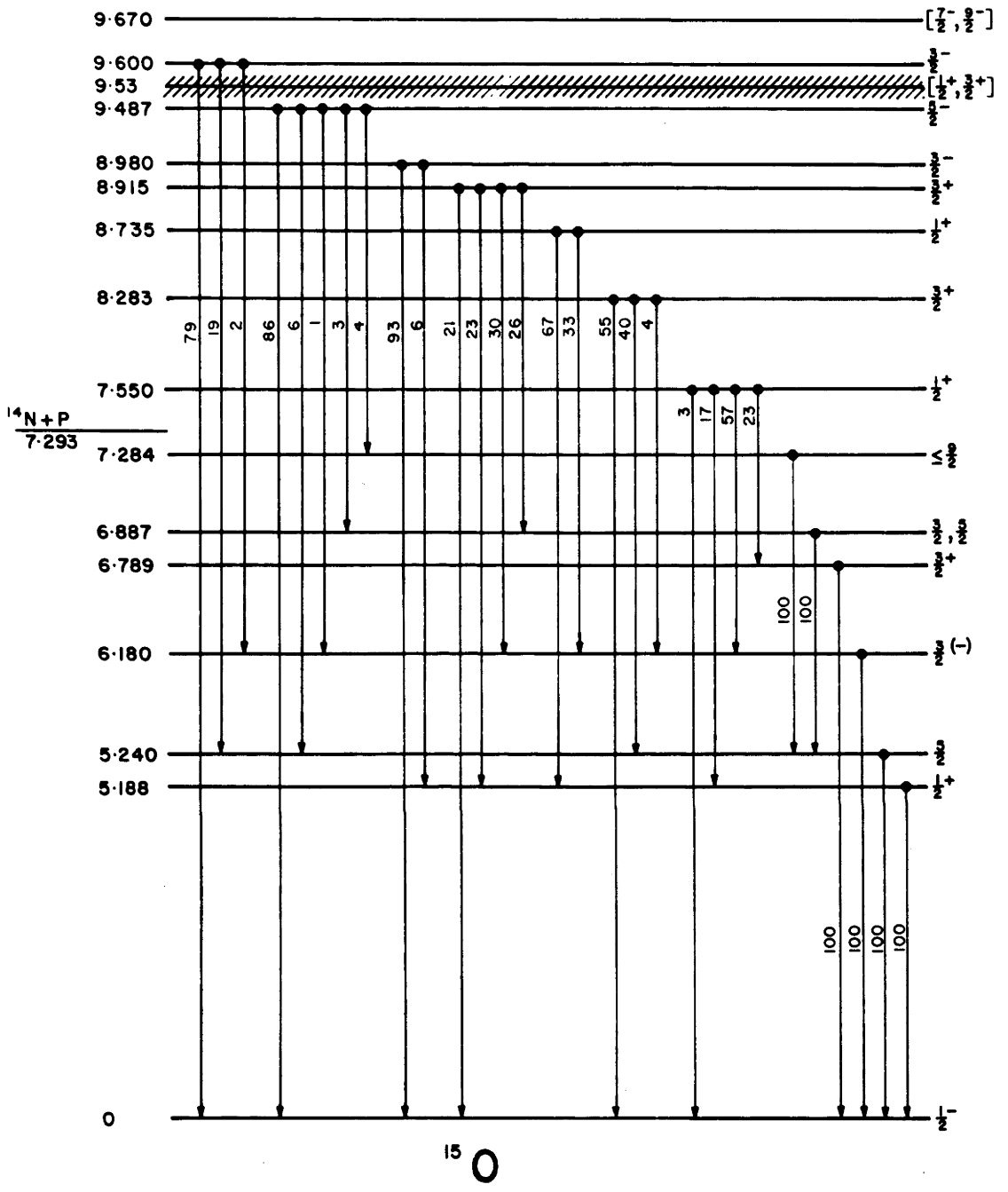
9·670
9·600
9·53
9·487
8·980
8·915
8·735
8·283
7·550
^{14}N+P
7·293
7·284
6·887
6·789
6·180
5·240
5·188
0
79
19
2
86
6
1
3
4
93
6
21
23
30
26
67
33
55
40
4
3
17
57
23
100
100
100
100
100
100
$[\frac{7}{2}^-, \frac{9}{2}^-]$
$[\frac{1}{2}^+, \frac{3}{2}^+]$
(-)
^{15}O

2.35 and 2.48 MeV which correspond to levels at 9.49 and 9.60 MeV in ^{15}O. Ferguson et al. (FE 59) suggested the broad level is most likely to have a J^{π} of $\frac{1}{2}^{+}$; however, the recent $^{14}N(p,p)$ experiment of Lambert et al. (LA 67) demonstrates that it is a $\frac{3}{2}^{+}$ level.

A level at 9.67 MeV was first reported by Olness et al. (OL 58) but not observed in recent work of Evans (EV 67). However, Lambert et al. (LA 67) observed the level and assigned the spin as either $\frac{7}{2}^{-}$ or $\frac{9}{2}^{-}$.

During the course of investigation of the present work, Evans (EV 67) reported measurements of the $^{14}N(p,\gamma)^{15}O$ reaction for proton energies between 1.85 to 2.60 MeV. He studied the decay schemes of the two narrow resonances at 9.49 MeV (Ep = 2.352 MeV) and 9.60 MeV (Ep = 2.480 MeV) in some detail. The broad resonance at 9.53 MeV was examined only qualitatively except for the ground state radiation.

Figure 4.1 summarizes the level and decay scheme of the ^{15}O nuclei from the work of Warburton et al. (WA 65a) and Evans (EV 67).

2. Specific problems

Experimental difficulties arise from the measurements of γ-ray spectra of the $^{14}N(p,\gamma)$ reaction with NaI(Tl) detectors since the available resolution is inadequate to

separate transitions to the doublets at 6.857 and 6.789 MeV and at 5.240 and 5.188 MeV, and to resolve the 6.180 MeV (6.180→0) γ-ray from the 6.129 MeV γ-ray due to possible fluorine contamination.

There are also problems associated with choice of target. If natural target material is used, the small proportion of ^{15}N produces a large yield of 4.43 MeV γ-ray from the $^{15}N(p,\alpha\gamma)^{12}C$ reaction. Though isotopic targets, made by bombarding tantalum with magnetically analyzed $(^{14}N)_2^+$ ions from a Van de Graaff, can reduce the strong 4.43 MeV radiation, the nitrogen distribution in the targets is not sufficiently uniform to measure reproducible excitation curves because of slight changes in the beam position between runs (EV 67). Thin targets made by sputtering tantalum in an atmosphere of nitrogen onto a tantalum backing were found (EV 67) to have considerable fluorine contamination, resulting in copious amounts of 6.13 to 7.12 MeV radiation. Targets made by diffusing nitrogen into a suitable backing by heating the backing material to red heat in an atmosphere of ammonia have been previously used in this laboratory at low proton energies (BA 63, HE 63). Careful manufacture is necessary to ensure that nitrogen does not diffuse deep into the target, thus smearing the excitation function. Target thicknesses of the order of 40-60 keV at 0.8 MeV

proton energy have been found previously for targets made by this method (BA 63). Targets made by evaporating adenine ($C_5H_5N_5$) onto a backing material have the advantage of well defined thickness; however, the compound is easily decomposed and introduces carbon as a source of background radiation.

3. Experimental details

The proton beam from the A.N.U. tandem Van de Graaff accelerator was used to provide proton beams of ~ 1 μa over the energy range of 1.7 to 3.0 MeV. Gamma-ray spectra were obtained at 20 keV intervals with an uncollimated 5" x 4" NaI(Tl) crystal, 5.62 cm from the target, at an angle of 55^{o} to the beam direction. Spectra were collected on an RIDL pulse height analyzer in the 200 channel mode.

In the later stage of this work, a 20 c.c. Ge(Li) detector became available and a number of spectra at selected energies were measured with the detector. These spectra were of great value in the accurate determination of the energies of γ-rays present in the spectra and served as a check on the analysis of the NaI(Tl) data.

For most of the measurements, nitrided tantalum targets, made by heating tantalum to a red heat in an

Figure 4.2

Experimental arrangement for the coincidence measurements.

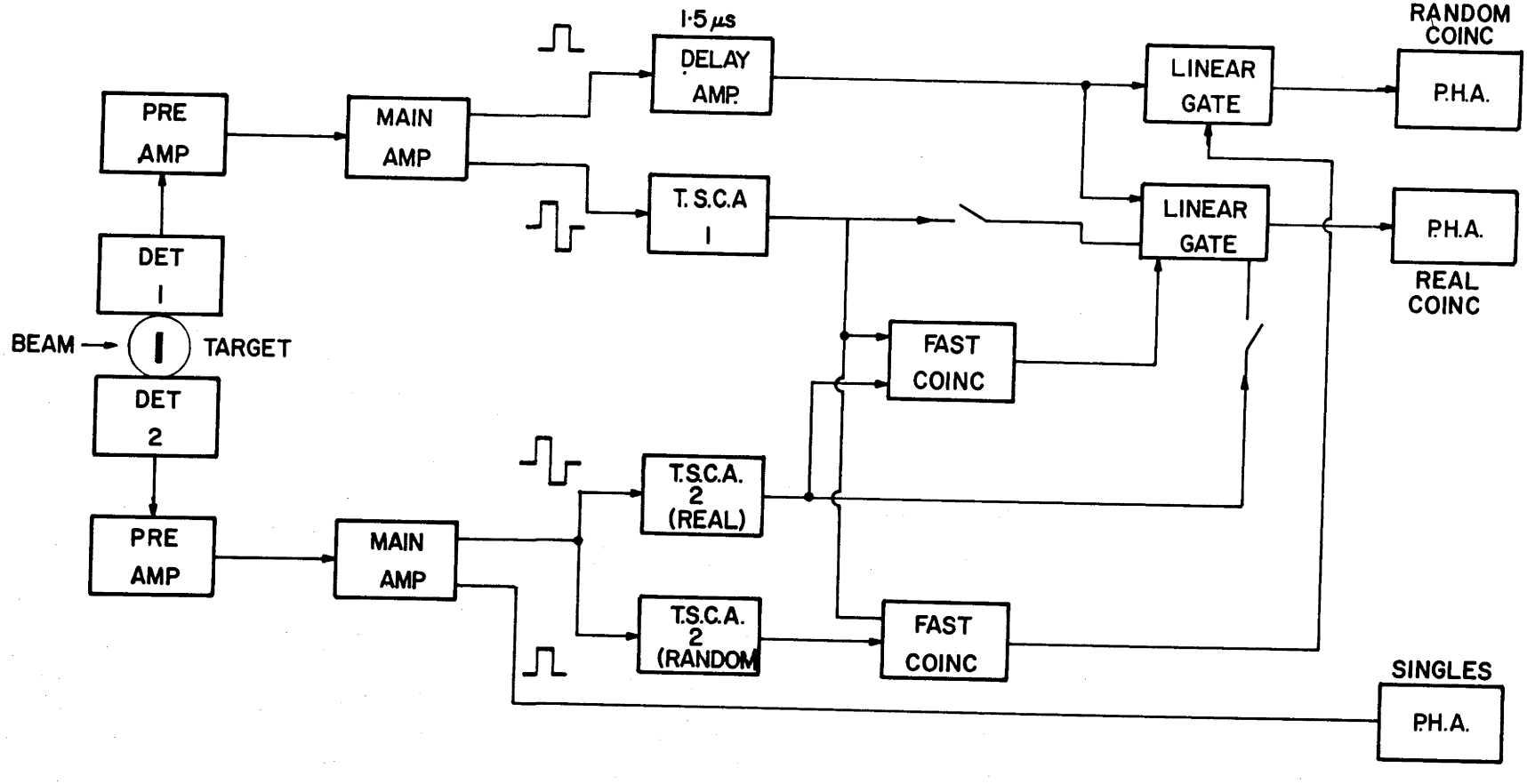
1·5 μs
DELAY AMP
RANDOM COINC
P.H.A.
LINEAR GATE
PRE AMP
MAIN AMP
T. S.C.A 1
LINEAR GATE
P.H.A.
REAL COINC
DET 1
BEAM
TARGET
FAST COINC
DET 2
T.S.C.A. 2 (REAL)
PRE AMP
MAIN AMP
T.S.C.A. 2 (RANDOM
FAST COINC
SINGLES
P.H.A.

atmosphere of ammonia containing natural nitrogen, were used. Such targets were available and no serious problem with fluorine contamination had been reported previously (BA 63, HE 63). However, after analysis of spectra obtained with the targets, it was found that the effects of fluorine contamination at higher proton energies were serious. Furthermore, nitrogen had diffused deep into the targets as was evident from the contributions to the γ-ray yield from resonances well below the bombarding energy.

To eliminate fluorine contamination and the strong 4.43 MeV γ-ray intensity, some coincidence measurements were performed with a tantalum nitride target and also with an adenine target of well defined thickness. The adenine target was made by evaporating a thin film of adenine on a gold covered copper backing which was screwed onto a water cooled target holder during the bombardment. The target proved to be not stable for beam currents of ~ 1 μa, losing nitrogen at a detectable rate. These spectra were used to check the results obtained from the NaI(Tl) spectra although some uncertainty was introduced by the nitrogen loss.

Figure 4.2 shows the experimental arrangement for the coincidence measurements. Two uncollimated 5" x 4" NaI(Tl) detectors, one inch apart with the target at the

center, were used to obtain coincidence spectra of cascade γ-rays. Timing single channel analyzers (T.S.C.A.) provided logic pulses after energy selection for the fast coincidence unit at the zero cross over point of the double delay line clipped linear pulses. The lower level discriminator of the timing single channel analyzer for detector 2 was set above 511 keV to minimize the contribution of non-cascade radiations in the gated spectra from detector 1.

4. Measurement of target composition

A knowledge on the distribution of nitrogen in the diffused nitrogen targets which were used for most of the experiment was necessary in order to calculate the cross section of the reaction.

The 0.4% concentration of ^{15}N in natural nitrogen enabled the nitrogen distribution to be calculated by measuring the yield of 4.43 MeV radiation from the narrow 429 keV resonance (Γ = 0.9 keV) in the $^{15}N(p,\alpha\gamma)^{12}C$ reaction as a function of energy. Figure 4.3 shows the measured yield curve. The excitation function was extended to 900 keV to allow the estimation of the contribution from the nitrogen deep in the target. The correction for the non-resonant radiation which contributes to the measured yield was estimated by using

Figure 4.3

The excitation function of the 4.43 MeV γ-ray from the $^{15}N(p,\alpha\gamma)$ reaction in the tantalum nitride target used for the $^{14}N(p,\gamma)$ measurements (Set 2 and 3).

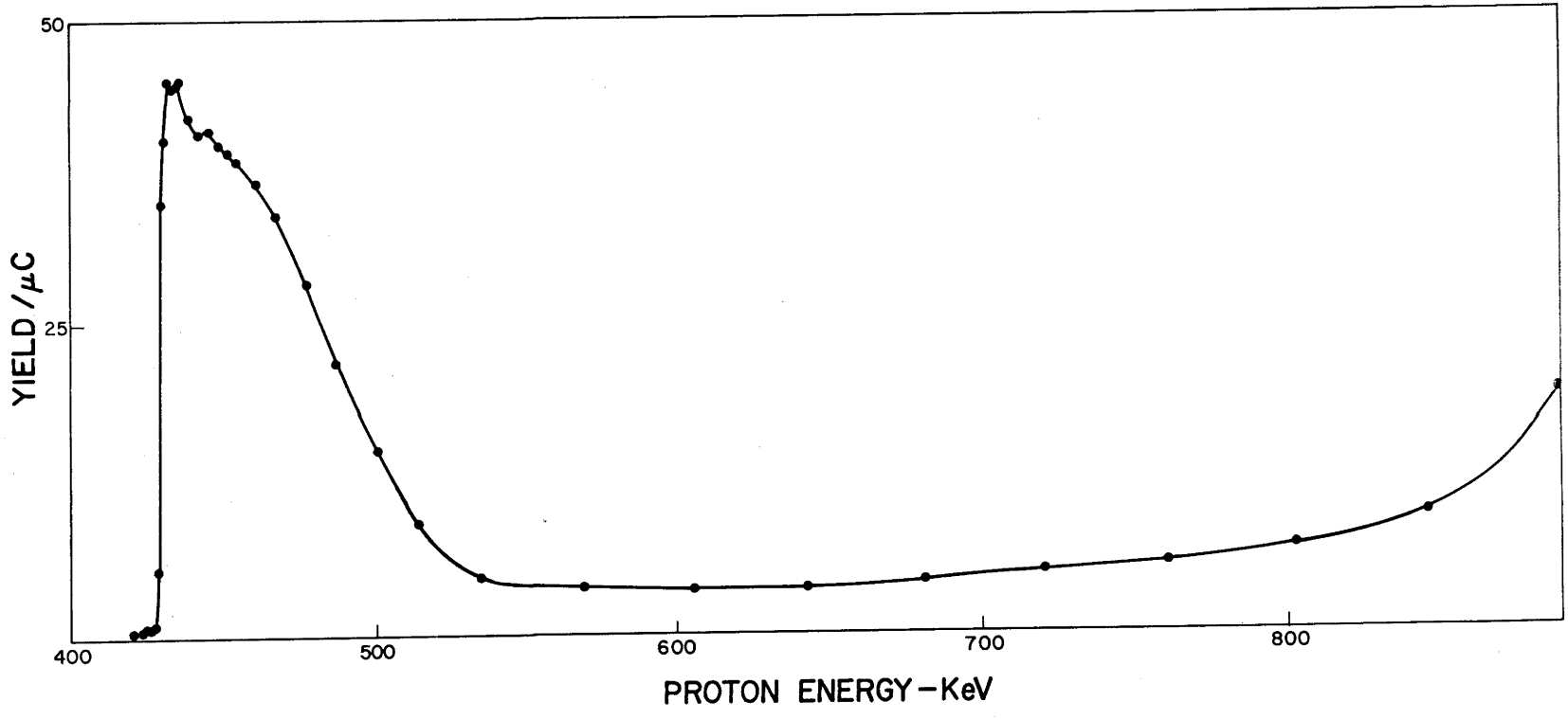
50
25
YIELD / μC
400
500
600
700
800
PROTON ENERGY – KeV

the excitation function of the 4.43 MeV γ-ray measured by Hebbard (HE 64) between proton energies of 300 to 1000 keV.

The yield is related to the stopping cross section per ^{15}N atom by the following equation:

$$Y = \left[\frac{2\pi^2 \lambda\!\!\!^{-2} w \Gamma_p \Gamma_{\alpha 1}}{\Gamma}\right] \frac{1}{\epsilon_N 15} \frac{EWQ}{e} \qquad \ldots\ldots (4.1)$$

where $\epsilon_N 15$ = the average stopping cross section per ^{15}N atom

E = efficiency of the detector

W = a correction factor for the angular distribution of the resonant radiation at the angle of detection (KR 53)

$\frac{Q}{e}$ = the number of protons incident on the target

A value of 0.260 keV barn was used for the integrated cross section, $2\pi^2 \lambda\!\!\!^{-2} w \Gamma_p \Gamma_{\alpha 1}/\Gamma$, of the resonance. Hebbard et al. (HE 63) have discussed the corrections involved in obtaining this figure from the data of Schardt et al. (SC 52) and Kraus et al. (KR 53).

The average stopping cross section per ^{15}N atom is also given by

$$\epsilon_N 15 = \frac{\Delta E}{N_N 15} \quad \text{eV-cm}^2 \qquad \ldots\ldots (4.2)$$

where ΔE is the energy loss in the target.

Equation 4.1 enabled the calculation of $\epsilon_N 15$ and euation 4.2 the calculation of $N_N 15$, the number of ^{15}N atoms/cm^2 in the target, which, in turn, determined $N_N 14$, the number of ^{14}N atoms/cm^2 in the target from the known proportion of ^{14}N and ^{15}N in natural nitrogen.

ΔE can have a value equivalent to total target thickness for a well defined target or can be divided into layers of desired thickness so that the number of nitrogen atoms/cm^2 for each layer can be calculated. ΔE is related to $N_N 14$ and N_{Ta}, which is the number of tantalum atoms/cm^2 in the target, by equation 4.3.

$$\Delta E = N_N 14 . \epsilon_N 14 + N_{Ta} . \epsilon_{Ta} \quad \ldots\ldots (4.3)$$

$\epsilon_N 14$ and ϵ_{Ta} are the stopping cross sections per atom for nitrogen-14 and tantalum at the average proton energy within the target.

An iterative calculation was performed in which the total number of nitrogen-14 and tantalum atoms was calculated layer by layer in 5 keV steps within the target. The composition of the front layer of the target, where the density of nitrogen atoms was greatest, gave a tantalum to nitrogen ratio of 0.62. This is in agreement with the composition of a previous target made by the same method (HE 63).

5. Analysis of data

(a). Singles NaI(Tl) data

The singles spectra obtained with a NaI(Tl) detector comprised the main part of the data of this experiment. The general methods of analysis have been discussed in Chapter 2 but several details are noted.

The coincidence sum spectra from simultaneous detection of cascade γ-rays, which were not included in the analysis of the $^{13}C(p,\gamma)^{14}N$ data, were found to be necessary as components in the fits. The transition from the resonance and off resonance level to the ground state constituted about 80% of the total decay in the $^{13}C(p,\gamma)^{14}N$ reaction. However, this is not the case for the present study as the spectra were collected over a wide range of proton energies and the relative intensity of each cascade was not known before the analysis. From Figure 4.1, it is observed that the ground state transition ranges from 3 to 93% for resonances observed between Ep = 275 to 2480 keV. The coincidence sum spectra included were the cascades from the compound state to the 5.2 and the 6.8 MeV doublets. The cascade through the 6.18 MeV state was found to be very weak throughout the analysis and was not included in final fits.

The 4.43 MeV γ-ray is a particular problem as the yield was found to be an order of magnitude larger than the yields of cascade γ-rays through the bound states. Furthermore, it is strongly broadened; the broadening increases markedly with energy and a resonance for the $^{15}N(p,\alpha\gamma)$ reaction exists at 3.12 MeV. Thus it was found impossible to fit the data over any part of the 4.43 MeV γ-ray peak without seriously affecting the fit in the region of the 5.2 MeV doublet, except for the spectra taken at lower proton energies.

Another problem was the presence of 6.13, 6.92 and 7.12 MeV γ-rays from $^{19}F(p,\alpha\gamma)^{16}O$ reaction which had an intensity of the same order as the $^{14}N(p,\gamma\gamma)$ gamma-rays in the same energy region. An additional feature of the problem was the considerable Doppler broadening of the 6.92 and 7.12 MeV γ-ray peaks. Calculations of the maximum Doppler shift at the angle of detection for the emission of the intermediate α-particles at different angles indicate a possible broadening of up to 90 keV. This broadening caused the extracted intensity of the 6.79 MeV γ-ray to spread considerably between different runs at the same proton energy. The presence of the 6.13 MeV γ-ray prevented meaningful extraction of the 6.18 MeV γ-ray intensity since the intensity of the latter was found to be much weaker from the Ge(Li) spectra. The

Figure 4.4

NaI(Tl) spectra of the $^{14}N(p,\gamma)$ reaction at Ep = 1.80, 2.48 and 2.90 MeV. Circles are the data and least squares line shape fit is the solid line.

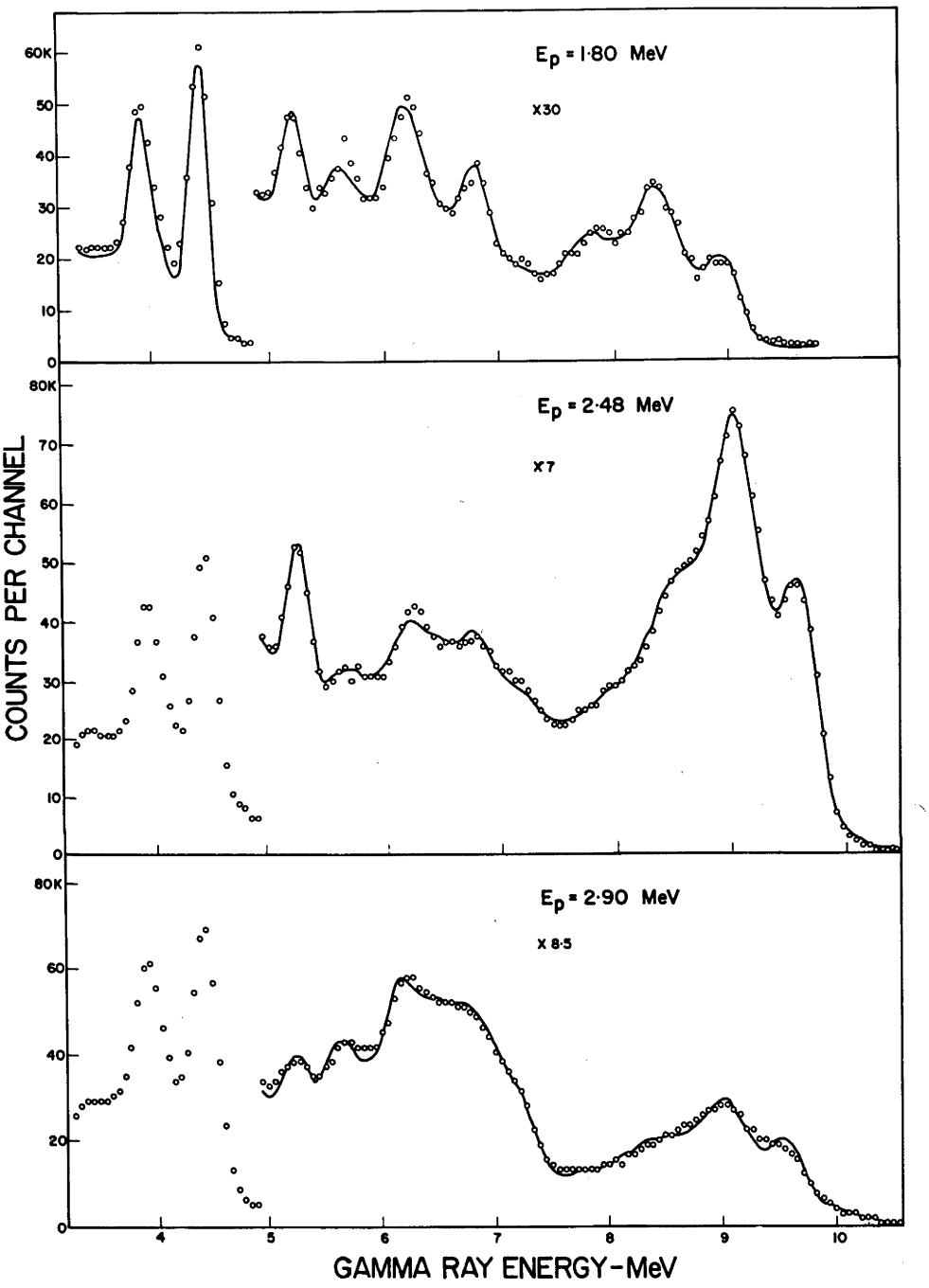
E_p = 1·80 MeV
X30
E_p = 2·48 MeV
X7
E_p = 2·90 MeV
X 8·5
COUNTS PER CHANNEL
GAMMA RAY ENERGY-MeV

extracted intensity of the 6.13 MeV γ-ray provided only an upper limit to the intensity of the 6.18 MeV γ-ray as the NaI(Tl) detector can not resolve these two γ-ray energies.

It was found necessary to include the ground state transition of resonances which were excited deep in the target as components in the fit due to the nitrogen distribution. This was especially important for spectra taken with proton energies above 2.40 MeV, because of the ground state γ-ray corresponding to either or both of the 9.49 and 9.60 MeV resonance levels is several times stronger than that of the compound state formed at the bombarding energy. The exclusion of these two components made the fits unacceptable. The contributions from these two resonances to the 5.24 MeV γ-ray intensity were subtracted in proportion to the extracted ground state γ-ray intensities according to the decay scheme shown in Figure 4.1. The corrections for the 6.79 MeV and the 6.18 MeV γ-ray intensities were not necessary since the contributions from these levels are insignificant and furthermore, the scatter of the data points due to fluorine contamination makes the correction meaningless.

Figure 4.4 shows the fits of NaI(Tl) data taken at Ep = 1.80, 2.48 and 2.90 MeV respectively.

Figure 4.5

Ge(Li) spectra of the $^{14}N(p,\gamma)$ reaction at Ep = 2.51 and 2.60 MeV.

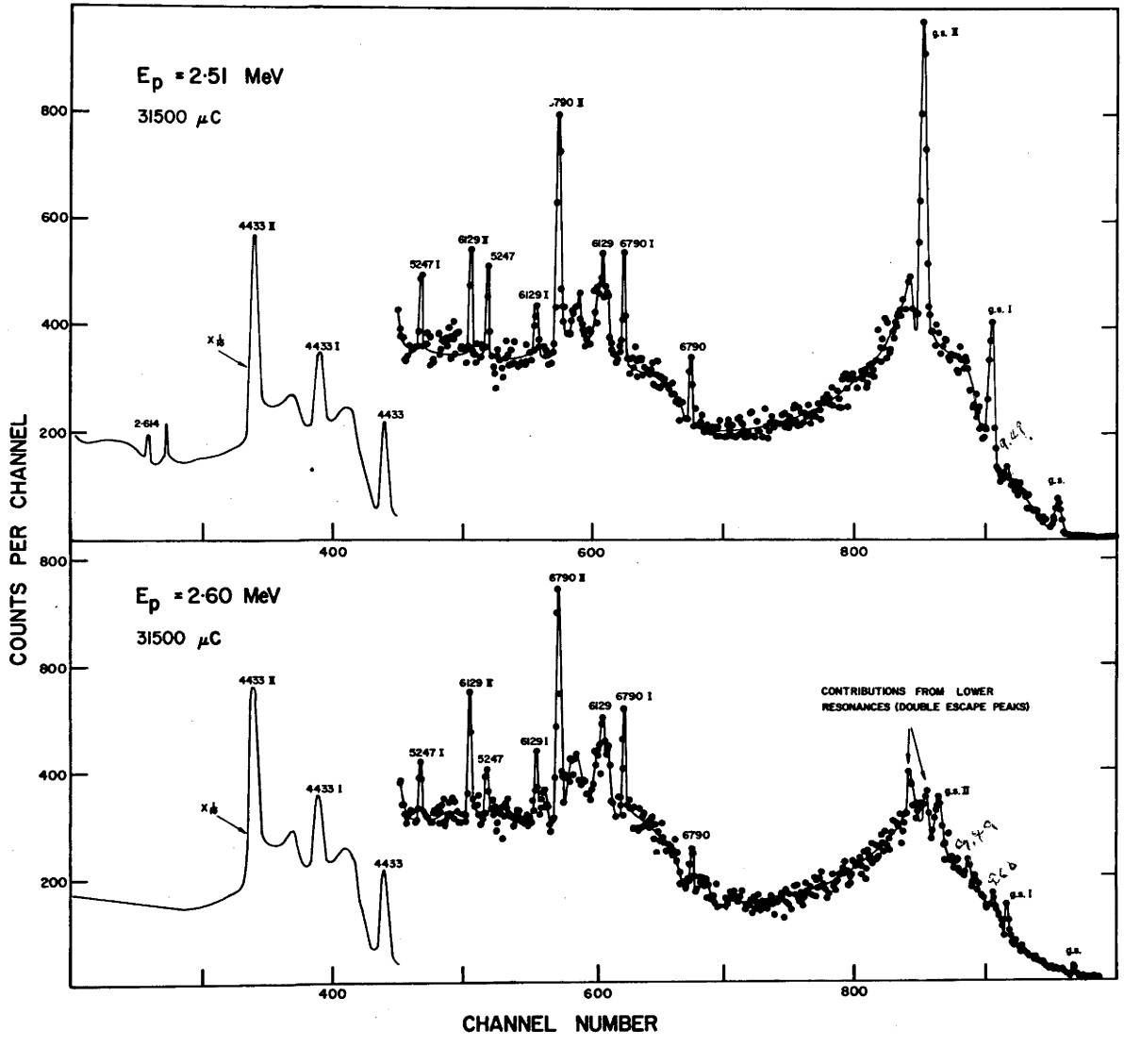
E_p = 2·51 MeV
31500 μC
4433 II
6129 II
5247 I
6790 II
6129 6790 I
6129 I
5247
6790
g.s. II
g.s. I
g.s.
x.e.
4433 I
2·614
4433
E_p = 2·60 MeV
31500 μC
6790 II
CONTRIBUTIONS FROM LOWER RESONANCES (DOUBLE ESCAPE PEAKS)
COUNTS PER CHANNEL
CHANNEL NUMBER
200
400
600
800

(b). Singles Ge(Li) data

The singles Ge(Li) spectra measured at Ep = 2.36, 2.51 and 2.60 MeV identified which of the doublet states were excited by the cascade γ-rays and allowed examination of the 6 MeV peak. The 6 MeV peak was determined to be 6.13 MeV and the 6.18 MeV peak was too weak for definite identification. The doublet member associated with the gamma-ray near 6.8 MeV was found to be the 6.79 MeV level in agreement with the observation that the 6.86 MeV state decays 100% to the 5.24 MeV state (WA 65a) and likewise the gamma-ray near 5.2 MeV was identified as being associated with the 5.24 MeV level.

The Ge(Li) spectra justify the inclusion of resonance components from resonances excited deep in the target in the fit for the analysis of NaI(Tl) spectra. Figure 4.5 shows spectra measured at Ep = 2.51 and 2.60 MeV. The peak observed at 9.72 MeV is due to interactions of 2.60 MeV protons with the nitrogen in the front layers of the target where the nitrogen concentration is high whereas the peak at 9.60 MeV is due to the ground state transition from the 9.60 MeV state which is excited deep in the target. Thus it was possible to derive the 'thin target' yield of the ground

Figure 4.6

Coincidence spectra measured with an adenine target, (a) Ep = 2.36 MeV, (b) Ep = 2.48 MeV, (c) Ep = 2.60 MeV and a TaN target (d) Ep = 2.48 MeV. (a) and (b) were fitted with γ-ray components which cascade through the bound states of ^{15}O and including as a component the background spectrum taken at Ep = 2.40 MeV. It is apparent that spectrum (d) corresponds to an energy just off resonance.

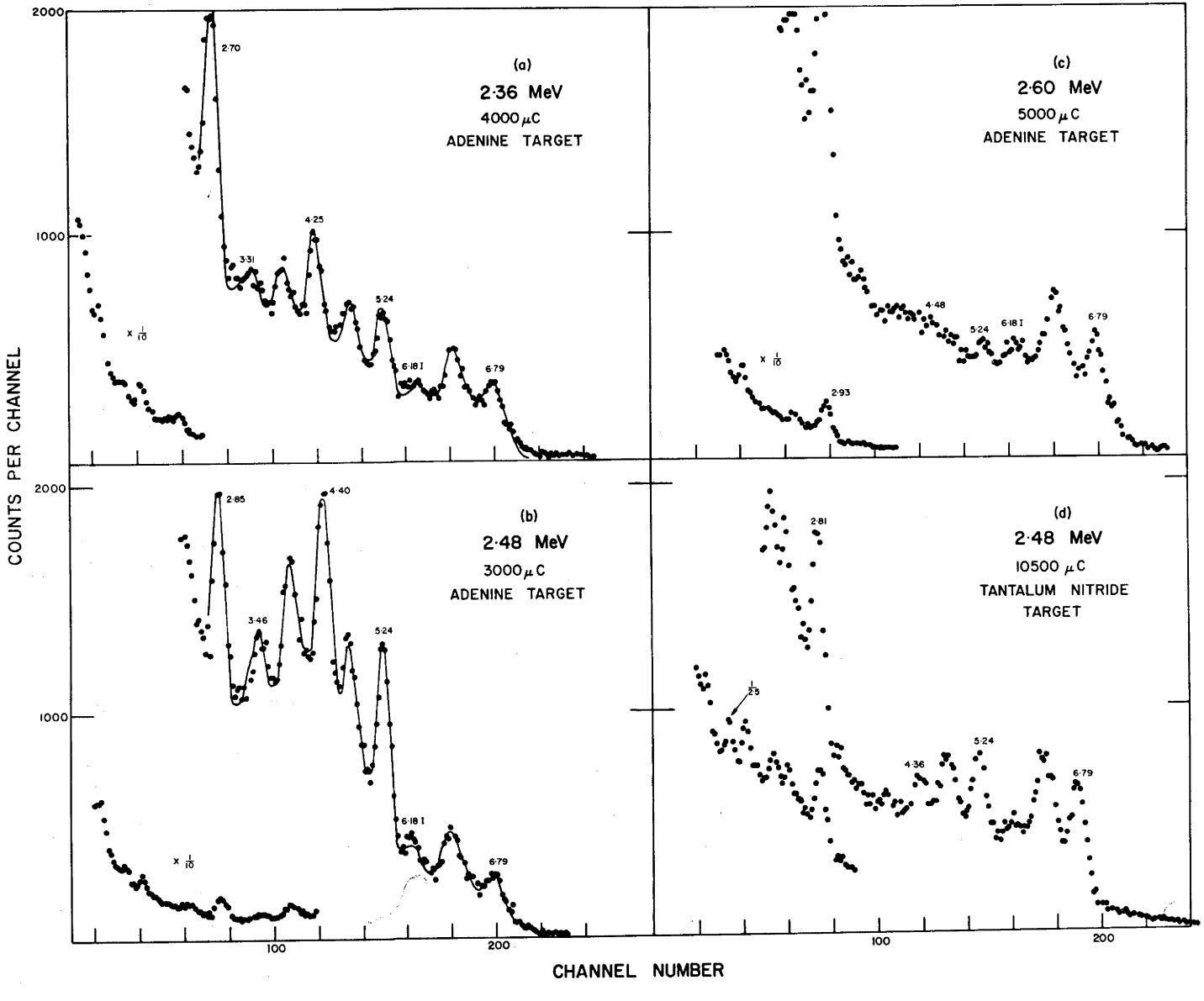
(a)
2·36 MeV
4000 μC
ADENINE TARGET
(b)
2·48 MeV
3000 μC
ADENINE TARGET
(c)
2·60 MeV
5000 μC
ADENINE TARGET
(d)
2·48 MeV
10500 μC
TANTALUM NITRIDE
TARGET
COUNTS PER CHANNEL
CHANNEL NUMBER
2000
1000
100
200
2·70
3·31
4·25
5·24
6·18 I
6·79
2·85
3·46
4·40
2·93
4·48
2·81
4·36
× 1/10
× 1/25

state transition at energies where Ge(Li) spectra were recorded and compare the results with the corrected NaI data.

(c). Coincidence spectra

Coincidence spectra were measured with tantalum nitride and adenine target at four proton energies, viz., 2.36 and 2.48 MeV to observe the cascade radiation at the two narrow resonances and 2.40 and 2.60 MeV to observe the underlying contributions. The spectra gave positive identification of the existence of the 6.18 MeV γ-ray which was not possible from the singles spectra. Figure 4.6 shows coincidence spectra at Ep = 2.36 MeV (a) and 2.48 MeV (b) fitted with γ-ray components which cascade through the bound states of ^{15}O and including as a component the 'background' spectrum taken at Ep = 2.40 MeV. The extracted intensity of 6.18 MeV γ-ray indicates that the 9.49 and 9.60 MeV levels decay through the 6.18 MeV level.

6. Results

Three sequences of runs were made with the NaI(Tl) detector. The first of these, at 20 keV intervals, was rejected because of the large amount of $^{19}F(p,\alpha\gamma)$ contamination which was apparent after line shape analysis of the spectra. The second sequence (Set 2), at

intervals of 100 keV up to Ep = 2.4 MeV and 20 keV intervals thereafter, was carried out to check the main sources of contamination (believed to be collimators rather than the target) had been removed and Set 3 was subsequently obtained at 20 keV intervals over most of the region using both NaI(Tl) and Ge(Li) detectors.

The excitation functions derived from the NaI(Tl) data of Set 2 and Set 3 were compared with the Ge(Li) detector and coincidence data in two ways. Firstly, the intensities of cascade radiation derived from the Ge(Li) detector measurements and the coincidence measurements with nitrided tantalum targets were compared with the raw NaI data before correction for the target 'tail' was made. Secondly, the ground state yield determined with the Ge(Li) detector and the cascade yields from the coincidence measurements using the adenine target were compared with the corrected NaI data. The cascade yields were extracted by line shape analysis of the coincidence spectra and compared, after appropriate correction for the relative efficiency of the coincidence arrangement, by normalizing to the NaI result for the 5.24 MeV γ-ray yield at 2.36 MeV.

(1). The ground state γ-ray

Figure 4.7 shows the excitation function of the ground state γ-ray. The upper curve is a raw yield curve which includes the contribution due to resonances excited deep in the target and the lower curves show the two results obtained for the 'thin target' yield by subtracting the contribution from the tail of the target. The apparent discrepancy between the Set 2 and Set 3 corrected results in the vicinity of 2.5 MeV is due to the few points recorded in this region for Set 2 and a small energy shift between the two runs. The data of Set 3 are preferred because sufficient points were taken to define the narrow resonance region but the corrected result of Set 2 is included to assess the overall accuracy of the results where Set 2 and 3 can be compared, viz., below and above the narrow resonances. The thin target yield shows significant reduction of intensity above Ep = 2.40 MeV compared to that of the thick target yield; this is because the 9.49 and 9.60 MeV levels which were excited deep in the target decay mostly to the ground state. The shape of the thin target yield is in agreement with the reference (EV 67) in which only dotted line was shown for proton energies above 2.6 MeV.

Figure 4.7

The excitation function of the ground state and the 5.24 MeV gamma-ray, showing the raw NaI result and the yields corrected for nitrogen distribution.

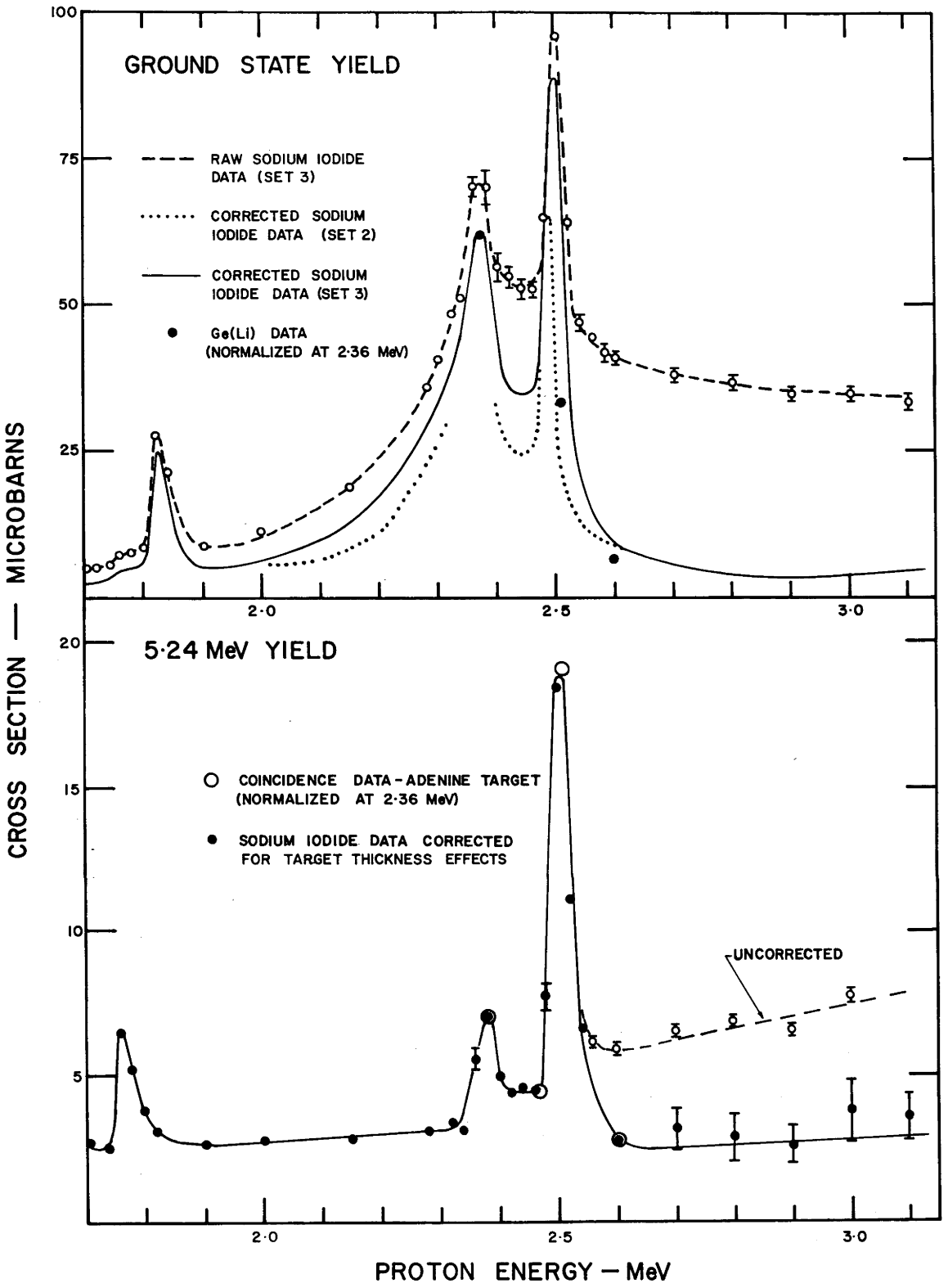
GROUND STATE YIELD
RAW SODIUM IODIDE DATA (SET 3)
CORRECTED SODIUM IODIDE DATA (SET 2)
CORRECTED SODIUM IODIDE DATA (SET 3)
Ge(Li) DATA (NORMALIZED AT 2·36 MeV)
5·24 MeV YIELD
COINCIDENCE DATA - ADENINE TARGET (NORMALIZED AT 2·36 MeV)
SODIUM IODIDE DATA CORRECTED FOR TARGET THICKNESS EFFECTS
UNCORRECTED
CROSS SECTION — MICROBARNS
PROTON ENERGY — MeV
100
75
50
25
20
15
10
5
2·0
2·5
3·0

Figure 4.8

The excitation function of the 6.79 MeV gamma-ray.

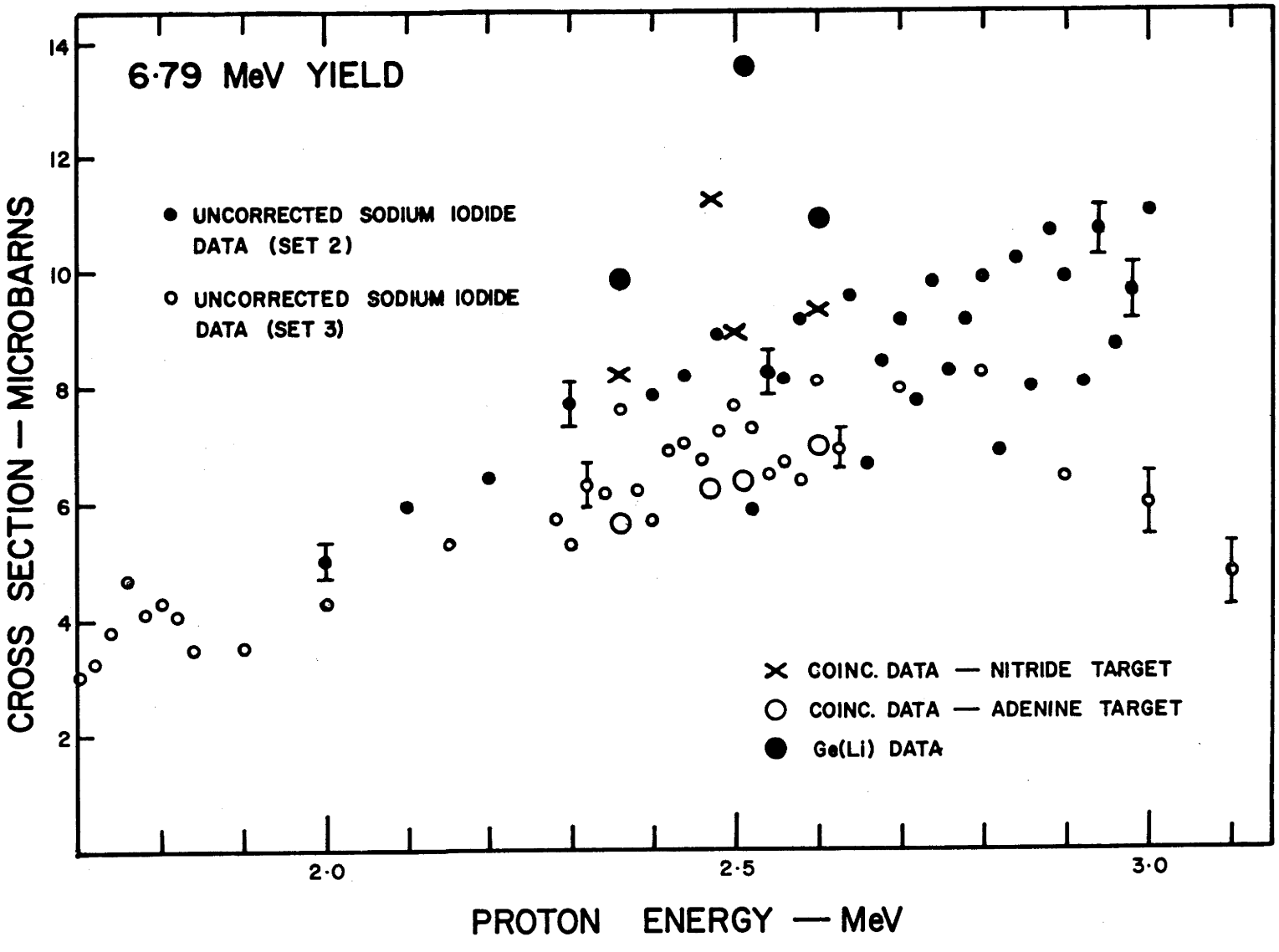
6·79 MeV YIELD
UNCORRECTED SODIUM IODIDE DATA (SET 2)
UNCORRECTED SODIUM IODIDE DATA (SET 3)
COINC. DATA — NITRIDE TARGET
COINC. DATA — ADENINE TARGET
Ge(Li) DATA
CROSS SECTION — MICROBARNS
PROTON ENERGY — MeV
14
12
10
8
6
4
2
2·0
2·5
3·0

Figure 4.9

The excitation function for the 6.13 MeV γ-ray (^{19}F contamination) is shown giving an upper limit for the 6.18 MeV γ-ray (^{15}O).

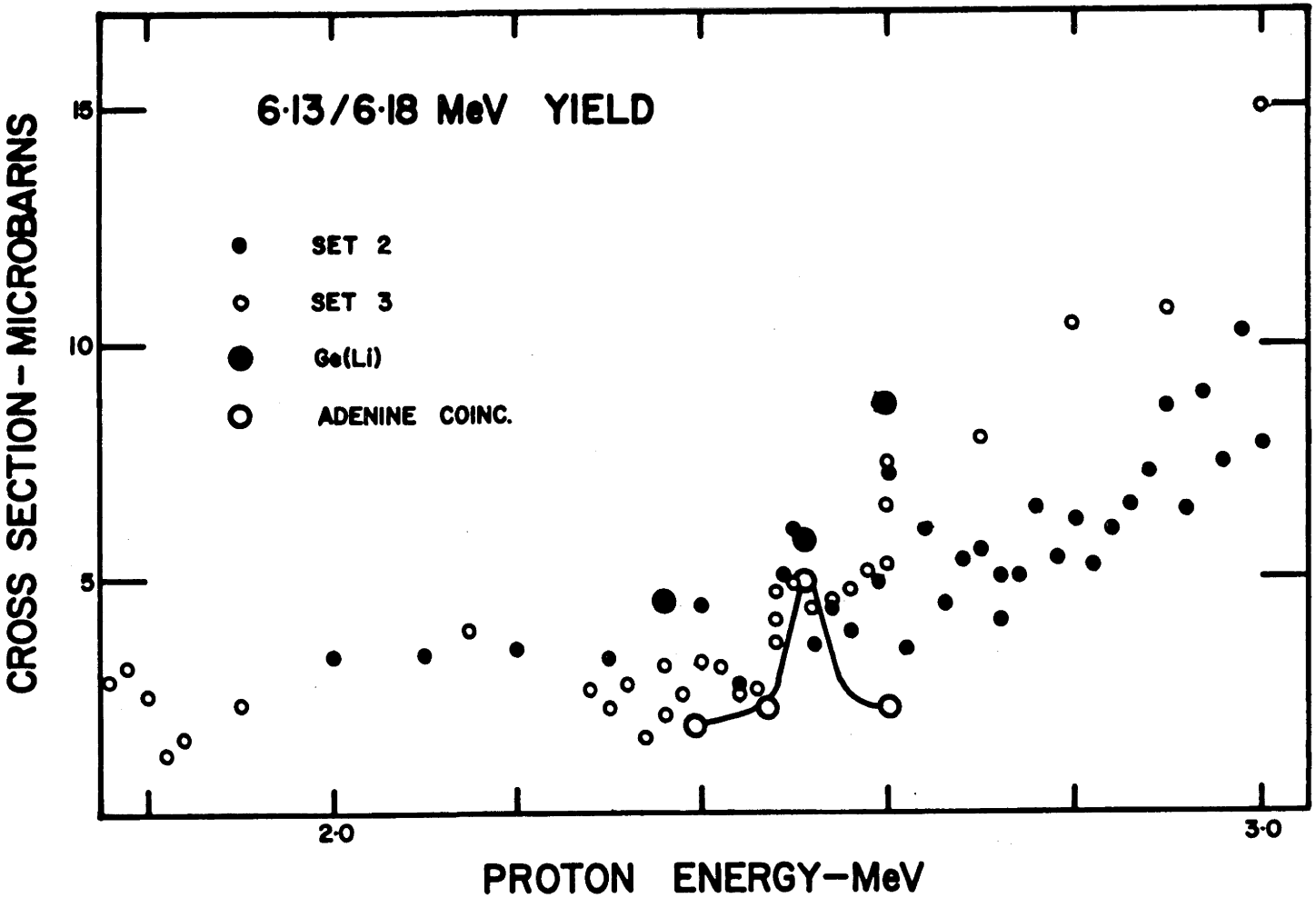
6·13/6·18 MeV YIELD
SET 2
SET 3
Ge(Li)
ADENINE COINC.
CROSS SECTION-MICROBARNS
15
10
5
2·0
3·0
PROTON ENERGY-MeV

As shown in the figure, the Ge(Li) data gave reasonable agreement with the corrected result of the NaI data from line shape analysis.

(2). The 6.79 MeV γ-ray

The results obtained for the excitation function of the 6.79 MeV γ-ray are given in Figure 4.8. Although both runs show considerable scatter, it is evident that there is no structure in the 6.79 MeV γ-ray yield and that the yield rises slowly with energy. These results are in accord with the view that the 6.79 MeV γ-ray is mainly due to direct capture (HE 63, EV 67).

The Ge(Li) data are slightly higher than the average cross section, however, the coincidence data taken with both adenine and nitride target agree fairly well with singles NaI data.

(3). The 6.18 MeV γ-ray

The excitation function for the 6.13 MeV γ-ray is shown in Figure 4.9. The extracted cross section gives only an upper limit for the 6.18 MeV γ-ray. The actual cross section of the 6.18 MeV γ-ray can be estimated by using the branching ratios of the γ-rays de-exciting the 9.60 and the 9.49 MeV levels (EV 67) and the measured ground state and the 5.24 MeV γ-ray cross sections. This estimation gives 15 - 40% of the measured 6.13 MeV γ-ray

cross section as attributed to the 6.18 MeV γ-ray. The scattered data points make it impossible to assess any resonance structure. However, the coincidence data obtained from the adenine target clearly show a resonance at Ep = 2.48 MeV. The observed cross section obtained from coincidence data and singles Ge(Li) data are in reasonable agreement with that of NaI data.

(4). The 5.24 MeV γ-ray

The excitation function of the 5.24 MeV γ-ray is shown in Figure 4.7. The coincidence data from the adenine target give very good agreement with the results for the NaI data. This fact further indicates that the present line shape analysis of NaI data is a satisfactory one. The observed peaks at Ep = 2.36 and 2.48 MeV are in agreement with previous studies (EV 67). The observed peak at Ep = 1.76 MeV is mainly the 5.188 MeV γ-ray cross section due to the resonance at Ep = 1.74 MeV (WA 65a). The slowly rising yields for proton energies above 2.60 MeV could be partly due to the contributions from the 4.43 MeV γ-ray which increases in intensity as the proton energy approaches the 3.12 MeV proton resonance in $^{15}N(p,\alpha\gamma)$ reaction. The non-resonant yield underlying the resonances is about 2.5 μb corresponding to a cross section factor of about 0.5 keV barn in proton energy region of 2.0 to 2.5 MeV.

(5). The resonance levels

The decay of the resonances at 2.36 and 2.48 MeV as derived from the coincidence and NaI measurements of the present work are in reasonable quantitative agreement with Evans (EV 67) with regard to the relative strengths of branches to various ^{15}O states but differ in some important respects at the lower resonance. In particular, Evans reported 2.75 and 1.62 MeV γ-rays corresponding to excitation and decay of the 6.86 MeV level both at and below the resonance whereas the present work finds no evidence for these low energy γ-rays. Likewise, Evans reported appreciable excitation of the 7.28 MeV level. Both levels (6.86 and 7.28) decay via the 5.24 MeV level but the present coincidence results find no surplus 5.24 MeV intensity in addition to that required by the intensity of the 4.25 MeV gamma-ray which feeds the 5.24 MeV level directly. The low energy gamma-rays, which serve as the most direct indication of whether or not the 6.86 and 7.28 MeV levels are excited, are obscured completely in the NaI spectra by the intense 4.43 MeV radiation and to only a slightly lesser extent in the Ge(Li) spectra since the primary γ-rays are broadened by the target thickness. Some low energy gamma rays were evident in the Ge(Li) spectra but did not appear to be associated with the $^{14}N(p,\gamma)$ reaction because their

intensities were not correlated with the intensities of the higher energy gamma-rays at the various bombarding energies.

The coincidence measurements made with the adenine target reveal only one gamma-ray at about 2.8 MeV (depending on bombarding energy) which corresponds to the transition feeding the 6.79 MeV level (Figure 4.6.c). A small peak at about 1.6 MeV results from random coincidences and is due to the strong 1.63 MeV radiation from the contaminant $^{23}Na(p,\alpha\gamma)$ reaction. On the other hand, the coincidence measurements with the nitrided tantalum (Figure 4.6.d) show many peaks below the 2.8 MeV transition and the energies of these peaks are in close agreement with those observed by Evans. Clearly these gamma-rays are associated with contamination, probably of the tantalum since Evans also used tantalum backings.

The excitation functions of the ground state, 6.79, 6.18 and 5.24 MeV γ-rays of the present measurements indicate that the decay of the broad level centered at Ep = 2.40 MeV is mostly direct to the ground state.

7. Discussion

The measured cross section of the ground state γ-ray which comprised the main yield of total γ-ray intensity is comparable to the corrected integrated total cross

section of Duncan et al. (DU 51). The correction to the cross section of Duncan et al. has been discussed by Hebbard et al. (HE 63).

The ground state and the 5.2 MeV γ-ray transitions were found previously (HE 63) to be not as important in the estimation of the total cross section factor at stellar proton energies as the 6.18 and 6.79 MeV γ-ray transitions. The present data obtained for the 6.18 and 6.79 MeV γ-ray cross section are considered too inaccurate to attempt any detailed analysis directed toward corrections of available estimates for the $^{14}N(p,\gamma)$ reaction rate at stellar proton energies. The cross section factors ($S = \sigma E_{CM} \exp(2\pi\eta)$ where η is the Coulomb parameter) calculated for the 6.18 MeV transition (regarded as an upper limit only) and the 6.79 MeV transition, using in each case the uncorrected NaI data, are within 20 - 30% of the values found by Hebbard et al. (HE 63) for the proton energy region 700 - 1000 keV. The result of the present work appears to be that only the ground state is excited by the broad level at Ep = 2.40 MeV whereas the transitions to 5.24, 6.18 and 6.79 MeV levels arise from a direct capture process between resonances. Indeed resonance excitation of the 6.79 MeV was not observed at all within the energy range of the present work. In a simple approach, this would mean that

the contributions from distant broad resonances are not important in determining methods of extrapolation of the cross section factors to zero proton energy.

Perhaps the most important feature of the present measurements is the positive demonstration of the difficulties introduced by the use of the nitrided tantalum targets. For the present work, strong contributions from the 2.36 MeV resonance were observed at the highest bombarding energy of 3.0 MeV. Thus appreciable nitrogen is present at depth beyond 14 mgm/cm^2. This effect can be observed in the region of Ep between 2.4 and 3.0 MeV since both of the resonances at 2.36 and 2.48 MeV decay strongly to the ground state. The low energy measurements of Hebbard et al. (HE 63) used corrections deduced indirectly from fits to the 6.79 MeV cross section factor. Neither the 278 keV resonance (only 3% to the ground state) nor measurements of the 429 keV resonance of the $^{15}N(p,\alpha\gamma)$ reaction are sufficiently sensitive to probe the nitrogen distribution deep in the target. The latter reaction is unsuitable because of the uncertainty of the tail of the higher resonance at 900 keV. Comparison of the target distribution measurement of the present work (Figure 4.3) and that of Hebbard et al. (HE 63) shows that their target was thicker so far as the front layer was

concerned and the tail beyond the resonance anomaly higher by 30 - 40%. In so far as the corrections required are large, as much as a factor of 2 (HE 63), and could have applied to a larger energy range than was appreciated, it is felt that re-measurement of the low energy data, using targets other than nitrided tantalum, is necessary to resolve the existing ambiguities of the cross section factor in that region. The depth of 14 mgm/cm^2 observed in the present target would mean that contributions from the 278 keV resonance would result in all data points up to at least 1100 keV.

In the light of experience from the present work, such a re-measurement would be best made using a coincidence arrangement to eliminate many of the uncertainties introduced by singles spectra and with targets other than nitrided tantalum. Estimates of the coincidence yield show that the count rate would be adequate.

FIGURE CAPTIONS

Figure 4.1 Energy levels and decay scheme of ^{15}O.

Figure 4.2 Experimental arrangement for the coincidence measurements.

Figure 4.3 The excitation function of the 4.43 MeV γ-ray from the $^{15}N(p,\alpha\gamma)$ reaction in the tantalum nitride target used for the $^{14}N(p,\gamma)$ measurements (Set 2 and 3).

Figure 4.4 NaI(Tl) spectra of the $^{14}N(p,\gamma)$ reaction at Ep = 1.80, 2.48 and 2.90 MeV. Circles are the data and least squares line shape fit is the solid line.

Figure 4.5 Ge(Li) spectra of the $^{14}N(p,\gamma)$ reaction at Ep = 2.51 and 2.60 MeV.

Figure 4.6 Coincidence spectra measured with an adenine target, (a) Ep = 2.36 MeV, (b) Ep = 2.48 MeV, (c) Ep = 2.60 MeV and a TaN target (d) Ep = 2.48 MeV.

(a) and (b) were fitted with γ-ray components which cascade through the bound states of ^{15}O and including as a component the background spectrum taken at Ep = 2.40 MeV. It is apparent that spectrum (d) corresponds to an energy just off resonance.

Figure 4.7 The excitation function of the ground state and the 5.24 MeV gamma-ray, showing the raw NaI result and the yields corrected for nitrogen distribution.

Figure 4.8 The excitation function of the 6.79 MeV gamma-ray.

Figure 4.9 The excitation function for the 6.13 MeV γ-ray (^{19}F contamination) is shown giving an upper limit for the 6.18 MeV γ-ray (^{15}O).

CHAPTER V

THE 20 c.c. Ge(Li) DETECTOR

1. Introduction

Lithium drifted germanium detectors are becoming increasingly important in the field of γ-ray spectroscopy because of their high resolution. Their fabrication, characteristics and applications have been discussed in detail by Goulding (GO 66a), Mayer (MA 66) and Hollander (HO 66).

The lithium drift process produces a region of intrinsic type material which is sensitive to nuclear radiation. To obtain good efficiency, larger active volumes are desirable. The method of coaxial lithium-drift has resulted in the production of germanium γ-ray detectors with many times larger sensitive volumes than that possible by using a planar method of drift.

A low energy γ-ray incident on the sensitive volume may be absorbed by photoelectric effect or be Compton scattered. At higher γ-ray energies, above 1.022 MeV, it is also possible to have γ-ray absorption by pair production. The hole-electron pairs produced by electrons resulting from these processes are separated

and collected by an electric field applied across the detector.

The direct collection of charge is in striking contrast with the method employed by scintillation detectors, in which the scintillation mechanisms, light collection and photoelectron emission result in large statistical fluctuations in the number of photo-electrons emitted from the cathode of photomultiplier for a given amount of γ-ray energy deposited. The inefficiency of the scintillator-photomultiplier systems requires more than 300 eV of energy absorbed in the crystal to release a photo-electron while in average semiconductor detectors, a hole-electron pair is produced for only about 3 eV of photon energy absorbed. For this reason, statistical fluctuations in the charge production process in Ge(Li) detector are small and high resolution is possible.

The high resolution provided by the Ge(Li) detector enables accurate determination of γ-ray energies and thus of level energies. Precise determination of these energies makes it possible to deduce the decay scheme of a capture resonance level from one singles spectrum otherwise many NaI(Tl) coincidence spectra would be required to attain a comparable result. A doublet of energy levels separated by the order of 20 keV can be

Figure 5.1

The A.N.U. 20 c.c. lithium drifted germanium detector is drawn to scale, the shaded part indicates the volume that is not depleted by the coaxial drift process.

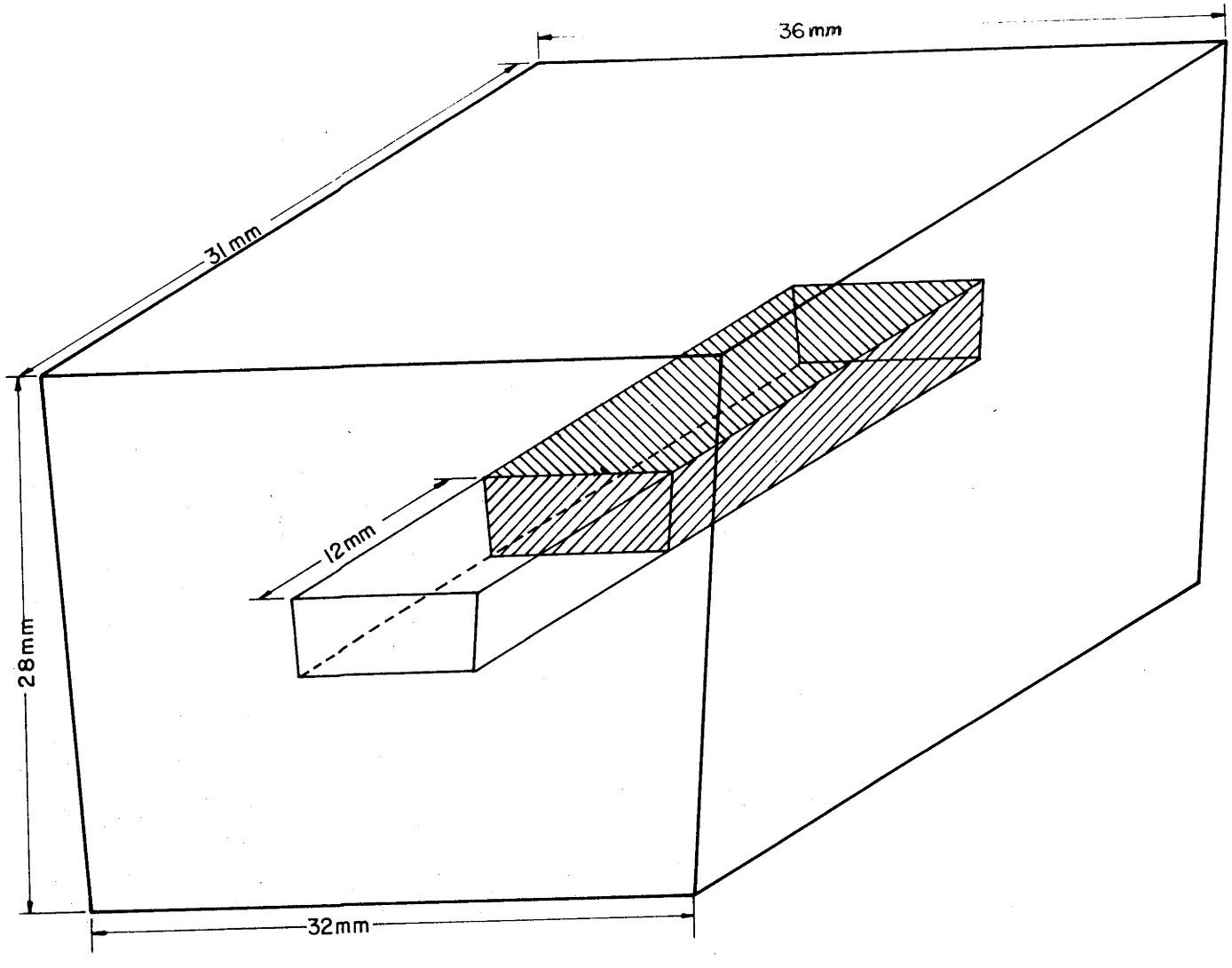
36 mm
31 mm
12 mm
28 mm
32 mm

well resolved by Ge(Li) detector which can determine level energies with a precision of 1 keV, and the word 'doublet' is hardly applicable to them.

In γ-ray angular correlation measurements with NaI(Tl) crystals it is highly likely that the window set to select the γ-rays of the cascade studied may contain other unsuspected peaks hidden under the main peak. A prior measurement with a Ge(Li) detector will resolve these peaks and allow a more justified choice of γ-rays for angular correlation measurement with NaI(Tl) detectors.

The purpose of the present work was to investigate the performance and characteristics of the newly acquired 20 c.c. coaxially drifted Ge(Li) detector and apply it to the study of nuclear reactions which result in the emission of γ-rays. Figure 5.1 shows the trapezoidal and rectangular cross sections of the detector after being drifted approximately 12 m.m. from the front side and each of the four sides. It was operated with a bias voltage of -1200 volts at liquid nitrogen temperature to reduce the leakage current in germanium.

2. Performance of the spectrometer

The characteristics of the coaxial diode as a γ-ray spectrometer were investigated with the system shown in

Figure 5.2

The experimental set up of the Ge(Li) γ-ray spectrometer.

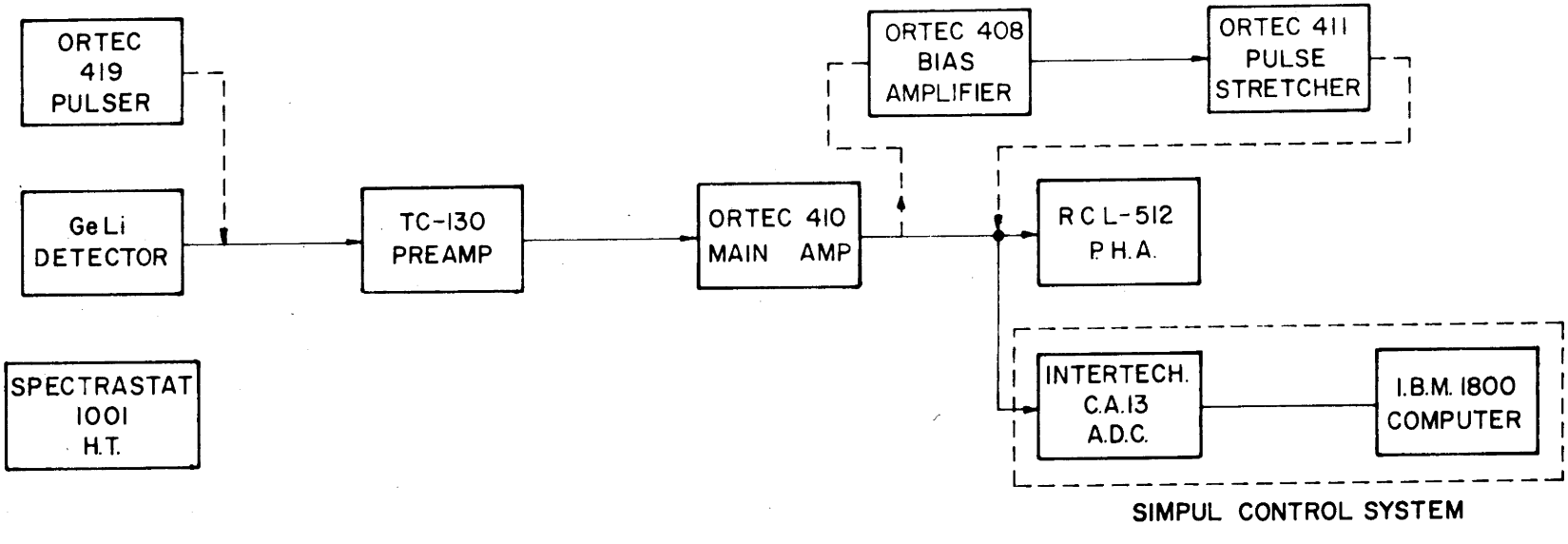

EXPERIMENTAL SETUP OF Ge(Li) γ-RAY SPECTROMETER

Figure 5.2. The SIMPUL program was developed in the Nuclear Physics department to control an Intertechnique CA - 13 analog to digital converter interfaced to an IBM - 1800 digital computer so as to provide a pulse height analyzer of up to 4096 channels. Pulses from the Ge(Li) detector (capacity 17 pf) were amplified by a TC - 130 preamplifier which has at the input field effect transistors operating at room temperature. The signal was further amplified by an ORTEC -410 main amplifier and analyzed and stored in either an RCL-512 channel pulse height analyzer or in the IBM - 1800 computer. Before the SIMPUL system was available, an ORTEC-408 bias amplifier followed by an ORTEC-411 pulse stretcher enabled expansion of small portions of a spectrum. Investigations of the various characteristics of the detection system are described below.

2.1 Resolution

The energy resolution (full width at half maximum) of the detector system for ^{60}Co γ-rays was investigated using various combinations of preamplifiers and main linear amplifiers available in the laboratory. The widths observed for the full energy peak of the 1.333 MeV γ-ray is summarized in Table 5.1.

Figure 5.3

The ^{60}Co spectrum with optimum resolution of 4.2 keV for the 1.333 MeV γ-ray.

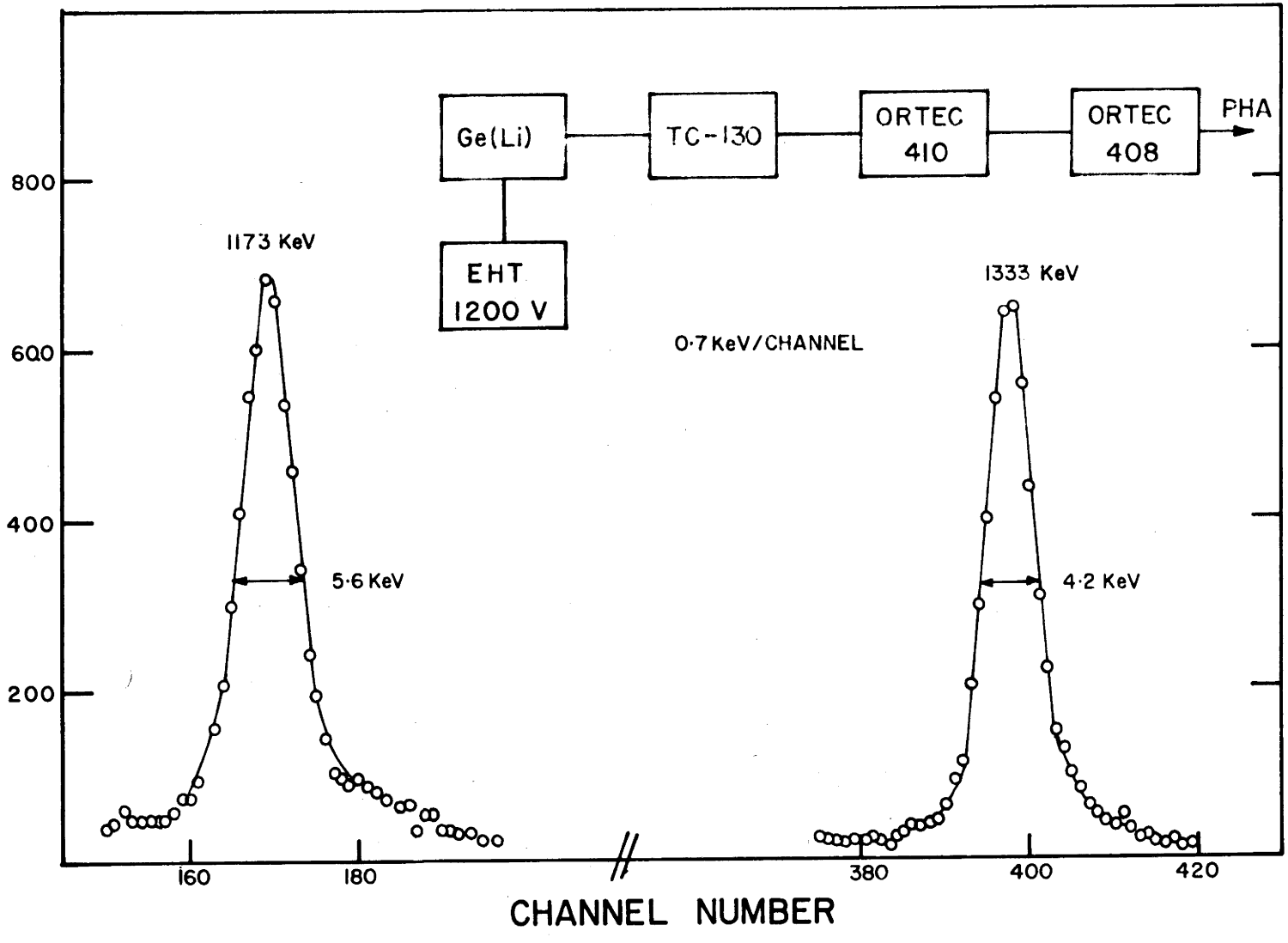
Ge(Li)
TC-130
ORTEC 410
ORTEC 408
PHA
EHT 1200 V
1173 KeV
1333 KeV
0·7 KeV/CHANNEL
5·6 KeV
4·2 KeV
800
600
400
200
160
180
380
400
420
CHANNEL NUMBER

Table 5.1

Resolution

Preamplifier		Main amplifier		Resolution (keV)
Make	Mode	Make	Mode	
ORTEC-103	RC (a)	ORTEC-203	RC	9.6
ORTEC-103	DL (b)	ORTEC-410	RC	8.7
ORTEC-103	DL	ORTEC-410	RC	10.2 (c)
TC-130		ORTEC-410	RC	4.2
ORTEC-109		ORTEC-410	RC	5.5

(a) RC : RC pulse shaping
(b) DL : indicates delay line mode but actually no shaping is done by preamplifier
(c) with pulse stretcher 2 μs.

Figure 5.3 shows the ^{60}Co spectrum corresponding to the best resolution obtained with the TC-130 and ORTEC-410 combination. The main amplifier was found to require integration and differentiation time constants of 2 μs - 2 μs - 1 μs for optimum resoltuion.

Factors that determine the energy resolution of a germanium detector system have been discussed by Goulding (GO 66a). These include:

(1) statistical spread in the detector signal

(2) noise in the associated electronic system, i.e., preamplifier and main amplifier

(3) noise due to detector leakage current.

For a given system, the latter two factors are constant whereas the first factor depends on the incident

Figure 5.4

Comparison of the line width of the full energy peak of a 10.76 MeV γ-ray to that of a 1.78 MeV γ-ray obtained in the same spectrum.

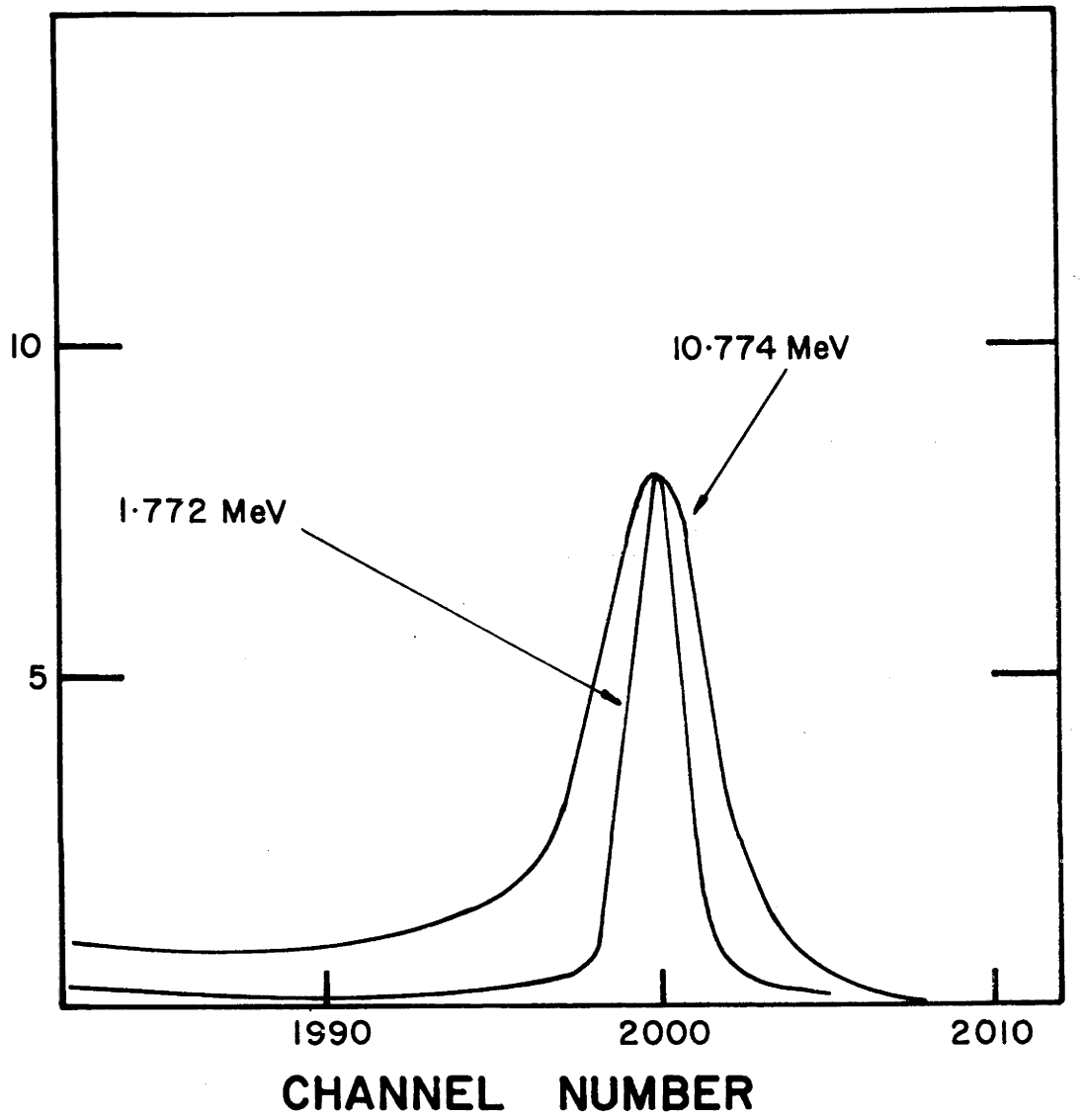
10
5
10·774 MeV
1·772 MeV
1990
2000
2010
CHANNEL NUMBER

γ-ray energy. At low energies, the statistical spread due to the electron-hole production mechanism is usually small compared with the amplifier noise, so that the observed line widths (typically 2 to 3 keV) are mainly due to noise associated with electronic system and detector leakage current. At higher energies, the square of the line width increases linearly with energy, as shown in equation (5.1).

$$(FWHM)^2 = F(E\gamma/\epsilon) \quad \ldots\ldots (5.1)$$

where E_γ = gamma energy absorbed by the detector

ϵ = average energy required to produce a hole-electron pair (~ 2.85 eV for germanium)

F = Fano factor.

The slope of the plot of $(\text{resolution})^2$ versus energy establishes the 'Fano factor' which would be zero if there were no statistical fluctuation in the amount of charge produced and collected per unit energy of γ-ray absorbed. Figure 5.4 shows the line widths of the full energy peaks of 10.76 and 1.78 MeV γ-rays after the full energy peaks have been normalized to the same height. The γ-ray line widths were obtained from a spectrum of the $^{27}Al(p,\gamma)^{28}Si$ resonance at Ep = 992 keV (AZ 66) using a 5 keV thick target. The width of 10.76 MeV γ-ray is 22 keV and is 2.5 times that of 1.78 MeV γ-ray as one would expect from equation (5.1). The line widths

obtained from nuclear reactions are broader than those obtained from sources due to Doppler effect. For a given (p,γ) reaction, the line widths are also affected by the thickness of the target used, a thick target gives broader peaks than a thin target if the resonance width is broader than the resolution of the system. The counting rate of the detection system also affects the resolution. This was particularly so in collecting the 6.129 MeV γ-ray line shape from $^{19}F(p,\alpha\gamma)^{16}O$ resonance in which the γ-ray yield was very high. Good resolution was obtained by reducing the bombarding proton beam intensity so that no appreciable dead time loss occurred due to very high counting rate. In general, to obtain an optimum resolution it is necessary to keep the dead time loss to within one per cent.

2.2 Energy linearity and calibration

One of the principal functions of a γ-ray spectrometer is to measure radiation energies. The advantage of the high resolution of a Ge(Li) detector over NaI(Tl) detectors is the possibility of more precise determination of γ-ray energies. In fact level energies can be assigned with comparable or even better accuracy than with high resolution magnets. Magnetic spectrometers are superior only in low energy region

Figure 5.5

The ThC" spectrum collected with SIMPUL 2048 channels. Peak energies are from reference (EM 60).

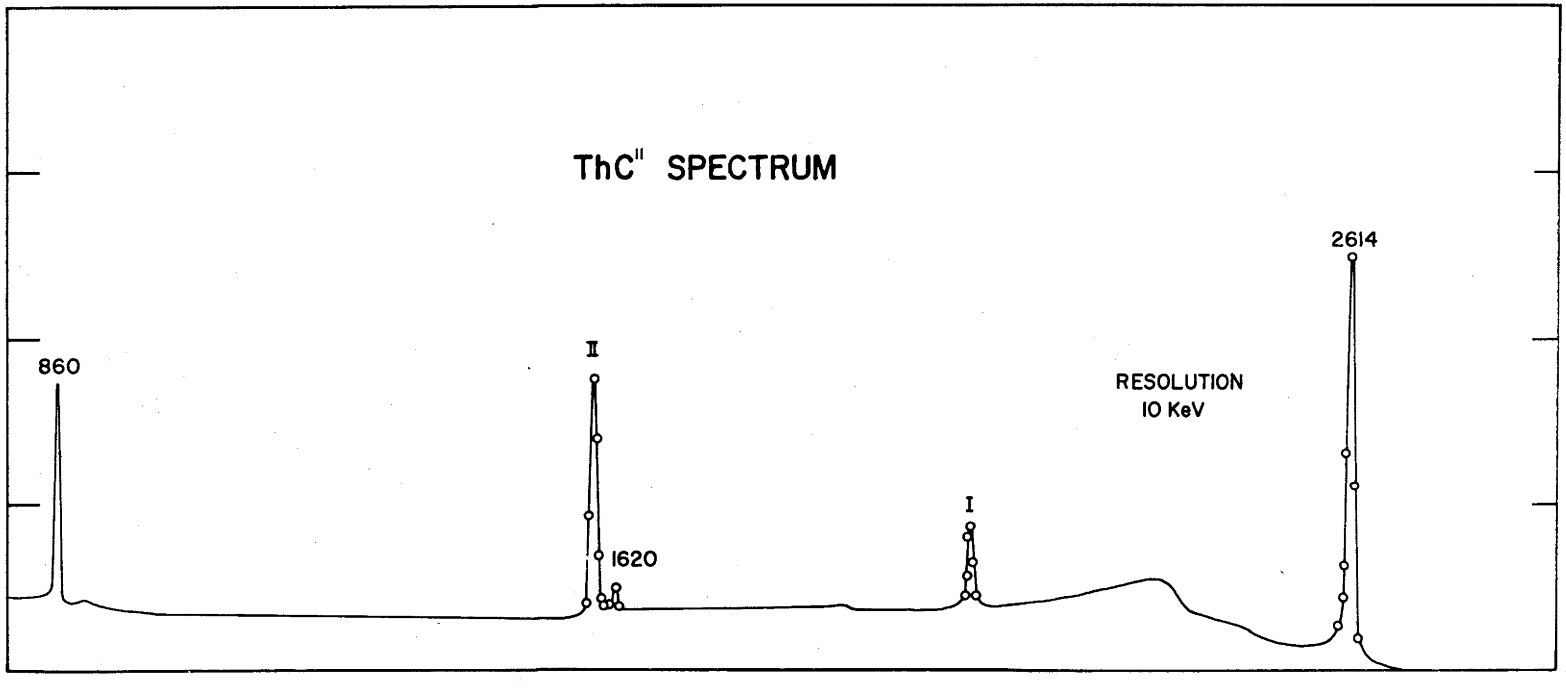
ThC'' SPECTRUM
860
II
1620
I
RESOLUTION
10 KeV
2614

where the electron conversion efficiency is high. Principal sources of error which arise in the energy calibration of a germanium detector system are:

(1) error in determining the peak positions

(2) non-linearity of the pulse height analyzer

(3) uncertainties in Doppler shifts corrections due to limited information of the life times of the levels emitting γ-rays

(4) for (p,γ) reactions the uncertainty in the incident proton energy which is usually known to within 1 or 2 keV and in the Q-value of a particular reaction which may be known to within 2 or 3 keV

(5) gain drifts in the associated electronic amplifier system

To eliminate any possible contribution from the latter three sources of error, a moderately strong γ-ray source of well known γ-ray energies was used to check the linearity of the system. Figure 5.5 shows a spectrum from a 5 mC thorium (B+C'+C") source collected for a period of 20 minutes on SIMPUL system with 2048 channels. The source was also used to check the linearity of the RCL-512 pulse height analyzer and SIMPUL system with 1024 and 4096 channels respectively. The energy calibrations of the two systems were derived with least squares fits

of two parameters (linear : $E = Bx + C$) and three parameters (parabolic : $E = Ax^2 + Bx + C$). The results are shown in Tables 5.2-5.5.

Table 5.2

Linearity of RCL-512 pulse height analyzer (ThC" source)

E (KeV)	Peak position	Linear		Parabolic	
		FIT	FIT-DATA	FIT	FIT-DATA
511.01	104.29	508.95	-2.06	510.33	-0.68
583.14	117.87	583.17	0.03	583.84	0.70
1592.45	303.21	1596.12	3.67	1592.70	0.25
2103.46	396.23	2104.51	1.05	2102.06	-0.50
2614.47	489.04	2611.76	-2.71	2614.68	0.21
A				0.15167×10^{-3}	
B		5.4654		5.3794	
C		-61.035		-52.335	

Differential linearity 2.35%
Integral linearity 0.14%

Table 5.3

Linearity of SIMPUL system 1024 channels (ThC" source)

E (KeV)	Peak position	Linear		Parabolic	
		FIT	FIT-DATA	FIT	FIT-DATA
511.01	185.41	511.24	0.23	510.98	-0.03
583.14	211.39	583.25	0.11	583.12	-0.02
1592.45	575.37	1592.08	-0.37	1592.72	0.27
2103.46	759.63	2102.79	-0.67	2103.37	-0.38
2614.47	944.49	2615.16	0.69	2614.60	0.13
A		2.7716		-0.73249×10^{-5}	
B		2.7716		2.7795	
C		-2.6508		-4.1219	

Differential linearity 0.27%
Integral linearity 0.026%

Table 5.4

Linearity of SIMPUL system 2048 channels (ThC" source)

E (KeV)	Peak position	Linear		Parabolic	
		FIT	FIT-DATA	FIT	FIT-DATA
511.01	370.30	511.18	0.17	511.02	0.01
583.14	422.35	583.20	0.06	583.12	-0.02
1592.45	1151.50	1592.12	-0.33	1592.53	0.08
2103.46	1520.81	2103.13	-0.33	2103.32	-0.14
2614.47	1890.65	2614.87	0.40	2614.52	0.05
A				-0.11616×10^{-5}	
B		1.3836		1.3861	
C		-1.1961		-2.1280	

Differential linearity 0.16%
Integral linearity 0.015%

Table 5.5

Linearity of SIMPUL system 4096 channels (ThC" source)

E (KeV)	Peak position	Linear		Parabolic	
		FIT	FIT-DATA	FIT	FIT-DATA
511.01	743.26	511.13	0.12	510.98	-0.03
583.14	848.25	583.21	0.07	583.13	-0.01
1592.45	2318.24	1592.32	-0.13	1592.71	0.26
2103.46	3062.03	2102.91	-0.55	2103.09	-0.37
2614.47	3807.91	2614.94	0.47	2614.61	0.14
A				-0.27067×10^{-6}	
B		0.68647		0.68764	
C		0.90884		0.02869	

Differential linearity 0.19%
Integral linearity 0.021%

The energies of γ-rays were obtained from reference (MU 65), and the peak positions were determined from a parabolic fit to the three highest points comprising the peak. The degree of uncertainty involved in locating the peak position depends on statistics of each point and on the shape of each peak. With an ORTEC-419 precision pulser the 'peaks' often comprised only of two channels in the spectrum; in this case the peak positions were determined by weighted means according to the counts in each channel. In general, it was possible to determine a peak position to within 0.1 of a channel. The linearity obtained from the precision pulser is shown in Table 5.6 and 5.7.

Before the SIMPUL system was available, an ORTEC-408 biased amplifier and an ORTEC-411 pulse stretcher with an RCL-512 pulse height analyzer were used to collect γ-ray spectra in the energy region of 2.5-5.0 MeV from $^{26}Mg(p,\gamma)^{27}Al$ resonance at Ep = 809 KeV. Table 5.8 shows the linearity of the detection system checked with a pulser.

From Tables 5.2-5.8, it can be seen that better energy calibrations are obtained from parabolic fits for both systems. The necessity for parabolic fitting of channel energies to attain accurate measurement of γ-ray energies was also reported by Van der Leun et al. (VA 67)

Table 5.6

Linearity of RCL-512 pulse height analyzer (pulser)

Pulser dial	Peak position	Linear		Parabolic	
		FIT	FIT-DATA	FIT	FIT-DATA
540	15.93	536.77	-3.23	539.59	-0.41
570	50.07	569.09	-0.91	570.72	0.72
600	82.73	600.01	0.01	600.66	0.66
630	113.90	629.52	-0.48	629.40	-0.60
660	146.80	660.66	0.66	659.90	-0.10
690	178.81	690.96	0.96	689.74	-0.26
720	210.05	720.54	0.54	719.01	-0.99
750	242.90	751.64	1.64	749.96	-0.04
780	275.10	782.12	2.12	780.47	0.47
810	306.20	811.56	1.56	810.09	0.09
840	337.85	841.53	1.53	840.38	0.38
870	369.10	871.11	1.11	870.46	0.46
900	399.94	900.31	0.31	900.28	0.28
930	430.00	928.76	-1.24	929.50	-0.50
960	460.98	958.09	-1.91	959.76	-0.24
990	491.78	987.25	-2.75	990.00	0.00

Differential linearity 7.17%
Integral linearity 0.33%

Table 5.7

Linearity of SIMPUL system 1024 channel (pulser)

Pulser dial	Peak position	Linear		Parabolic	
		FIT	FIT-DATA	FIT	FIT-DATA
50	65.01	50.27	0.27	49.94	-0.06
100	125.98	100.63	0.63	100.44	0.44
150	185.42	149.73	-0.27	149.64	-0.36
200	246.20	199.93	-0.07	199.94	-0.06
250	306.52	249.75	-0.25	249.84	-0.16
300	367.29	299.95	-0.05	300.09	0.09
350	427.70	349.85	-0.15	350.02	0.02
400	488.12	399.75	-0.25	399.95	-0.05
450	548.71	449.80	-0.20	450.00	0.00
500	609.30	499.85	-0.15	500.02	0.02
550	669.73	549.76	-0.24	549.90	-0.10
600	730.78	600.19	0.19	600.27	0.27
650	791.00	649.93	-0.07	649.94	-0.06
700	851.98	700.30	0.30	700.21	0.21
750	911.92	749.81	-0.19	749.61	-0.39
800	973.19	800.42	0.42	800.09	0.09

Differential linearity 1.85%
Integral linearity 0.079%

Table 5.8

Linearity of RCL-512, ORTEC-411 and ORTEC-408 system (pulser)

Pulser dial	Peak position	Linear		Parabolic	
		FIT	FIT-DATA	FIT	FIT-DATA
290	19.60	288.37	-0.63	290.05	0.05
315	65.00	314.36	-0.64	315.10	0.10
340	109.70	339.96	-0.04	339.96	-0.04
365	154.04	365.34	0.34	364.80	-0.20
390	198.96	391.06	1.06	390.16	0.16
415	241.96	415.68	0.68	414.62	-0.38
440	286.06	440.93	0.93	439.88	-0.12
465	329.98	466.08	1.08	465.23	0.23
490	373.33	490.90	0.90	490.43	0.43
515	415.13	514.83	-0.17	514.89	-0.11
540	457.60	539.15	-0.85	539.92	-0.08
565	499.70	563.26	-1.74	564.90	-0.10

Differential linearity 4.34% Integral linearity 0.31%

in their studies of $^{26}Mg(p,\gamma)^{27}Al$ reaction. Ewan and Tavendale (EW 64) have shown that the response of a Ge(Li) detector is linear from 0 to 2600 keV to within the $\pm$ 0.3% accuracy of the precision pulser used for the measurement, so that the non-linearities observed are attributed to the analog to digital converters used in the system. The differential and integral linearity of the Intertechnique CA-13 analog to digital converter used in the SIMPUL system have been investigated in this laboratory by other methods, their values are also listed in the tables.

Unfortunately the thorium source provides only low energy γ-rays. Accordingly, γ-rays from nuclear reactions must be used for high energy calibrations and corrections made for Doppler shifts. In the study of $^{26}Mg(p,\gamma)^{27}Al$ resonance at Ep = 809 keV, a maximum energy shift of 11 keV is possible for an 8 MeV γ-ray if the detector is at 0^{o} to the beam. Nevertheless two good calibration points were obtained in the spectra from the bombardment of ^{26}Mg target, viz., the 511 keV annihilation of radiation and 6.129 MeV γ-rays due to fluorine contamination of the target via the $^{19}F(p,\alpha\gamma)^{16}O$ reaction. The 6.129 MeV level of ^{16}O has a sufficiently long lifetime of about 10^{-11} sec that the energy is not

Doppler shifted since recoiling ^{16}O nuclei have completely stopped before the γ-ray is emitted.

To maintain high resolution during long data runs, more severe requirements in the gain stability of the electronic system are inevitable for Ge(Li) detector systems. Gain shifts in the system cause occasionally broadened peaks or even double peaks for a single γ-ray; these troubles were encountered in the course of study. Adequate gain stability was achieved if the A.D.C. and the associated amplififer system were maintained at a constant room temperature and operated from a well stabilized mains supply.

2.3 Calculation of detector efficiencies and angular correlation attenuation factors

As shown in Figure 5.1, the present detector has an irregular shape and a volume not accurately defined so that calculation of detector efficiencies for given geometries is difficult. In the following calculation, the trapezoidal detector was assumed to be rectangular and to have a completely sensitive volume. These assumptions will naturally result in higher detector efficiencies. The γ-ray mass attenuation coefficients were taken from the tables of Storm, Gilbert and Israel (ST 58) and multiplied by the density of germanium at 77^{o} K (5.325 g/cm^3) to obtain the linear attenuation

coefficients. In using the table, the total absorption for a given γ-ray energy was taken as the sum of τ, σ_α, σ_I and K_T, where

τ = the cross section for the production of photoelectron

σ_α = the absorption component of the total Compton cross section

σ_I = the incoherent scatter component for the total Compton cross section

K_T = the sum of the cross section for pair production in the field of the nucleus and of the atomic electrons.

The linear attenuation coefficients τ and K_T are tabulated in Table 5.9 and shown in Figure 5.6 since these data are used in the calculation of photopeak efficiency and pair production efficiency for comparison with experimental values.

If detector efficiency is defined as the ratio of the number of events detected to the number of γ-rays emitted, the efficiency ϵ can be expressed in terms of the linear total absorption coefficients μ by

$$\epsilon = \frac{1}{4\pi}\int \left\{ 1 - \exp(-\mu S) \right\} \, d\Omega \qquad \ldots\ldots (5.2)$$

where S is the length of path traversed by γ-rays in the detector, and $d\Omega$ is the solid angle subtended at the

Figure 5.6

The linear attenuation coefficients of γ-rays in germanium.

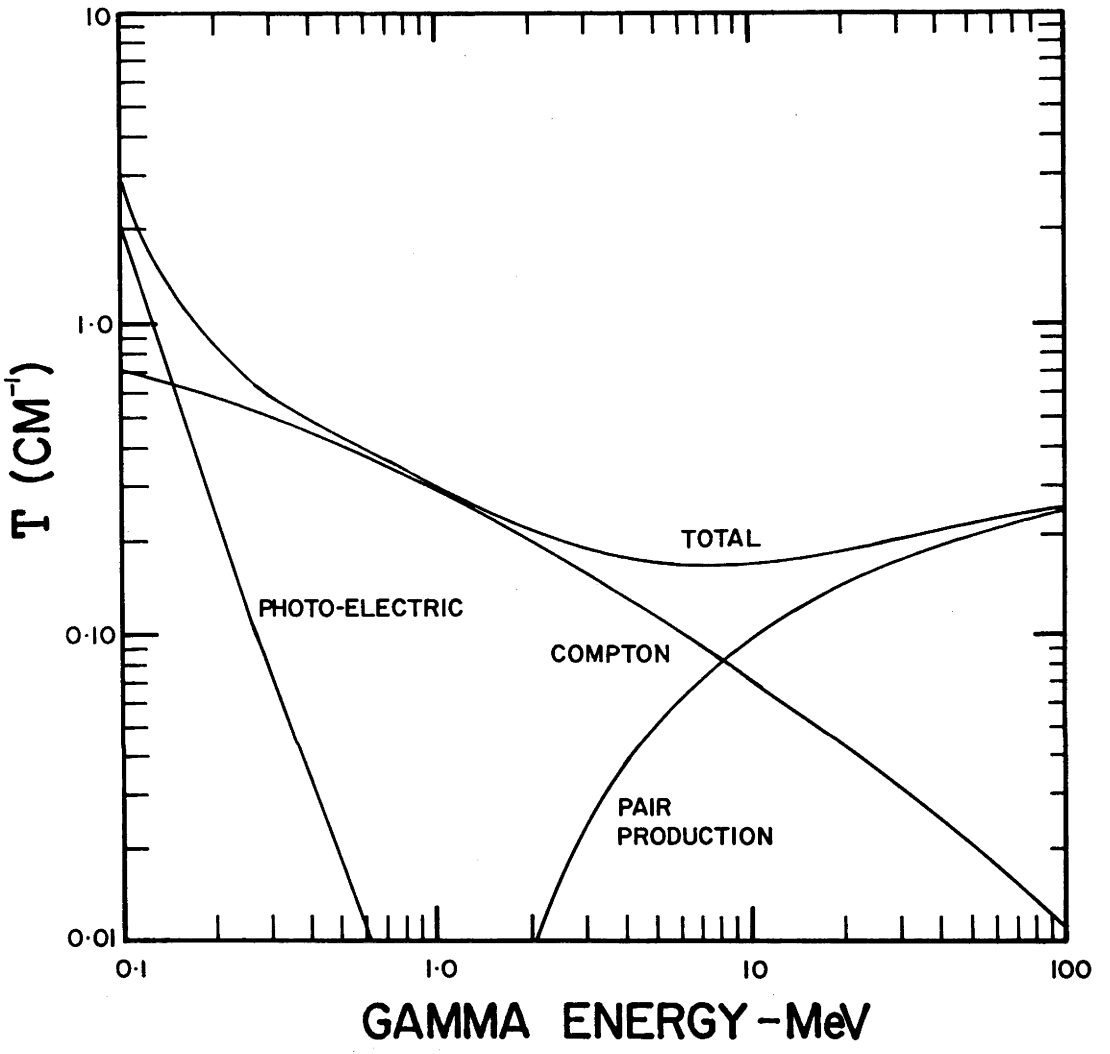
10
1·0
0·10
0·01
T (CM⁻¹)
TOTAL
PHOTO-ELECTRIC
COMPTON
PAIR
PRODUCTION
0·1
1·0
10
100
GAMMA ENERGY - MeV

Table 5.9

Gammay ray attenuation coefficients in germanium (cm^{-1})

E (MeV)	Photo-electric τ	Compton $\sigma=\sigma_\alpha+\sigma_I$	Pair production K_T	Total $\mu=\tau+\sigma+K_T$
0.01	160.815	0.916		161.731
0.015	503.745	0.872		504.617
0.02	226.313	0.880		227.193
0.03	71.355	0.840		72.195
0.04	30.619	0.799		31.418
0.05	15.815	0.809		16.624
0.06	9.372	0.767		10.139
0.08	3.999	0.731		4.730
0.10	2.066	0.699		2.765
0.15	0.586	0.627		1.213
0.20	0.256	0.575		0.831
0.30	0.075	0.500		0.575
0.40	0.034	0.448		0.482
0.50	0.019	0.409		0.428
0.60	0.011	0.378		0.389
0.80	0.0053	0.332		0.337
1.00	0.0037	0.298		0.302
1.50	0.0016	0.242	0.002	0.246
2.00	0.0011	0.207	0.009	0.217
3.00	0.00053	0.162	0.024	0.187
4.00		0.136	0.038	0.174
5.00		0.117	0.051	0.168
6.00		0.104	0.062	0.166
8.00		0.085	0.079	0.164
10.00		0.072	0.094	0.166
15.00		0.053	0.122	0.175
20.00		0.043	0.143	0.186
30.00		0.031	0.172	0.203
40.00		0.025	0.192	0.217
50.00		0.021	0.207	0.228
60.00		0.018	0.219	0.237
80.00		0.014	0.236	0.250
100.00		0.012	0.248	0.260

Figure 5.7

Geometry of a quarter section of a rectangular detector (HO 65).

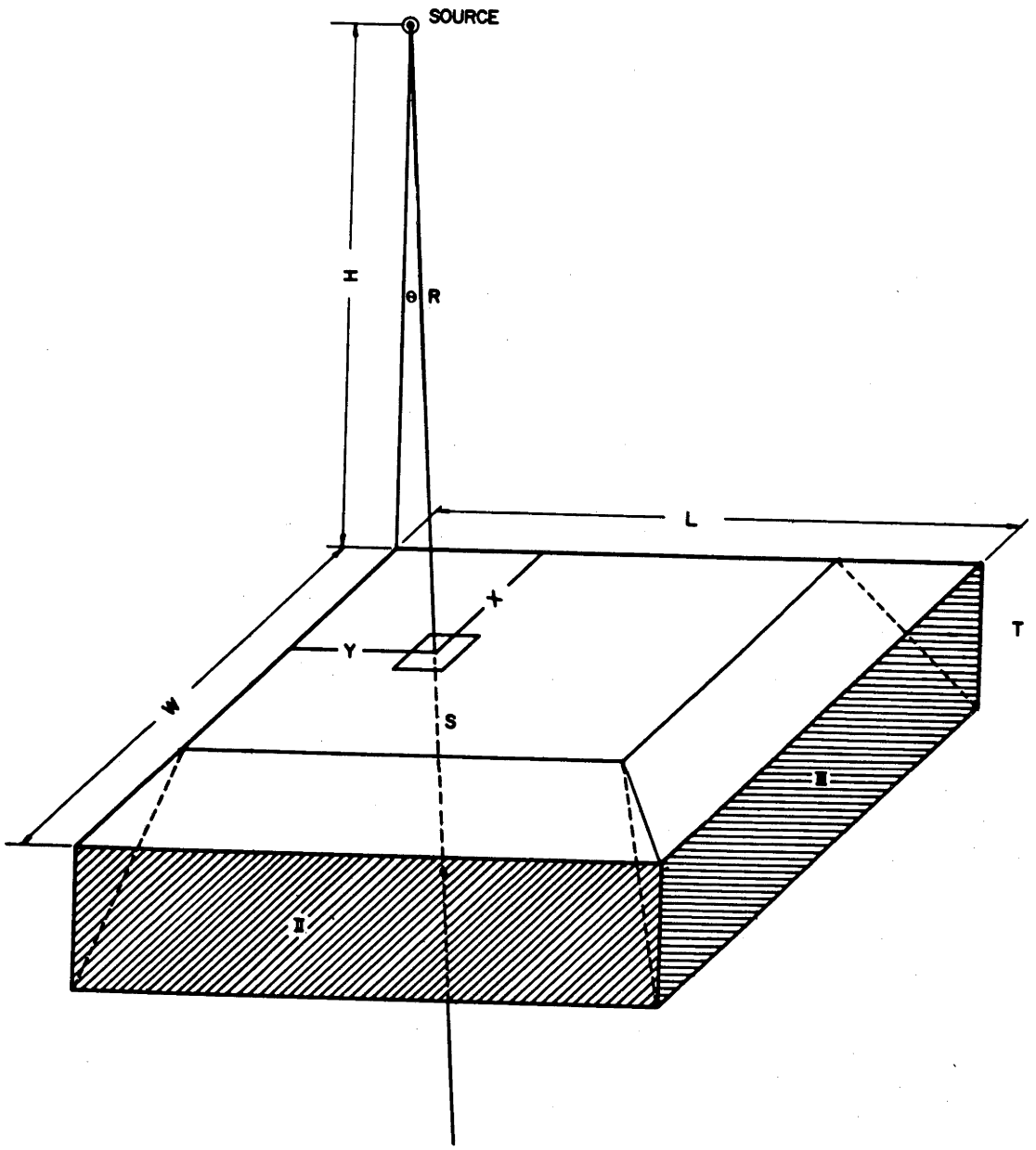
SOURCE
H
θ
R
L
X
Y
W
S
T
II
III

source by the detector. The calculation of a planar drifted Ge(Li) detector with rectangular shape has been carried out by Hotz et al. (HO 65). Their method was to divide a quarter section of the crystal into three regions according to the path of γ-ray through the crystal and perform the integration with respect to the solid angle subtended at each region (see Figure 5.7). The same scheme was used here and the calculations of detector efficiencies (equation 5.3) and angular correlation attenuation factors (equation 5.4) were carried out with a program GEEFFANG (see Appendix) using an IBM-360 computer.

The detector efficiency

$$\varepsilon = \frac{1}{\pi}\left\{ \int_0^{\frac{HW}{H+T}} \int_0^{\frac{HL}{H+T}} \left[1 - \exp\left(-\frac{\mu RT}{H}\right)\right] \frac{H}{R^3} dY dX \right.$$

$$+ \int_{\frac{HW}{H+T}}^{W} \int_0^{\frac{XL}{W}} \left[1 - \exp\left(-\mu R\left\{\frac{W}{X} - 1\right\}\right)\right] \frac{H}{R^3} dY dX$$

$$\left. + \int_{\frac{HL}{H+T}}^{L} \int_0^{\frac{YW}{L}} \left[1 - \exp\left(-\mu R\left\{\frac{L}{Y} - 1\right\}\right)\right] \frac{H}{R^3} dX dY \right\} \quad \ldots\ldots (5.3)$$

The angular correlation attenuation factor

$$Q_\ell = \frac{1}{\pi\epsilon}\left\{\int_0^{\frac{HW}{H+T}}\int_0^{\frac{HL}{H+T}} P_\ell(\text{ocs }\theta)\left[1 - \exp\left(-\frac{\mu RT}{H}\right)\right]\frac{H}{R^3}dYdX\right.$$

$$+ \int_{\frac{HW}{H+T}}^{W}\int_0^{\frac{XL}{W}} P_\ell(\cos\theta)\left[1 - \exp\left(-\mu R\left\{\frac{W}{X}-1\right\}\right)\right]\frac{H}{R^3}dYdX$$

$$\left. + \int_{\frac{HL}{H+T}}^{L}\int_0^{\frac{YW}{L}} P_\ell(\cos\theta)\left[1 - \exp\left(-\mu R\left\{\frac{L}{Y}-1\right\}\right)\right]\frac{H}{R^3}dXdY\right\} \quad \ldots\ldots (5.4)$$

where $R = (X^2 + Y^2 + H^2)^{\frac{1}{2}}$

$P_\ell(\cos\theta) = P_\ell\left(\frac{H}{R}\right)$ are Legendre polynomials.

In equation (5.3) and (5.4), the first term is for a γ-ray which enters the top face and exits through the bottom face, the second term is for a γ-ray entering the top face and leaving through one side and the third term is for a γ-ray entering the top face and leaving through the other side face. The results of calculations are shown in Table 5.10 for source - detector distance of 2.54 cm and 5.0 cm. Figure 5.8 shows the plots of detector efficiencies.

Figure 5.8

Calculated detector efficiencies at 2.54 and 5.0 cm.

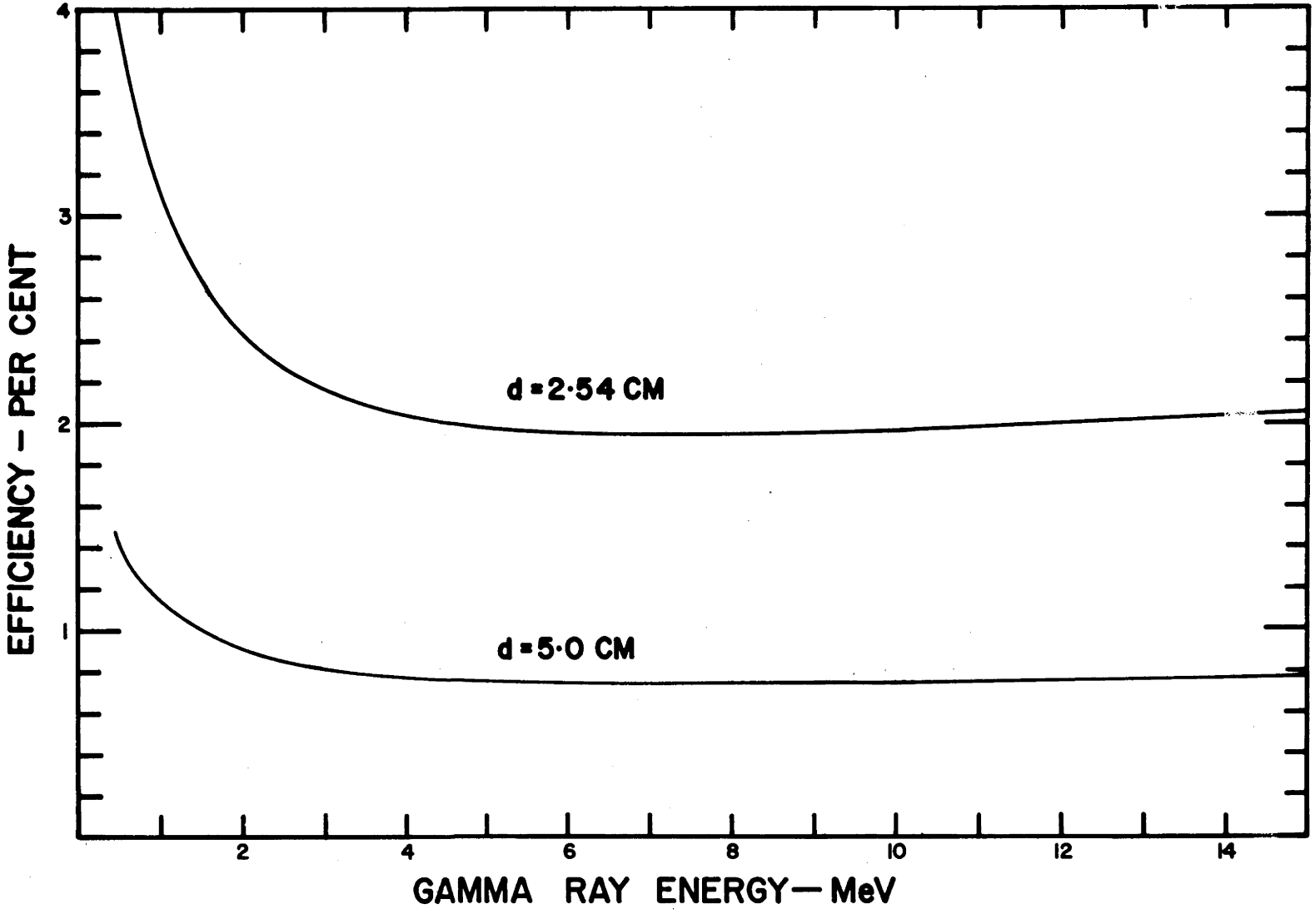
EFFICIENCY – PER CENT
4
3
2
1
d = 2·54 CM
d = 5·0 CM
2
4
6
8
10
12
14
GAMMA RAY ENERGY— MeV

Table 5.10

Detector efficiencies and angular correlation attentuation factors

E (MeV)	2.54 cm			5.00 cm		
	Eff(%)	J_2/J_0	J_4/J_0	Eff(%)	J_2/J_0	J_4/J_0
0.5	3.82	0.8261	0.5073	1.42	0.9362	0.7990
0.6	3.61	0.8275	0.5109	1.35	0.9366	0.8002
0.8	3.30	0.8295	0.5159	1.24	0.9372	0.8020
1.0	3.06	0.8310	0.5194	1.15	0.9376	0.8032
1.5	2.64	0.8332	0.5251	1.00	0.9383	0.8051
2.0	2.40	0.8345	0.5282	0.910	0.9386	0.8062
3.0	2.14	0.8357	0.5313	0.814	0.9390	0.8072
4.0	2.02	0.8363	0.5327	0.770	0.9391	0.8077
5.0	1.96	0.8365	0.5333	0.747	0.9392	0.8079
6.0	1.93	0.8367	0.5336	0.738	0.9392	0.8080
8.0	1.92	0.8367	0.5337	0.734	0.9392	0.8080
10.0	1.94	0.8366	0.5336	0.740	0.9392	0.8080
15.0	2.03	0.8362	0.5325	0.775	0.9391	0.8076

2.4 Photopeak efficiency

The intrinsic full energy peak efficiency of the detector was measured with ^{137}Cs and ^{22}Na sources. Since these were not calibrated standard sources, the source strengths were determined with a 3" x 3" NaI(Tl) scintillation counter for which the detector efficiency and peak to total ratio are well known. Each source was mounted on the axis of the two detectors 5 cm from the Ge(Li) crystal and 10 cm from the NaI(Tl) crystal. Figure 5.9 and Figure 5.10 shows the spectra obtained from ^{137}Cs and ^{22}Na sources respectively. Since the

Figure 5.9

The 662 keV γ-ray spectra measured with a 3" x 3" NaI(Tl) detector (A) and the Ge(Li) detector (B).
(^{137}Cs source).

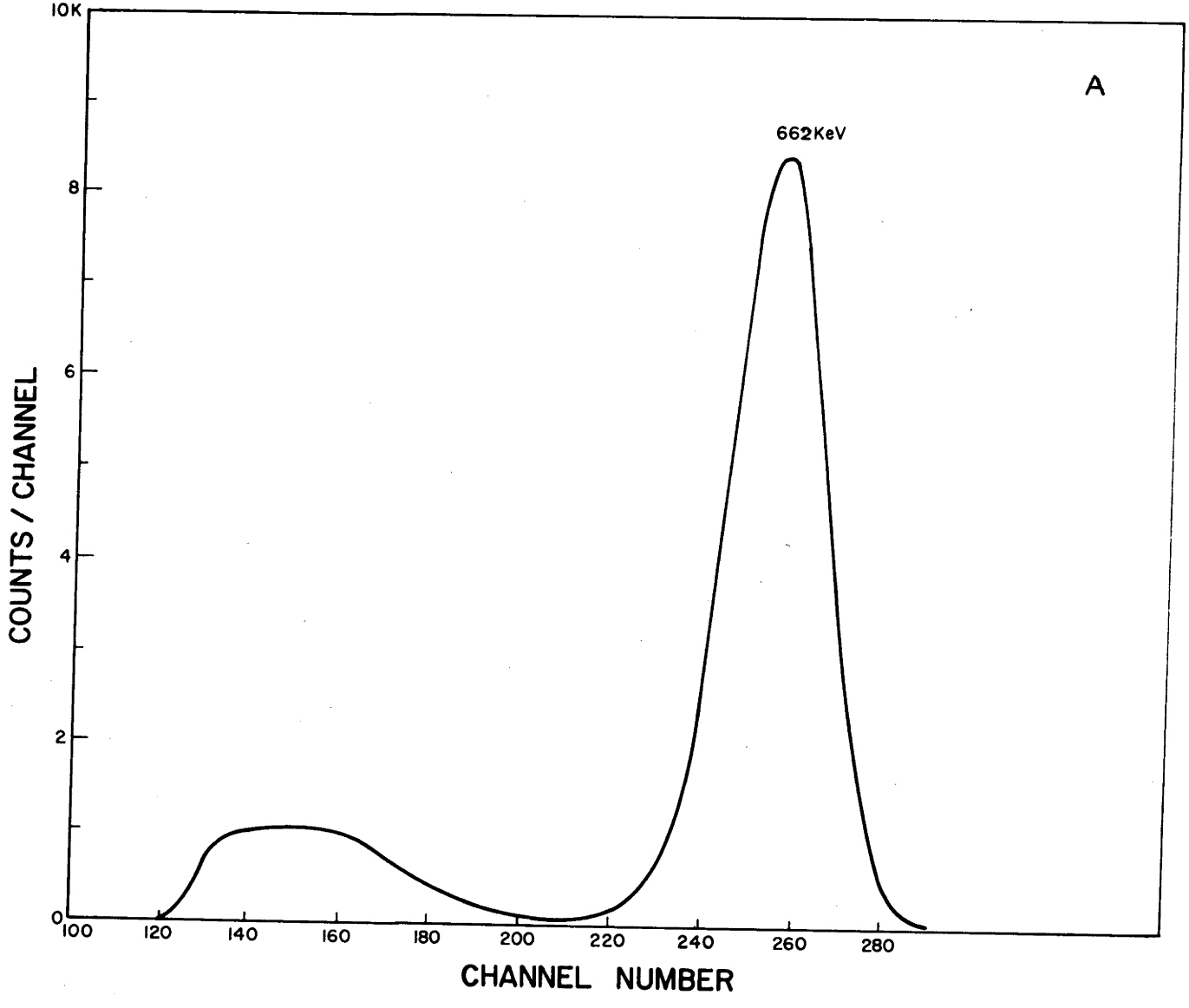
10K
8
6
4
2
0
A
662KeV
COUNTS / CHANNEL
100
120
140
160
180
200
220
240
260
280
CHANNEL NUMBER

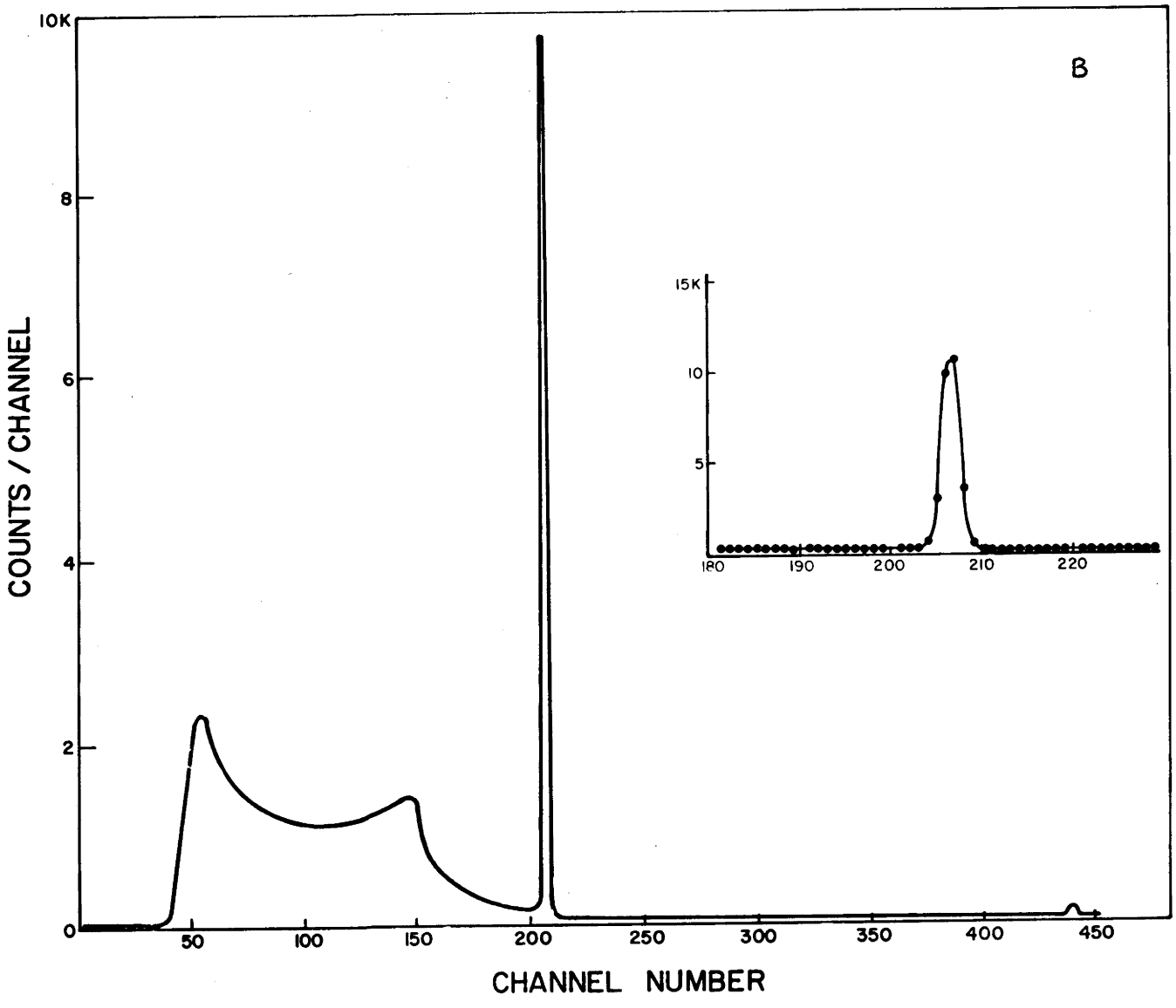
B
10K
8
6
4
2
0
COUNTS / CHANNEL
50
100
150
200
250
300
350
400
450
CHANNEL NUMBER
15K
10
5
180
190
200
210
220

Figure 5.10

The 511 and 1274 keV γ-ray spectra measured with a 3" x 3" NaI(Tl) detector (A) and the Ge(Li) detector (B).
(^{22}Na source).

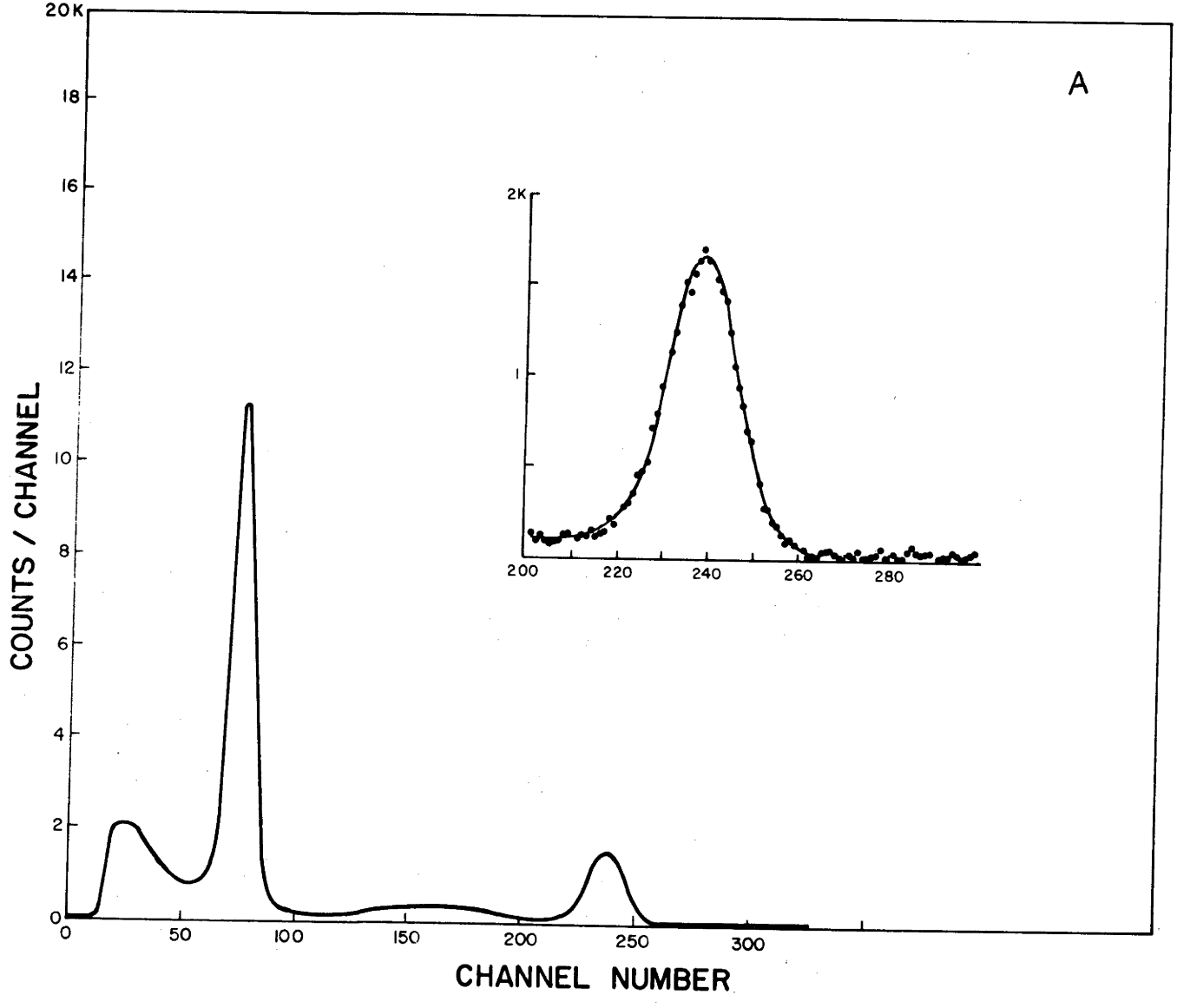
A
20K
18
16
14
12
10
8
6
4
2
0
COUNTS / CHANNEL
0
50
100
150
200
250
300
CHANNEL NUMBER
2K
1
200
220
240
260
280

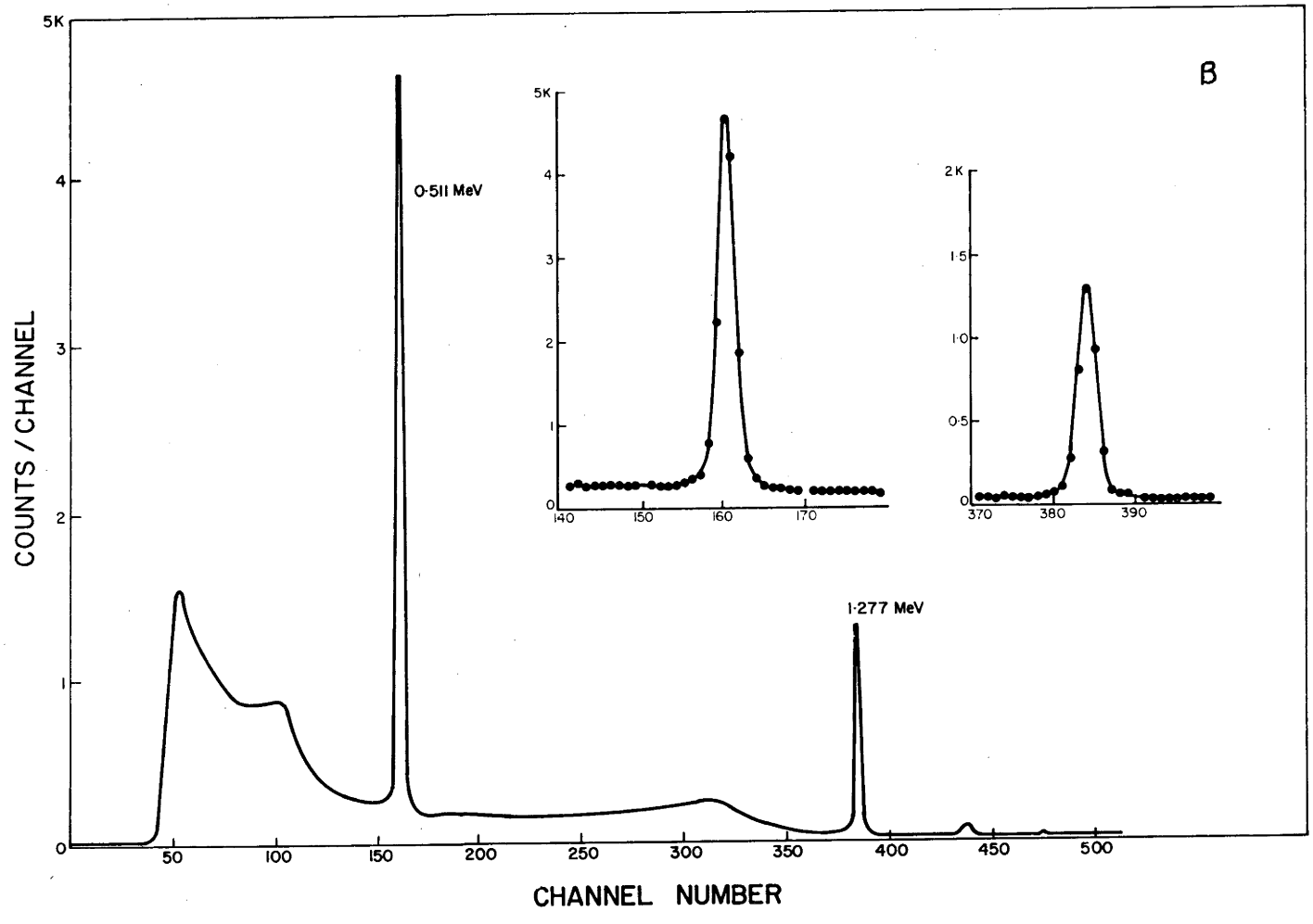
β
0·511 MeV
1·277 MeV
COUNTS / CHANNEL
CHANNEL NUMBER
5K
4
3
2
1
0
50
100
150
200
250
300
350
400
450
500
5K
4
3
2
1
0
140
150
160
170
2K
1·5
1·0
0·5
0
370
380
390

results obtained from these measurements, viz., intrinsic full energy peak efficiencies of the 511, 662 and 1274 keV γ-rays, are used to normalize the relative efficiencies of high energy γ-rays, it is important to measure them as accurately as possible. Table 5.11 shows the experimental results and the calculation used to obtain these values.

The observed counts of full energy peak in column 3 and 4 were obtained by summing the counts comprising the peak and subtracing appropriate background and contributions from higher energy γ-rays, if present. The 3" x 3" NaI(Tl) detector efficiencies and peak to total ratios at 10 cm were obtained from reference (MA 60). A check of the results is provided by the ratio of total 511 and 1274 keV γ-rays emitted by the source; the value obtained from Table 5.11 is 9.3106/5.1706 = 1.801 as compared to the theoretical ratio is 1.796 (EN 62).

For higher energy γ-rays, the relative efficiencies were measured for pairs of γ-rays from nuclear reactions and sources in which the relative intensities of the pairs of γ-rays were well known (Table 5.12). Figure 5.11 shows the plots of the full energy peak efficiency as a function of energy. The high energy end of the curve was extended pair by pair by interpolation and extrapolation until a smooth curve was obtained.

Figure 5.11

The intrinsic full energy peak efficiency of the 20 c.c. Ge(Li) detector.

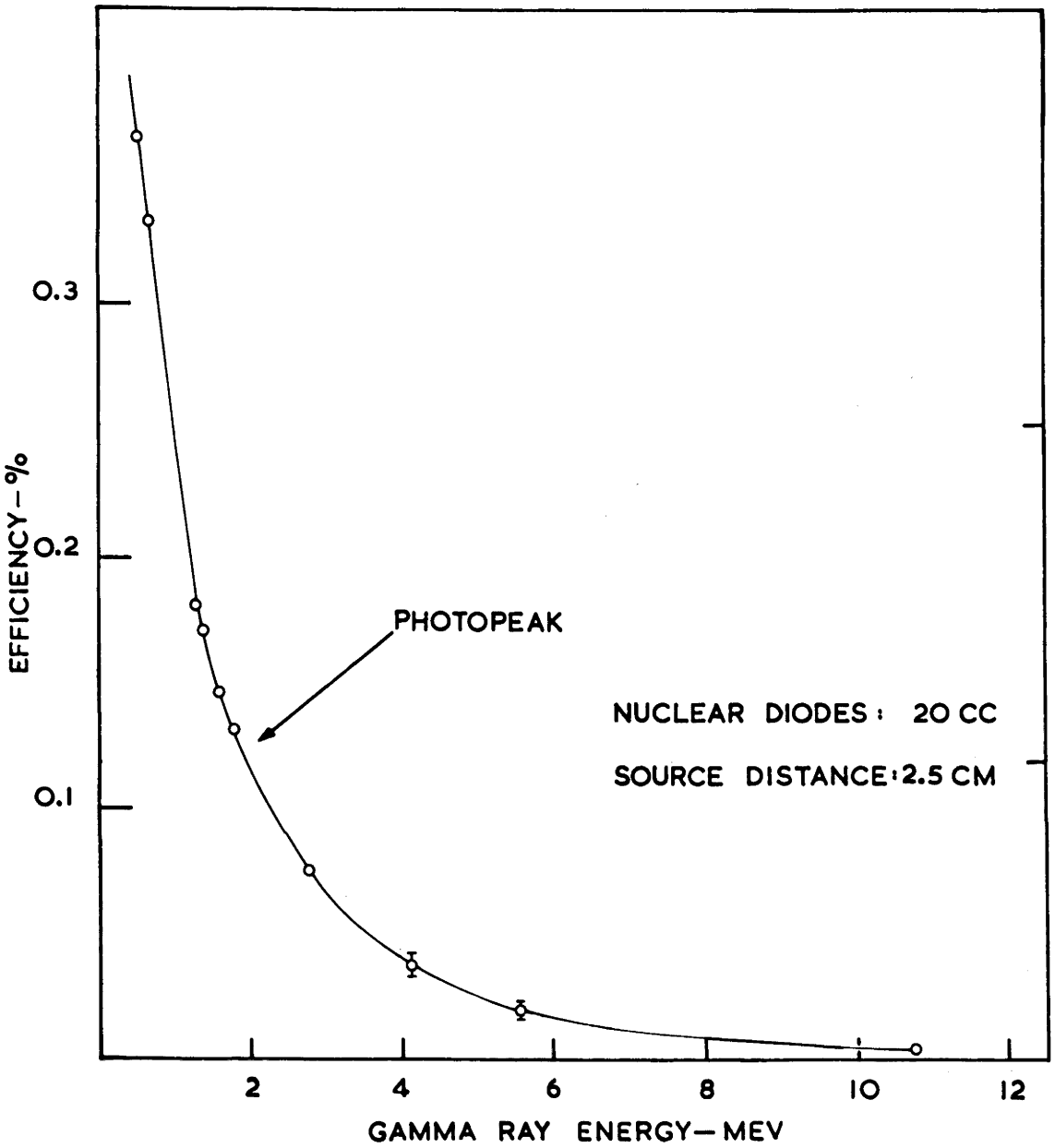
0.3
0.2
0.1
EFFICIENCY – %
PHOTOPEAK
NUCLEAR DIODES : 20 CC
SOURCE DISTANCE : 2.5 CM
2
4
6
8
10
12
GAMMA RAY ENERGY – MEV

Table 5.11

Intrinsic full energy peak efficiencies of 511, 662 and 1274 KeV γ-rays

Source	E_γ keV	Observed counts of full energy peak		Detector eff. 3" X 3" NaI(Tl) at 10 cm	Peak to total ratio 3" X 3" NaI(Tl)	γ-ray intensity emitted from source	Intrinsic full energy peak eff. Ge(Li) %
		NaI(Tl) Ns	Ge(Li) Ng	εs	R	No=Ns/(εsR)	Ng/No
^{22}Na	511	130162	13316	0.02167	0.645	9.3106×10^6	0.1430
^{137}Cs	662	224583	26640	0.02016	0.545	20.435×10^6	0.1304
^{22}Na	1274	30633	3664	0.01669	0.355	5.1701×10^6	0.0709

Table 5.12

Relative intensities of γ-rays

Reaction	Ep(KeV)	$E_{\gamma 1}$	$E_{\gamma 2}$	$E_{\gamma 1}$: $E_{\gamma 2}$
^{60}Co source		1.17	1.33	1 : 1
^{24}Na source		2.75	1.37	1 : 1
$^{26}Mg(p,\gamma)^{27}Al$	662	2.75	5.32	1 : 0.7 (VA 67)
$^{13}C(p,\gamma)^{14}N$	554	4.11	1.63	1 : 0.96 (AJ 59)
$^{27}Al(p,\gamma)^{28}Si$	992	10.76	1.78	1 : 1.22 (AZ 66)

Figure 5.12

The intrinsic full energy peak efficiency of the 20 c.c. Ge(Li) detector is compared with those of 3" x 3" and $1\frac{3}{4}$" x 2" NaI(Tl) crystals. The dotted line shows the calculated photopeak efficiency using the photoelectric cross section of Table 5.9.

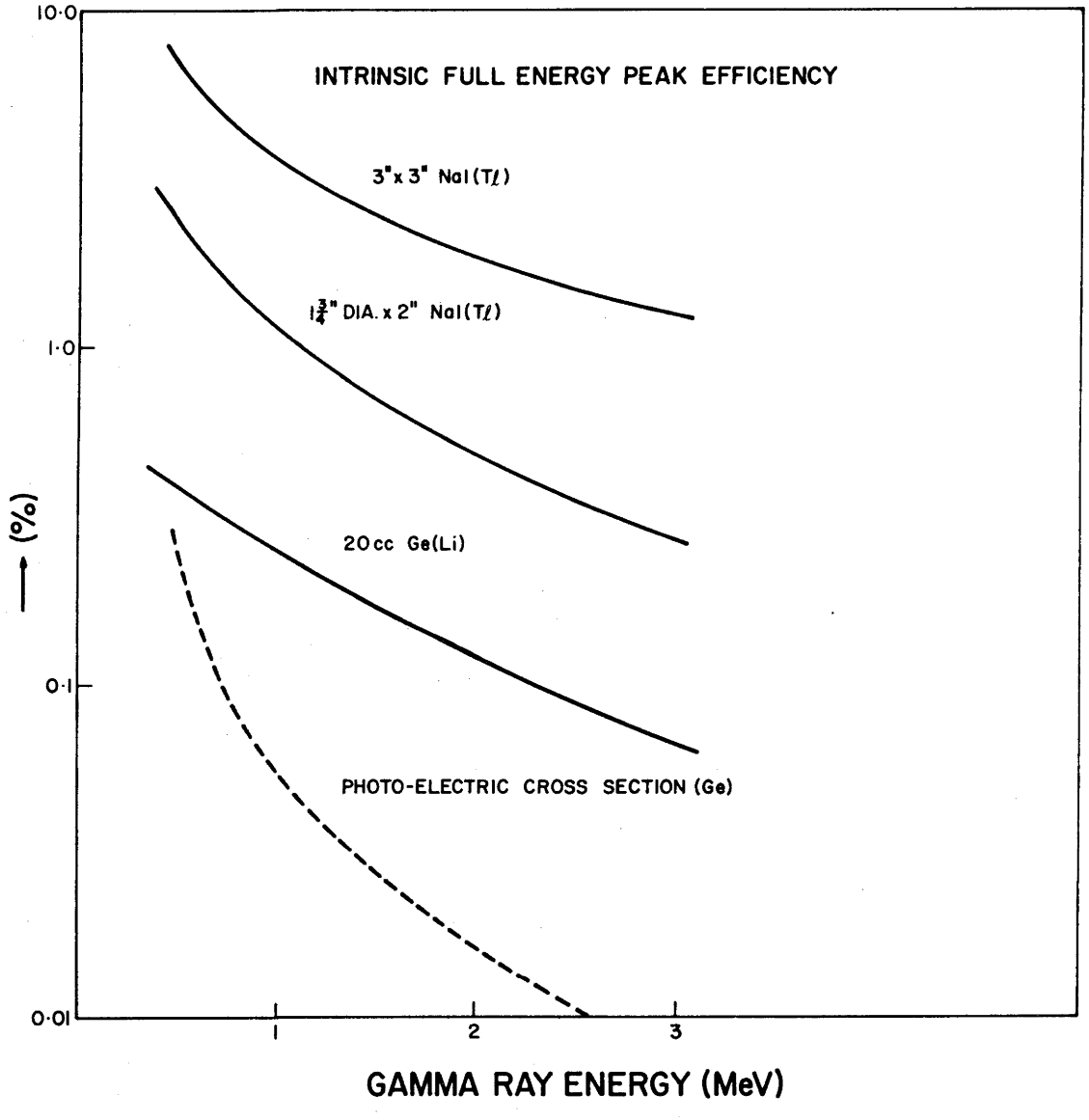
INTRINSIC FULL ENERGY PEAK EFFICIENCY
3"x 3" NaI(Tℓ)
1¾" DIA. x 2" NaI(Tℓ)
20cc Ge(Li)
PHOTO-ELECTRIC CROSS SECTION (Ge)
10·0
1·0
0·1
0·01
(%)
1
2
3
GAMMA RAY ENERGY (MeV)

As the γ-ray energy increases the photoelectric cross section drops very rapidly (Figure 5.6) and the photopeak efficiency drops accordingly. However, because of the photoelectric absorption of Compton scattered γ-rays and of two annihilation gamma quanta simultaneously in the pair production process, the total full energy absorption efficiency exceeds the photoelectric efficiency. Figure 5.12 shows the difference between the experimental efficiency curve and the calculated curve using the photoelectric cross section (Table 5.9). This difference will increase as the sensitive volume of the detector becomes larger. It is important to know the full energy peak efficiency of a particular detector experimentally so that the γ-ray intensities can be extracted accurately. The word 'full energy peak' is preferred to that of 'photopeak', since all the γ-ray energies studied were above 1 MeV, where the full energy peak is not due only to the photoelectric effect. The full energy peak efficiencies of 3" x 3" and $1\frac{3}{4}$" x 2" NaI(Tl) crystals are also shown in Figure 5.12 for comparison with 20 c.c. Ge(Li) detector, they were obtained from reference (MA 60).

2.5 Double escape peak efficiency

A γ-ray with energy greater than 1.022 MeV incident on the detector can produce an electron-positron pair and many of the electrons and positrons deposit most of the energy in the detector. As shown in Figure 5.6, the cross section for pair production rises rapidly above the threshold and at about 1.5 MeV γ-ray energy begins to exceed that of the photoelectric effect. For each electron-positron pair produced, two 511-keV photons are created from positron annihilation. Because of the limited size of the detector most of the annihilation photons escape. If both quanta escape a peak corresponding to an energy of E_γ - 1.022 MeV, the 'double escape peak', results. There is also a weaker peak corresponding to energy of E_γ - 0.511 MeV, since the probability of the energy of one of the 511-keV γ-rays being completely deposited within the detector is much smaller; this is the 'single escape peak'. A full energy peak corresponding to photoelectric absorption of incident and Compton scattered γ-rays and re-absorption of both the anniliation quanta due to pair production is also observed in high energy γ-ray line shapes. Figure 5.13 shows the variation of the ratio of double escape peak to full energy peak with respect to the incident

Figure 5.13

Ratio of double escape peak to full energy peak efficiency and relative double escape peak efficiency of γ-rays of the 20 c.c. Ge(Li) detector.

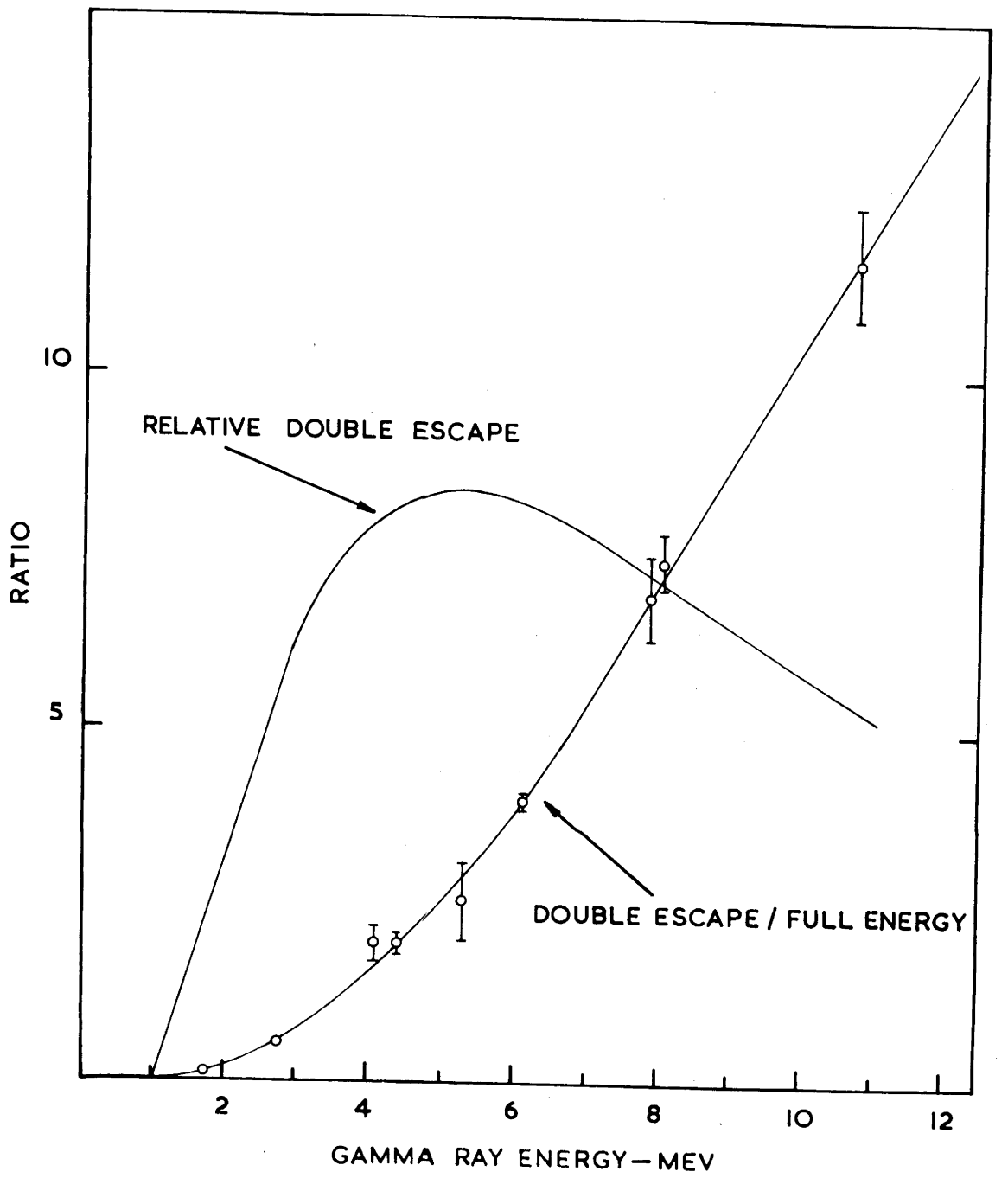
RELATIVE DOUBLE ESCAPE
DOUBLE ESCAPE / FULL ENERGY
RATIO
10
5
2
4
6
8
10
12
GAMMA RAY ENERGY—MEV

γ-ray energy. The curve was obtained from the measurement of the ratio of γ-rays listed in Table 5.13.

Table 5.13

Double escape peak to full energy peak ratio of γ-rays

Reaction	Ep (KeV)	E_γ (MeV)	Ratio
$^{27}Al(p,\gamma)^{28}Si$	992	1.78	0.10
$^{26}Mg(p,\gamma)^{27}Al$	662	2.75	0.50
$^{13}C(p,\gamma)^{14}N$	554	4.11	1.85
$^{11}B(p,\gamma)^{12}C$	600	4.43	1.95
$^{26}Mg(p,\gamma)^{27}Al$	662	5.32	2.57
$^{19}F(p,\alpha\gamma)^{16}O$	597	6.13	4.01
$^{30}Si(p,\gamma)^{31}P$	620	7.89	6.89
$^{13}C(p,\gamma)^{14}N$	554	8.06	7.39
$^{27}Al(p,\gamma)^{28}Si$	992	10.76	11.62

From Figure 5.13, it is seen that above a γ-ray energy of 3.4 MeV, the double escape peak is the most intense peak in the spectrum of a single γ-ray. Thus the double escape peak is used most often for the identication of high energy γ-rays and for the estimation of the full energy peak intensity via the double escape peak to full energy peak ratio. The fact that the double escape peak to full energy peak ratio is greater than 1.0 at 3.4 MeV instead of at 1.5 MeV as would be expected from the photopeak and pair production cross section is further indication that the detector has a large sensitive

Figure 5.14

Double escape peak efficiency of the 20 c.c. Ge(Li) detector. Curve A is experimentally obtained and curve B is calculated from the pair production cross section.

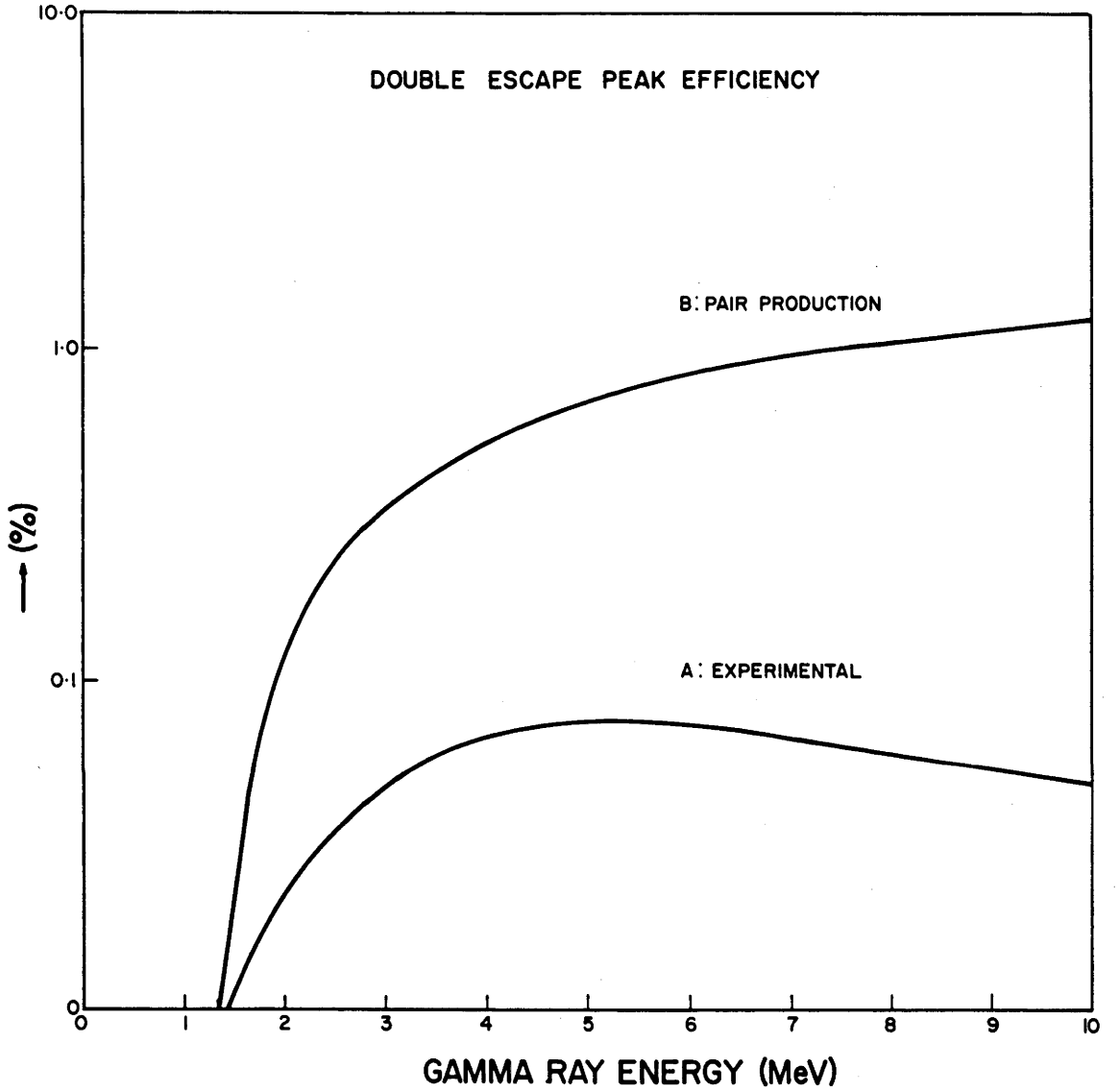
DOUBLE ESCAPE PEAK EFFICIENCY
B: PAIR PRODUCTION
A: EXPERIMENTAL
10·0
1·0
0·1
0
(%)
0
1
2
3
4
5
6
7
8
9
10
GAMMA RAY ENERGY (MeV)

volume and that multiple absorption processes are contributing to the full energy peak.

Figure 5.14 shows the double escape peak efficiencies of the detector. Curve A is obtained by multiplying the values obtained from Figure 12 and Figure 13, and curve B is calculated from pair production cross section. The experimentally obtained curve A has a much smaller efficiency at higher energies as compared to the calculated result and in fact the efficiency decreases as gamma energy increases. Ewan and Tavandale (EW 64) studied this effect for a relatively small crystal of 3.5 m.m. depth and gave as two reasons:

(1) A large number of electrons and positrons created by the pair production process have sufficient energy to escape from the detector before losing all of their energy.

(2) High energy electrons and positrons in slowing down lose energy by emission of bremsstrahlung which can escape from the detector.

3. Line shape analysis

Though the methods described in Chapter 2 for the analysis of scintillation spectra are applicable to Ge(Li) spectra, the increased number of channels which are necessary for high resolution germanium spectra

Figure 5.15

The distributions of the ratio of double escape peak to full energy peak of γ-rays emitted from the 719 (crosses), 809 (dots) and 954 (open circles) keV resonances of $^{26}Mg(p,\gamma)^{27}Al$ reaction along with the measured curve.

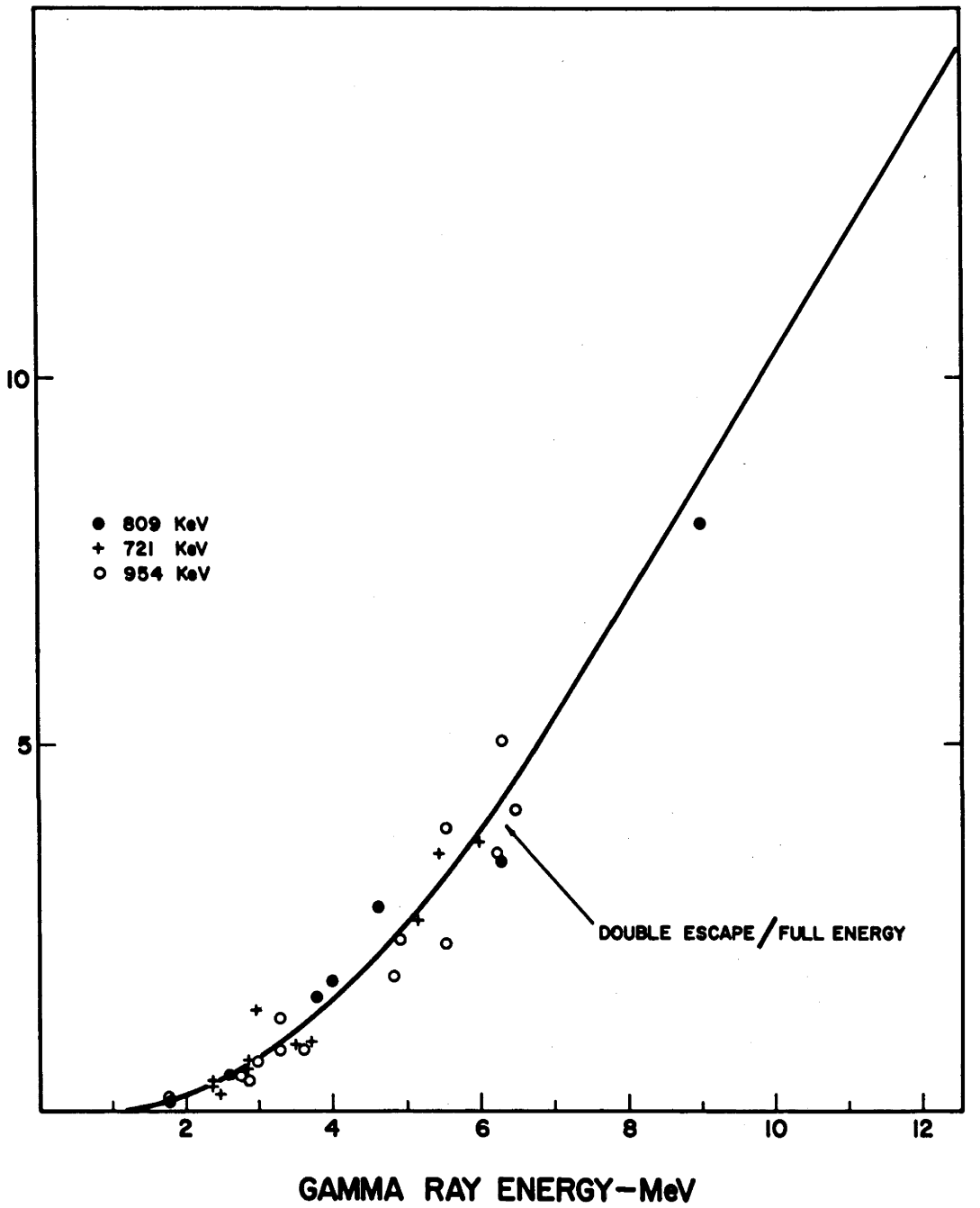
10
5
● 809 KeV
+ 721 KeV
○ 954 KeV
DOUBLE ESCAPE / FULL ENERGY
2
4
6
8
10
12
GAMMA RAY ENERGY—MeV

presents a problem for computer least squares analysis because of limited number of available core locations. The recent work of Van der Leun et al. (VA 67) derived γ-ray intensities from intrinsic full energy peak or double escape peak efficiencies without any attempt at line shape analysis. The present work, however, found that the line shape analysis was necessary to check the results obtained from the intrinsic full energy peak efficiency and that more accurate results were in fact obtained. This is because the data points comprising peaks in a Ge(Li) spectrum constitute only a small proportion of the total spectrum. Figure 5.15 shows the distributions of the ratio of double escape peak to full energy peak as compared to the measured line of Figure 5.13 for γ-rays emitted from the $^{26}Mg(p,\gamma)^{27}Al$ resonances at Ep = 719 (crosses), 809 (dots) and 954 (open circles) keV. The considerable scatter of points indicates the inaccuracies of intensities determined in this way ($\sim \pm$ 20%) and indicates the necessity of a more accurate method.

The standard γ-ray line shapes of energies 1.780, 2.367, 4.433, 6.129, 8.060 and 10.760 MeV were measured in 2048 channels. Since the storage of these line shapes would occupy 49 kilo bytes of computer core, they were stored on disk and added to the main program only at

Figure 5.16

The standard γ-ray line shapes of energy 1.780, 2.367, 4.433, 6.129, 8.060 and 10.760 MeV with each normalized to have a unique integrated intensity of 10^6 counts.

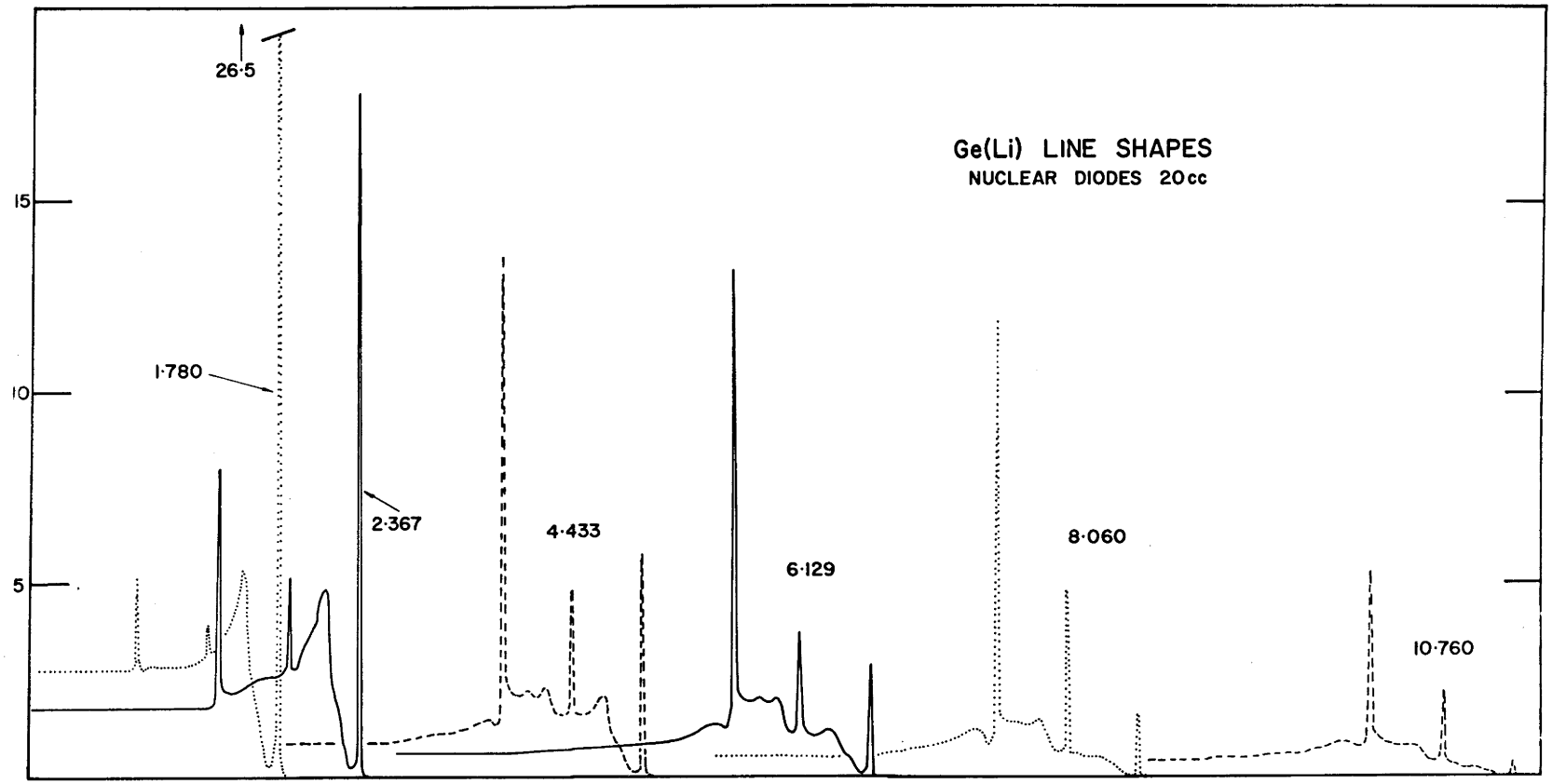
Ge(Li) LINE SHAPES
NUCLEAR DIODES 20cc
26·5
1·780
2·367
4·433
6·129
8·060
10·760
15
10
5

Figure 5.17

The standrd γ-ray line shape of energy 1.780, 2.367, 4.433, 6.129, 8.060 and 10.760 MeV with the full energy peaks aligned and normalized to the same height.

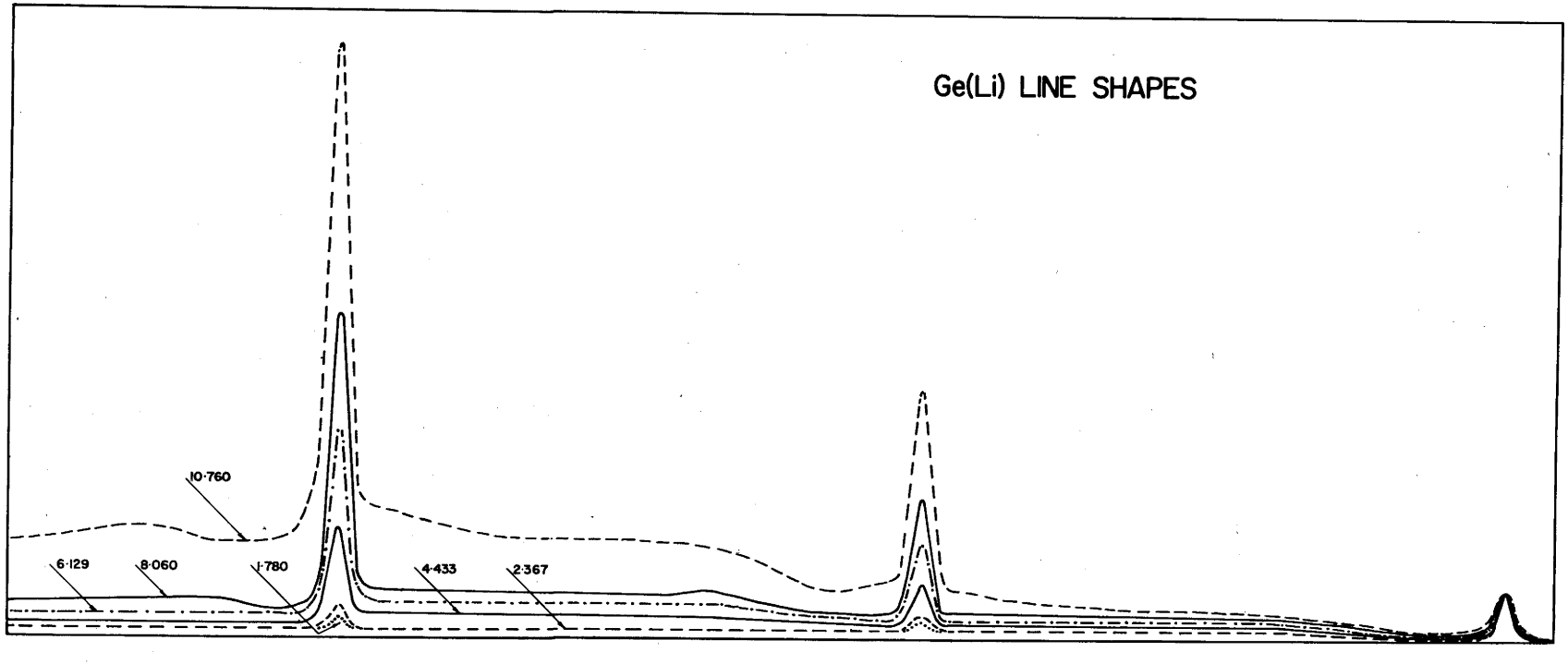
Ge(Li) LINE SHAPES
10·760
6·129
8·060
1·780
4·433
2·367

Figure 5.18

The 6.129 MeV γ-ray line shape using the $^{19}F(p,\alpha\gamma)^{16}O$ resonance at 597 keV. The bump on the low energy side of each of the three peaks indicates that γ-rays were emitted from ^{16}O nuclei recoiling into vacuum in the backward direction.

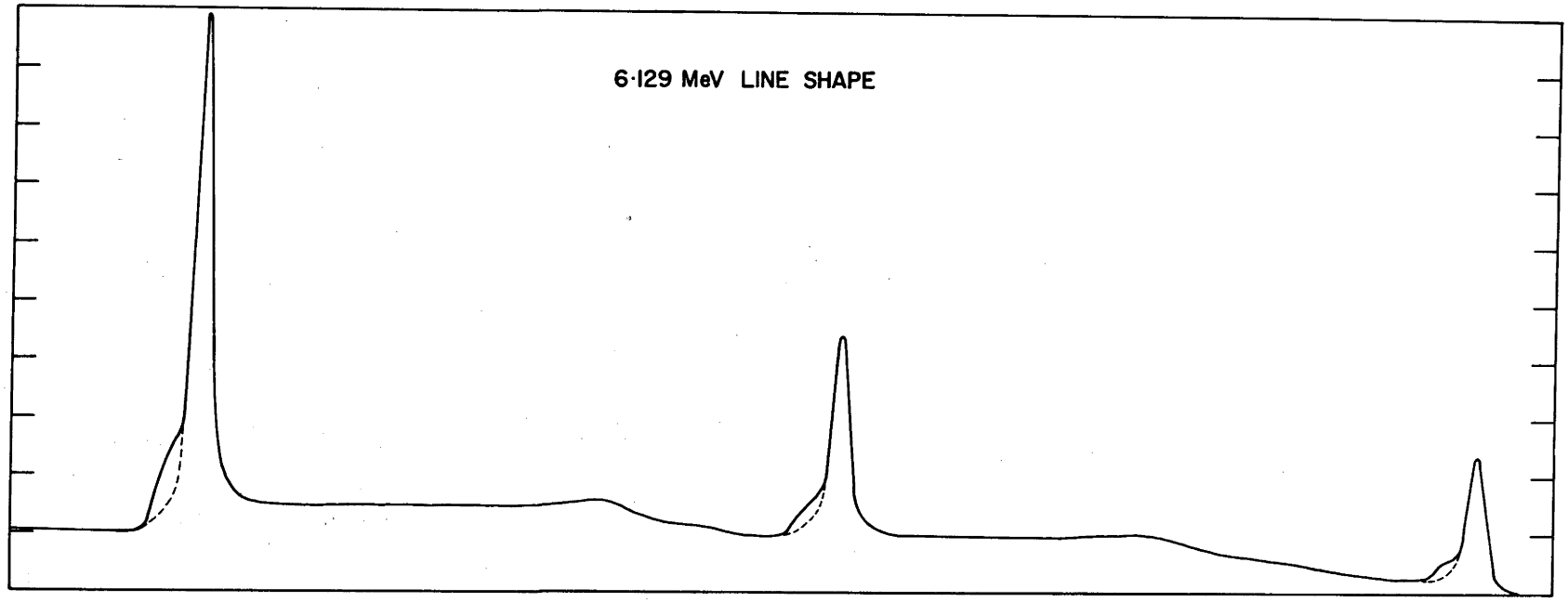
6·129 MeV LINE SHAPE

the time when they were used. A least squares fit program called FITTER (see Appendix) was developed for the IBM-360 computer to analyze complex γ-ray spectra of up to 2048 channels with the number of components (more than 20) adjustable according to the size of the energy interval fitted. Figure 5.16 shows the line shapes each normalized to have a unique integrated intensity of 10^6 counts and Figure 5.17 shows the line shapes with the full energy peaks aligned to the same position and normalized to the same height. The 1.780 and 10.760 MeV γ-ray line shapes were obtained from the $^{27}Al(p,\gamma)^{28}Si$ resonance at Ep = 992 keV (AZ 66). The 4.433 MeV γ-ray line shape was obtained from the $^{11}B(p,\gamma)^{12}C$ reaction at Ep = 600 keV. This was found necessary to replace the $^{15}N(p,\alpha\gamma)^{12}C$ resonance which was used in NaI(Tl) line shapes due to the Doppler broadening of peaks resulting from the recoil of α-particles significantly affects the resolution of the Ge(Li) line shape. This effect became serious in the measurement of 6.129 MeV γ-ray line shape using the $^{19}F(p,\alpha\gamma)^{16}O$ resonance at 597 keV. The line shape taken with the detector at 0^o to the beam is shown in Figure 5.18. The bump on the low energy side of each of the three peaks indicates that γ-rays were emitted from ^{16}O nuclei recoiling into vacuum in the backward

direction. To prevent this effect, a thin film of gold was evaporated on to the surface of the fluorine target.

The ^{13}C target which was used in the measurement of 8.06 MeV γ-ray line shape for the NaI(Tl) detector was found too thick to use for the line shape of Ge(Li) detector. The resonance width of 33 keV at Ep = 554 keV is broad compared to the resolution of the detection system. A thin ^{13}C target of about 5 keV thick which was prepared by cracking enriched methyl iodide on a tantalum foil was used instead for the measurement of 8.06 MeV γ-ray line shape.

The quality of the fits and the intensities obtained are discussed in the study of $^{26}Mg(p,\gamma)^{27}Al$ reaction at 954 keV resonance in which the intensities obtained from the intrinsic full energy peak efficiencies were compared.

4. Application

The high resolution obtainable from a Ge(Li) γ-ray spectrometer enables accurate measurement of γ-ray energies, Doppler shifts and broadenings thus providing accurate assessments of level energies, decay schemes and life times of excited states and the elimination of ambiguities and incorrect assignments of spins which have arisen from measurements made with inadequate resolution.

The application of the 20 c.c. Ge(Li) detector is demonstrated in the study of the $^{26}Mg(p,\gamma)^{27}Al$ resonances at Ep = 662, 719, 809, 839, 954 and 982 keV.

FIGURE CAPTIONS

Figure 5.1 The A.N.U. 20 c.c. lithium drifted germanium detector is drawn to scale, the shaded part indicates the volume that is not depleted by the coaxial drift process.

Figure 5.2 The experimental set up of the Ge(Li) γ-ray spectrometer.

Figure 5.3 The ^{60}Co spectrum with optimum resolution of 4.2 keV for the 1.333 MeV γ-ray.

Figure 5.4 Comparison of the line width of the full energy peak of a 10.76 MeV γ-ray to that of a 1.78 MeV γ-ray obtained in the same spectrum.

Figure 5.5 The ThC" spectrum collected with SIMPUL 2048 channels. Peak energies are from reference (EM 60).

Figure 5.6 The linear attenuation coefficients of γ-rays in germanium.

Figure 5.7 Geometry of a quarter section of a rectangular detector (HO 65).

Figure 5.8 Calculated detector efficiencies at 2.54 and 5.0 cm.

Figure 5.9 The 662 keV γ-ray spectra measured with a 3" x 3" NaI(Tl) detector (A) and the Ge(Li) detector (B).
(^{137}Cs source).

Figure 5.10 The 511 and 1274 keV γ-ray spectra measured with a 3" x 3" NaI(Tl) detector (A) and the Ge(Li) detector (B).
(^{22}Na source).

Figure 5.11 The intrinsic full energy peak efficiency of the 20 c.c. Ge(Li) detector.

Figure 5.12 The intrinsic full energy peak efficiency of the 20 c.c. Ge(Li) detector is compared with those of 3" x 3" and $1\frac{3}{4}$" x 2" NaI(Tl) crystals. The dotted line shows the calculated photopeak efficiency using the photoelectric cross section of Table 5.9.

Figure 5.13 Ratio of double escape peak to full energy peak efficiency and relative double escape peak efficiency of γ-rays of the 20 c.c. Ge(Li) detector.

Figure 5.14 Double escape peak efficiency of the 20 c.c. Ge(Li) detector. Curve A is experimentally obtained and curve B is calculated from the pair production cross section.

Figure 5.15 The distributions of the ratio of double escape peak to full energy peak of γ-rays emitted from the 719 (crosses), 809 (dots) and 954 (open circles) keV resonances of $^{26}Mg(p,\gamma)^{27}Al$ reaction along with the measured curve.

Figure 5.16 The standard γ-ray line shapes of energy 1.780, 2.367, 4.433, 6.129, 8.060 and 10.760 MeV with each normalized to have a unique integrated intensity of 10^6 counts.

Figure 5.17 The standard γ-ray line shape of energy 1.780, 2.367, 4.433, 6.129, 8.060 and 10.760 MeV with the full energy peaks aligned and normalized to the same height.

Figure 5.18 The 6.129 MeV γ-ray line shape using the $^{19}F(p,\alpha\gamma)^{16}O$ resonance at 597 keV. The bump on the low energy side of each of the three peaks indicates that γ-rays were emitted from ^{16}O nuclei recoiling into vacuum in the backward direction.

CHAPTER VI

THE $^{26}Mg(p,\gamma)^{27}Al$ REACTION

1. Introduction

The ^{27}Al nucleus has been widely discussed in terms of a strong coupling collective rotational model (NI 55, GO 60, OP 64) and the excited core model (TH 66, EV 67a). The collective rotational model, which explains with some success the structure of ^{25}Mg, ^{25}Al and other light nuclei in the 2s-1d shell (GO 60, BI 60), has been applied to the decay scheme of ^{27}Al. Figure 6.1 shows the low lying level scheme taken from Ophel and Lawergren (OP 64) and Lawergren (LA 64). The level energies were taken from Van der Leun and Sheppard (VA 67). The level sequence 0.843 MeV ($\frac{1}{2}^+$), 1.013 MeV ($\frac{3}{2}^+$) and 2.732 MeV ($\frac{5}{2}^+$) forms a rotational band on orbit 9 of the Nilson model (NI 55). A rotational band with $K = \frac{5}{2}$ based on the ground state with the 2.209 MeV level ($\frac{7}{2}^+$) as the second member and the 3.000 MeV level ($\frac{9}{2}^+$) as the third member was suggested by Gove (GO 60). The application of this model to the experimentally obtained transition strengths, E2/M1 mixing ratios and branching ratios were discussed by Ophel *et al*. (OP 64) and

Figure 6.1

Decay schame of the low-lying levels of ^{27}Al.

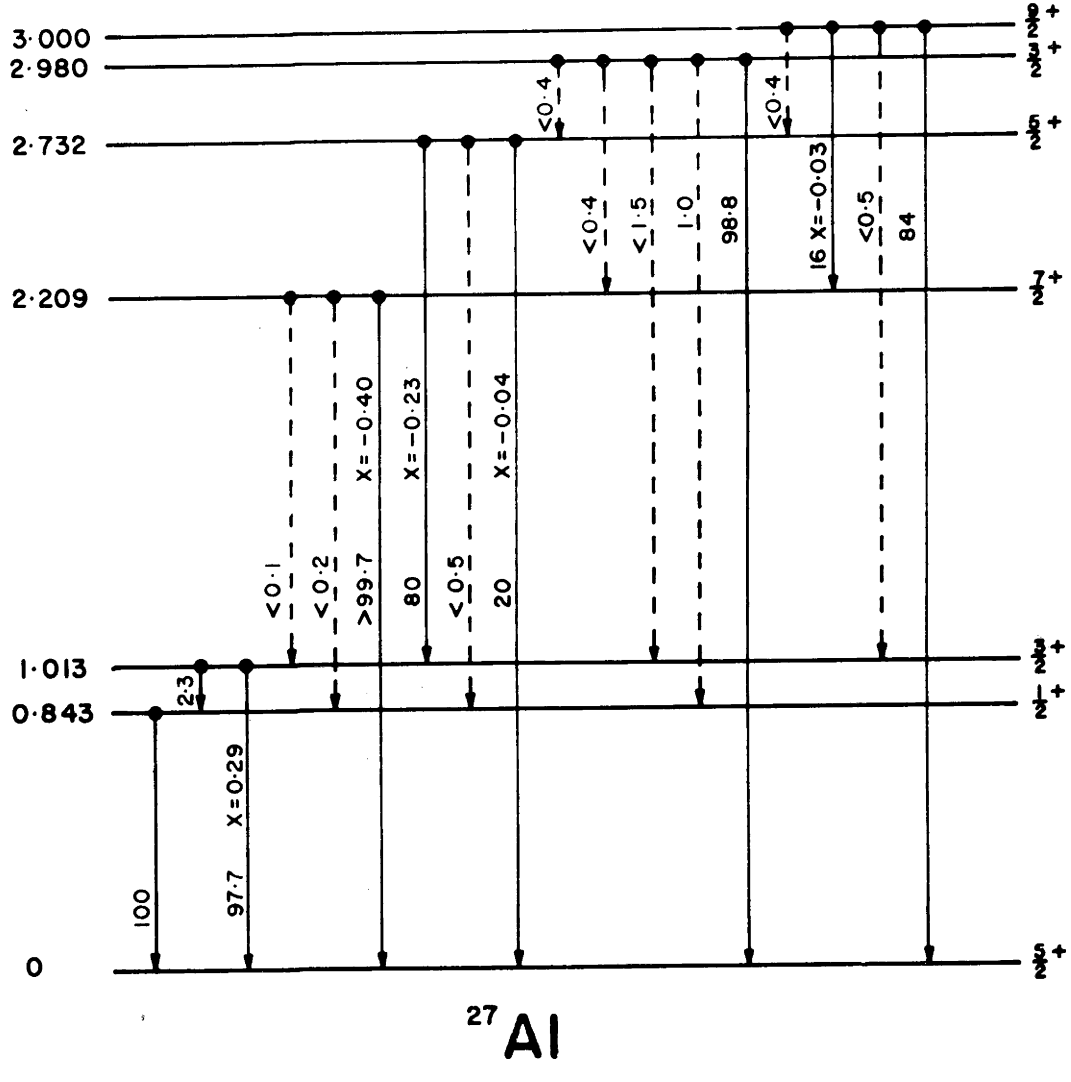
3·000
2·980
2·732
2·209
1·013
0·843
0
<0·4
<0·4
<0·4
<1·5
1·0
98·8
16 X=-0·03
<0·5
84
<0·1
<0·2
>99·7
X=-0·40
80
X=-0·23
<0·5
20
X=-0·04
2·3
100
97·7
X=0·29
^{27}Al

Lawergren (LA 64). Satisfactory qualitative interpretation of the experimental information is possible but numerous exceptions exist.

The weak coupling core excited model has been applied to heavy and medium weight nuclei and found to be rather successful (LA 57, DE 60, DE 65a). This model suggests that low lying levels of odd mass nuclei could be interpreted as resulting from the coupling of a particle or a hole to the first excited state of a doubly even core. The theoretical calculation of the level structure of ^{27}Al with this model has recently been carried out by Thankappan (TH 66) and applied by Evers et al. (EV 67a) to compare the decay properties such as M1, E2 transition strengths, mixing ratios and branching ratios of low lying levels of ^{27}Al with experimental and theoretical values. The nucleus ^{27}Al is described as a $d_{5/2}$ hole in the ground state of ^{28}Si. The coupling of this hole to the quadrupole excitation $\ell = 2$ of the surface of the core gives rise to five excited states of angular momentum $\frac{1}{2}^+$, $\frac{3}{2}^+$, $\frac{5}{2}^+$, $\frac{7}{2}^+$ and $\frac{9}{2}^+$. The observed levels at 0.843 MeV ($\frac{1}{2}^+$), 1.013 MeV ($\frac{3}{2}^+$), 2.209 MeV ($\frac{7}{2}^+$), 2.732 MeV ($\frac{5}{2}^+$) and 3.000 MeV ($\frac{9}{2}^+$) have spin and parity as predicted by this model. The transition from strong coupling to weak coupling going from ^{25}Mg to ^{27}Al has been described by Crawley et al. (CR 65) for the (p,p')

scattering at Ep = 17.5 MeV. Similar results were obtained by Niewodniczanski (NI 64) for (d,d') scattering at Ed = 12.8 MeV and by Kokame (KO 65) for (α,α') scattering at E_α = 28.5 MeV. However, Van der Leun et al. (VA 67) from his recent experimental results of $^{26}Mg(p,\gamma)^{27}Al$ reaction indicated that the core excited model cannot explain the decay properties of the 2.732 MeV level and the mixing ratio of the 2.980 MeV γ-ray. It also cannot explain the data of Lawergren (LA 67a) for the $^{26}Mg(d,n)^{27}Al$ reaction. These experiments favour a description of the ^{27}Al level scheme in terms of the rotational collective model. The theoretical predictions based on different models need systematic studies to gather adequate experimental information of level properties. Due to the narrow separation of levels in ^{27}Al, the previous experimental data obtained from the study of $^{26}Mg(p,\gamma)^{27}Al$ reaction with NaI(Tl) detectors are shown by Van der Leun et al. (VA 67) to yield erroneous information as a result of the insufficient resolution of the NaI(Tl) crystals. Systematic studies of ^{27}Al nucleus have been carried out in this department (LA 62, OP 62, OP 62a, OP 63, OP 64, LA 64, OS 65). With the advent of the Ge(Li) detector, measurement of decay schemes using high resolution Ge(Li) detectors is necessary to identify γ-rays which were not possible to

resolve in the previous measurements with NaI(Tl) crystals. This is especially important if high efficiency NaI(Tl) crystals are to be used in angular correlation measurements. The possibility exists that the cascade γ-rays selected for the correlation measurement may contain other peaks hidden under the main peak. A prior measurement with a Ge(Li) detector will allow a more justified choice of γ-rays in cascade for angular correlation measurement with NaI(Tl) detectors. The high resolution of the Ge(Li) detector provides more precise determinations of γ-ray energies and thus of more precise level energies. Accurate information of these energies increases the reliability of decay schemes deduced from them. The theoretical calculation of ^{27}Al model schemes need more correlation measurements to establish branching ratios and quadrupole/dipole mixing ratios of low-lying levels especially. Since the efficiency of the available Ge(Li) detectors is not large enough for γ-γ correlation measurements, NaI(Tl) detectors are still resorted to for such measurements. Additionally, the systematic survey of the resonance levels may extend information about the group decay properties of two or more neighbouring levels. This was reported by Van der Leun in ^{27}Al (VA 67) for resonance

levels of 2293 and 2323 keV, 662 and 719 keV, and 338 and 454 keV.

2. Specific problems concerning levels of ^{27}Al

2.1 The spin of the 3.00 MeV level

The spin of the 3.00 MeV level is a key property to the success of the prediction of the core excited model which explains better level energies of lower value with a high spin, however, there still remains some uncertainty about the assignment of $\frac{9}{2}$ to this level. The spin $\frac{9}{2}$ has been assigned to this level by Towle and Gilboy (TO 62) from the analysis of the differential cross section for inelastic scattering of neutrons.

Lawergren (LA 64) measured the γ-ray triple correlations of the cascade 3.00→2.21→0 and showed that an assignment of $\frac{9}{2}$ to this level was consistent with the measurements, but analysis for spins other than $\frac{9}{2}$ was not attempted.

Wakatsuki et al. (WA 65b, WA 66) made a firm assignment of $\frac{7}{2}$ from γ-ray correlation measurements for the $(p,p'\gamma)$ reaction leading to this level. The 3.00 MeV level was interpreted by them as the fourth member of a $k = \frac{1}{2}$ rotational band based on the first excited level, i.e., 0.843 MeV $(\frac{1}{2}^+)$, 1.013 MeV $(\frac{3}{2}^+)$, 2.732 MeV $(\frac{5}{2}^+)$, 3.000 MeV $(\frac{7}{2}^+)$.

Sheppard et al. (SH 67) studied the $^{26}Mg(p,\gamma)^{27}Al$ reaction using a Ge(Li) crystal as γ-ray detector which has no problem in separating the doublet 2.980 and 3.000 MeV γ-rays. The angular correlation measurements at Ep = 2323 and 2574 keV resonance both lead to the assignment of $\frac{9}{2}$ or $\frac{5}{2}$ to 3.00 MeV level. However, a unique solution was claimed at Ep = 1733 keV resonance where the decay sequence $\frac{7}{2} \rightarrow \frac{9}{2} \rightarrow \frac{5}{2}$ gave a much better fit than that from $\frac{7}{2} \rightarrow \frac{5}{2} \rightarrow \frac{5}{2}$ sequence.

Recently Gove et al. (GO 67) reported a spin of $\frac{3}{2}$ or $\frac{5}{2}$ for this level from the study of $^{28}Si(d,^{3}He)^{27}Al$ reaction using a magnetic spectrograph to resolve the 2.980 and 3.000 MeV levels. Kean et al. (KE 67) found that either $\frac{5}{2}$ or $\frac{9}{2}$ was consistent with measurements of the $^{24}Mg(\alpha,p\gamma)^{27}Al$ reaction using NaI(Tl) crystals in conjunction with a double focussing magnetic spectrometer where the doublet is adequately separated. From the experimental evidence discussed above, assignments ranging from $\frac{3}{2}$ up to $\frac{9}{2}$ have been assigned to 3.00 MeV level.

2.2 The 3.68 MeV level

The spin of this level was first reported by Van der Leun et al. (VA 56) to be $\frac{1}{2}$ from the measurement of angular distribution of 4.91 MeV γ-ray emitted from

Ep = 339 keV resonance level to 3.68 MeV level. Recently Sheppard and Van der Leun (SH 67) using Ge(Li) γ-ray spectrometer studied $^{26}Mg(p,\gamma)^{27}Al$ reaction and found a number of resonance levels with spin $\frac{1}{2}$ or $\frac{3}{2}$ which de-excite through this level; furthermore, they found that the level de-excites 65% to 0.843 MeV ($\frac{1}{2}$) level and 35% to 1.013 MeV ($\frac{3}{2}$) level. They concluded that the spin of 3.68 MeV level is $\frac{1}{2}$ or $\frac{3}{2}$; a definite assignment of spin to this level, however, was not made.

Osgood (OS 65) extensively studied the Ep = 721 keV resonance, measuring the angular distributions of the transitions from resonance to the 3.68 MeV level and 3.68 → 0.84 MeV level. The anisotropy of the 2.84 MeV (3.68 → 0.84) γ-ray was regarded as evidence that the 3.68 MeV level could not have a spin of $\frac{1}{2}$. The analysis of angular correlation measurements of the cascade r → 3.68 → 0.84 (r stands for resonance) was made with spin sequences of $\frac{5}{2} \rightarrow \frac{3}{2} \rightarrow \frac{1}{2}$ and $\frac{3}{2} \rightarrow \frac{3}{2} \rightarrow \frac{1}{2}$, since the spin of the resonance level was not known. Osgood concluded that the measurements were consistent with $\frac{5}{2} \rightarrow \frac{3}{2} \rightarrow \frac{1}{2}$ for geometries I and II, i.e., he proposed the 721 keV resonance level to have spin $\frac{5}{2}$ and the 3.68 MeV level spin $\frac{3}{2}$. Osgood also studied the decay scheme of the 3.68 MeV level by measuring the low energy γ-rays in

coincidence with 5.24 MeV (r → 3.68) γ-ray. He found only 2.34 MeV (r → 6.6) and 2.84 MeV (3.68 → 0.84) γ-rays and concluded that 3.68 MeV level decays at least 97% via 0.84 MeV level.

Wakatsuki et al. (WA 66) studied the decay scheme of 3.68 MeV level with (p,p'γ) reaction. They found the 3.68 MeV level decays 50% to 0.84 MeV level and 50% to 1.01 MeV level in contradiction to the result of Osgood, but in a better agreement to that of Van der Leun.

This indicates that the decay scheme of 3.68 MeV level obtained by Osgood is incorrect and the assignment of the spin $\frac{3}{2}$ to this level is possibly in error since the angular distribution of the 2.84 MeV (3.68 → 0.84) γ-ray measured by Osgood contained also the 2.67 MeV (3.68 → 1.01) γ-ray. In fact, a strong γ-ray from 721 keV resonance decays to 6.16 MeV level with energy 2.80 MeV. The coincidence spectrum failed to distinguish the r → 3.68 → 0.84 cascade from r → 6.16 → 0.84 cascade due to the fact that 5.32 MeV (6.16 → 0.84) γ-ray is not resolved from 5.24 MeV γ-ray (r → 3.68) which was chosen as the energy window in the coincidence measurement. This fact demonstrates the importance of pre-identification of γ-rays to guide γ-γ angular correlation measurements. Precise determinations of the energies of levels and

γ-rays will reduce the chance of mistakenly inverting the order of two cascading γ-rays. The decay scheme of the 719 keV resonance and the angular correlation measurements of the cascade r → 6.16 → 0.84 and r → 3.68 → 0.84 were re-studied in detail by this work.

Lawergren (LA 67a) using neutron time of flight technique studied the angular distribution of neutron groups from the $^{26}Mg(d,n)^{27}Al$ reaction, and $\ell = 0$ result was observed to the 3.68 MeV level corresponding to a spin and parity of 3.68 MeV level of $\frac{1}{2}^+$.

2.3 The 3.96 MeV level

The decay scheme of the 3.96 MeV level was studied by Wakatsuki et al. (WA 66) from (p,p'γ) reaction, the branching ratio of 45 : 18 : 20 : 12 : 5 was reported by them from this level decaying to the ground state ($\frac{5}{2}^+$), 0.843 MeV ($\frac{1}{2}^+$), 1.013 MeV ($\frac{3}{2}^+$), 2.212 MeV ($\frac{7}{2}^+$) and 2.732 MeV ($\frac{5}{2}^+$) states. They suggest a spin of $\frac{3}{2}$ for this level.

This result is however in serious disagreement from that of Van der Leun and Sheppard (VA 67), who found that the level decays only to the ground state. The spin of the level was suggested as $\frac{3}{2}$ from the fact that the level was excited by resonance levels which of spin either $\frac{1}{2}$, $\frac{3}{2}$, or $\frac{5}{2}$ and decays only to ground state which has spin of $\frac{5}{2}$.

Valter et al. (VA 65) studied the decay scheme of the 10.48 MeV resonance level corresponding to Ep = 2.293 MeV with NaI(Tl) detectors. The γ-γ triple correlation measurements of r → 3.96 → 0 cascade established a spin of $\frac{7}{2}$ for the 3.96 MeV level. Recent measurement with a Ge(Li) detector by Van der Leun et al. (VA 67), however, shows that the 10.48 MeV level decays to 6.48 MeV level which was not identified by Valter et al., and the 3.96 MeV level was not excited from the decay of 10.48 MeV level. Again, the measurement of Valter et al. with NaI(Tl) detectors could not resolve the 3.96 MeV (3.96 → 0) and 6.52 MeV (10.48 → 3.96) γ-rays from 4.00 MeV (10.48 → 6.48) and 6.48 MeV (6.48 → 0) γ-rays.

The $^{26}Mg(d,n)^{27}Al$ reaction of Lawergren (LA 67a) seems to indicate the spin and parity of this state is $\frac{7}{2}^-$.

2.4 The 4.41 MeV level

The decay scheme of the 4.41 MeV level was studied by Metzger (ME 65), Van der Leun (VA 67) and recently by Spear (SP 67). All works indicated that the level decays directly to the ground state and through 1.01 MeV level. However, the intensity of the transition 4.41 → 2.21 ($\frac{7}{2}^+$) was very different between their results, 11% by Metzger, 25% by Van der Leun and less than 5% by Spear. Metzger

also measured the angular distributions of the 4.41 MeV (4.41 → 0) and the 3.40 MeV (4.41 → 1.01) γ-rays, the results being consistent with the assignment of $\frac{5^+}{2}$ to 4.41 MeV level. Sheppard and Van der Leun (SH 67) suggested the spin to be $\frac{5}{2}$ from the combined evidence that the level is excited by decay of resonance levels of spins $\frac{3}{2}$, $\frac{5}{2}$ or $\frac{7}{2}$ and that the decay of this level proceeds via $\frac{3}{2}$, $\frac{5}{2}$ and $\frac{7}{2}$ states. However, Lawergren's $^{26}Mg(d,n)^{27}Al$ results suggest that the spin and parity of this level is $\frac{3^-}{2}$ (LA 67a).

3. Experimental Methods

All investigations of $^{26}Mg(p,\gamma)^{27}Al$ resonance levels were carried out using the proton beam of the A.N.U. 2 MeV Van de Graaff accelerator. The proton beam was analyzed by a 25^o magnet with an energy stability of ± 1 keV. The low detector efficiency of Ge(Li) crystal required beam currents greater than 15 μa for a reasonable running time for each spectrum collected. Depending on the yield of the reaction at different proton energies, spectra were obtained in periods ranging from three to five hours.

The targets were prepared by evaporating ^{26}MgO from a tantalum strip in vacuo onto copper. The heat process reduces the oxide, hence liberating the magnesium. The

^{26}MgO, supplied by A.E.R.E., Harwell, England, was enriched to contain >98% of ^{26}Mg. Targets prepared in this way were usually about 5 keV thick at 1 MeV proton energy. The copper backings, sand blasted beforehand to remove any contaminants, had a thickness of about 2 mm and were designed to screw onto a water-cooled target holder. The target holder was surrounded by a liquid air trap to prevent deposits of carbon on the target. The method was used previously by Bashkin and Ophel (BA 61). The water cooled target allowed bombardment of the target with greater beam currents (up to 30 W) without deterioration. The target chamber was cylindrical in shape and made of brass. A glass window on the chamber wall at 90^{o} to the beam direction facilitated optical alignment.

The Ge(Li) γ-ray spectrometer as described in Chapter V was used for all of the measurements. The resonance spectra were obtained at 2.54 cm from the target and at $\theta = 55^{o}$ with respect to the proton beam thus averaging out any dipole angular distribution effect. The decay scheme for each resonance level was investigated firstly; the angular distributions of cascade γ-rays were then measured after all γ-rays in the single spectrum had been identified. Though no serious effort was put into establishing level energies with high

precision, internal consistency was obtained between cascade γ-ray energies. In fact a number of levels were established more accurately than previous measurements. In the early stage of investigation before the 4096 channel analyzer provided by the SIMPUL system was available, spectra were collected with an RCL-512 pulse height analyzer. Due to the limited number of channels available, some portions of spectra were remeasured with expanded gain by a biased amplifier and it was found also necessary to perform some coincidence measurements between a 5" x 4" NaI(Tl) crystal and the Ge(Li) detector. The results of these measurements however agree with the corresponding single spectra recorded with 2048 channels, demonstrating the fact that a high resolution Ge(Li) detector combined with a multichannel analyzer which provides enough channels with respect to the resolution required can eliminate most if not all of the coincidence measurements usually necessary to achieve identification of γ-rays.

Initially, the angular distributions were measured at six equal intervals of $\cos^2\theta$ = 0.0(0°), 0.2 (63.45°), 0.4 (50.75°), 0.6 (39.25°), 0.8 (26.55°) and 1.0 (90°). Since no appreciable P_4 terms were observed at any of the resonance levels studied, measurements were reduced to 0°, 45° and 90°, and sometimes only at 0° and 90°. The

alignment of detector assembly with respect to beam spot on the target was checked by measuring at different angles the isotropic 8.07 MeV ($r \rightarrow 1.01$) γ-ray from the 839 keV resonance level (OP 62). Any deviations from isotropy were used to correct subsequent measurements. To check the stability of beam energy which might occasionally drift from the resonance energy, a 5" x 4" NaI(Tl) crystal fixed at 90^{o} to the beam was used as a monitor throughout the angular distribution measurements. In general, the monitor count and the yield/integrated charge agreed to within $\pm$ 3%. The angular distributions were analyzed in terms of Legendre Polynomials:

$$W(\theta) \sim 1 + a_2 P_2(\cos \theta)$$

with the coefficient $a_2 = A_2 Q_2$, where A_2 is the theoretical coefficient and Q_2 is the attenuation factor due to the finite size of the detector. Where the measurements were made at more than two angles, the value of a_2 was obtained by the method of least squares as described by Ferguson (FE 65).

Theoretical calculations of angular distributions for various spin sequences were carried out using tables of Sharp et al. (SH 54), and are listed in Table 6.1. The target ^{26}Mg has $J^{\pi} = 0^{+}$, simplifies the analysis of angular distribution since a unique ℓ_p value and channel spin is associated with each possible resonance spin.

Table 6.1

Theoretical angular distributions for gamma radiation emitted in transitions between states of definite spin. Compound state (J_1) formed by capture of p-wave and d-wave protons with entrance spin $\frac{1}{2}^+$. Case (a) first radiation ($J_1 \rightarrow J_2$) observed; Case (b) first radiation unobserved, second radiation ($J_2 \rightarrow J_3$) observed.

$J_1 J_2 J_3$	Angular Distribution
(a)	
A. $\frac{3}{2}\rightarrow\frac{1}{2}$	$W(\theta)=P_0-\frac{0.5 - 1.732X - 0.5X^2}{1 + X^2}P_2$
B. $\frac{3}{2}\rightarrow\frac{3}{2}$	$W(\theta)=P_0+\frac{0.4 + 1.55X}{1 + X^2}P_2$
C. $\frac{3}{2}\rightarrow\frac{5}{2}$	$W(\theta)=P_0-\frac{0.1 + 1.184X + 0.357X^2}{1 + X^2}P_2$
D. $\frac{5}{2}\rightarrow\frac{3}{2}$	$W(\theta)=P_0-\frac{0.4 - 2.03X - 0.204X^2}{1 + X^2}P_2+\frac{0.653X^2}{1 + X^2}P_4$
E. $\frac{5}{2}\rightarrow\frac{5}{2}$	$W(\theta)=P_0+\frac{0.457 + 1.084X - 0.204X^2}{1 + X^2}P_2-\frac{0.367X^2}{1 + X^2}P_4$
F. $\frac{5}{2}\rightarrow\frac{7}{2}$	$W(\theta)=P_0-\frac{0.143 + 1.484X + 0.347X^2}{1 + X^2}P_2+\frac{0.109X^2}{1 + X^2}P_4$
(b)	
G. $\frac{3}{2}\rightarrow\frac{1}{2}\rightarrow\frac{1}{2}$	$W(\theta)=P_0$
H. $\frac{3}{2}\rightarrow\frac{1}{2}\rightarrow\frac{3}{2}$	$W(\theta)=P_0$
I. $\frac{3}{2}\rightarrow\frac{3}{2}\rightarrow\frac{1}{2}$	$W(\theta)=P_0-\frac{(0.1-0.3t)+(0.346-1.04t)X-(0.1-0.3t)X^2}{(1 + X^2)(1 + t)}P_2$
J. $\frac{3}{2}\rightarrow\frac{3}{2}\rightarrow\frac{3}{2}$	$W(\theta)=P_0+\frac{(0.08 - 0.24t) - (0.31 - 0.432t)X}{(1 + X^2)(1 + t)}P_2$
K. $\frac{3}{2}\rightarrow\frac{5}{2}\rightarrow\frac{3}{2}$	$W(\theta)=P_0-\frac{(0.28-0.04t)+(1.42-0.203t)X-(0.143-0.02t)X^2}{(1 + X^2)(1 + t)}P_2$
L. $\frac{5}{2}\rightarrow\frac{5}{2}\rightarrow\frac{3}{2}$	$W(\theta)=P_0-\frac{(0.263+0.04t)+(1.333+0.203t)X-(0.134+0.0204t)X^2}{(1 + X^2)(1 + t)}P_2$ $-\frac{(0.093+0.3265t)X^2}{(1+X^2)(1+t)}P_4$

Transitions with $\Delta J \geq 3$ were ignored throughout. In Table 6.1, X is the mixing ratio (quadrupole/dipole) of the observed γ-ray and t is that of the unobserved γ-ray.

4. The 662 keV resonance (Ex = 8.908 MeV)

The decay scheme of the 662 keV resonance level was previously studied by Van der Leun et al. (VA 56) and Ophel et al. (OP 62a) with NaI(Tl) detectors. Both groups assigned the most intense γ-rays with energies of 5.25 and 2.80 MeV to the cascade r → 3.68 (5.23 MeV) and 3.68 → 0.84 (2.84 MeV). The improved resolution of Ge(Li) detectors enabled the present work and that of Van der Leun et al. (VA 67) to identify 2.80 and 5.25 MeV γ-rays with the cascade r → 6.160 (2.748 MeV) and 6.160 → 0.843 (5.317 MeV).

Figure 6.2 shows the spectrum and the decay scheme obtained from the present work and Table 6.2 lists the γ-rays observed with the results of Van der Leun et al. listed in column 5 for comparison. In general the agreement is excellent.

The slight discrepancy in the intensity of the cascade r → 6.160, 36% as compared to 43% of Van der Leun, occurred also at 719 keV resonance level in which the intensity of the cascade r → 6.160 was 34% from the present work while that of Van der Leun was 41%. Since

Figure 6.2

Resonance spectrum and decay scheme of the 662 keV resonance. Circles are data and the least squares line shape fit is the solid line.

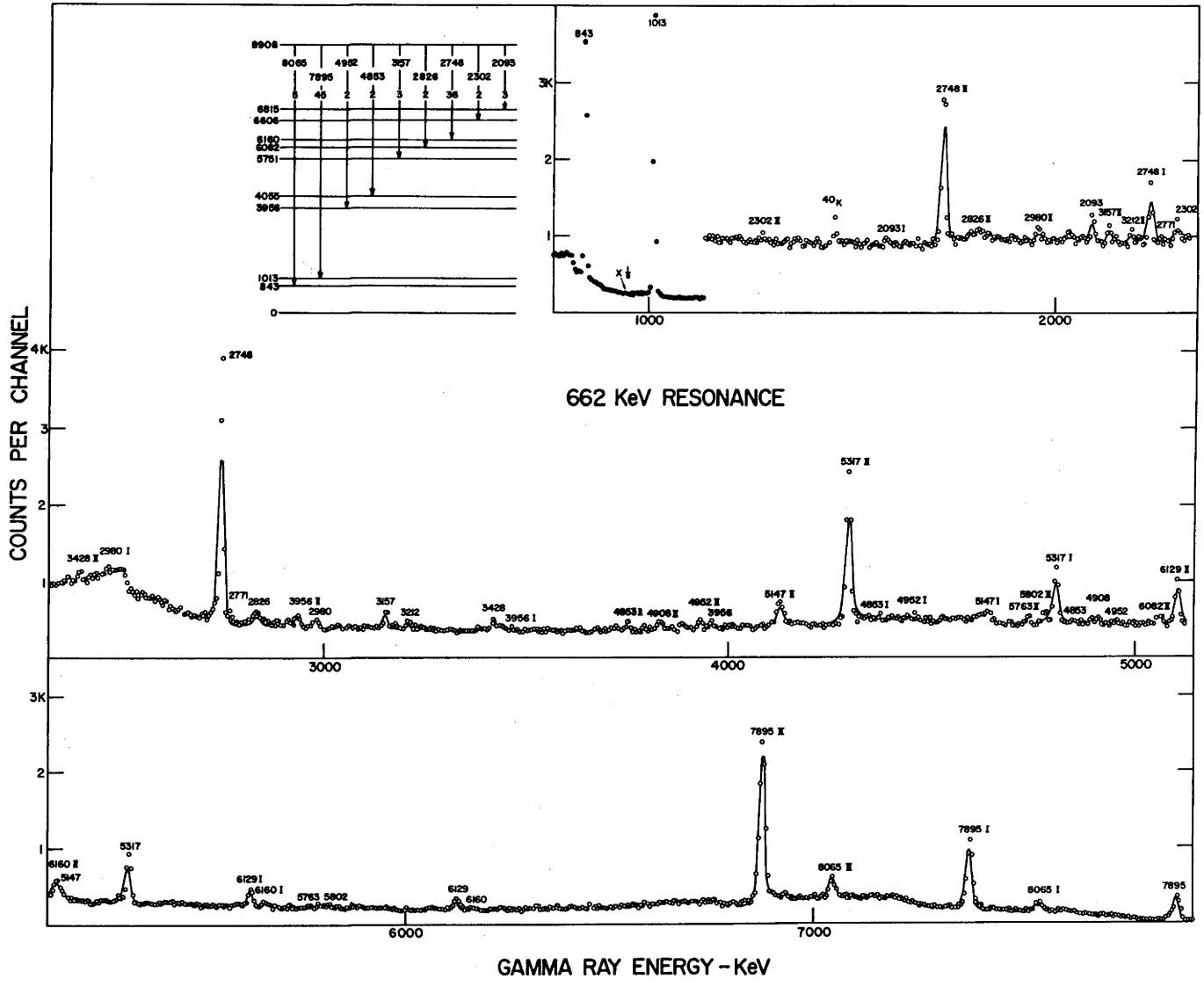
662 KeV RESONANCE
COUNTS PER CHANNEL
GAMMA RAY ENERGY - KeV
8908
8065
4952
357
2748
2093
7895
4853
2826
2302
6815
6606
6180
6082
5751
4055
3956
1013
843
0
2748
5317
7895
6129
6160
5147
3428
2980
2771
2826
3956
3212
4853
4908
5763
5802
2302
2093
3571
3212
2771
2980
4952
6082
5471

Table 6.2

Gamma-rays observed at 662 keV resonance

Eγ(MeV)	Interpretation	Relative intensity	Branching ratio % (resonance level)	(VA 67) %
0.843	0.843 → 0.	77		
1.013	1.013 → 0.	100		
2.093	8.908 → 6.815	6	3	2
2.302	8.908 → 6.606	4	2	-
2.748	8.908 → 6.160	81	36	43
2.771	5.751 → 2.980	2		
2.826	8.908 → 6.082	4	2	3
2.980	2.980 → 0.	5		
3.157	8.908 → 5.751	7	3	2
3.212	4.055 → 0.843	4		
3.428	6.160 → 2.732	4		
3.956	3.956 → 0.	5		
4.853	8.908 → 4.055	4	2	1
4.908	5.751 → 0.843	4		
4.952	8.908 → 3.956	4	2	2
5.147	6.160 → 1.013	11		
5.317	6.160 → 0.843	62		
5.763	6.606 → 0.843	3		
5.802	6.815 → 1.013	4		
6.082	6.082 → 0.	4		
6.129	$^{19}F(p,\alpha\gamma)^{16}O$	20		
6.160	6.160 → 0.	5		
7.895	8.908 → 1.013	102	45	42
8.065	8.908 → 0.843	12	5	5

the relative intensities of the present work were deduced from intrinsic full energy peak efficiencies as well as line shape analysis and the measurements made at 55^{o} rather than 45^{o} as chosen by Van der Leun *et al*. (VA 67), more accurate results are expected from the present work.

The cascade r → 6.606 (2.302 MeV) was not reported by Van der Leun et al. The observed peak at 2.302 MeV was further supported by the existence of 5.763 MeV γ-ray from the cascade 6.606 → 0.843 which accounts 75% of the decay of the 6.606 MeV level (VA 67).

The decay of the 5.751 MeV level has not been reported previously. The decay of this level to the 0.843 and 2.980 MeV levels is consistent with the measurement at the 954 keV resonance in which the 5.751 MeV level was rather strongly excited enabling the observation of the cascade 5.751 → 1.013 as well.

The spin of the 6.082 MeV level so far has not been proposed. The observation of the 6.082 MeV (6.082 → 0) γ-ray suggests the spin of the level is $\frac{3}{2}$, since the level was excited by the resonance level with spin $\frac{1}{2}$ (EN 62) and decays to the ground state ($\frac{5}{2}$). The existence of the cascade 6.082 → 0 was also observed at 839 keV resonance which also has a spin of $\frac{1}{2}$ (OP 62).

5. The 719 keV resonance (E_x = 8.963 MeV)

5.1 Decay scheme of the 719 keV resonance level

The decay scheme of the 719 keV resonance was measured previously by Van der Leun (VA 56), Ophel and Lawergren (OP 62) and Osgood (OS 65) using NaI(Tl) crystals as γ-ray detectors. Each measurement failed to

resolve the γ-rays from the transitions r → 6.16 (2.80 MeV) and 3.68 → 1.01 (2.67 MeV) from the 2.84 MeV (3.68 → 0.84) γ-ray. Another feature of the previous measurements was the transition from the resonance to the 2.21 MeV ($\frac{7}{2}$) level, reported as 28% and 16% of the total decay by Van der Leun and Ophel and Lawergren respectively. Osgood succeeded in finding an alternate explanation of the cascade r → 2.21 → 0 in terms of a cascade r → 6.6 → 0, however, the coicidence measurement of the unresolved 2.84 MeV γ-ray led him to the incorrect assignments of spin $\frac{5}{2}$ and $\frac{3}{2}$ for the resonance level and 3.68 MeV level respectively. During the present investigation, Van der Leun (VA 67) published the decay scheme of this 719 keV resonance, the two results agree within experimental errors. However, the cascade r → 7.00 MeV (3% by Van der Leun) was not observed in this work.

Osgood had studied the 719 keV resonance (he reported as 721 keV) in great detail by measuring but not interpreting correctly a number of coicidence spectra (Figure 6.3), which are in good agreement with the decay scheme of present work. The γ-ray spectrum in coincidence with 0.84 MeV γ-ray has prominent 5.3 and 2.8 MeV γ-rays, supporting the cascades r → 6.16 (2.80 MeV),

Figure 6.3

The γ-ray spectra observed in coincidence with the energy intervals shown at the 719 keV resonance. All spectra collected for 10^6 monitor counts (OS 65).

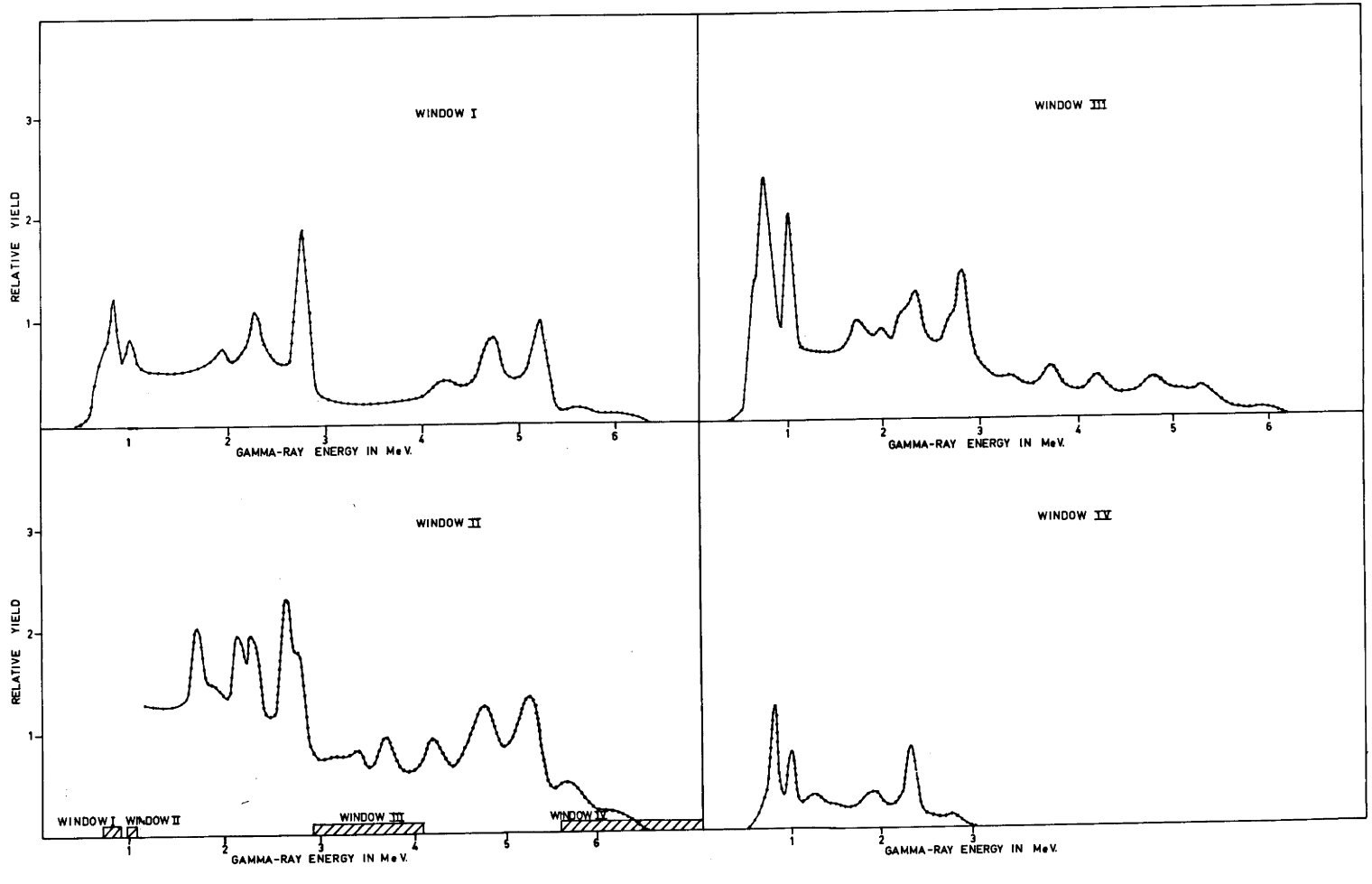
WINDOW I
WINDOW II
WINDOW III
WINDOW IV
RELATIVE YIELD
GAMMA-RAY ENERGY IN MeV.
WINDOW I WINDOW II
WINDOW III
WINDOW IV

6.16 → 0.84 (5.32 MeV), r → 3.68 (5.28 MeV), 3.68 → 0.84 (2.84 MeV).

The γ-ray spectrum in coincidence with 1.01 MeV γ-ray indicates γ-rays at 1.7, 2.3, 2.7, 2.8, 3.4, 3.8, 4.2, 5.3, 5.6, 6.2 MeV, in agreement with the decay of r → 2.73 (6.23 MeV), 2.73 → 1.01 (1.72 MeV), r → 3.68 (5.28 MeV), 3.68 → 1.01 (2.67 MeV), r → 6.16 (2.80 MeV), 6.16 → 2.73 (3.43 MeV), 6.16 → 1.01 (5.15 MeV), r → 6.65 (2.31 MeV), 6.65 → 1.01 (5.64 MeV), r → 4.81 (4.15 MeV), 4.81 → 1.01 (3.80 MeV).

The γ-ray spectrum in coincidence with γ-rays between 2.8-4.2 MeV region, has prominent peaks at 0.84 and 1.01 MeV and is in accord with the present decay scheme. The prominent peaks at 2.7, 4.2, 5.3 and 6.0 MeV are consistent with the cascades r → 6.16 (2.80 MeV), 6.16 → 1.01 (5.15 MeV), 6.16 → 0 (6.16 MeV), r → 3.68 (5.28 MeV), 3.68 → 0.84 (2.84 MeV), 3.68 → 1.01 (2.67 MeV), r → 4.81 (4.15 MeV), 4.81 → 1.01 (3.80 MeV), r → 5.24 (3.72 MeV), 5.24 → 1.01 (4.24 MeV).

Likewise, the spectrum in coincidence with γ-rays above 4.6 MeV has prominent peaks at 0.84, 1.01 and 2.3 MeV, the latter resulting from the transition of r → 6.65 (2.31 MeV), 6.65 → 0 (6.65 MeV).

Figure 6.4 shows the 719 keV resonance measured at 55°, the circles are data and the least squares line

Figure 6.4

Resonance spectrum and decay scheme of the 719 keV resonance. Circles are data and the least squares line shape fit is the solid line.

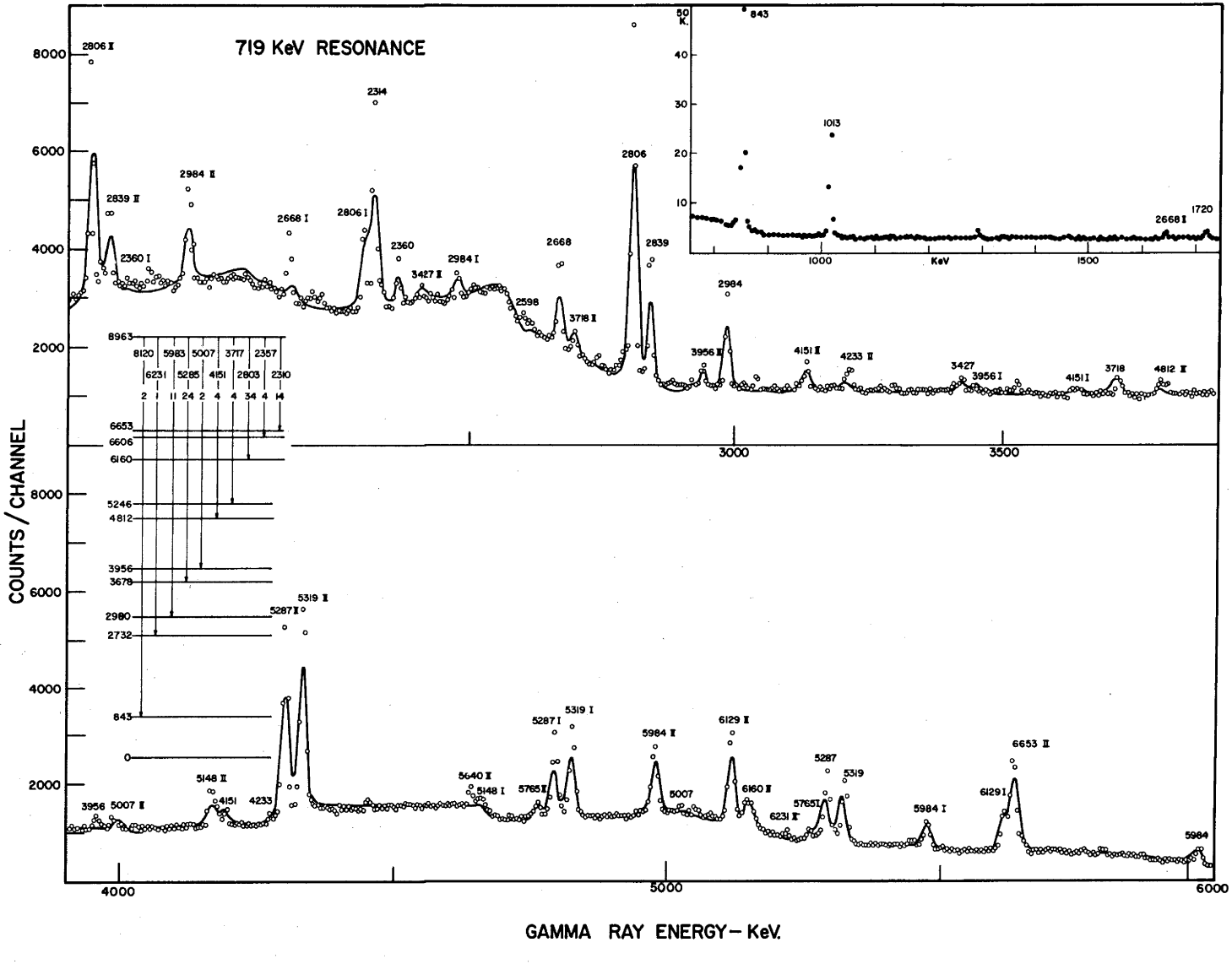
719 KeV RESONANCE
COUNTS / CHANNEL
GAMMA RAY ENERGY – KeV.
2806 I
2839 II
2984 II
2360 I
2668 I
2314
2806 I
2360
3427 II
2984 I
2668
2806
2839
2598
3718 I
2984
3956 II
4151 II
4233 II
3427
3956 I
4151 I
3718
4812 II
1013
843
1720
2668 I
KeV
8963
8120
5983
5007
3717
2357
6231
5285
4151
2803
2310
2 1 11 24 2 4 4 34 4 14
6653
6606
6160
5246
4812
3956
3678
2980
2732
843
0
5319 II
5287 II
5148 II
3956
5007 II
4151
4233
5640 II
5148 I
5765 II
5287 I
5319 I
5984 II
5007
6129 II
6160 II
6231 II
5765 I
5287
5319
5984 I
6129 I
6653 II
5984

shape fit is the solid line. Table 6.3 lists the relative intensities of γ-rays and the branching ratio of the resonance level. The result of Van der Leun et al. is listed in colum 5 for comparison with the present work.

Table 6.3

Gamma rays observed at the 719 keV resonance

E_γ(MeV)	Interpretation	Relative intensity	Branching ratio % (resonance level)	(VA 67) %
0.843	0.843 → 0.	100		
1.013	1.013 → 0.	54		
1.720	2.732 → 1.013	9		
2.314	8.963 → 6.653	30	14	14
2.360	8.963 → 6.606	9	4	4
2.598	4.812 → 2.209	2		
2.668	3.678 → 1.013	18		
2.806	8.963 → 6.160	75	34	41
2.839	3.678 → 0.843	30		
2.984	2.980 → 0.	27		
3.037	5.246 → 2.209	3		
3.427	6.160 → 2.732	6		
3.718	8.963 → 5.246	9	4	2
3.956	3.956 → 0.	7		
4.151	8.963 → 4.812	9	4	3
4.233	5.245 → 1.013	8		
4.812	4.812 → 0.	4		
5.007	8.963 → 3.956	4	2	1
5.148	6.160 → 1.013	8		
5.287	8.963 → 3.678	53	24	20
5.319	6.160 → 0.843	60		
5.640	6.653 → 1.013	4		
5.765	6.606 → 0.843	5		
5.984	8.963 → 2.980	25	11	10
6.160	6.160 → 0.	8		
6.129	$^{19}F(p,\alpha\gamma)^{16}O$	30		
6.232	8.963 → 2.732	2	1	1
6.606	6.606 → 0.	1		
6.653	6.653 → 0.	33		
8.115	8.963 → 0.843	4	2	1
-	(8.963 → 7.000)	-	-	3

5.2 Angular correlation measurements at the 719 keV resonance

The 719 keV resonance level decays 34% to the 6.16 MeV level, 24% to the 3.68 MeV level enabling determinations of the spins of the resonance level, the 6.16 MeV level and the 3.68 MeV level. Preliminary measurements at six angles found no appreciable P_4 terms, consequently spectra were measured at 0^o and 90^o. Table 6.4 summarizes the results (which assumed no P_4 terms).

Table 6.4

E_γ(MeV)	Interpretation	A_2
0.843	0.843 → 0	0.00 ± 0.01
1.013	1.013 → 0	0.03 ± 0.02
2.665	3.678 → 1.013	0.00 ± 0.13
2.803	r → 6.160	0.34 ± 0.05
2.835	3.678 → 0.843	0.00 ± 0.06
5.285	r → 3.678	-0.38 ± 0.03
5.317	6.160 → 0.843	-0.11 ± 0.03
5.285+5.317		-0.23 ± 0.03
2.665+2.803+2.835		0.21 ± 0.04

The isotropic distribution obtained for the 0.843 MeV γ-ray shows that the geometrical arrangement of the detector and target is consistent at both angles.

The isotropic distributions of both the 2.665 MeV (3.678 → 1.013) and 2.835 MeV (3.678 → 0.843) γ-rays and the pure dipole transition ($\frac{3}{2} \rightarrow \frac{1}{2}$) of the 5.285 MeV

(r → 3.678) γ-ray are consistent with decay sequences of $\frac{3}{2} \rightarrow \frac{1}{2} \rightarrow \frac{3}{2}$ (for 2.665 MeV) and $\frac{3}{2} \rightarrow \frac{1}{2} \rightarrow \frac{1}{2}$ (for 2.835 MeV). (See Table 6.1, G & H). The pure dipole nature of the 5.285 MeV γ-ray was deduced from Figure 6.5, by assuming that the resonance level has a spin $\frac{3}{2}$ and decay to $\frac{1}{2}$ state with mixing ratio X. The experimental value of the anisotropy $A_2 = -0.38 \pm 0.03$ determines that the value of X≈0. The isotropic nature of both the 2.665 MeV and 2.835 MeV γ-rays was further confirmed in the study of 954 keV resonance level which decays 16% to 3.678 MeV level. These are considered conclusive evidence that the 3.678 MeV level has $J = \frac{1}{2}$ in agreement with the assignment of Lawergren (LA 67a).

The assumption that the 719 keV resonance has spin $\frac{3}{2}$ is consistent with the decay scheme; only states with spin of $\frac{1}{2}$, $\frac{3}{2}$ and $\frac{5}{2}$ are found excited by de-excitation of this level. This assignment agrees with previous suggestions (VA 67).

The analysis of the spin of the 6.16 MeV level was based on the resonance level having a definite $J = \frac{3}{2}$. The fact that the 6.16 MeV level is strongly excited at 662 keV resonance ($\frac{1}{2}$), limits the spin of this state to $\frac{1}{2}$, or $\frac{3}{2}$, from the criterion that for $\Delta J = 2$, the transition strength is < 2% (VA 67). The first γ-ray 2.803 MeV in the cascade r → 6.160 → 0.843 was analyzed

Figure 6.5

Plot of the coefficient of $P_2(\cos\theta)$ term versus arctangent of X, the quadrupole/dipole mixing ratio, for the transition $\frac{3}{2} \rightarrow \frac{1}{2}$ (Table 6.1,A).

Figure 6.6

Plot of the coefficient of $P_2(\cos\theta)$ term versus arctangent of X, the quadrupole/dipole mixing ratio, for the transition $\frac{3}{2} \rightarrow \frac{3}{2}$ (Table 6.1,B).

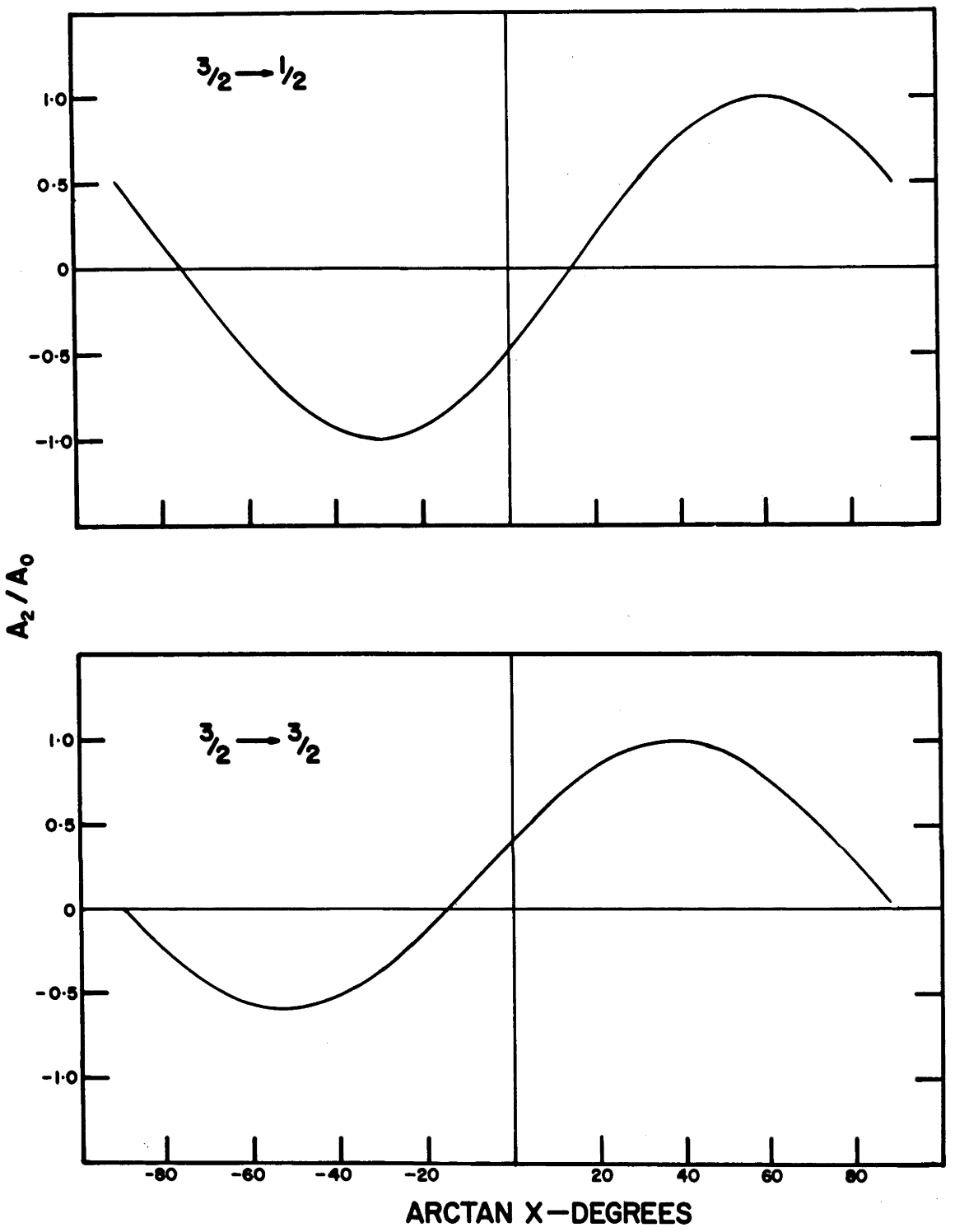
3/2 → 1/2
1·0
0·5
0
-0·5
-1·0
A2 / A0
3/2 → 3/2
1·0
0·5
0
-0·5
-1·0
-80
-60
-40
-20
20
40
60
80
ARCTAN X—DEGREES

Figure 6.7

The contour plot of the coefficient of $P_2(\cos\theta)$ term for the spin sequence $\frac{3}{2} \rightarrow \frac{3}{2} \rightarrow \frac{1}{2}$ with first γ-ray unobserved (Table 6.1 I). The hatched area indicates the possible region determined by the experimental value.

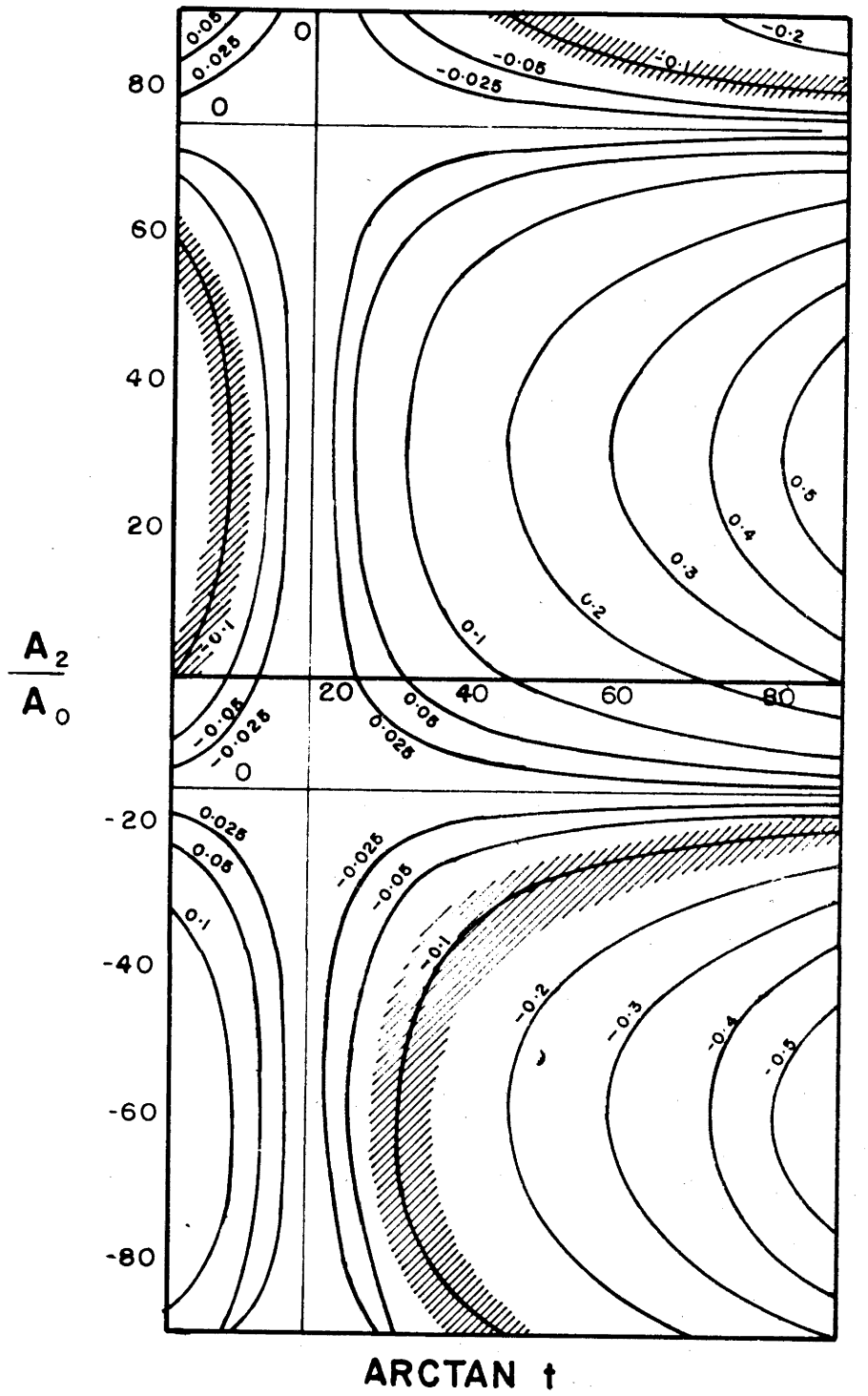
$\frac{A_2}{A_0}$
80
60
40
20
-20
-40
-60
-80
20
40
60
80
0
0.05
0.025
0.1
0.2
0.3
0.4
0.5
-0.05
-0.025
-0.1
-0.2
-0.3
-0.4
-0.5
ARCTAN t

for the spin sequence of $\frac{3}{2} \rightarrow \frac{3}{2}$, since the anisotropic distribution of the second γ-ray of energy 5.317 MeV (6.16 → 0.843) shows that the spin of the 6.16 MeV level is not $\frac{1}{2}$. Figure 6.6 shows the plot of mixing ratio X vs A_2. The experimental value $A_2 = 0.34 \pm 0.05$, again corresponds to a value of $X \approx 0$, i.e., the 2.803 MeV γ-ray is a pure dipole transition.

The contour plot of the second γ-ray (5.317 MeV) is shown in Figure 6.7, assuming the spin sequence of $\frac{3}{2} \rightarrow \frac{3}{2} \rightarrow \frac{1}{2}$ with first γ-ray not observed. The experimental value of $A_2 = -0.11 \pm 0.03$ defines three possible regions (shown as hatched areas). One of these regions corresponds to both members of the cascade being pure dipole. One can conclude with fair certainty that the spin of the 6.160 MeV level is $\frac{3}{2}$. This assignment supports the tentative assignment of $\frac{3}{2}$ by Sheppard et al. (SH 67) based only on intensity arguments.

As mentioned by Van der Leun et al. (VA 67), the 6.160 MeV level is excited strongly only at 662 keV and 719 keV resonances. Since the spin of the 662 keV resonance level is $\frac{1}{2}$, the information obtainable from angular correlation measurements is severely limited because the γ-ray distributions are isotropic. The 719 keV resonance level with spin $\frac{3}{2}$ is suitable for the study of angular correlation but the presence of γ-rays with

energies 2.665, 2.803 and 2.835 MeV means that the use of high resolution Ge(Li) detector is necessary. In consequence, more detailed correlation work was not considered practicable.

It is interesting to compare the results of Osgood (OS 65) with the present work, Osgood measured the angular distribution of the 5.28 MeV (r → 3.68) γ-ray which in fact contained also the 5.32 MeV γ-ray from the transition 6.16 MeV level to 0.84 MeV level, and obtained the value $A_2 = -0.22 \pm 0.05$, this is in agreement with the angular distribution of the sum of 5.285 and 5.317 MeV γ-ray (Row 8, Table 6.4) obtained from this work. Also the angular distribution of the 2.84 MeV (3.68 → 0.84) γ-ray was found to be not isotropic $A_2 = 0.22 \pm 0.01$; in fact the 2.84 MeV γ-ray also contained 2.80 MeV (r → 6.16) and 2.67 MeV (3.68 → 1.01) γ-rays. His value of A_2 is also in agreement with that of the sum of 2.665, 2.803 and 2.835 MeV γ-rays of this work (Row 9, Table 6.4), providing confirmation of the present measurements.

6. The 809 keV resonance (Ex = 9.052 MeV)

6.1 Decay scheme of the 809 keV resonance

The decay scheme of the 809 keV resonance level was previously studied with NaI(Tl) detectors by Ophel *et al.* (OP 62) and the spin determined as $\frac{5}{2}$ from the analysis of

double and triple correlation measurements of the cascades r → 0, r → 1.013 and r → 2.732.

The resonance spectrum and the decay scheme of the present work is shown in Figure 6.8. The relative intensities of γ-rays were deduced from line shape analysis and peak intensities. Circles are the data and least squares line shape fit is the solid line. Table 6.5 summarizes the γ-rays observed at the 809 keV resonance with the results of Ophel et al. in column 5. The transition r → 4.410, which was not previously reported (OP 62), was excited rather strongly (8%) enabling further study of the decay scheme of the 4.410 MeV level.

6.2 Decay scheme of the 4.410 MeV level

The discrepancy observed in the decay scheme of the 4.410 MeV level between Metzger (ME 65), Van der Leun (VA 67) and Spear (SP 67) was discussed in section 2.4 of this chapter.

The present measurement found that 4.410 MeV level decays 67% to the ground state and 33% to the 1.013 MeV state with no positive evidence for the transition 4.410 → 2.209 MeV state. Since the decay of the resonance level to the 2.209 and 2.732 MeV levels is strong, the first escape peak of the 2.732 MeV (2.732 → 0) γ-ray with

energy 2.221 MeV is closely adjacent to the 2.201 MeV (4.410 → 2.209) and 2.209 MeV (2.209 → 0) peaks. The original decay scheme, which was deduced from a spectrum contained in 2048 channels, was re-measured with 4096 channels in order to investigate the possible γ-ray at 2.201 MeV. Indeed no γ-ray of this energy was observed. It was felt that an upper limit of 5% on this transition could be made, in agreement with the result of Spear. Since Van der Leun also used a Ge(Li) γ-ray spectrometer for studying $^{26}Mg(p,\gamma)^{27}Al$ reaction, his claim of 25% cascade from the 4.410 MeV level to the 2.209 MeV level might have been distorted by the first escape peak of the 2.732 MeV γ-ray although it would seem that the energy difference is sufficient to avoid mis-interpretation.

6.3 Angular correlation measurements at the 809 keV resonance

The results of the measurements at three angles 0^{o}, 45^{o} and 90^{o} to the beam direction are summarized in Table 6.6. The angular distributions of the cascades r → 0, r → 1.013 and r → 2.732 of the NaI(Tl) results are from the reference (OP 62).

Table 6.5

Gamma-rays observed at the 809 keV resonance

E_γ(MeV)	Interpretation	Relative intensity	Branching ratio % (resonance level)	OP 62
0.843	0.843 → 0.	6.0		
1.013	1.013 → 0.	150.		
1.720	2.732 → 1.013	52.0		
1.822	9.052 → 7.230	1.5	<1	
2.057	9.052 → 6.997	1.2	<1	
2.211	2.209 → 0.	20.0		
2.587	6.997 → 4.410	1.0		
2.732	2.732 → 0.	14.0		
2.982	2.980 → 0.	5.6		
3.396	4.410 → 1.013	8.0		
3.501	9.052 → 5.551	2.7	1	} 5
3.804	9.052 → 5.246	13.2	4	
3.957	3.956 → 0.	6.8		
4.236	5.246 → 1.013	11.4		
4.411	4.410 → 0.	18.0		
4.471	9.052 → 4.581	2.9	1	
4.581	4.581 → 0.	2.1		
4.643	9.052 → 4.410	26.0	8	
5.021	7.230 → 2.209	1.7		
5.099	9.052 → 3.956	8.0	2	
5.551	5.551 → 0.	0.9		
6.070	9.052 → 2.980	4.4	1	
6.319	9.052 → 2.732	72.0	21	21
6.840	9.052 → 2.209	7.2	2	2
8.040	9.052 → 1.013	100.	29	36
9.053	9.052 → 0.	100.	29	36

Table 6.6

E (MeV)	Interpretation	a_2 : Ge(Li)	A_2 : NaI(Tl)
9.052	r → 0.	0.25 ± 0.0.02	0.26 ± 0.02
8.039	r → 1.013	-0.39 ± 0.05	-0.37 ± 0.03
6.320	r → 2.732	-0.19 ± 0.02	-0.32 ± 0.06
4.642	r → 4.410	-0.20 ± 0.02	
3.806	r → 5.246	0.37 ± 0.02	
4.233	5.246 → 1.013	-0.20 ± 0.05	

The observed coefficients a_2 ($a_2 = A_2Q_2$) of the Ge(Li) data for the two strongest cascades r → 0 and r →1.013 are within experimental errors of the corrected values of the coefficients A_2 of the corresponding NaI(Tl) data. This fact indicates that the angular correlation attenuation factor Q_2 is approximately equal to unity. The calculation of the value under various assumptions discussed in previous chapter shows Q_2 is of the order of 0.84, the corrections were actually not made to obtain the value of A_2. This applies to the angular distributions measured at the 719 and 954 keV resonances.

The anisotropy for the cascade r → 1.013 corresponds to a pure dipole transition (Table 6.1, D), however, significant quadrupole and dipole mixings were observed for the cascades r → 0 (X = -0.18) and r → 2.732 (X = -0.59). This is a feature different from the decay observed at the 719 and 954 keV resonances in which strong transitions from the resonance level are of a pure dipole nature.

The spin of the 4.410 MeV level was assigned by Metzger (ME 65) and Sheppard et al. (SH 67) as $\frac{5}{2}$ and by Lawergren (LA 67a) as $\frac{3}{2}$. The present analysis of the angular distribution of the 4.642 MeV (r → 4.410) γ-ray for the spin sequences of $\frac{5}{2} \rightarrow \frac{3}{2}$, $\frac{5}{2} \rightarrow \frac{5}{2}$ and $\frac{5}{2} \rightarrow \frac{7}{2}$ shows

quadrupole and dipole mixing ratios of values 0.10, -0.60 and -0.04 is required respectively for the observed anisotropy of $A_2 = -0.20$. The assignment of $J = \frac{7}{2}$ can be excluded from the argument that the 4.410 MeV decays strongly to 1.013 MeV level $(\frac{3}{2})$ since $\Delta J = 2$ is very unlikely. The assignment of $J = \frac{3}{2}$ is most probable as this will give the transition $r \rightarrow 4.410$ a near dipole nature $(X = 0.10)$, however, from the strong mixing of quadrupole and dipole radiations evidenced at the 809 keV resonance, the assignment of $J = \frac{5}{2}$ is also possible $(X = -0.60)$. The assignment of $J = \frac{3}{2}$ to the 4.410 MeV level is consistent with the observed cascades $4.410 \rightarrow 0$ $(\frac{3}{2} \rightarrow \frac{5}{2})$ and $4.410 \rightarrow 1.013$ $(\frac{3}{2} \rightarrow \frac{3}{2})$ and no cascade of $4.410 \rightarrow 2.209$ $(\frac{3}{2} \rightarrow \frac{7}{2})$. Thus the present work favours an assignment of $J = \frac{3}{2}$ to the 4.410 MeV level; the decay scheme of the 4.410 MeV level derived by Metzger and Sheppard et al. is in error and the disputed cascade essentially determined the assignment of $J = \frac{5}{2}$ made by them.

The spin of the 5.246 MeV level was tentatively proposed by Sheppard et al. (SH 67) to be $\frac{5}{2}$. The present analysis of the anisotropies observed for the cascade $r \rightarrow 5.246$ $(X = -0.08)$ and $5.246 \rightarrow 1.013$ $(X = -0.04)$ is consistent with the spin sequence of $\frac{5}{2} \rightarrow \frac{5}{2} \rightarrow \frac{3}{2}$ (Table 6.1, E and L).

7. The 839 keV resonance (Ex = 9.081 MeV)

The decay scheme of the 839 keV resonance level was previously studied by Ophel and Lawergren (OP 62) with NaI(Tl) detectors. The relatively simple spectrum at this resonance enabled the accurate measurement of the γ-rays with NaI(Tl) detectors. The spin of the resonance level was deduced to be $\frac{1}{2}$ from the isotropic distributions of γ-rays from the cascades r → 1.013 ($\frac{1}{2} \rightarrow \frac{3}{2}$) and r → 3.68 ($\frac{1}{2} \rightarrow \frac{1}{2}$).

Table 6.7 lists the γ-rays observed at this resonance by the present study with a Ge(Li) detector. Column 4 lists the branching ratio of cascades from the resonance level and column 5 lists the result of Ophel et al. The agreement between the two results is excellent. The γ-rays of weak intensity which were not identified by Ophel et al., however, were assigned by the present work.

The presence of the cascades r → 5.751 and r → 5.828 suggests the spin of the 5.751 and 5.828 MeV levels to either $\frac{1}{2}$ or $\frac{3}{2}$. The discussion of the spins of these levels is given in the study of the 954 keV resonance.

The decay to the ground state from the 6.082 MeV level is consistent with the observation at the 662 keV resonance, where the spin of the 6.082 MeV was proposed as $\frac{3}{2}$.

Figure 6.9

Resonance spectrum and decay scheme of the 839 keV resonance. Circles are data and least squares line shape fit is the solid line.

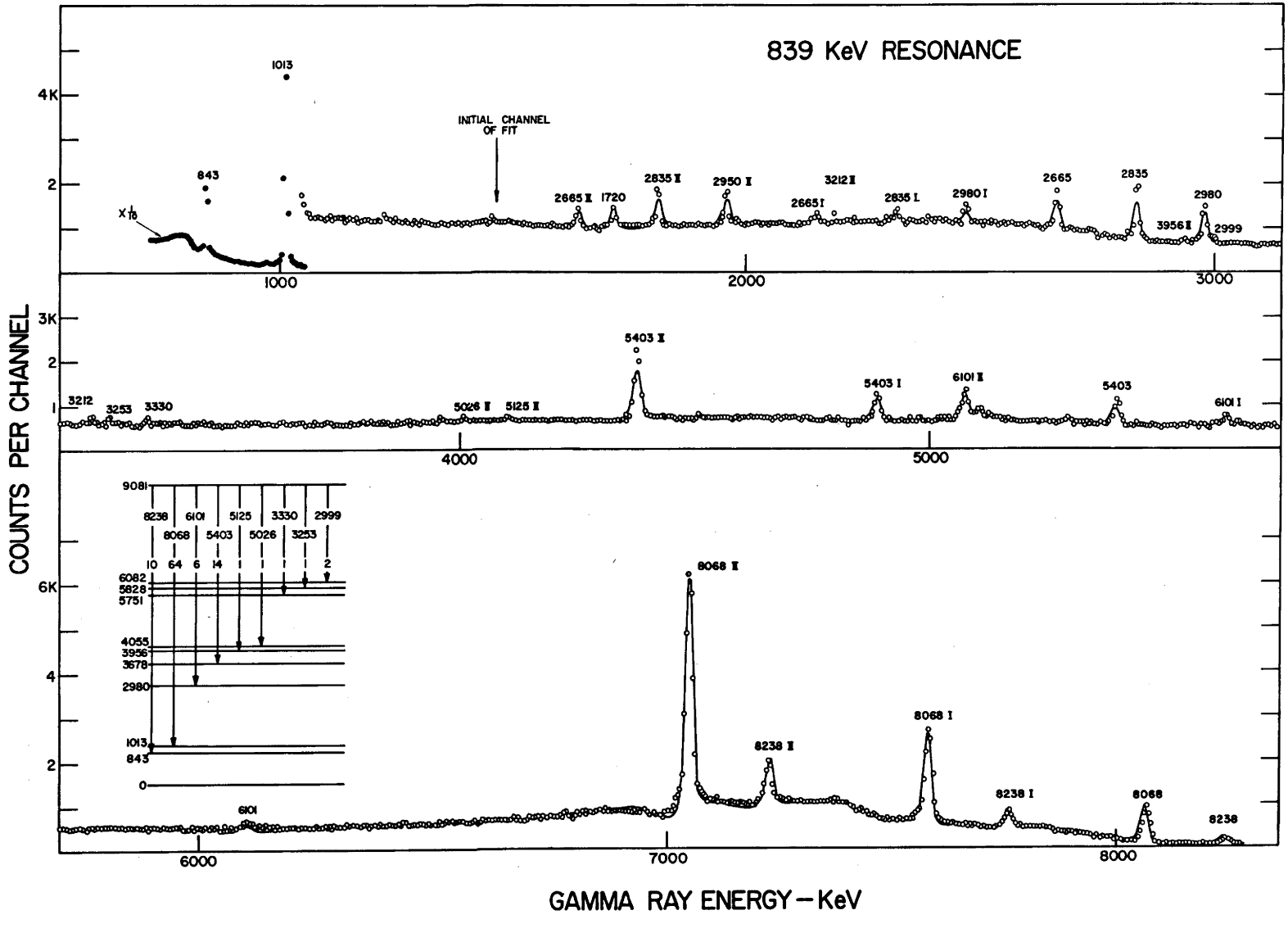
839 KeV RESONANCE
COUNTS PER CHANNEL
GAMMA RAY ENERGY – KeV
INITIAL CHANNEL OF FIT
1013
843
X 10
2665 I
1720
2835 I
2950 I
3212 I
2665 I
2835 I
2980 I
2665
2835
2980
3956 I
2999
5403 I
5403 I
6101 I
5403
6101 I
3212
3253
3330
5026 I
5125 I
9081
8238
6101
5125
3330
2999
8068
5403
5026
3253
10
64
6
14
1
1
1
2
6082
5828
5751
4055
3956
3678
2980
1013
843
0
8068 I
8238 I
8068 I
8238 I
8068
8238
6101
1K
2K
3K
4K
6K
1000
2000
3000
4000
5000
6000
7000
8000

Figure 6.9 shows the resonance spectra and the decay scheme of the 839 keV resonance level. The peak observed at 1.719 MeV is due to contamination from 809 keV resonance which is also apparent from the presence of the ground state transition of the appropriate energy. The error introduced from the 809 keV resonance is insignificant.

Table 6.7

Gamma-rays observed at the 839 keV resonance

E_γ(MeV)	Interpretation	Relative intensity	Branching ratio % (resonance level)	OP 62
0.843	0.843 → 0.	31		
1.013	1.013 → 0.	100		
2.664	3.678 → 1.013	9		
2.835	3.678 → 0.843	13		
2.981	2.980 → 0.	10		
2.998	9.081 → 6.082	3	2	-
3.212	4.055 → 0.843	2		
3.250	9.081 → 5.828	1	1	-
3.331	9.081 → 5.751	2	1	-
3.956	3.956 → 0.	2		
5.026	9.081 → 4.055	2	1	-
5.124	9.081 → 3.956	1	1	-
5.402	9.081 → 3.678	22	14	13
6.082	6.082 → 0.	2		
6.101	9.081 → 2.980	10	6	6
6.129	$^{19}F(p,\alpha\gamma)^{16}O$	2		
8.066	9.081 → 1.013	103	64	71
8.237	9.081 → 0.843	16	10	7
others				3

8. The 954 keV resonance (E_x = 9.191 MeV)

8.1 The decay scheme of the 954 keV resonance

A previous study of the decay scheme of this resonance level was reported by Ophel and Lawergren (OP 62) from measurements with NaI(Tl) detectors. The recent work by Van der Leun et al. (VA 67) who used a Ge(Li) γ-ray spectrometer to study thirty $^{26}Mg(p,\gamma)^{27}Al$ resonances between Ep = 0.3 - 2.8 MeV did not include this resonance. The γ-ray studies of Ophel et al. interpreted the 4.73 MeV and 3.41 MeV γ-rays as transitions r → 4.41 (4.78 MeV) and 4.41 → 1.01 (3.40 MeV); however, the present work re-assigns these γ-rays as transitions 5.828 → 1.013 (4.815 MeV) and r → 5.828 (3.363 MeV) and r → 5.751 (3.440 MeV) respectively.

The doublet at 5.751 MeV and 5.821 MeV is of considerable interest, if one searches through the decay scheme of the 30 resonances studied by Van der Leun et al. the 5.751 MeV level was excited only once at 662 keV resonance with intensity of 2%, while the 5.821 MeV level was not excited at all. The existence of the doublet has been confirmed by Browne et al. (BR 54, BR 59) from the studies of $^{27}Al(p,p')$ and $^{29}Si(d,\alpha)^{27}Al$ reactions with high resolution magnetic spectrograph to have level energies at 5.745 MeV and 5.820 MeV. The measurement of γ-ray energy by Van der Leun et al. with Ge(Li) detector

gave more accurate level energy of 5.751 MeV to the lower level and the present work found 5.828 MeV for upper level energy which was self consistent with the cascade γ-rays decaying through this level. The doublet was excited fairly strongly at 954 keV resonance; each member with the same intensity of 9%.

Figure 6.10 shows the resonance spectrum and the decay scheme, the solid line is the fit from line shape analysis and the circles are the experimental data recorded in 2048 channels. By examining the fit at each peak, it is obvious that the experimental data had a better resolution than the line shapes, this phenomenon severely affects the Chi-square test of the fit, however, the intensities deduced for γ-rays, except for very weak transitions, were not affected. The accuracy of the intensity so obtained could be checked by comparing the intensity of the γ-ray decaying from the resonance level to a low lying level and the sum of intensities of γ-rays decaying from this low lying level. In general total intensities were conserved to within experimental errors of 10 - 15% for cascade γ-rays in decaying to all low lying levels from the resonance level. In fact, in the first attempt to fit the experimental data, the standard line shape with 4.433 MeV γ-ray obtained from $^{15}N(p,\alpha\gamma)^{12}C$ reaction was used. Due to the α-particle

Figure 6.10

Resonance spectrum and decay scheme of the 954 keV resonance. Circles are data and the least squares line shape fit is the solid line.

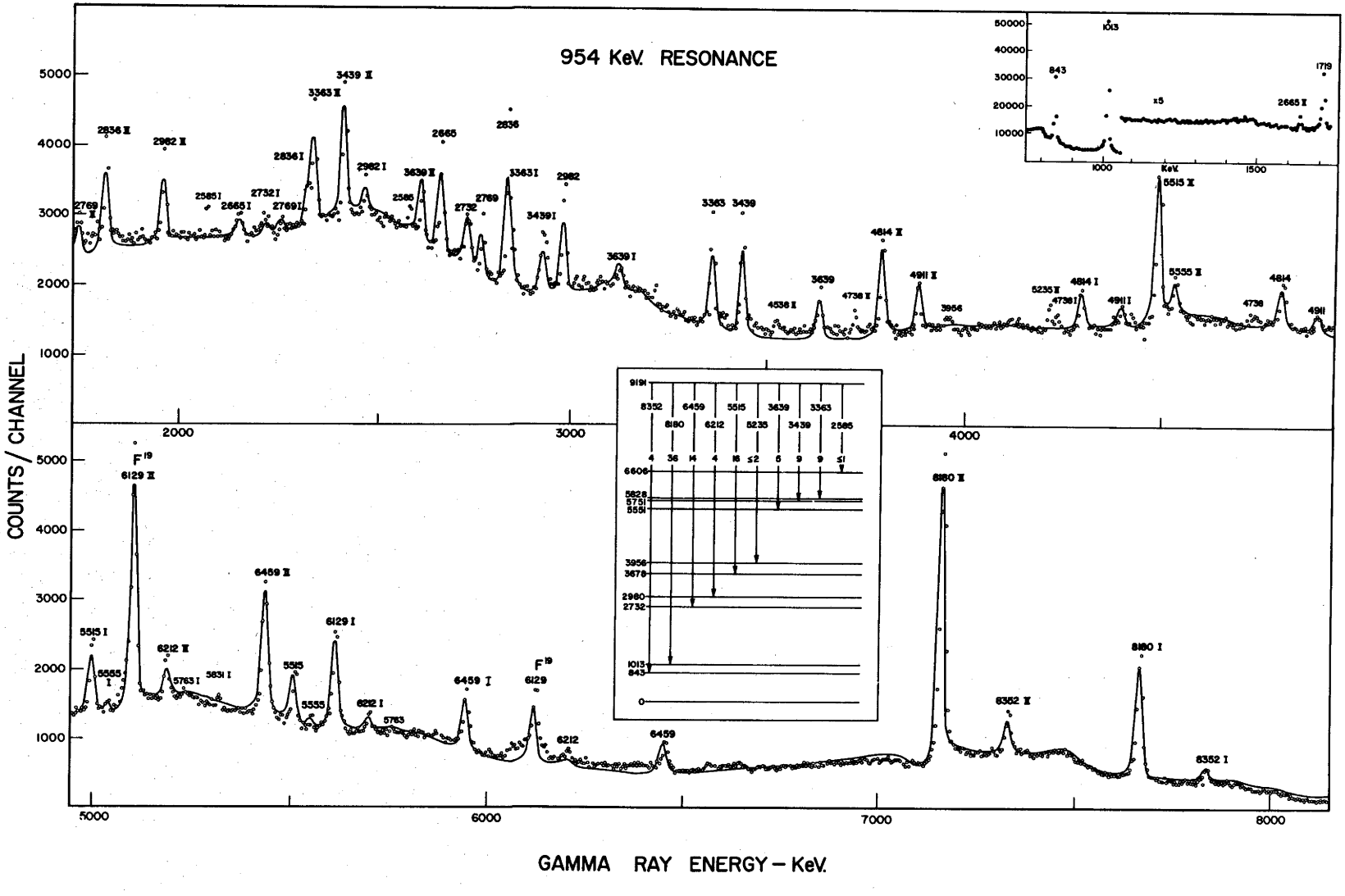
954 KeV. RESONANCE
COUNTS / CHANNEL
GAMMA RAY ENERGY – KeV.
F19
6129 II
6459 II
6212 II
5515 II
6880 II
6352 II
6880 I
6352 I
6459 I
6129 I
6212 I
5515 I
5555 II
5555 I
5763 I
5831 I
2836 II
2962 II
3363 II
3439 II
2665
2836
3363 I
2962
3639 II
3639 I
4536 I
4614 II
4911 II
5235 II
4614 I
5555 II
4911 I
4614
4911
2836 I
2732 I
2769 II
2665 I
2962 I
2732
2769
3439 I
3363 3439
3639
4738 I
3956
4738 I
4738
1013
843
1719
2665 I
x5
KeV.
9191
8352
6459
5515
3639
3363
8180
6212
5235
3439
2585
6606
5628
5751
5551
3956
3678
2960
2732
1013
843
0

recoil, the peaks of the line shape were Doppler broadened and the low energy γ-rays interpolated from the 4.433 MeV γ-ray line shape considerably broadened. The line shape of the 4.433 MeV γ-ray was re-measured using $^{11}B(p,\gamma)^{12}C$ reaction providing better resolution, however, the intensities obtained from the two different fits were not significantly different. This is due to the fact that peaks amount to only a small portion of the total line shape in the spectrum thus the total intensity of a γ-ray is defined more by the Compton distributions.

Discrepancies of the fit at the high energy end are mainly due to the non-linearity of the analyzing system. A parabolic fit to energy calibration ($E = ax^2 + bx + c$) was used for all energy assignments but, for fitting, intermediate γ-ray line shapes were interpolated with the gain and zero (b and c) of the experimental spectrum. The coefficient 'a' which has the value of the order of 10^{-4}~10^{-5} was ignored. This effect shows up at high energy end of the spectrum due to x^2 term, and was common to all the spectra fitted.

A number of γ-rays of small intensity were not included in the fit. The identification of these γ-rays were not very certain, the energy is marked on those peaks which most strongly support the identification. The γ-rays in this category are: 2.585 MeV (9.191 → 6.606),

3.956 MeV (3.956 → 0), 4.738 MeV (5.751 → 1.013), 5.235 MeV (9.191 → 3.956), 5.763 MeV (6.606 → 0.843) and 5.831 MeV (5.828 → 0). The three peaks for 2.585 MeV γ-ray seems to support the transition r → 6.606, however, the second escape peak of the 5.763 MeV (6.606 → 0.843) γ-ray at 4.741 MeV is difficult to distinguish from 4.738 MeV (5.751 → 1.013) γ-ray. The transition 6.606 MeV level to 0.843 MeV level is 75% (VA 67). The three peaks for 4.738 MeV γ-ray seem to support the assigned transition. The transition r → 3.956 (5.235 MeV) obtained from the double escape peak of the 5.235 MeV γ-ray is supported by the full energy peak of the 3.956 MeV γ-ray. The positive assignment cannot be made because the double escape peak of 3.956 MeV γ-ray at 2.934 MeV is not obvious due to the first escape peak of the 3.439 MeV (r → 5.751) γ-ray at 2.928 MeV which has a rather large peak intensity. The 5.831 MeV γ-ray has a double escape peak at 4.809 MeV, which cannot be identified because of the 4.814 MeV (5.828 → 1.013) γ-ray. An alternative assignment of the first escape peak of the 5.831 MeV γ-ray (5.320 MeV) to the double escape peak of the 6.342 MeV γ-ray was not successful because the identification of the 6.342 MeV γ-ray led to difficulty. The assignment of 5.831 MeV γ-ray to the transition 5.828 → 0 seems to be most probable.

The fit in the region 6.0 - 7.0 MeV is relatively poor because 6.92 MeV and 7.12 MeV γ-rays were not included in the fit. The strong intensity for the 6.129 MeV γ-ray indicates the background due to $^{19}F(p,\alpha\gamma)^{16}O$ reaction is strongly present in the spectrum, and the other γ-rays due to the de-excitation of ^{16}O cannot be ignored.

The reasons why some weak γ-ray components were not included in the fit were mainly due to the following:

(1) the limited amount of computer core locations cannot accommodate all components in the fitting program especially in a complicated decay spectrum,

(2) the weak components are usually associated with large errors and even negative intensities.

The relative intensities shown in the decay scheme were derived from line shape analysis and from the estimation of photopeak and double escape peak areas. Table 6.8 shows the results obtained from the two different methods. In general, they agree to within 20% on absolute basis. If the agreement between them was poor, the one considered most reliable was chosen otherwise the two results were averaged. Column 3 lists the intensities obtained from the estimations of photopeak and/or double escape peak areas using absolute photopeak efficiency as experimentally determined.

Table 6.8

E (MeV)	Interpretation	Peak Intensity x 10^7	Relative Intensity	Line Shape Fit x 10^7	Relative Intensity
0.843	0.843 → 0.	1.50	55	-	-
1.013	1.013 → 0.	4.20	150	-	-
1.719	2.732 → 1.103	0.70	25	-	-
2.665	3.678 → 1.013	0.58	21	0.48	17
2.733	2.732 → 0.	0.24	10	0.29	10
2.769	5.751 → 2.980	0.22	8	0.30	10
2.836	3.678 → 0.843	0.78	28	0.80	28
2.982	2.980 → 0.	0.64	23	0.56	20
3.363	9.191 → 5.828	0.74	26	0.74	26
3.439	9.191 → 5.751	0.90	32	0.88	31
3.639	9.191 → 5.551	0.34	12	0.50	18
4.814	5.828 → 1.013	0.76	27	0.74	26
4.911	5.751 → 0.843	0.30	11	0.39	14
5.515	9.191 → 3.678	1.20	41	1.30	45
5.555	5.551 → 0.	0.26	9	0.22	8
6.219	$^{19}F(p,\alpha\gamma)^{16}O$	2.40	90	1.90	67
6.212	9.191 → 2.980	0.32	11	0.24	8
6.459	9.191 → 2.732	1.20	44	1.10	39
8.180	9.191 → 1.013	2.80	100	2.80	100
8.352	9.191 → 0.843	0.32	11	0.34	12
2.585	9.191 → 6.606	0.10	3.6	-	-
4.538	5.551 → 1.013	0.07	2.5	-	-
4.738	5.751 → 1.013	0.12	4.3	-	-
5.235	9.191 → 3.956	0.15	5.4	-	-
5.831	5.828 → 0.	0.15	5.4	-	-

Column 5 lists the intensities obtained from the total counts to zero energy deduced from line shape fits divided by the calculated total detector efficiency.

8.2 Angular correlation measurements at the 954 keV resonance

The 954 keV resonance level decays 16% to the 3.678 MeV level, 9% to the 5.828 MeV level and another 9% to the 5.751 MeV level enabling measurement of the spin of the resonance level, the 3.678, 5.751 and 5.828 MeV levels. The spin of the resonance level was previously reported to be $\frac{3}{2}$ (OP 62), while those for 5.751 and 5.828 MeV levels have not been assigned. Since the 3.678 MeV level was assigned by the present work to have $J = \frac{1}{2}$ from the angular distribution measurements at the 719 keV resonance, the angular correlation measurements at 954 keV enable a further check on the assignment of this level. The spectra were measured at 0^{o}, 45^{o} and 90^{o}. Table 6.9 summarizes the results.

The anisotropic distributions of the 8.178 MeV ($r \rightarrow 1.013$) and 8.348 MeV ($r \rightarrow 0.843$) γ-rays correspond to pure dipole transitions of the spin sequence $\frac{3}{2} \rightarrow \frac{3}{2}$ and $\frac{3}{2} \rightarrow \frac{1}{2}$ respectively, providing further confirmation that the spin of the resonance level is $\frac{3}{2}$.

Table 6.9

E (MeV)	Interpretation	A_2
0.843	0.843 → 0.	0.00 ± 0.02
1.013	1.013 → 0.	-0.01 ± 0.03
1.719	2.732 → 1.013	-0.01 ± 0.05
2.665	3.678 → 1.013	0.00 ± 0.10
2.835	3.678 → 0.843	0.01 ± 0.02
3.363	9.191 → 5.828	0.33 ± 0.14
3.440	9.191 → 5.751	-0.35 ± 0.04
3.640	9.191 → 5.551	-0.08 ± 0.05
5.513	9.191 → 3.678	-0.44 ± 0.03
6.459	9.191 → 2.732	-0.04 ± 0.06
8.178	9.191 → 1.013	0.40 ± 0.06
8.348	9.191 → 0.843	-0.66 ± 0.10

The anisotropy observed for the 5.513 MeV (r → 3.678) γ-ray corresponds to a pure dipole transition corresponding to $\frac{3}{2} \rightarrow \frac{1}{2}$, which is consistent with the previous assignments of $J = \frac{3}{2}$ to the resonance level and $J = \frac{1}{2}$ to the 3.678 MeV level. Furthermore, the isotropic distributions of the 2.665 MeV (3.678 → 1.013) and 2.835 MeV (3.678 → 0.843) γ-rays are consistent with the measurements at the 719 keV resonance.

The spins of the 5.828 and 5.751 MeV levels have been discussed at the 839 keV resonance as $\frac{1}{2}$ or $\frac{3}{2}$. The anisotropy ($A_2 = 0.33 \pm 0.14$) observed for the 3.363 MeV (r → 5.828) γ-ray corresponds to a pure dipole transition for spin sequence $\frac{3}{2} \rightarrow \frac{3}{2}$, which determines the spin of the 5.828 MeV level to be $\frac{3}{2}$. The observed cascades of the

5.828 → 1.013 ($\frac{3}{2}$) and 5.828 → 0 ($\frac{5}{2}$) are consistent with the assignment.

The anisotropic distribution of the 3.440 MeV (r → 5.751) γ-ray ($A_2 = -0.35 \pm 0.04$) differs significantly from a pure dipole transition ($A_2 = -0.5$) corresponding to $\frac{3}{2} \rightarrow \frac{1}{2}$; however, a positive anisotropy $A_2 = +0.4$ is required for the spin sequence $\frac{3}{2} \rightarrow \frac{3}{2}$; hence it is very unlikely that the 5.751 MeV level is a $\frac{3}{2}$ state. The argument that the 5.751 MeV level cannot have a spin greater than $\frac{3}{2}$ leaves $\frac{1}{2}$ as the only possible assignment. This assignment is consistent with the observed decay of the 5.751 MeV level to the 0.843 ($\frac{1}{2}$), 1.013 ($\frac{3}{2}$) and 2.980 ($\frac{3}{2}$) MeV levels and no decay of this level to the ground state ($\frac{5}{2}$).

The angular distribution of the 3.640 MeV (r → 5.551) γ-ray has $A_2 = -0.08 \pm 0.05$ corresponding to a pure dipole transition for $\frac{3}{2} \rightarrow \frac{5}{2}$ (Table 6.1, C). This is in agreement with previous suggestion based on transition strengths (VA 67) that the 5.551 MeV level is a $\frac{5}{2}$ state. Thus the spin of the 5.551 MeV level can be assigned with fair certainty as $\frac{5}{2}$.

The observed anisotropy for the 6.459 MeV (r → 2.732) is consistent with a pure dipole transition for the spin sequence $\frac{3}{2} \rightarrow \frac{5}{2}$. The angular distribution observed for the 1.719 MeV (2.732 → 1.013) γ-ray ($A_2 = -0.01 \pm 0.05$)

determines the E2/M1 mixing ratio X = -0.10 ± 0.04, which is in agreement with the result of Ophel et al. (OP 64) and is in disagreement with that of Sheppard et al. (SH 67). (See Table 6.1, K).

9. The 982 keV resonance (Ex = 9.218 MeV).

The angular correlation measurements of Almqvist et al. (EN 62) at the 982 keV resonance indicated either $J^{\pi} = \frac{7}{2}^{+}$ or $\frac{3}{2}^{+}$ for the resonance level and $J^{\pi} = \frac{5}{2}^{+}$ for the 2.732 MeV level. Since the transition strength from the resonance level to the 0.843 ($\frac{1}{2}^{+}$) and 1.013 ($\frac{3}{2}^{+}$) MeV levels was found at most 3% of the ground state transition, the assignment of $\frac{7}{2}^{+}$ to the resonance level was favoured by Almqvist et al.

Osgood (OS 65) identified the main cascades at this resonance as r → 0, r → 2.73, r → 2.98, r → 6.15 and measured angular distributions of the first three gamma rays and the triple correlation for the cascade r → 2.73 → 1.01. The measurements were consistent with either $J = \frac{5}{2}$ or $\frac{7}{2}$ for the resonance level.

A spectrum measured at 55° and the decay scheme deduced from it (Figure 6.11) confirmed all cascades deduced by Osgood; however, the resonance level also decays weakly to higher energy bound states at 6.778, 7.471 and 8.184 MeV. A level at 8.2 MeV was excited in

Figure 6.11

Resonance spectrum and decay of the 982 keV resonance. Circles are data and the least squares line shape fit is the solid line.

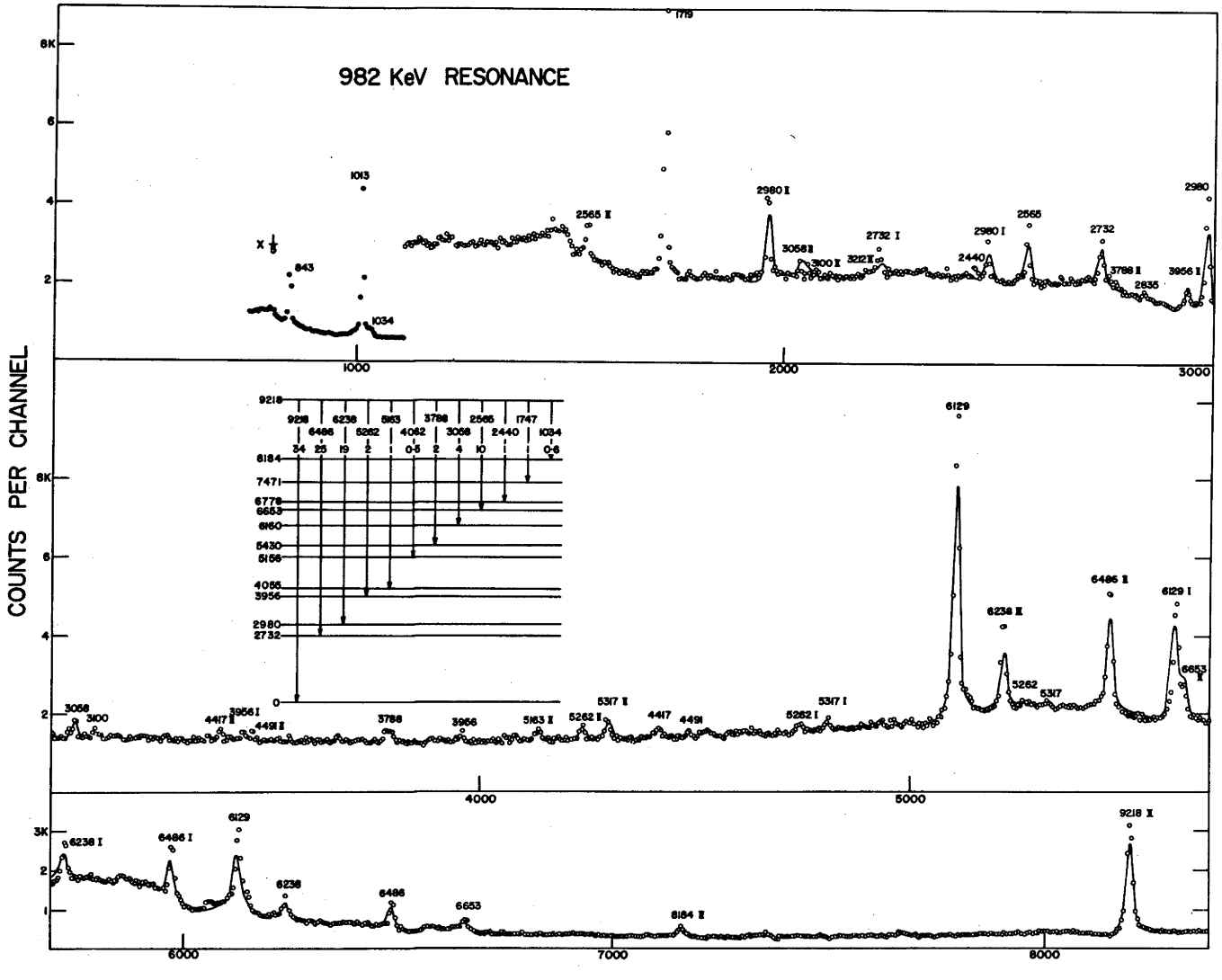
982 KeV RESONANCE
COUNTS PER CHANNEL
GAMMA RAY ENERGY - KeV
1719
1013
843
1034
2565 II
2980 I
3058 I
3300 I
3212 II
2732 I
2440
2980 I
2565
2732
3788 II
2835
3956 I
2980
9218
6238
5262
4082
3058
2440
1034
6184
7471
6778
6653
6160
5430
5156
4086
3956
2980
2732
0
3058
3300
4417 II
3956 I
4491 II
3788
3956
5163 I
5262 II
5317 II
4417
4491
5317 I
6129
6238 II
6486 II
6129 I
5262
5317
6653
6238 I
6486 I
6129
6238
6486
6653
6184 II
9218 II

the $^{26}Mg(d,n)^{27}Al$ reaction and the spin determined from angular distribution measurements as $\frac{1}{2}^-$ or $\frac{3}{2}^-$ (TR 56). The present measurement establishes the level energy as 8184 $\pm$ 4 keV from the γ-ray energies observed in the cascade r $\rightarrow$ 8.184 $\rightarrow$ 0. Clearly the $\frac{3}{2}^-$ assignment is to be preferred.

The 7.471 MeV level was excited in the $^{26}Mg(p,\gamma)$ reaction at Ep = 1733 keV and found to decay partly to the 2.21 MeV level (VA 67) whereas the present spectrum provides evidence for decay to only the 2.98 MeV level.

The level at 6.778 MeV was reported to decay to the ground state (20%), the 0.843 MeV level (55%), the 2.980 MeV level (25%) and the 3.678 MeV level ($\leq$ 20%) (VA 67); of these branches, decay to the 3.678 MeV level was evident in the spectrum at the 982 keV resonance. The reported strong branching from the 6.778 MeV level to the 0.843 MeV level, however, was not observed.

The spin of the resonance level can not be uniquely determined from the transition strengths alone. The decay of the resonance level to the ground state ($\frac{5}{2}$), the 2.732 MeV level ($\frac{5}{2}$), the 2.980 MeV level ($\frac{3}{2}$), the 6.653 MeV level ($\frac{3}{2}$) and the 6.160 MeV level ($\frac{3}{2}$) suggests the resonance level is either $\frac{3}{2}$ or $\frac{5}{2}$. The proposition of $J^\pi = \frac{7}{2}^+$ is rejected conclusively by the strong transition r $\rightarrow$ 2.980 (19%).

The gamma-rays observed at the 982 keV resonance are listed in Table 6.10. The relative intensity of γ-rays were determined from line shape analysis and intrinsic full energy peak efficiencies.

Table 6.10

Gamm-rays observed at the 982 keV resonance

E_γ(MeV)	Interpretation	Relative Intensity	Branching ratio (%) (Resonance Level)
0.843	0.843 → 0	32.9	
1.013	1.013 → 0	107.	
1.034	9.218 → 8.184	2.5	0.6
1.720	2.732 → 1.013	76.8	
1.747	9.218 → 7.471	4.0	1
2.441	9.218 → 6.778	3.8	1
2.565	9.218 → 6.653	38.7	10
2.665	3.678 → 1.013	1.7	
2.736	2.732 → 0	23.2	
2.836	3.678 → 0.843	3.2	
2.983	2.980 → 0	72.9	
3.057	9.218 → 6.160	14.2	4
3.100	6.778 → 3.678	3.9	
3.212	4.055 → 0.843	3.7	
3.788	9.218 → 5.430	8.0	2
3.958	3.956 → 0	11.6	
4.063	9.218 → 5.156	2.1	0.5
4.417	5.430 → 1.013	8.0	
4.492	7.471 → 2.980	4.0	
5.156	5.156 → 0	1.5	
5.163	9.218 → 4.055	4.3	1
5.262	9.218 → 3.956	9.7	2
5.319	6.160 → 0.843	13.5	
6.129	$^{19}F(p,\alpha\gamma)^{16}O$	339.	
6.238	9.218 → 2.980	76.8	19
6.486	9.218 → 2.732	100	25
6.653	6.653 → 0	42.6	
8.184	8.184 → 0	2.6	
9.218	9.218 → 0	134	34

10. Branching ratios of bound states

The branching ratios for a number of bound states which are excited by any of the 662, 719, 809, 839, 954 and 982 keV resonances are summarized below. The branchings of levels below 3 MeV are well established (OP 64, LA 64) and are not included.

The 3.678 MeV level was excited by the decay of the 719 (24%), 839 (14%) and 954 (16%) keV resonance levels. The branching ratio of the 3.678 MeV level was obtained by averaging the results of the three resonances giving 3.678 → 0.843 (60%) and 3.678 → 1.013 (40%) in agreement with previous results (VA 67, WA 66).

The 3.956 MeV level was weakly excited (2%) at the 662, 719, 809 and 982 keV resonances and only the ground state transition which had comparable strength to the primary γ-ray was observed. Van der Leun et al. (VA 67) has reported >80% to the ground state whereas Spear et al. (SP 67) find evidence for weak transitions to the 1.013 and 2.732 MeV levels.

The 4.410 MeV level was excited (8%) at the 809 keV resonance level. The branchings from the 4.410 MeV level are 4.410 → 0 (67%) and 4.410 → 1.013 (33%). No branching to the 2.209 MeV level was observed.

The 4.581 MeV level was observed (1%) at the 809 keV resonance level; only the ground state transition was

identified. A weak transition via the 2.209 MeV level (SP 67) could not be observed due to intense gamm-rays in the vicinity of the expected transitions.

The 4.812 MeV level was previously reported (VA 67) to decay to the ground state (40%), the 1.013 MeV level (25%) and the 2.209 MeV level (35%). At the 719 keV resonance, the cascades 4.812 → 0 and 4.812 → 2.209 were both observed. The cascade 4.812 → 1.013 (3.799 MeV) was not positively identified. This is because the full energy peak (3.799 MeV) and the double escape peak (2.777 MeV) of the 3.799 MeV γ-ray were obscured by the cascade γ-rays 4.812 MeV (4.812 → 0) which has double escape peak energy 3.790 MeV and the 2.803 MeV (8.963 → 6.160) which is strong (34%). There is surplus γ-ray intensity feeding the 4.812 MeV level compared to that de-exciting the 4.812 MeV level.

The 5.156 MeV level was excited weakly at 982 keV resonance and only the ground state transition was observed.

The 5.246 MeV level has been reported (VA 67) to decay to the ground state (10%), the 1.013 MeV level (70%) and the 2.209 MeV level (20%). The present study could only identify the cascade 5.246 → 1.013 and 5.246 → 2.209 transitions at the 719 and 809 keV resonance levels with a branching ratio 25:75.

The 5.430 MeV level was excited at the 982 keV resonance and only transition to the ground state was observed.

The 5.551 MeV level was excited at the 809 (1%) and 954 (5%) keV resonances. The study at the latter resonance identified the cascades 5.551 → 0 (80%) and 5.551 → 1.013 (20%) whereas a previous report (VA 67) suggested only a ground state transition.

The 5.751 MeV level was excited at the 662 (3%), 839 (1%) and 954 (9%) keV resonances. The study at the 954 keV resonance determined the branchings as 5.751 → 0.843 (50%), 5.751 → 1.013 (14%) and 5.751 → 2.980 (36%). A suggested ground state transition (VA 67) was not observed.

The 5.828 MeV level was excited with intensities of 9% and 1% at the 954 and 839 keV resonances respectively. The branching ratio was determined as 5.828 → 0 (16%) and 5.828 → 1.013 (84%).

The 6.082 MeV level was observed to decay to the ground state from the study at the 662 and 839 keV resonances which both excite the 6.082 MeV level weakly (2%).

The 6.160 MeV level was strongly excited at the 662 (36%), 719 (34%) keV resonances and weakly at the 982 keV resonance (4%). The branchings were determined as

6.160 → 0 (8%), 6.160 → 0.843 (74%), 6.160 → 1.013 (12%) and 6.160 → 2.732 (6%) in accord with (VA 67).

The 6.606 MeV level was previously reported (VA 67) to decay to the ground state (15%), the 0.843 MeV level (75%) and the 1.013 MeV level (10%). The present work found that the 6.606 MeV level was weakly excited at the 662 (2%), 719 (4%) and 954 (<1%) keV resonances. The investigation at the 719 keV resonance could only confirm the cascades 6.606 → 0 and 6.606 → 0.843 with 1:5 ratio.

The 6.653 MeV level was found previously (VA 67) to have the branchings 6.653 → 0 (85%), 6.653 → 0.843 (5%) and 6.653 → 1.013 (10%). The level was excited rather strongly at the 719 (14%) and 982 (10%) keV resonances but the measurement at the 719 keV resonance could only confirm the cascades 6.653 → 0 and 6.653 → 1.013 with a ratio 88:12. The cascade gamma-ray 6.653 → 0.843 (5.810 MeV) has a double escape peak at 4.788 MeV which was obscured by the first escape peaks of two strong γ-rays 5.317 MeV (6.160 → 0.843) and 5.285 MeV (8.963 → 3.678). At the 982 keV resonance, only the ground state transition was identified.

The 6.778 MeV level was reported (VA 67) to have the cascades 6.778 → 0 (20%), 6.778 → 0.843 (55%), 6.778 → 2.980 (25%) and 6.778 → 3.678 (≤20%). The present

measurement at the 982 keV resonance, which excites the 6.778 MeV level with 1% intensity, only revealed the cascade 6.778 → 3.678.

The 6.815 MeV level was reported to decay to the 0.843 MeV level (20%), 1.013 MeV level (70%) and the 3.678 MeV level (10%) (VA 67). The 6.815 MeV level was weakly excited (3%) at the 662 keV resonance and allowed only the observation of the cascade 6.815 → 1.013.

The 6.997 MeV level was excited 4% at the 809 keV resonance. The cascade from the 6.997 MeV level to the 4.410 MeV level was observed.

The 7.230 MeV level was excited <1% at the 809 keV resonance and was observed to decay to the 2.209 MeV level in agreement with a previous suggestion (VA 67).

The 7.471 MeV level was excited (1%) at the 982 keV resonance and observed to decay to the 2.980 MeV level. The suggested decay via the 2.209 MeV level (VA 67) was obscured in the present work. The 5.262 MeV (7.471 → 2.209) γ-ray has the same energy as the γ-ray from the cascade 9.218 → 3.956 (5.262 MeV) while the second γ-ray of the cascade 7.471 → 2.209 → 0 was masked by the strong first escape peak of the 2.732 MeV γ-ray at 2.221 MeV.

The 8.184 MeV level was excited <1% at the 982 keV resonance. The ground state transition from the level was observed.

11. Spins

The present study confirms the previous spin assignments of the 662 ($\frac{1}{2}$), 719 ($\frac{3}{2}$), 809 ($\frac{5}{2}$), 839 ($\frac{1}{2}$) and 954 ($\frac{3}{2}$) keV resonance levels. The previous assignment $\frac{7}{2}$ to the 982 keV resonance level is conclusively rejected by the present work which favours the assignment $\frac{3}{2}$ or $\frac{5}{2}$.

The angular distribution measurements at the 719, 809 and 954 keV resonance are considered to uniquely determine the spins of the 3.678 ($\frac{1}{2}$), 5.246 ($\frac{5}{2}$), 5.551 ($\frac{5}{2}$), 5.751 ($\frac{1}{2}$), 5.828 ($\frac{3}{2}$) and 6.160 ($\frac{3}{2}$) MeV levels.

The spin of the 6.082 MeV level was proposed as $\frac{3}{2}$ from the intensity measurement alone.

The spin of the 4.410 MeV level was assigned previously as $\frac{5}{2}$ (ME 65, VA 67). The present work suggests $\frac{3}{2}$ is more likely.

The spin of the 3.000 MeV level was discussed in section 2.1 of this chapter. The decay of the resonance levels examined in the present work found no evidence for excitation of the 3.000 MeV level. The decay through the 2.209 MeV level with spin of $\frac{7}{2}$ was the highest spin state observed. This fact alone indicates the 3.000 MeV level is a high spin state consistent with the assignment of $\frac{9}{2}$ which is currently favoured.

12. Discussion

The present investigations, combined with the results of Van der Leun et al. (VA 67) serve as an illustration of the potential features of systematic studies of capture reactions with Ge(Li) detectors.

The question of group properties of resonances requires much more study. While closely spaced levels with the same spin and parity and virtually identical (and simple) decay schemes (e.g. the 2293 and 2323 keV levels) can be understood in a simple approach and similar examples occur in other reactions (ER 66), the case of the 662 and 719 keV resonance levels is less readily accounted for. Both levels decay strongly to the 6.16 MeV level in contrast to all other levels studied (34 in total) but otherwise have dissimilar decay and different spins. Little more information concerning the levels can be derived from gamma-ray measurements - perhaps particle reactions leading to the levels as final states would aid an understanding of them.

The value of Ge(Li) spectra in determining decay schemes is obvious but less so until the measurements are made, is the fact that the spectra serve mainly to only indicate the branchings of the higher levels (i.e. above 4 MeV). Accurate branching ratios are not possible

except at particularly favourable resonances. Thus not only do surveys with Ge(Li) detectors establish resonances at which correlation measurements may be made with NaI detectors but they also serve to locate resonances at which coincidence measurements may be used to establish branching ratios. Such measurements will constitute the next phase of the program.

FIGURE CAPTIONS

Figure 6.1 Decay scheme of the low-lying levels of ^{27}Al.

Figure 6.2 Resonance spectrum and decay scheme of the 662 keV resonance. Circles are data and the least squares line shape fit is the solid line.

Figure 6.3 The γ-ray spectra observed in coincidence with the energy intervals shown at the 719 keV resonance. All spectra collected for 10^6 monitor counts (OS 65).

Figure 6.4 Resonance spectrum and decay scheme of the 719 keV resonance. Circles are data and the least squares line shape fit is the solid line.

Figure 6.5 Plot of the coefficient of $P_2(\cos\theta)$ term versus arctangent of X, the quadrupole/dipole mixing ratio, for the transition $\frac{3}{2} \rightarrow \frac{1}{2}$ Table 6.1, A).

Figure 6.6 Plot of the coefficient of $P_2(\cos\theta)$ term versus arctangent of X, the quadrupole/dipole mixing ratio, for the transition $\frac{3}{2} \rightarrow \frac{3}{2}$ (Table 6.1, B).

Figure 6.7 The contour plot of the coefficient of $P_2(\cos\theta)$ term for the spin sequence $\frac{3}{2} \rightarrow \frac{3}{2} \rightarrow \frac{1}{2}$ with first γ-ray unobserved (Table 6.1 I). The hatched area indicates the possible region determined by the experimental value.

Figure 6.8 Resonance spectrum and decay scheme of the 809 keV resonance. Circles are data and the least squares line shape fit is the solid line.

Figure 6.9 Resonance spectrum and decay scheme of the 839 keV resonance. Circles are data and least squares line shape fit is the solid line.

Figure 6.10 Resonance spectrum and decay scheme of the 954 keV resonance. Circles are data and the least squares line shape fit is the solid line.

Figure 6.11 Resonance spectrum and decay of the 982 keV resonance. Circles are data and the least squares line shape fit is the solid line.

REFERENCES

AJ 59 : F. Ajzenberg-Selove and T. Lauritsen, Nucl. Phys. 11 (1959) 1.

AR 61 : Armstrong, Marion, Detenbeck and Hornyak, Bull. Amer. Phys. Soc. 6 (1961) 37.

AZ 66 : Azuma, Carlson, Charlesworth, Jackson, Anyas-Weiss and Lalovic, Can. J. Phys. 44 (1966) 3075.

BA 61 : S. Bashkin and T.R. Ophel, Australian J. Phys. 14 (1961) 335.

BA 63 : G.M. Bailey and D.F. Hebbard, Nucl. Phys. 46 (1963) 529.

BI 60 : G.R. Bishop, Nucl. Phys. 14 (1960) 376.

BI 64 : Bishop, Bernheim and Kossanyi-Demay, Nucl. Phys. 54 (1964) 353.

BR 54 : Browne, Zimmerman, and Buechner, Phys. Rev. 96 (1954) 725.

BR 59 : C.P. Browne, Phys. Rev. 114 (1959) 807.

CH 61 : R.F. Christy and I. Duck, Nucl. Phys. 24 (1961) 89.

CR 65 : M. Crawley and G.T. Garvet, Phys. Lett. 19 (1965) 228.

DE 60 : A. De-Shalit, Phys. Rev. 122 (1960) 1530.

DE 65 : Detenbeck, Armstrong, Figuera and Marion, Nucl. Phys. 72 (1965) 552.

DE 65a : A. De-Shalit, Phys. Lett. 15 (1965) 170.

DE 67 : R.W. Detenbeck, private communication.

DU 51 : D.B. Duncan and J.E. Perry, Phys. Rev. 82 (1951) 809.

EA 64 : L.G. Earwaker and D.F. Hebbard, Nucl. Phys. 53 (1964) 252.

EM 60 : G.T. Emery and W.R. Kane, Phys. Rev. 118 (1960) 755.

EN 62 : P.M. Endt and C. Van der Leun, Nucl. Phys. 34 (1962) 1.

ER 66 : Erné, Veltman and Wintermans, Nucl. Phys. 88 (1966) 1.

EV 66 : A.E. Evans, B. Brown and J.B. Marion, Phys. Rev. 149 (1966) 863.

EV 67 : A.E. Evans, Phys. Rev. 155 (1967) 1047.

EV 67a : Evers, Hertel, Retz-Schmidt and Skorka, Nucl. Phys. A91 (1967) 492.

EW 64 : G.T. Ewan and A.J. Tavendale, Can. J. Phys. 42 (1964) 2286.

FE 59 : A.J. Ferguson, Phys. Rev. 115 (1959) 1660.

FE 62 : A.J. Ferguson, A Least Squares Program for the Analysis of Gamma-Ray Spectra (Atomic Energy of Canada Ltd, Chalk River, Canada, 1962) AECL-1398, unpublished.

FE 65 : A.J. Ferguson, Angular Correlation Methods in Gamma-Ray Spectroscopy (North-Holland Publishing Company, Amsterdam, 1965) Chapter 4.

GA 68 : Gallmann, Haas and Heusch, Phys. Rev. to be published.

GO 60 : H.E. Gove, Proceedings of Kingston Conference on Nuclear Structure (North-Holland Publishing Company, Amsterdam, 1960) p.438.

GO 66 : Gorodetzky, Freeman, Gallmann and Haas, Phys. Rev. 149 (1966) 801.

GO 66a : F.S. Goulding Nucl. Instr. and Meth. 43 (1966) 1.

GO 67 : Gove, Purser, Schwartz, Alford and Cline, Contributions to International Conference on Nuclear Structure, Tokyo (1967).

HE 54 : W. Heitler, The Quantum Theory of Radiation (Clarendom Press, Oxford, 1954).

HE 60 : D.F. Hebbard and J.L. Vogl, Nucl. Phys. 21 (1960) 652.

HE 63 : D.F. Hebbard and G.M. Bailey, Nucl. Phys. 49 (1963) 666.

HE 64 : D.F. Hebbard, private communication.

HE 66 : R.L. Heath, Nucl. Instr. and Meth. 43 (1966) 209.

HE 67 : Heath, Helmer, Schmittroth and Cazier, Nucl. Instr. and Meth. 47 (1967) 281.

HE 67a : Helmer, Heath, Schmittroth, Jayne and Wagner, Nucl. Instr. and Meth. 47 (1967) 305.

HO 65 : Hotz, Mathiesen and Hurley, Nucl. Instr. and Meth. 37 (1965) 93.

HO 66 : J.M. Hollander, Nucl. Instr. and Meth. 43 (1966) 65.

KE 67 : Kean, Elliott and Spear, ANU-P/396 (1967).

KO 65 : Kokame, Fukunaya and Nakamura, Phys. Lett. 14 (1965) 234.

KR 53 : Kraus, French, Fowler and Lauritsen, Phys. Rev. 89 (1953) 299.

LA 57 : R.D. Lawson and J.L. Uretsky, Phys. Rev. 108 (1957) 1300.

LA 62 : B.T. Lawergren and T.R. Ophel, Proc. Phys. Soc. 79A (1962) 881.

LA 64 : B.T. Lawergren, Nucl. Phys. 53 (1964) 417.

LA 67 : M. Lambert and M. Durand, Phys. Lett. 24B (1967) 287.

LA 67a : B. Lawergren, Nucl. Phys. A90 (1967) 311.

MA 60 : J.B. Marion, 1960 Nuclear Data Tables, Part 3.

MA 66 : J.W. Mayer, Nucl. Instr. and Meth. 43 (1966) 55.

ME 65 : F.R. Metzger, Phys. Rev. 139 (1965) B1464.

MI 56 : Miller, Carmichael, Gupta, Rasmussen and Sampson, Phys. Rev. 101 (1956) 740.

MU 65 : Murray, Graham and Geiger, Nucl. Phys. 63 (1965) 353.

NI 55 : S.G. Nilsson, Mat. Fys. Medd. Dan. Vid. Selsk. 29 (1955) No.16.

NI 64 : Niewodniczanski, Nurzynski, Strzalkowski, Wilczynski, Rook and Hodgson, Nucl. Phys. 55 (1964) 386.

NE 65 : Newton, Blake, Jacobs and Schapira, Nucl. Phys. 71 (1965) 113.

OL 58 : Olness, Verona and Lewis, Phys. Rev. 112 (1958) 475.

OP 62 : T.R. Ophel and B.T. Lawergren, Nucl. Phys. 30 (1962) 215.

OP 62a : T.R. Ophel and B.T. Lawergren, Phys. Lett. 2 (1962) 167.

OP 63 : T.R. Ophel and B.T. Lawergren, Phys. Lett. 6 (1963) 230.

OP 64 : T.R. Ophel and B.T. Lawergren, Nucl. Phys. 52 (1964) 417.

OS 65 : D.R. Osgood, M.Sc. thesis, the Australian National University (1965).

RO 53 : M.E. Rose, Phys. Rev. 91 (1953) 610.

SC 52 : Schardt, Fowler and Lauritsen, Phys. Rev. 86 (1952) 527.

SH 54 : Sharp, Kennedy, Sears and Hoyle, Tables of Coefficients for Angular Distribution Analysis (Atomic Energy of Canada Ltd., Chalk River, Canada, 1954) AECL-97, unpublished.

SH 67 : D.M. Sheppard and C. Van der Leun, Nucl. Phys. A100 (1967) 333.

SP 67 : R.H. Spear, private communication.

ST 58 : Storm, Gilbert and Israel, Los Alamos Sci. Lab. Rep. LA-2237 (1958).

TH 66 : V.K. Thankappan, Phys. Rev. 141 (1966) 957.

TO 62 : J.H. Towle and W.B. Gilboy, Nucl. Phys. 39 (1962) 300.

TR 56 : B. Trumpy and A. Graue, Physica 22 (1956) 1155(A).

VA 56 : Van der Leun, Endt, Kluyver and Vrenken, Physica 22 (1956) 1223.

VA 65 : Valter, Kopanetz and Tsytko, Izv. Akad. Nauk. SSSR, Ser. Fiz. 29 (1965) 803.

VA 67 : Van der Leun, Sheppard and Endt, Nucl. Phys. A100 (1967) 316.

WA 58 : E.K. Warburton, Phys. Rev. Lett. 1 (1958) 68.

WA 59 : Warburton, Rose and Hatch, Phys. Rev. 114 (1959) 214.

WA 60 : E.K. Warburton and W.T. Pinkston, Phys. Rev. 118 (1960) 733.

WA 64 : Warburton, Olness, Alburger, Bredin and Chase, Phys. Rev. 134 (1964) B 338.

WA 65 : Warburton, Lopes, Ollerhead, Poletti and Thomas, Phys. Rev. 138 (1965) B 104.

WA 65a : Warburton, Olness and Alburger, Phys. Rev. 140 (1965) B 1202.

WA 65b : T. Wakatsuki and B.D. Kern, Conference on Bases for Nuclear Spin-Parity Assignment, Gatlinburg, Nov. (1965).

WA 66 : Wakatsuki, Hirao, Miura and Shimizu, J. Phys. Soc. Japan 21 (1966) 834.

WH 44 : E. Whittaker and G. Robinson, The Calculus of Observation, (Blackie & Son Ltd, London, 1944, fourth edition) p.28.

WI 60 : D.H. Wilkinson, Nuclear Spectroscopy, Part B, ed, by F. Ajzenberg-Selove (Academic Press, New York, 1960).

APPENDIX

COMPUTER PROGRAMS

1. FUNFIT (Function Fit) A 1

2. GEEFFANG (Germanium Detector Efficiencies and Angular Correlation Attenuation Factors) A12

3. FITTER

   a. LNESHAPE (Generate Line Shapes and Store on Disk) A16

   b. LEASTFIT (Least Squares Line Shape Fit) A23

      PUSH

      PULL

      PARAB

      MATINV

      SUMSPE

      LSTSQR

      PLTFIT

```
C      PROGRAM FUNCTION FIT
C      USE PROCEDURE FOR CARD OUTPUT
0001        DOUBLE PRECISION AMTX(50,17),B(10),CMTX(17,17),D(2100),P(20),
           1COEFFT(17),DATA(2100)
0002        DIMENSION FIT(25,25),OP(485),LOP(100),IDENT(20),FITB(21,20),FB(5)
0003       1 FORMAT (4X,F5.0,9F6.0)
0004       2 FORMAT(I4,5D13.7)
0005       3 FORMAT(F5.1,F7.3,F8.2,F6.2,F6.1,A4)
0006       4 FORMAT(39X,F9.2)
0007       5 FORMAT ('0','INTERVAL',3X,'MEAN SQU. RESIDUAL')
0008       6 FORMAT ('0','FIXED PARAMETERS')
0009       7 FORMAT (' ',' INT ',5X,'A',12X,'B',12X,'B1',11X,'B2',11X,'B3')
0010       8 FORMAT (1H0,2X,8HINT PMTR,9H  L.B.USE,4X,7HL.B.FIT,4X,
           17HU.B.FIT,3X,8HRSDL LMT)
0011       9 FORMAT(1H ,12HEXPTL GAIN =,F8.2,10HKEV/100CH.)
0012      10 FORMAT (1H ,12HEXPTL ZERO =F7.2,3H CH)
0013      12 FORMAT (1H ,2I4,5F11.3)
0014      13 FORMAT (1H ,28HTOO MANY INTERVALS SPECIFIED)
0015      14 FORMAT (1H ,21HTOO MANY CHS IN INTVL,I4)
0016      15 FORMAT (1H ,25HNESTING ERROR IN INTERVALI4)
0017      16 FORMAT (1H ,27HHIGHEST CHAN.NO.GT.THAN 199)
0018      17 FORMAT (1H ,35HTOO MANY PARAMETERS SPECIFIED,INTVLI4)
0019      18 FORMAT (2I4,E13.7)
0020      19 FORMAT (' ',2X,I4,7X,E13.7)
0021      21 FORMAT (1H ,I4,10F7.0)
0022      22 FORMAT ('+',30X,'TOO LARGE. REPEAT WITH 1 MORE PARAMETER')
0023     108 FORMAT (2I4,5F11.3)
0024     109 FORMAT(1H1,3HRUN,F5.1)
0025     110 FORMAT('0','O/P SPECTRUM WITH ORIGINAL INTENSITY, GAIN AND ZERO',
           117X,F7.3,4H MEV)
0026     111 FORMAT('0','NORMALISED OUTPUT FUNCTIONS WITH ORIGINAL INTENSITY',
           117X,F7.3,4H MEV)
0027     112 FORMAT(8(I4,F6.0))
0028     113 FORMAT (20A4)
0029     114 FORMAT(1H ,20A4)
0030     115 FORMAT(1H0,33HINDIVIDUAL CHANNELS CORRECTED ARE)
0031     119 FORMAT(1H ,12HMAX CHANNEL=,I4,8H, SMULT=,E14.7)
0032     120 FORMAT(1H ,8(I5,F8.0))
0033     139 FORMAT(1H0,14HBACKGROUND RUN,F5.1,12H, LIVE TIME=,F9.2,4H SEC,
           14H, AT,F6.1,7H DEGREE,15H, TOTAL COUNTS=,E14.7)
0034     140 FORMAT(1H ,40HSET OF FUNCTIONS INCOMPLETE, START AGAIN)
0035     213 FORMAT (1H ,49HRANGE RESTRICTED. STOP AT CHANNEL 519 IN INTERVAL,
           I13)
0036     225 FORMAT(1H0,47HTOTAL O/P SPECTRUM WITH ORIGINAL GAIN AND ZERO=,
           1E14.7,7H COUNTS)
0037     226 FORMAT(1H ,46HNORMALISED OUTPUT FUNCTION WITH UNIT INTENSITY,
           122X,F7.3,4H MEV)
0038     229 FORMAT(1H ,I4,5E16.7)
0039     239 FORMAT(1H0,51HORIGINAL SPECTRUM AFTER ADDITION OR SUBSTRACTION OF,
           117H ANOTHER SPECTRUM,F7.3,4H MEV)
0040     245 FORMAT(1H0,30HNORMALISED TOTAL O/P SPECTRUM=,E14.7,7H COUNTS)
0041     246 FORMAT(1H0,51HNORMALISED O/P SPECTRUM WITH 500000 TOTAL INTENSITY,
           117X,F7.3,4H MEV)
0042     250 FORMAT(I4,5(E14.7))
0043      23 READ(1,3)EXPT,EGAM,GAINI,ZEROI,ANGLE,IBLANK
0044         IF(EXPT)238,238,124
0045     124 WRITE(3,109)EXPT
0046      11 READ(1,113)(IDENT(J),J=1,20)
```

```
0047                IF(IDENT(1)-IBLANK)24,107,24
0048             24 WRITE(3,114)(IDENT(J),J=1,20)
0049                GO TO 11
0050            107 WRITE(3,9)GAINI
0051                WRITE(3,10)ZEROI
0052                LB=0
0053                NN=0
0054                JJ=0
0055                N=1
0056                DO 25 I=1,25
0057                DO 25 J=1,25
0058             25 FIT(I,J)=0.0
0059                ISTOP=0
                C       READ IN INTVL DEFN CARDS
0060                INTVL=0
0061             26 READ(1,108)LBL,NPAR,B(2),B(3),B(1),B(4),B(5)
0062                IF(LBL-24) 27,27,28
                C       CHECK SPECIFICATION OF INTERVALS
0063             27 INTVL=INTVL+1
0064                IF(LBL) 34,34,29
0065             28 WRITE(3,13)
0066                ISTOP=1
0067             29 DO 33 J=2,5
0068             33 FIT(LBL,J)=B(J)
0069                FIT(LBL,1)=NPAR
0070                FIT(LBL+1,3)=B(1)
0071                FIT(25,4)=B(4)
0072                GO TO 26
0073             34 INTVL=INTVL-1
0074                DO 46 LBL=1,INTVL
0075                IF(FIT(LBL+1,3)-FIT(LBL,3)) 35,35,36
0076             35 WRITE(3,15)LBL
0077                ISTOP=1
0078             36 IF(FIT(LBL,2)-FIT(LBL,3)) 38,38,37
0079             37 WRITE(3,15)LBL
0080                ISTOP=1
0081             38 IF(FIT(LBL,4)-FIT(LBL+1,3)) 39,40,40
0082             39 WRITE(3,15)LBL
0083                ISTOP=1
0084             40 DO 42 J=2,4
0085                IF(FIT(LBL,J)-2047.)42,42,41
0086             41 WRITE(3,16)
0087                ISTOP=1
0088             42 CONTINUE
0089                IF(FIT(LBL,1)-17.0) 44,44,43
0090             43 WRITE(3,17)LBL
0091                ISTOP=1
0092             44 IF(FIT(LBL,1)+FIT(LBL,2)-FIT(LBL,4)-1.) 46,46,45
0093             45 WRITE(3,15)LBL
0094                ISTOP=1
0095             46 CONTINUE
0096                IF(ISTOP) 47,47,234
0097             47 WRITE(3,8)
0098                DO 48 I=1,INTVL
0099                NPAR=FIT(I,1)
0100             48 WRITE(3,12)I,NPAR,FIT(I,3),FIT(I,2),FIT(I,4),FIT(I,5)
0101                NPAR=0
0102                I=INTVL+1
```

```
      WRITE(3,12)I,NPAR,FIT(I,3)
      GAIN=550./GAINI
      DO 49 I=1,20
   49 P(I)=0.0
      WRITE(3,6)
      WRITE(3,7)
C     READ IN COEFFT DEFN CDS FOR NON.FITTED INTVLS
   50 READ(1,2)LBL,(P(I),I=4,8)
      IF(LBL) 52,52,51
   51 WRITE(3,229)LBL,(P(I),I=4,8)
      FIT(LBL,1)=-2.0
      LAB=LBL
      NCARD=-FIT(LAB,1)
      DO 302 J=2,3
  302 P(J-1)=(FIT(LAB,J)-ZERO1)/GAIN
      P(3)=3.1415927*GAIN/(FIT(LAB,4)-FIT(LAB,2))
      P(5)=GAIN*P(5)
      DO 303 J=4,20
  303 P(J)=P(J)*GAIN
      M=NCARD*5
      DO 304 L=1,M
      K=L+NN
  304 OP(K)=P(L)
      NN=NN+M
      DO 305 J=1,NCARD
      M=100*J+LAB
      JJ=JJ+1
  305 LOP(JJ)=M
      GO TO 50
   52 DO 53 I=1,2100
   53 DATA(I)=0.0
      MAXM=FIT(25,4)
      NCARD=MAXM
C     K=3, READ DATA IN RIDL FORMAT
C     K=2, READ BACKGROUND SOURCE FUNCTIONS
C     K=1, USE PREVIOUS BACKGROUND SOURCE FUNCTIONS
   54 READ(1,18)K,MAXM,SMULT
      WRITE(3,119)MAXM,SMULT
      IF(K-2)60,59,55
C     READ IN DATA,R.I.D.L. FORMAT
   55 N=MAXM/10+1
      DO 57 I=1,N
      READ(1,1)(B(K),K=1,10)
      DO 57 J=1,10
      LBL=(I-1)*10+J
   56 DATA(LBL)=B(J)*SMULT+DATA(LBL)
   57 CONTINUE
   58 READ(1,18)K
C     POSSIBILITY OF ADDING OR SUBTRACTING ANOTHER SPECTRUM
      IF(K-1)121,121,54
  121 WRITE(3,239)
      DO 123 I=1,N
      DO 122 J=1,10
      LBL=(I-1)*10+J
  122 B(J)=DATA(LBL)
      L=10*(I-1)
  123 WRITE(3,21)L,(B(K),K=1,10)
      WRITE(2,239)EGAM
```

```
0155                  DO 129 J=1,MAXM
0156                  K=MAXM+51-J
0157              129 DATA(K)=DATA(K-50)
0158                  N=MAXM+50
0159                  CALL RIDL(DATA,N)
0160                  DO 130 J=1,MAXM
0161              130 DATA(J)=DATA(J+50)
0162                  GO TO 64
                C     READ IN BACKGROUND FUNCTIONS
0163               59 DO 131 I=1,20
0164                  DO 131 J=1,21
0165              131 FITB(J,I)=0.0
0166                  READ(1,4)TIMEB
0167              132 READ(1,250)M,(FB(I),I=1,5)
0168                  NCARD=M/100
0169                  LBL=M-100*NCARD
0170                  IF(NCARD-9)133,135,135
0171              133 FITB(1,LBL)=NCARD
0172                  DO 134 I=1,5
0173                  J=5*NCARD+I-4
0174              134 FITB(J,LBL)=FB(I)
0175                  GO TO 132
0176              135 FITB(3,LBL)=FB(2)
0177                  INTVLB=LBL-1
0178                  RUN=FB(1)
0179                  COUNT=FB(4)
0180                  ANGLE=FB(5)
0181                  WRITE(3,139)RUN,TIMEB,ANGLE,COUNT
0182                  DO 137 I=1,INTVLB
0183                  IF(FITB(1,I))137,136,137
0184              136 WRITE(3,140)
0185                  GO TO 238
0186              137 CONTINUE
0187                  GAINB=5000.0
0188                  ZEROB=0.0
0189               60 CALL SUB2(FITB,D,GAINI,ZEROI,INTVLB,GAINB,ZEROB)
0190                  DO 138 I=1,200
0191              138 DATA(I)=DATA(I)+D(I+50)*SMULT
0192                  GO TO 58
                C     POSSIBILITY OF CHANGING INDIVIDUAL CHANNELS
0193               64 WRITE(3,115)
0194               65 READ(1,112)(IDENT(I),B(I),I=1,8)
0195                  L=0
0196                  DO 126 I=1,8
0197                  K=IDENT(I)
0198                  IF(K)125,127,125
0199              125 L=L+1
0200              126 DATA(K+1)=B(I)
0201                  WRITE(3,120)(IDENT(J),B(J),J=1,8)
0202                  GO TO 65
0203              127 IF(L)128,116,128
0204              128 WRITE(3,120)(IDENT(J),B(J),J=1,L)
0205              116 WRITE(3,5)
                C     START FITTING
0206                  LB=1
0207                  DO 67 LBL=1,INTVL
0208                  NPAR=FIT(LBL,1)
0209                  IF(NPAR) 67,67,68
```

```
0210            68 J=FIT(LBL,2)
0211               B(1)=J
0212               IF(B(1)-FIT(LBL,2))69,70,70
0213            69 B(1)=B(1)+1.
0214            70 B(2)=B(1)
0215               B(4)=3.1415927/(FIT(LBL,4)-FIT(LBL,2))
0216            71 B(3)=B(2)-FIT(LBL,2)
0217               L=B(2)-B(1)+1.
0218               NM=NPAR-2
0219               DO 72 K=1,NM
0220               B(5)=K
0221            72 AMTX(L,K+2)=DSIN(B(3)*B(4)*B(5))
0222               AMTX(L,1)=1.
0223               AMTX(L,2)=B(3)
0224               B(2)=B(2)+1.
0225               IF(FIT(LBL,4)-B(2)) 73,71,71
0226            73 MAXM=L
0227               DO 77 I=LBL,INTVL
0228               MP=0
0229               B(3)=FIT(I,2)-FIT(LBL,2)
0230               P(1)=FIT(I,4)-FIT(LBL,4)
0231               IF(B(3)-P(1)) 77,74,77
0232            74 K=B(3)
0233               B(5)=K
0234               IF(B(3)-B(5)) 77,75,77
0235            75 MINM=FIT(I,1)
0236               IF(MINM-NPAR) 82,76,78
0237            76 IF(I-LBL) 88,82,88
0238            78 B(3)=B(1)-FIT(LBL,2)
0239               NM=NM+3
0240               DO 81 L=1,MAXM
0241               DO 80 K=NM,MINM
0242            79 B(5)=K-2
0243               AMTX(L,K)=DSIN(B(3)*B(4)*B(5))
0244            80 AMTX(L,2)=B(3)
0245            81 B(3)=B(3)+1.
0246               NM=NPAR-2
0247            82 DO 83 J=1,MINM
0248               DO 83 K=1,MINM
0249               CMTX(J,K)=0.0
0250               DO 83 L=1,MAXM
0251            83 CMTX(J,K)=AMTX(L,J)*AMTX(L,K)+CMTX(J,K)
0252               DO 87 J=1,MINM
0253               B(9)=CMTX(J,J)
0254               CMTX(J,J)=1.
0255               DO 84 K=1,MINM
0256            84 CMTX(J,K)=CMTX(J,K)/B(9)
0257               DO 87 L=1,MINM
0258               IF(L-J) 85,87,85
0259            85 B(9)=CMTX(L,J)
0260               CMTX(L,J)=0.0
0261               DO 86 K=1,MINM
0262            86 CMTX(L,K)=CMTX(L,K)-B(9)*CMTX(J,K)
0263            87 CONTINUE
0264            88 DO 89 J=1,20
0265            89 P(J)=0.0
0266               M=FIT(I,2)
0267               B(9)=M
```

```
0268                IF(B(9)-FIT(I,2)) 90,91,91
0269             90 M=M+1
0270             91 DO 92 J=1,MINM
0271                DO 92 L=1,MAXM
0272                N=L+M
0273                DO 92 K=1,MINM
0274             92 P(J+3)=CMTX(J,K)*AMTX(L,K)*DATA(N)+P(J+3)
0275                FIT(I,1)=(MINM+7)/(-5)
0276                B(5)=0.0
0277                B(10)=0.0
0278                DO 96 J=1,MAXM
0279                N=J+M
0280                B(6)=N-1
0281                IF(B(6)-FIT(I,3)) 96,93,93
0282             93 IF(FIT(I+1,3)-B(6)) 97,94,94
0283             94 B(5)=B(5)+1.
0284                B(9)=0.0
0285                DO 95 K=1,MINM
0286                B(7)=P(K+3)*AMTX(J,K)
0287             95 B(9)=B(9)+B(7)
0288                B(8)=DATA(N)-B(9)
0289                B(10)=B(8)*B(8)+B(10)
0290             96 CONTINUE
0291             97 B(10)=B(10)/B(5)
0292                WRITE(3,19)I,B(10)
0293                MP=MP+1
0294                N=1
0295                LAB=I
0296                IF(B(10)-FIT(I,5))101,101,98
0297             98 IF(MP-1) 99,99,101
0298             99 IF(MINM-17) 100,101,101
0299            100 MINM=MINM+1
0300                WRITE(3,22)
0301                GO TO 78
0302            101 NCARD=-FIT(LAB,1)
0303                DO 102 J=2,3
0304            102 P(J-1)=(FIT(LAB,J)-ZERO1)/GAIN
0305                P(3)=3.1415927*GAIN/(FIT(LAB,4)-FIT(LAB,2))
0306                P(5)=GAIN*P(5)
0307                DO 103 J=4,20
0308            103 P(J)=P(J)*GAIN
                C       PUTS OUTPUT FUNCTIONS INTO OP(DIM=405).LABELS ARE PUT INTO
                C       LOP(DIM.=81). FOR ELEMENTS 1-5 IN OP, LOP(1) APPLIES,
                C       FOR ELEMENTS 6-10 IN OP,LOP(2) APPLIES. E.T.C.
                C       FINAL CARD.. (LABEL),EXPT,MAX CH.NO.,GAIN,ZERO,SOURCE(42.111)
                C       ARE STORED IN OIDENT(1-6)
0309                M=NCARD*5
0310                DO 104 L=1,M
0311                K=L+NN
0312            104 OP(K)=P(L)
0313                NN=NN+M
0314                DO 105 J=1,NCARD
0315                M=100*J+LAB
0316                JJ=JJ+1
0317            105 LOP(JJ)=M
0318             77 CONTINUE
0319             67 CONTINUE
0320            106 LOP(JJ+1)=901+INTVL
```

```
0321                OP(K+1)=EXPT
0322                OP(K+2)=(FIT(INTVL+1,3)-ZEROI)/GAIN
0323                OP(K+3)=EGAM
0324                OP(K+4)=0.0
0325                OP(K+5)=ANGLE
0326                KS=K
0327                DO 203 I=1,25
0328                DO 203 J=1,25
0329           203  FIT(J,I)=0.0
0330                M=1
0331                I=1
0332           204  NCARD=LOP(I)/100
0333                LBL=LOP(I)-100*NCARD
0334                IF(NCARD-9)205,207,207
0335           205  FIT(1,LBL)=NCARD
0336                DO 206 K=1,5
0337                J=5*NCARD+K-4
0338                L=K+(M-1)*5
0339           206  FIT(J,LBL)=OP(L)
0340                M=M+1
0341                I=I+1
0342                GO TO 204
0343           207  FIT(3,LBL)=OP(L+2)
0344                INTVL=LBL-1
0345                NORM=0
0346                GAINT=GAIN
0347                INTVLT=INTVL
0348                GAIN=1.0
0349                ZERO=0.0
0350                GO TO 241
0351           242  GAIN=GAINT
0352                ZERO=ZEROI
0353                INTVL=INTVLT
0354           241  GAIN=1./GAIN
0355                DO 202 I=1,2100
0356           202  D(I)=0.0
0357                DO 209 J=1,INTVL
0358                DO 208 I=4,21
0359           208  FIT(I,J)=FIT(I,J)*GAIN
0360                FIT(6,J)=FIT(6,J)*GAIN
0361                DO 209 I=2,3
0362           209  FIT(I,J)=FIT(I,J)/GAIN+ZERO
0363                FIT(3,INTVL+1)=FIT(3,INTVL+1)/GAIN+ZERO
0364                COEFFT(1)=1.0
0365                LBL=1
0366                CHAN=-50.0
0367                K=INTVL+1
0368                DO 210 J=1,K
0369                IF(FIT(3,J)-2047.)210,210,211
0370           210  CONTINUE
0371                GO TO 212
0372           211  INTVL=J-1
0373                KJ=J
0374                T=FIT(3,J)
0375                FIT(3,J)=519.0
0376                WRITE(3,213)INTVL
0377           212  IF(CHAN-FIT(3,1)) 214,215,215
0378           214  CHAN=CHAN+1.0
```

```
0379                GO TO 212
0380           215  DO 216 K=1,15
0381                J=22-K
0382                IF(FIT(J,LBL)) 217,216,217
0383           216  CONTINUE
0384           217  NSIN=J-6
0385                NPAR=NSIN+2
0386                B(4)=FIT(4,LBL)
0387                B(2)=FIT(2,LBL)
0388           218  B(3)=CHAN-B(2)
0389                DO 219 K=1,NSIN
0390                B(5)=K
0391           219  COEFFT(K+2)=DSIN(B(3)*B(4)*B(5))
0392                COEFFT(2)=B(3)
0393                N=CHAN+51.0
0394                DO 220 J=1,NPAR
0395           220  D(N)=D(N)+COEFFT(J)*FIT(J+4,LBL)
0396                CHAN=CHAN+1.0
0397                IF(CHAN-FIT(3,LBL+1))218,240,222
0398           240  IF(LBL-INTVL)222,218,218
0399           222  LBL=LBL+1
0400                IF(LBL-INTVL) 215,215,223
0401           223  TOTAL=0.0
0402                DO 224 J=1,N
0403           224  TOTAL=TOTAL+D(J)
0404                FIT(3,KJ)=T
0405                IF(NORM)244,243,244
0406           244  WRITE(3,225)TOTAL
               C    PRINT OUTPUT SPECTRUM,ORIGINAL GAIN AND ZERO
0407                WRITE(3,110)
0408                DO 228 J=51,N,10
0409                DO 227 K=1,10
0410                L=J+K-1
0411           227  B(K)=D(L)
0412                LBL=J-51
0413           228  WRITE(3,21)LBL,(B(K),K=1,10)
0414                WRITE(2,110)EGAM
0415                CALL RIDL(D,N)
               C    PRINT OUTPUT FUNCTIONS, RUN NUMBER, MAX CH, ENERGY, INTENSITY
0416                I=1
0417                WRITE(3,111)
0418                WRITE(2,111)EGAM
0419                OP(KS+4)=TOTAL
0420           117  LBL=LOP(I)
0421                DO 118 J=1,5
0422                L=J+(I-1)*5
0423           118  FB(J)=OP(L)
0424                WRITE(3,229)LBL,(FB(J),J=1,5)
0425                WRITE(2,250)LBL,(FB(J),J=1,5)
0426                I=I+1
0427                IF(LOP(I-1)-900)117,117,23
0428           243  WRITE(3,246)
0429                RATIO=1000000.0/TOTAL
0430                DO 252 K=1,N
0431           252  D(K)=D(K)*RATIO
0432                DO 248 J=51,N,10
0433                DO 247 K=1,10
0434                L=J+K-1
```

```
0435          247 B(K)=D(L)
0436              LBL=J-51
0437          248 WRITE(3,21)LBL,(B(K),K=1,10)
0438              WRITE(2,246)EGAM
0439              CALL PIDL(D,N)
0440              WRITE(3,245)TOTAL
0441              NOR=1
0442              I=1
0443              WRITE(3,226)
0444              WRITE(2,226)EGAM
0445          230 LBL=LOP(I)
0446              L=LOP(I)/100
0447              IF(L-1)233,231,233
0448          231 DO 232 J=1,3
0449              K=J+(I-1)*5
0450          232 FB(J)=OP(K)
0451              FB(4)=OP(K+1)/TOTAL
0452              FB(5)=OP(K+2)/TOTAL
0453              GO TO 235
0454          233 DO 234 J=1,5
0455              K=J+(I-1)*5
0456          234 FB(J)=OP(K)/TOTAL
0457          235 WRITE(3,229)LBL,(FB(J),J=1,5)
0458              WRITE(2,250)LBL,(FB(J),J=1,5)
0459              I=I+1
0460              IF(LOP(I)-900)230,236,236
0461          236 LBL=LOP(I)
0462              DO 237 J=1,3
0463              K=J+(I-1)*5
0464          237 FB(J)=OP(K)
0465              FB(4)=1.0
0466              FB(5)=ANGLE
0467              WRITE(3,229)LBL,(FB(J),J=1,5)
0468              WRITE(2,250)LBL,(FB(J),J=1,5)
0469              GO TO 242
0470          238 STOP
0471              END
```

```
0001                  SUBROUTINE RIDL(A,N)
0002                  DOUBLE PRECISION A(2100)
0003                  DIMENSION IA(2100),IOP(63),IBI(6),IO(12),IC(5)
0004                1 FORMAT(I3,1X,59A1)
0005                  M=N/10*10
0006                  IF(M-N)14,15,15
0007               14 N=M+10
0008               15 DO 4 I=51,N
0009                  IF(A(I)-99999.)2,3,3
0010                3 IA(I)=99999
0011                  GO TO 4
0012                2 IF(A(I))11,11,12
0013               11 IA(I)=0
0014                  GO TO 4
0015               12 IA(I)=A(I)
0016                4 CONTINUE
0017                  IO(1)=-264224704
0018                  IO(2)=-247447488
0019                  IO(3)=-230670272
0020                  IO(4)=-213893056
0021                  IO(5)=-197115840
0022                  IO(6)=-180338624
0023                  IO(7)=-163561408
0024                  IO(8)=-146784192
0025                  IO(9)=-130006976
0026                  IO(10)=-113229760
0027                  IO(11)=1346386032
0028                  IO(12)=1077952576
0029                  DO 10 IJ=51,N,10
0030                  DO 8 I=1,10
0031                  LBL=I+IJ-1
0032                  DO 5 J=1,6
0033                5 IBI(J)=IA(LBL)/(10**(J-1))
0034                  DO 6 K=1,5
0035                6 IC(K)=IBI(K)-IBI(K+1)*10
0036                  L=5+6*(I-1)
0037                  M=L+4
0038                  DO 7 IK=L,M
0039                  IL=M-IK+1
0040                  KK=IC(IL)
0041                7 IOP(IK)=IO(KK+1)
0042                8 IOP(M+1)=IO(11)
0043                  IOP(64)=IO(12)
0044                  LBL=(IJ-51)/10
0045               10 WRITE(2,1)LBL,(IOP(I),I=5,63)
0046                  RETURN
0047                  END
```

```
0001            SUBROUTINE SUB2(FIT,D,GAINI,ZEROI,INTVL,GAINB,ZEROB)
0002            DOUBLE PRECISION D(570)
0003            DIMENSION FIT(21,20),B(10),COEFF(17)
0004          1 FORMAT(' ','NORMALISED BACKGROUND TOTAL COUNTS=',E14.7)
0005         65 FORMAT(1H ,24HERROR IN LAST INPUT CARD)
0006         69 FORMAT(1H ,48HRANGE RESTRICTED,STOP AT CHANNEL 519 IN INTERVAL,I3)
0007            GAIN=GAINI/GAINB
0008            DO 24 I=1,570
0009         24 D(I)=0.0
0010            DO 26 J=1,INTVL
0011            DO 25 I=4,21
0012         25 FIT(I,J)=FIT(I,J)*GAIN
0013            FIT(6,J)=FIT(6,J)*GAIN
0014            DO 26 I=2,3
0015         26 FIT(I,J)=(FIT(I,J)-ZEROB)/GAIN+ZEROI
0016            FIT(3,INTVL+1)=(FIT(3,INTVL+1)-ZEROB)/GAIN+ZEROI
0017            COEFF(1)=1.0
0018            LBL=1
0019            CHAN=-50.0
0020            K=INTVL+1
0021            DO 67 J=1,K
0022            IF(FIT(3,J)-519.0)67,67,68
0023         67 CONTINUE
0024            GO TO 27
0025         68 INTVL=J-1
0026            FIT(3,J)=519.0
0027            WRITE(3,69)INTVL
0028         27 IF(CHAN-FIT(3,1))28,29,29
0029         28 CHAN=CHAN+1.0
0030            GO TO 27
0031         29 DO 44 K=1,15
0032            J=22-K
0033            IF(FIT(J,LBL))45,44,45
0034         44 CONTINUE
0035         45 NSIN=J-6
0036            NPAR=NSIN+2
0037            B(4)=FIT(4,LBL)
0038            B(2)=FIT(2,LBL)
0039         30 B(3)=CHAN-B(2)
0040            DO 31 K=1,NSIN
0041            B(5)=K
0042         31 COEFF(K+2)=SIN(B(3)*B(4)*B(5))
0043            COEFF(2)=B(3)
0044            N=CHAN+51.0
0045            DO 32 J=1,NPAR
0046            CHAN=CHAN+1.0
0047         32 D(N)=D(N)+COEFF(J)*FIT(J+4,LBL)
0048            IF(CHAN-FIT(3,LBL+1))30,33,34
0049         33 IF(LBL-INTVL)34,30,64
0050         64 WRITE(3,65)
0051            STOP
0052         34 LBL=LBL+1
0053            IF(LBL-INTVL)29,29,35
0054         35 TOTAL=0.0
0055            DO 42 J=1,N
0056            IF(D(J))40,42,41
0057         40 D(J)=0.0
0058         41 TOTAL=TOTAL+D(J)
```



```
0059         42 CONTINUE
0060            WRITE(3,1)TOTAL
0061            GAINB=GAINI
0062            ZEROB=ZEROI
0063            RETURN
0064            END
```

```
      C     CALCULATE EFF AND ANGULAR CORRELATION CORRECTION FACTORS FOR
      C     RECTANGULAR GERMANIUM DECTOR
0001        DIMENSION TOTAL(3),EGAMMA(33),TAU(33)
0002        COMMON/COMA/W,FL,T,H,TOR,L,K
0003        COMMON/COMB/X,DH,Y1,Y2,N,SUM
      C     SPECIFY DIMENSION OF THE DETECTOR IN CM
0004        DATA HEIGHT,WIDTH,THICK/2.8,3.4,3.1/
      C     SPECIFY RANGE OF GAMMA ENERGY TO BE CALCULATED
0005        DATA NR1,NR2/14,26/
      C     LIST OF GAMMA ENERGIES AND LINEAR ATTENUATION FACTORS(TAU)
0006        DATA EGAMMA/0.01,0.015,0.02,0.03,0.04,0.05,0.06,0.08,0.1,0.15,
           10.2,0.3,0.4,0.5,0.6,0.8,1.0,1.5,2.0,3.0,4.0,5.0,6.0,8.0,10.0,15.0,
           120.0,30.0,40.0,50.0,60.0,80.0,100.0/
0007        DATA TAU/161.731,504.617,227.193,72.195,31.418,16.624,10.139,
           14.730,2.765,1.213,0.831,0.575,0.482,0.428,0.389,0.337,0.302,0.246,
           10.217,0.187,0.174,0.168,0.166,0.164,0.166,0.175,0.186,0.203,0.217,
           10.228,0.237,0.250,0.260/
0008        31 FORMAT('0',' EGAM TAU DET EFF J2/J0',
           1' J4/J0')
0009        32 FORMAT('1','DETECTOR DIMENSION HEIGHT=',F6.2,' CM, WIDTH=',
           1F6.2,' CM, THICK=',F6.2,' CM')
0010        33 FORMAT(' ',F10.3,F10.4,E12.5,2F10.4)
0011        34 FORMAT('0','SOURCE TO DETECTOR DISTANCE=',F6.2,' CM')
0012        35 FORMAT('0','SOLID ANGLE=',E12.5,' ST RADIAN')
0013        36 FORMAT(F10.2)
0014           WRITE(3,32)HEIGHT,WIDTH,THICK
0015           W=HEIGHT/2.0
0016           FL=WIDTH/2.0
0017           T=THICK
0018           M=10
0019           N=10
      C     READ IN SOURCE TO DETECTOR DISTANCE
0020        77 READ(1,36)H
0021           WRITE(3,34)H
0022           SUM4=0.0
0023           DO 78 NG=NR1,NR2
0024           TOR=TAU(NG)
0025           EGAM=EGAMMA(NG)
0026           DO 4 L=1,3
      C     CALCULATE FIRST INTEGRAL
0027           SUM1=0.0
0028           X1=0.0
0029           X2=H*W/(H+T)
0030           DH=(X2-X1)/(2.0*M)
0031           Y1=0.0
0032           Y2=H*FL/(H+T)
0033           DO 1 I=1,M
0034           K=1
0035           X=X1+(I-1)*2.0*DH
0036           CALL DINTEG
0037           SUM1=SUM1+SUM
0038           IF(NG-NR1)14,14,1
0039        14 IF(L-1)11,11,1
0040        11 K=4
0041           CALL DINTEG
0042           SUM4=SUM4+SUM
0043         1 CONTINUE
      C     CALCULATE SECOND INTEGRAL
```

```
0044                SUM2=0.0
0045                X1=H*W/(H+T)
0046                X2=W
0047                DH=(X2-X1)/(2.0*M)
0048                Y1=0.0
0049                DO 2 I=1,M
0050                K=2
0051                X=X1+(I-1)*2.0*DH
0052                Y2=X*FL/W
0053                CALL DINTEG
0054                SUM2=SUM2+SUM
0055                IF(NG-NR1)15,15,2
0056             15 IF(L-1)12,12,2
0057             12 K=4
0058                CALL DINTEG
0059                SUM4=SUM4+SUM
0060              2 CONTINUE
                C   CALCULATE THIRD INTEGRAL
0061                SUM3=0.0
0062                X1=H*FL/(H+T)
0063                X2=FL
0064                DH=(X2-X1)/(2.0*M)
0065                Y1=0.0
0066                DO 3 I=1,M
0067                K=3
0068                X=X1+(I-1)*2.0*DH
0069                Y2=X*W/FL
0070                CALL DINTEG
0071                SUM3=SUM3+SUM
0072                IF(NG-NR1)16,16,3
0073             16 IF(L-1)13,13,3
0074             13 K=4
0075                CALL DINTEG
0076                SUM4=SUM4+SUM
0077              3 CONTINUE
0078                TOTAL(L)=SUM1+SUM2+SUM3
0079              4 CONTINUE
0080                IF(NG-NR1)17,17,18
0081             17 WRITE(3,35)SUM4
0082                WRITE(3,31)
0083             18 EFF=TOTAL(1)/3.14159
0084                Q2=TOTAL(2)/TOTAL(1)
0085                Q4=TOTAL(3)/TOTAL(1)
0086                WRITE(3,33)EGAM,TOR,EFF,Q2,Q4
0087             78 CONTINUE
0088                GO TO 77
0089                END
```

```
0001                SUBROUTINE DINTEG
0002                DOUBLE PRECISION Z
0003                COMMON/COMB/X1,DH,Y1,Y2,N,SUM
0004                COMMON/COMC/X,Y,Z
0005                DK=(Y2-Y1)/(2.0*N)
0006                G=2.0*DH*(Y2-Y1)/(36.0*N)
0007                SUM1=0.0
0008                N1=N+1
0009                DO 7 I=1,3
0010                X=X1+(I-1)*DH
0011                DO 7 J=1,N1
0012                Y=Y1+(J-1)*DK*2.0
0013                IF(J-1)1,1,2
0014              2 IF(J-N1)3,1,1
0015              1 CM=1.0
0016                GO TO 4
0017              3 CM=2.0
0018              4 IF(I-2)6,5,6
0019              5 CM=4.0*CM
0020              6 CALL ZFUNC
0021                SUM1=SUM1+Z*CM
0022              7 CONTINUE
0023                SUM2=0.0
0024                DO 11 I=1,3
0025                X=X1+(I-1)*DH
0026                DO 11 J=1,N
0027                Y=Y1+(2*J-1)*DK
0028                IF(I-2)9,8,9
0029              8 CM=16.0
0030                GO TO 10
0031              9 CM=4.0
0032             10 CALL ZFUNC
0033                SUM2=SUM2+CM*Z
0034             11 CONTINUE
0035                SUM=(SUM1+SUM2)*G
0036                RETURN
0037                END
```

```
0001                  SUBROUTINE ZFUNC
0002                  DOUBLE PRECISION E,R,R3,COSTH1,COSTH2,COSTH4,Z
0003                  COMMON/COMA/W,FL,T,H,TOR,L,K
0004                  COMMON/COMC/X,Y,Z
0005                  DIMENSION P(3)
0006                  E=X*X+Y*Y+H*H
0007                  R=DSQRT(E)
0008                  R3=R*R*R
0009                  COSTH1=H/R
0010                  COSTH2=COSTH1*COSTH1
0011                  COSTH4=COSTH2*COSTH2
0012                  P(1)=1.0
0013                  P(2)=(3.0*COSTH2-1.0)/2.0
0014                  P(3)=(35.0*COSTH4-30.0*COSTH2+3.0)/8.0
0015                  GO TO(1,2,3,4),K
0016                1 E=-1.0*TOR*R*T/H
0017                  E=(1.0-DEXP(E))*H/R3
0018                  Z=P(L)*E
0019                  RETURN
0020                2 E=-1.0*TOR*R*(W/X-1.0)
0021                  E=(1.0-DEXP(E))*H/R3
0022                  Z=P(L)*E
0023                  RETURN
0024                3 E=-1.0*TOR*R*(FL/X-1.0)
0025                  E=(1.0-DEXP(E))*H/R3
0026                  Z=P(L)*E
0027                  RETURN
0028                4 Z=H/R3
0029                  RETURN
0030                  END
```

```
      C     PROGRAM FITTER
      C     PROGRAM LNESHAPE
      C     ALIGN PHOTOPEAK OF EACH LINE SHAPE TO THE SAME POSITION AND
      C     NORMALIZE TO THE SAME HEIGHT
      C     STORE LINE SHAPES ON DISK
      C
            INTEGER PRINT
0001        DIMENSION A(2048,10),X(10),P(10),Y(10),NX(10),R(2048),TITLE(20),
0002       1S(2048),T(2048)
            COMMON S,T
0003  C     READ RUN DESCRIPTION - UP TO 80 CHARACTERS
            READ(1,360)TITLE
0004
0005  360   FORMAT(20A4)
0006        WRITE(3,3645)TITLE
0007  3645  FORMAT('1',20A4)
      C     READ IN THE HIGHEST NUMBER OF CHANNEL WHICH CONTAINS ALL LINE
      C     SHAPES AND PRINT OPTION, KDISK=1 OR GREATER IF THE LINE SHAPES ARE
      C     TO BE STORED IN THE DISK
            READ(1,117)K,PRINT,KDISK
0008
0009        K=K+1
0010  117   FORMAT(3I5)
      C     READ IN NUMBER OF LINE SHAPES - MAXIMUM OF TEN
            READ(1,1)NUM
0011
0012  1     FORMAT(I5)
0013        DO 22 I=1,10
0014        DO 22 J=1,2048
0015  22    A(J,I)=0.0
      C     READ IN LINE SHAPES, STARTING FROM LOW ENERGY IN INCREASING ORDER
0016        DO 20 J=1,NUM
      C     READ IN THE HIGHEST NUMBER OF CHANNEL OF EACH LINE SHAPE
0017        READ(1,1)NOCH
0018        NOCH=NOCH+1
0019        READ(1,2)(A(I,J),I=1,NOCH)
0020  2     FORMAT(3X,10F6.0)
      C     READ IN THREE HIGHEST CHANNELS OF PHOTOPEAK
0021        READ(1,3)K1,K2,K3
0022  3     FORMAT(3I5)
0023        M1=K1+1
0024        M2=K2+1
0025        M3=K3+1
      C     PEAK POSITION DETERMINED BY PARABOLIC FIT
0026        CALL PARAB(A(M1,J),A(M2,J),A(M3,J),K1,K2,K3,U,V,W)
0027        X(J)=-V/(2.*U)
0028        P(J)=X(J)*(U*X(J)+V)+W
0029        IF(PRINT)21,20,21
0030  21    WRITE(3,4)X(J),P(J)
0031  4     FORMAT(22HOPHOTOPEAK PARAMETERS,,19HPOSITION AND HEIGHT,2F10.2)
0032  20    CONTINUE
      C     READ IN ENERGIES APPROPRIATE TO LINE SHAPES
0033        READ(1,6)(Y(J),J=1,NUM)
0034  6     FORMAT(8F10.3)
      C     ENERGY CALIBRATION DETERMINED BY LEAST SQUARES FIT
0035        CALL LSTSQ(X,Y,NUM,SLOPE,RINT,SSD)
0036        IF(PRINT)471,470,471
0037  471   WRITE(3,7)SLOPE,RINT
0038  7     FORMAT(19HOENERGY CALIBRATION,5X,6HSLOPE=E15.5,5X,5HRINT=E15.5)
      C     TEST OF ENERGY CALIBRATION
0039  470   DO 50 J=1,NUM
0040        EN=SLOPE*X(J)+RINT
```

```
0041            IF(PRINT)51,50,51
0042      51    WRITE(3,8)EN,Y(J)
0043      8     FORMAT(31HOCOMPARISON WITH INPUT ENERGIES,5X,3HEN=F10.3,5X,7HACTUA
                1L=F10.3)
0044      50    CONTINUE
          C     GAIN ADJUSTED SO THAT PEAK OCCURS AT INTEGRAL CHANNEL
0045            DO 60 J=1,NUM
0046            NX(J)=X(J)+0.5
0047            XF=NX(J)
0048            RAT=(XF*SLOPE+RINT)/(X(J)*SLOPE+RINT)
0049            RATE=SLOPE*X(J)/XF
0050            DO 220 LX=1,K
0051      220   R(LX)=A(LX,J)
0052            IF(RAT-1.)141,141,142
0053      141   CALL PUSH(R,SLOPE,RINT,RATE,RINT,K)
0054            GO TO 607
0055      142   CALL PULL(R,SLOPE,RINT,RATE,RINT,K)
0056      607   DO 210 LX=1,K
0057      210   A(LX,J)=R(LX)
0058      60    CONTINUE
0059            IF(PRINT)473,472,473
0060      473   WRITE(3,9)(NX(J),J=1,NUM)
0061      9     FORMAT(27HORDUNDED OFF PEAK POSITIONS,10I5)
          C     SPECTRA NORMALIZED TO SAME PEAK HEIGHT
0062      472   NM=NUM-1
0063            DO 30 J=1,NM
0064            JZ=NX(NUM)+1
0065            JY=NX(J)+1
0066            FACTOR=A(JZ,NUM)/A(JY,J)
0067            IF(PRINT)474,475,474
0068      474   WRITE(3,5)FACTOR
0069      5     FORMAT(32HOLINE SHAPE NORMALIZATION FACTOR,F10.3)
0070      475   DO 40 I=1,K
0071            A(I,J)=FACTOR*A(I,J)
0072      40    CONTINUE
0073      30    CONTINUE
          C     SPECTRA TRANSLATED SO THAT PHOTOPEAKS ALIGNED
0074            DO 70 J=1,NUM
0075            DO 69 I=1,K
0076         69 R(I)=A(I,J)
0077            DO 80 I=1,K
0078            N=I+NX(NUM)-NX(J)
0079            IF(N-2048)652,652,651
0080       652  A(N,J)=R(I)
0081      651   XJ=J
0082            XZ=NM
0083            IF(XJ-XZ-0.1)778,778,80
0084      778   KR=NX(NUM)-NX(J)+1
          C     LOW ENERGY TAILS EXPTRAPOLATED TO ZERO
0085            KB=KR+1
0086            DO 90 KP=1,KR
0087      90    A(KP,J)=A(KB,J)
0088      80    CONTINUE
0089      70    CONTINUE
0090            IF(PRINT)78,77,78
0091      78    WRITE(3,71)
0092      71    FORMAT(31HOALIGNED AND NORMALIZED SPECTRA)
0093            WRITE(3,10)((A(I,J),I=1,K),J=1,NUM)
```



```
0094      10    FORMAT(' ',10F10.1)
0095      77    IF(KDISK)74,74,72
0096      72    REWIND 4
0097            WRITE(4)NUM,K,SLOPE,RINT,NX(NUM),(Y(L),L=1,NUM)
0098            REWIND 6
0099            DO 73 J=1,NUM
0100      73    WRITE(6)(A(I,J),I=1,K)
0101      74    IF(PRINT)75,76,75
0102      75    CALL MULPLT(NUM,A,K)
0103      76    STOP
0104            END
```

```
0001          SUBROUTINE LSTSQ(A,B,N,SLOPE,RINT,SSD)
              C LINEAR LEAST SQUARES FIT
0002          DIMENSION A(10),B(10)
0003          XN=N
0004          SUMA=0.
0005          SUMB=0.
0006          SUMAB=0.
0007          SUMAA=0.
0008          DO 1 I=1,N
0009          SUMA=SUMA+A(I)
0010          SUMB=SUMB+B(I)
0011          SUMAB=SUMAB+A(I)*B(I)
0012          SUMAA=SUMAA+A(I)*A(I)
0013        1 CONTINUE
0014          WA=SUMA*SUMB/XN-SUMAB
0015          WB=(SUMA**2)/XN-SUMAA
0016          SLOPE=WA/WB
0017          RINT=SUMB/XN-SLOPE*SUMA/XN
0018          SSD=0.
0019          DO 2 I=1,N
0020          DELTA=SLOPE*A(I)+RINT-B(I)
0021        2 SSD=SSD+DELTA*DELTA
0022          RETURN
0023          END
```

```
0001            SUBROUTINE PUSH(A,B,C,D,E,M)
          C     COMPRESS ORIGINAL SPECTRUM
0002            DIMENSION A(2048),S(2048),T(2048)
0003            COMMON S,T
0004            DO 1 NX=1,2048
0005            T(NX)=0.
0006          1 S(NX)=0.0
0007            DO 3 NM=1,M
0008            X=NM
0009            ORD=B*X+C-B*0.5
0010            Y=(ORD-E+0.5*D)/D
0011            IF(Y)3,9,9
0012          9 J=Y
0013            K=J+1
0014            WIDTH=B/D
0015            HT=(D/B)*A(NM)
0016            IF(WIDTH-FLOAT(K)+Y)10,10,12
0017         10 IF(J)3,3,11
0018         11 T(J)=A(NM)
0019            N1=J
0020            N2=J
0021            GO TO 6
0022         12 TA=HT*(K-Y)
0023            IF(J)15,15,13
0024         15 N1=J+1
0025            GO TO 14
0026         13 T(J)=TA
0027            N1=J
0028         14 T(K)=A(NM)-TA
0029            N2=K
0030          6 DO 4 L=N1,N2
0031            S(L)=S(L)+T(L)
0032          4 T(L)=0.
0033          3 CONTINUE
0034            DO 5 L=1,M
0035          5 A(L)=S(L)
0036            RETURN
0037            END
```

```
0001            SUBROUTINE PULL(A,B,C,D,E,M)
              C EXPAND ORIGINAL SPECTRUM
0002            DIMENSION A(2048),S(2048),T(2048)
0003            COMMON S,T
              C MAXIMUM NUMBER OF OUTPUT CHANNEL IS 2047
0004            DO 1 NX=1,2048
0005            T(NX)=0.
0006          1 S(NX)=0.
0007            DO 3 NM=1,M
0008            X=NM
0009            ORD=B*X+C-B*0.5
0010            Y=(ORD-E+0.5*D)/D
0011            IF(Y)3,9,9
0012          9 J=Y
0013            K=J+1
0014            WIDTH=B/D
0015            HT=(D/B)*A(NM)
0016            IF(WIDTH-K-1+Y)10,10,13
0017         10 TA=HT*(K-Y)
0018            IF(J)19,19,16
0019         19 N1=J+1
0020            GO TO 12
0021         16 IF(J-2048)11,11,6
0022         11 T(J)=TA
0023            N1=J
0024            IF(K-2048)12,12,6
0025         12 T(K)=A(NM)-TA
0026            N2=K
0027            GO TO 7
0028         13 TA=HT*(K-Y)
0029            IF(J)20,20,17
0030         20 N1=J+1
0031            GO TO 15
0032         17 IF(J-2048)14,14,6
0033         14 T(J)=TA
0034            N1=J
0035            IF(K-2048)15,15,6
0036         15 T(K)=HT
0037            IF(K-2047)18,18,6
0038         18 T(K+1)=A(NM)-TA-HT
0039            N2=K+1
0040            GO TO 7
0041          6 N1=J
0042            N2=2048
0043          7 DO 4 L=N1,N2
0044            S(L)=S(L)+T(L)
0045          4 T(L)=0.
0046          3 CONTINUE
0047            DO 5 L=1,M
0048          5 A(L)=S(L)
0049            RETURN
0050            END
```

```
0001          C     SUBROUTINE PARAB(X,Y,Z,I,J,K,U,V,W)
                    DETERMINE PEAK POSITION BY PARABOLIC FIT TO THREE POINTS
0002                XI=I
0003                XJ=J
0004                XK=K
0005                U=((X-Y)/(XI-XJ)-(X-Z)/(XI-XK))/(XJ-XK)
0006                V=(X-Z)/(XI-XK)-U*(XI+XK)
0007                W=X-U*(XI**2)-V*XI
0008                RETURN
0009                END
```

```
0001            SUBROUTINE MULPLT(ND,DATA,MUPPER)
          C     PLOT LINE SHAPES
0002            DIMENSION DATA(2048,10),IO(116)
0003         30 FORMAT('0','SCALE FACTOR=',F7.2,' COUNTS')
0004         31 FORMAT('0',4X,'0',8X,'10',8X,'20',8X,'30',8X,'40',8X,'50',8X,'60',
                18X,'70',8X,'80',8X,'90',8X,'100',7X,'110')
0005         32 FORMAT(' ',4X,116A1)
0006         33 FORMAT(' ',I4,116A1)
0007            DMAXM=0.0
0008            DO 2 I=1,MUPPER
0009            DO 2 J=1,ND
0010            IF(DMAXM-DATA(I,J))1,2,2
0011          1 DMAXM=DATA(I,J)
0012          2 CONTINUE
0013            SCALE=DMAXM/115.0
0014            WRITE(3,30)SCALE
0015            WRITE(3,31)
0016            DO 3 I=1,116
0017          3 IO(I)=1262501952
0018            DO 4 I=1,12
0019            J=(I-1)*10+1
0020          4 IO(J)=-918536128
0021            WRITE(3,32)(IO(J),J=1,116)
0022            DO 7 I=1,MUPPER
0023            DO 5 K=1,116
0024          5 IO(K)=1077952576
0025            DO 6 J=1,ND
0026            P=DATA(I,J)/SCALE+1.
0027            MP=P+0.5
0028          6 IO(MP)=1547714624
0029            LBL=I-1
0030            WRITE(3,33)LBL,(IO(K),K=1,116)
0031          7 CONTINUE
0032            RETURN
0033            END
```

```
                C       PROGRAM FITTER
                C       PROGRAM LEASTFIT
                C       LEAST SQUARES ANALYSIS OF GAMMA RAY COMPLEX SPECTRA          HUANG
0001                    DOUBLE PRECISION EGAM(25),Z1
0002                    DIMENSION Y(10),NX(10),XP(2048),R(2048),TITLE(20),A(1340,20),
                       1P(25),F(2048,2),FATRIX(25,25),ATRIX(25,1),EN(10),S(2048),T(2048),
                       2ZA(2048),ZB(2048),B(2048),D(2048)
0003                    KA1=1340
0004                    KA2=20
                C       READ EXPERIMENTAL SPECTRUM
0005                77  READ(1,360)TITLE
                C       READ PARAMETERS APPROPRIATE TO EXPERIMENTAL SPECTRUM
0006                    READ(1,362)KW,KST,NOLINE,OPTION,GLOPE,GINT,CHOICE,FMULT,NRAN,KEND
0007                362 FORMAT(3I5,5F10.5,2I5)
0008                    KW=KW+1
0009                    KST=KST+1
0010                    KEND=KEND+1
0011                    KM=KEND
0012                    GLOPE=GLOPE/1000.
0013                    GINT=GINT/1000.
0014                    READ(1,78)CHARGE
0015                 78 FORMAT(F10.2)
0016                    READ(1,2)(XP(I),I=1,KW)
0017                    IF(CHOICE)787,710,782
0018                782 READ(1,2)(B(J),J=1,KW)
0019                787 DO 781 I=1,2048
0020                781 R(I)=0.0
0021                    DO 786 I=1,KW
0022                786 R(I)=B(I)
                C       SPECIFY GAIN AND ZERO OF THE BACKGROUND SPECTRUM
0023                    QB1=0.05954
0024                    QB2=-0.1602
0025                    QB3=GLOPE/QB1
0026                    IF(QB3-1.0)783,784,784
0027                783 CALL PULL(R,QB1,QB2,GLOPE,GINT,KW,S,T)
0028                    GO TO 785
0029                784 CALL PUSH(R,QB1,QB2,GLOPE,GINT,KW,S,T)
0030                785 DO 701 LX=1,KW
0031                701 XP(LX)=XP(LX)-FMULT*R(LX)
0032                710 CONTINUE
0033                    WRITE(3,361)TITLE
0034                    WRITE(3,3666)GLOPE,GINT
0035                    WRITE(3,712)
0036                712 FORMAT(16HOINPUT SPECTRUM,,32HRANDOMS OR BACKGROUND SUBTRACTED)
0037                    WRITE(3,711)(XP(J),J=1,KW)
0038                    REWIND 4
0039                    READ(4)NUM,K,SLOPE,RINT,NX(NUM),(Y(L),L=1,NUM)
0040                    DO 437 MA=1,NOLINE
0041                    IF(NRAN)161,160,161
0042                161 IF(MA-NOLINE)160,162,160
0043                162 EGAM(NOLINE)=-99.999
0044                    GO TO 437
                C       READ ENERGY TO BE FITTED AND IDENTIFY ADJACENT LINE SHAPES
                C       ADD BYPASS IF GAIN ITERATION NOT REQUIRED
0045                160 READ(1,12)EGAM(MA),J,M,ELIM1,ELIM2,BYPASS,DECIDE,IDENT,EPEAK
0046                12  FORMAT(F10.3,2I5,4F10.3,I5,F10.2)
0047                    E=EGAM(MA)
0048                    IF(E-0.001)163,163,165
```

```
0049          163 DO 164 I=1,KA1
0050          164 A(I,MA)=0.0005
0051              GO TO 437
0052          165 PP=(E-RINT)/SLOPE
0053              KI=PP+0.5
0054              KX=NX(NUM)-KI+1
                  C     LINE SHAPE OF INTERMEDIATE GAMMA RAY GENERATED BY LINEAR
                  C     INTERPOLATION AND TRANSLATED TO THE APPROPRIATE POSITION
0055              REWIND 6
0056              DO 109 MB=1,J
0057          109 READ(6)(F(L,1),L=1,K)
0058              REWIND 6
0059              DO 114 MB=1,M
0060          114 READ(6)(F(L,2),L=1,K)
0061              DO 111 I=1,2048
0062          111 R(I)=0.0
0063              DO 110 N=KX,K
0064              I=N-NX(NUM)+KI
0065              R(I)=F(N,1)+(F(N,2)-F(N,1))*(E-Y(J))/(Y(M)-Y(J))
0066          110 CONTINUE
0067              JA=K-NX(NUM)+KI+1
0068              DO 931 MB=JA,K
0069          931 R(MB)=0.0
                  C     COMPUTED LINE SHAPE GAIN ADJUSTED TO CORRECT POSITION
0070              ZINT=(KI-PP)*SLOPE+RINT
0071              CALL PUSH(R,SLOPE,RINT,SLOPE,ZINT,K,S,T)
0072              IF(OPTION)239,245,239
0073          239 RAT=GLOPE/SLOPE
0074              IF(RAT-1.0)242,242,241
0075          241 CALL PUSH(R,SLOPE,RINT,GLOPE,GINT,K,S,T)
0076              GO TO 243
0077          242 CALL PULL(R,SLOPE,RINT,GLOPE,GINT,K,S,T)
0078          243 CONTINUE
0079              IF(OPTION)664,245,664
0080          245 GLOPE=SLOPE
0081              GINT=RINT
0082          664 XD=(E-GINT)/GLOPE
0083              XD=EPEAK
0084              WRITE(3,692)XD
0085          692 FORMAT(100X,F10.3)
0086              IF(BYPASS)666,662,666
0087          662 ND=XD+1
0088              NDO=ND-7
0089              NDU=ND+7
0090          677 DO 650 LC=NDO,NDU
0091              IF(R(LC+1)-R(LC))650,650,651
0092          651 IF(R(LC+1)-R(LC+2))650,650,652
0093          650 CONTINUE
0094              WRITE(3,653)
0095          653 FORMAT('0',80X,'PHOTO PEAK NOT FOUND')
0096              NDO=NDO-5
0097              NDU=NDU+5
0098              GO TO 677
0099          652 NPP=LC+1
0100              NP=NPP-1
0101              WRITE(3,691)NP
0102              CALL PARAB(R(NPP-1),R(NPP),R(NPP+1),NP-1,NP,NP+1,U,V,W)
0103              PEAK=-V/(2.*U)
```

```
0104                  WRITE(3,692)PEAK
0105                  IF(ABS(XD-PEAK)-0.1)666,957,957
0106            957   ZINT=(PEAK-XD)*GLOPE+GINT
0107                  CALL PUSH(R,GLOPE,GINT,GLOPE,ZINT,KW,S,T)
0108                  GO TO 677
0109            666   CONTINUE
0110                  IF(DECIDE)807,801,807
0111            807   IF(IDENT-1)808,802,808
0112            808   DO 803 LM=1,KW
0113            803   ZB(LM)=R(LM)
0114                  Z1=Z1+E
0115                  EGAM(MA)=Z1
0116                  GO TO 804
0117            802   DO 805 LM=1,KW
0118            805   ZA(LM)=R(LM)
0119                  Z1=E*10.0E+04
0120                  GO TO 160
0121            804   CALL SUMSPE(ZA,ZB,R,KW,GLOPE,GINT,S,T)
0122            801   CONTINUE
0123                  PRINT=0
0124                  IF(PRINT)479,476,479
0125            479   WRITE(3,413)EGAM(MA)
0126            413   FORMAT('0','GAIN ADJUSTED COMPUTED SHAPE',F14.3,' MEV')
0127                  WRITE(3,13)(R(I),I=1,KW)
0128            13    FORMAT(' ',10F10.1)
0129            476   CONTINUE
0130                  IF(ELIM1+ELIM2)493,581,493
0131            581   SUM=0.0
0132                  DO 494 I=1,KW
0133            494   SUM=SUM+R(I)
0134                  DO 495 I=1,KW
0135              495 R(I)=R(I)/SUM
0136                  DO 496 I=KST,KM
0137                  II=I-KST+1
0138              496 A(II,MA)=R(I)
0139                  GO TO 437
0140            493   CONTINUE
                C     LINE SHAPE NORMALIZED BY SUMMING INTERVAL NOMINATED
0141                  PS=(ELIM1-GINT)/GLOPE
0142                  QS=(ELIM2-GINT)/GLOPE
0143            244   KS=PS+1.5
0144                  KQ=QS+1.5
0145                  ZL=0.
0146                  DO 277 LA=KS,KQ
0147            277   ZL=ZL+R(LA)
0148                  ZX=0.
0149                  DO 278 LB=KS,KQ
0150            278   ZX=ZX+XP(LB)
0151                  WRITE(3,497)ZL,ZX
0152            497   FORMAT(100X,2F10.3)
0153                  FACTOR=ZX/ZL
0154                  WRITE(3,113)FACTOR
0155                  DO 120 I=1,K
0156                  R(I)=FACTOR*R(I)
0157            120   CONTINUE
0158                  WRITE(3,112)
0159                  WRITE(3,13)(R(I),I=1,KW)
                C     RESIDUAL SPECTRUM GENERATED
```

```
0160                DO 150 I=1,K
0161          150   XP(I)=XP(I)-R(I)
0162                DO 152 I=KST,KM
0163                II=I-KST+1
0164          152   A(II,MA)=R(I)
0165                WRITE(3,15)EGAM(MA)
0166          15    FORMAT(18HRESIDUAL SPECTRUM,5X,2HE=F14.3,10HSUBTRACTED)
0167                WRITE(3,16)(XP(I),I=1,KW)
0168          16    FORMAT(' ',10F10.1)
              C     RETURNS TO PEEL OFF THE NEXT GAMMA RAY
0169          437   CONTINUE
0170                IF(NRAN)187,179,180
0171          180   READ(1,2)(D(I),I=1,KW)
0172          187   DO 184 I=1,2048
0173          184   R(I)=0.0
0174                DO 186 I=1,KW
0175          186   R(I)=D(I)
              C     SPECIFY GAIN AND ZERO OF THE RANDOM BACKGROUND
0176                Q2=0.23026
0177                Q1=0.03460
0178                Q3=GLOPE/Q1
0179                IF(Q3-1.0)181,182,182
0180          181   CALL PULL(R,Q1,Q2,GLOPE,GINT,KW,S,T)
0181                GO TO 183
0182          182   CALL PUSH(R,Q1,Q2,GLOPE,GINT,KW,S,T)
0183          183   SUM=0.0
0184                DO 148 I=1,KW
0185          148   SUM=SUM+R(I)
0186                DO 149 I=1,KW
0187          149   R(I)=R(I)/SUM
0188                DO 151 I=KST,KM
0189                II=I-KST+1
0190          151   A(II,NOLINE)=R(I)
0191          179   CONTINUE
0192                IF(ELIM1+ELIM2)821,498,821
0193          821   DO 948 LX=1,KW
0194                R(LX)=0.
0195                DO 948 JC=1,NOLINE
0196                IF(JC-NOLINE)499,500,499
0197          500   IF(NRAN)948,499,948
0198          499   CONTINUE
0199                R(LX)=R(LX)+A(LX,JC)
0200          948   CONTINUE
0201                WRITE(3,949)
0202                WRITE(3,13)(R(I),I=1,KW)
              C     RECONSTITUTE THE EXPERIMENTAL SPECTRUM
0203                DO 508 LX=1,KW
0204          508   XP(LX)=XP(LX)+R(LX)
0205                WRITE(3,528)
0206                WRITE(3,13)(XP(I),I=1,KW)
0207          498   CONTINUE
0208                CALL LSTSQR(A,XP,KST,KM,NOLINE,FATRIX,ATRIX,FINISH,R,KA1,KA2)
0209                WRITE(3,522)
0210                WRITE(3,13)(R(LC),LC=KST,KM)
0211                SUMA=0.
0212                DO 520 LX=KST,KM
0213          520   SUMA=SUMA+(R(LX)-XP(LX))*(R(LX)-XP(LX))
0214                DF=KM-KST+1-NOLINE
```

```
0215                WS=SUMA/DF
0216                DO 521 LX=1,NOLINE
0217          521   FATRIX(LX,LX)=FATRIX(LX,LX)*WS
0218                CALL PLTFIT(R,XP,KST,KM)
0219                WRITE(3,400)
0220                DO 402 I=41,KW,10
0221                LX=I-1
0222                DO 401 LO=1,10
0223                JC=LX+LO-1
0224          401   EN(LO)=JC*GLOPE+GINT
0225          402   WRITE(3,403)LX,(EN(LO),LO=1,10)
0226                I=KM-KST+1
0227                DO 525 LO=1,NOLINE
0228                DO 526 LX=1,I
0229          526   R(LX)=ATRIX(LO,1)*A(LX,LO)
0230                WRITE(3,529)EGAM(LO)
0231                WRITE(3,13)(R(LX),LX=1,I)
0232          525   CONTINUE
0233                DO 530 LX=1,NOLINE
0234          530   ATRIX(LX,1)=ATRIX(LX,1)/CHARGE
0235                WRITE(3,361)TITLE
0236                WRITE(3,3666)GLOPE,GINT
0237                WRITE(3,519)
0238                DO 523 LX=1,NOLINE
0239          523   P(LX)=SQRT(FATRIX(LX,LX))/CHARGE
0240                DO 531 LX=1,NOLINE
0241          531   WRITE(3,518)EGAM(LX),ATRIX(LX,1),P(LX)
0242          518   FORMAT(' ',F14.3,4X,E12.5,2X,E12.5)
0243                RATIO=FINISH/DF
0244                WRITE(3,968)FINISH,DF,RATIO
0245          968   FORMAT('0','CHI-SQUARE=',E12.5,' DEGREE OF FREEDOM=',F6.0,
                   1' RATIO=',E12.5)
0246            360 FORMAT(20A4)
0247              2 FORMAT(3X,10F6.0)
0248            361 FORMAT('1',20A4)
0249         3666   FORMAT('0','SLOPE=',F10.5,' MEV/CH, INTERCEPT=',F10.5,' MEV')
0250          711   FORMAT(' ',10F10.1)
0251          691   FORMAT(100X,I5)
0252          113   FORMAT(22HONORMALIZATION FACTOR=F10.5)
0253          112   FORMAT(20HOCOMPUTED LINE SHAPE)
0254          529   FORMAT('0','FITTED LINE SHAPE ',F14.3,' MEV')
0255          519   FORMAT('0','    GAMMA ENERGY    INTENSITY   STD DEVIATION')
0256          949   FORMAT(18HOCOMPUTED SPECTRUM)
0257          528   FORMAT(15HOINPUT SPECTRUM)
0258          522   FORMAT(16HOFITTED SPECTRUM)
0259          400   FORMAT('0','ENERGY OF EACH CHANNEL IN MEV')
0260          403   FORMAT(' ',I5,10F10.3)
0261                GO TO 77
0262                END
```

```
0001                  SUBROUTINE PUSH(A,B,C,D,E,M,S,T)
                C     COMPRESS ORIGINAL SPECTRUM
0002                  DIMENSION A(2048),S(2048),T(2048)
0003                  DO 1 NX=1,2048
0004                  T(NX)=0.
0005            1     S(NX)=0.0
0006                  DO 3 NM=1,M
0007                  X=NM
0008                  ORD=B*X+C-B*0.5
0009                  Y=(ORD-E+0.5*D)/D
0010                  IF(Y)3,9,9
0011            9     J=Y
0012                  K=J+1
0013                  WIDTH=B/D
0014                  HT=(D/B)*A(NM)
0015                  IF(WIDTH-FLOAT(K)+Y)10,10,12
0016           10     IF(J)3,3,16
0017           16     IF(J-2048)11,11,3
0018           11     T(J)=A(NM)
0019                  N1=J
0020                  N2=J
0021                  GO TO 6
0022           12     TA=HT*(K-Y)
0023                  IF(J)15,15,17
0024           15     N1=J+1
0025                  GO TO 14
0026           17     IF(J-2048)13,13,3
0027           13     T(J)=TA
0028                  N1=J
0029                  IF(K-2048)14,14,18
0030           14     T(K)=A(NM)-TA
0031                  N2=K
0032                  GO TO 6
0033           18     N2=J
0034            6     DO 4 L=N1,N2
0035                  S(L)=S(L)+T(L)
0036            4     T(L)=0.
0037            3     CONTINUE
0038                  DO 5 L=1,2048
0039            5     A(L)=S(L)
0040                  RETURN
0041                  END
```

```
0001                  SUBROUTINE PULL(A,B,C,D,E,M,S,T)
                C     EXPAND ORIGINAL SPECTRUM
0002                  DIMENSION A(2048),S(2048),T(2048)
0003                  DO 1 NX=1,2048
0004                  T(NX)=0.
0005            1     S(NX)=0.
0006                  DO 3 NM=1,M
0007                  X=NM
0008                  ORD=B*X+C-B*0.5
0009                  Y=(ORD-E+0.5*D)/D
0010                  IF(Y)3,9,9
0011            9     J=Y
0012                  K=J+1
0013                  WIDTH=B/D
0014                  HT=(D/B)*A(NM)
0015                  IF(WIDTH-FLOAT(K+1)+Y)10,10,13
0016               10 TA=HT*(K-Y)
0017                  IF(J)19,19,16
0018               19 N1=J+1
0019                  GO TO 12
0020               16 IF(J-2048)11,11,3
0021               11 T(J)=TA
0022                  N1=J
0023                  IF(K-2048)12,12,3
0024               12 T(K)=A(NM)-TA
0025                  N2=K
0026                  GO TO 7
0027               13 TA=HT*(K-Y)
0028                  IF(J)20,20,17
0029               20 N1=J+1
0030                  GO TO 15
0031               17 IF(J-2048)14,14,3
0032               14 T(J)=TA
0033                  N1=J
0034                  IF(K-2048)15,15,3
0035               15 T(K)=HT
0036                  IF(K-2047)18,18,3
0037               18 T(K+1)=A(NM)-TA-HT
0038                  N2=K+1
0039                7 DO 4 L=N1,N2
0040                  S(L)=S(L)+T(L)
0041            4     T(L)=0.
0042            3     CONTINUE
0043                  DO 5 L=1,2048
0044                5 A(L)=S(L)
0045                  RETURN
0046                  END
```

```
0001            SUBROUTINE PARAB(X,Y,Z,I,J,K,U,V,W)
          C     DETERMINE PEAK POSITION BY PARABOLIC FIT TO THREE POINTS
0002            XI=I
0003            XJ=J
0004            XK=K
0005            U=((X-Y)/(XI-XJ)-(X-Z)/(XI-XK))/(XJ-XK)
0006            V=(X-Z)/(XI-XK)-U*(XI+XK)
0007            W=X-U*(XI**2)-V*XI
0008            RETURN
0009            END
```

```
0001                  SUBROUTINE MATINV(A,N,B,M,DETERM)
                C     INVERT A MATRIX
0002                  DIMENSION IPIVOT(25),INDEX(25,2),PIVOT(25),A(25,25),B(25,1)
0003                  EQUIVALENCE (IROW,JROW),(ICOLUM,JCOLUM),(AMAX,T,SWAP)
0004            10    DETERM=1.0
0005            15    DO 20 J=1,N
0006            20    IPIVOT(J)=0
0007            30    DO 550 I=1,N
0008            40    AMAX=0.
0009            45    DO 105 J=1,N
0010            50    IF(IPIVOT(J)-1)60,105,60
0011            60    DO 100 K=1,N
0012            70    IF(IPIVOT(K)-1)80,100,740
0013            80    IF(ABS(AMAX)-ABS(A(J,K)))85,100,100
0014            85    IROW=J
0015            90    ICOLUM=K
0016            95    AMAX=A(J,K)
0017           100    CONTINUE
0018           105    CONTINUE
0019           110    IPIVOT(ICOLUM)=IPIVOT(ICOLUM)+1
0020           130    IF(IROW-ICOLUM)140,260,140
0021           140    DETERM=-DETERM
0022           150    DO 200 L=1,N
0023           160    SWAP=A(IROW,L)
0024           170    A(IROW,L)=A(ICOLUM,L)
0025           200    A(ICOLUM,L)=SWAP
0026           205    IF(M)260,260,210
0027           210    DO 250 L=1,M
0028           220    SWAP=B(IROW,L)
0029           230    B(IROW,L)=B(ICOLUM,L)
0030           250    B(ICOLUM,L)=SWAP
0031           260    INDEX(I,1)=IROW
0032           270    INDEX(I,2)=ICOLUM
0033           310    PIVOT(I)=A(ICOLUM,ICOLUM)
0034           320    DETERM=DETERM*PIVOT(I)
0035           330    A(ICOLUM,ICOLUM)=1.0
0036           340    DO 350 L=1,N
0037           350    A(ICOLUM,L)=A(ICOLUM,L)/PIVOT(I)
0038           355    IF(M)380,380,360
0039           360    DO 370 L=1,M
0040           370    B(ICOLUM,L)=B(ICOLUM,L)/PIVOT(I)
0041           380    DO 550 L1=1,N
0042           390    IF(L1-ICOLUM)400,550,400
0043           400    T=A(L1,ICOLUM)
0044           420    A(L1,ICOLUM)=0.
0045           430    DO 450 L=1,N
0046           450    A(L1,L)=A(L1,L)-A(ICOLUM,L)*T
0047           455    IF(M)550,550,460
0048           460    DO 500 L=1,M
0049           500    B(L1,L)=B(L1,L)-B(ICOLUM,L)*T
0050           550    CONTINUE
0051           600    DO 710 I=1,N
0052           610    L=N+1-I
0053           620    IF(INDEX(L,1)-INDEX(L,2))630,710,630
0054           630    JROW=INDEX(L,1)
0055           640    JCOLUM=INDEX(L,2)
0056           650    DO 705 K=1,N
0057           660    SWAP=A(K,JROW)
```



```
0058           670    A(K,JROW)=A(K,JCOLUM)
0059           700    A(K,JCOLUM)=SWAP
0060           705    CONTINUE
0061           710    CONTINUE
0062           740    RETURN
0063           750    END
```

```
0001            SUBROUTINE SUMSPE(A,B,G,K,D,E,H,C)
                C   GENERATE COINCIDENCE SUM SPECTRUM
0002            DIMENSION A(2048),B(2048),G(2048),H(2048),C(2048)
0003            KY=2*K
0004            CALL PUSH(A,D,E,D,0.,K,H,C)
0005            CALL PUSH(B,D,E,D,0.,K,H,C)
0006            DO 5 M=1,2048
0007            H(M)=0.0
0008          5 C(M)=0.
0009            DO 1 M=1,K
0010            HT=A(M)/1000.
0011            DO 2 J=1,K
0012          2 G(J)=HT*B(J)
0013            DO 3 J=1,K
0014            LX=J+M
0015            IF(LX-2048)7,7,3
0016          7 H(LX)=G(J)
0017          3 CONTINUE
0018            DO 4 J=1,KY
0019            IF(J-2048)6,6,4
0020          6 C(J)=C(J)+H(J)
0021            H(J)=0.
0022          4 CONTINUE
0023          1 CONTINUE
0024            DO 8 I=1,2048
0025          8 G(I)=C(I)
0026            M=2048
0027            CALL PUSH(G,D,0.,D,E,M,H,C)
0028            RETURN
0029            END
```

```
0001                  SUBROUTINE LSTSQR(A,XP,KST,KW,NOLINE,FATRIX,ATRIX,FINISH,R,KA1,
                     1KA2)
                C     LEAST SQUARES ANALYSIS
0002                  DIMENSION A(KA1,KA2),XP(2048),TEMP(25),WEIGHT(2048),R(2048),
                     1FATRIX(25,25),ATRIX(25,1)
                C     INITIALIZE THE RESPONSE MATRIX
                C     COMPUTE THE NORMAL MATRIX
0003                  DO 512 LO=1,NOLINE
0004                  DO 512 LX=1,NOLINE
0005                  SUMA=0.
0006                  DO 513 LP=KST,KW
0007                  LY=LP-KST+1
0008            513   SUMA=SUMA+A(LY,LO)*A(LY,LX)
0009            512   FATRIX(LO,LX)=SUMA
                C     COMPUTE THE ASSOCIATED MATRIX
0010                  DO 516 LO=1,NOLINE
0011                  SUMA=0.
0012                  DO 517 LX=KST,KW
0013                  LY=LX-KST+1
0014            517   SUMA=SUMA+A(LY,LO)*XP(LX)
0015            516   ATRIX(LO,1)=SUMA
0016                  CALL MATINV(FATRIX,NOLINE,ATRIX,1,DETERM)
0017            720   DO 711 LX=KST,KW
0018                  LY=LX-KST+1
0019                  SUMA=0.
0020                  DO 712 LO=1,NOLINE
0021                  TEMP(LO)=ATRIX(LO,1)
0022            712   SUMA=SUMA+ATRIX(LO,1)*A(LY,LO)
0023            711   R(LX)=SUMA
0024                  DO 713 LX=KST,KW
0025                  IF(R(LX)-100.)800,800,714
0026            800   WEIGHT(LX)=0.01
0027                  GO TO 713
0028            714   WEIGHT(LX)=1./R(LX)
0029            713   CONTINUE
0030                  SUMA=0.
0031                  DO 213 LT=KST,KW
0032            213   SUMA=SUMA+WEIGHT(LT)*(XP(LT)-R(LT))**2
0033                  FINISH=SUMA
0034                  RETURN
0035                  END
```

```
0001            SUBROUTINE PLTFIT(FIT,OD,MLOWER,MUPPER)
                C       PLOT DATA AND FIT
0002            DIMENSION OD(2048),FIT(2048),IO(116)
0003         30 FORMAT('0','SCALE FACTOR=',F7.2,' COUNTS')
0004         31 FORMAT('0',4X,'0',8X,'10',8X,'20',8X,'30',8X,'40',8X,'50',8X,'60',
                18X,'70',8X,'80',8X,'90',8X,'100',7X,'110')
0005         32 FORMAT(' ',4X,116A1)
0006         33 FORMAT(' ',I4,116A1)
0007         34 FORMAT('+',4X,116A1)
0008            DO 27 I=MLOWER,MUPPER
0009            IF(OD(I))26,26,27
0010         26 OD(I)=0.0
0011         27 CONTINUE
0012            DO 29 I=MLOWER,MUPPER
0013            IF(FIT(I))28,28,29
0014         28 FIT(I)=0.0
0015         29 CONTINUE
0016            BMAXM=0.0
0017            DO 2 I=MLOWER,MUPPER
0018            IF(BMAXM-OD(I))1,2,2
0019          1 BMAXM=OD(I)
0020          2 CONTINUE
0021            DO 4 I=MLOWER,MUPPER
0022            IF(BMAXM-FIT(I))3,4,4
0023          3 BMAXM=FIT(I)
0024          4 CONTINUE
0025            BMAXM=BMAXM+SQRT(BMAXM)
0026            SCALE=BMAXM/115.
0027            WRITE(3,30)SCALE
0028            WRITE(3,31)
0029            DO 5 I=1,116
0030          5 IO(I)=1262501952
0031            DO 6 I=1,12
0032            J=(I-1)*10+1
0033          6 IO(J)=-918536128
0034            WRITE(3,32)(IO(J),J=1,116)
0035            DO 23 I=MLOWER,MUPPER
0036            P=OD(I)/SCALE+1.
0037            MP=P
0038            IF(P-MP-0.5)8,7,7
0039          7 MP=MP+1
0040          8 IF((I-1)/10*10-(I-1))24,25,25
0041         24 MQ=0
0042            GO TO 10
0043         25 P=SQRT(OD(I))/SCALE
0044            MQ=P
0045            IF(P-MQ-0.5)10,10,9
0046          9 MQ=MQ+1
0047         10 MR1=MP+MQ
0048            MR2=MP-MQ
0049            DO 11 J=1,MR1
0050         11 IO(J)=1077952576
0051            IO(MR1)=-918536128
0052            IF(MR2)13,13,12
0053         12 IO(MR2)=-918536128
0054         13 IO(MP)=-700432320
0055            MQ=I-1
0056            WRITE(3,33)MQ,(IO(J),J=1,MR1)
```

```
0057                P=(FIT(I)-OD(I))/SCALE
0058                MQ=P
0059                IF(P)16,18,14
0060             14 IF(P-MQ-0.5)18,15,15
0061             15 MQ=MQ+1
0062                GO TO 18
0063             16 IF(P-MQ+0.5)17,17,18
0064             17 MQ=MQ-1
0065             18 MR1=MP+MQ-1
0066                MR2=MR1+1
0067                IF(MR1)21,21,19
0068             19 DO 20 J=1,MR1
0069             20 IO(J)=1077952576
0070             21 IF(MR2)23,23,22
0071             22 IO(MR2)=1312833600
0072                WRITE(3,34)(IO(J),J=1,MR2)
0073             23 CONTINUE
0074                RETURN
0075                END
```